UNIVERSITY OF NATAL

CORDLESS LINEAR SYNCHRONOUS MOTOR MATERIAL HANDLING SYSTEM FOR COMPUTER INTEGRATED MANUFACTURING

Craig Vaughn Lindsay

BSc Eng

School of Mechanical Engineering

University of Natal

Durban

2000

Submitted in fulfilment of the academic requirements for the degree of Masters of Science in Engineering in the School of Mechanical Engineering, University of Natal.

Combined Research Project

Schools of Mechanical

and

Electrical Engineering

University of Natal

Durban

South Africa

PREFACE

The author hereby states that this entire thesis, unless specifically indicated otherwise, is his own original work, and has not been submitted in part or in whole to any other University. This dissertation records the work completed by the author at the School of Mechanical Engineering at the University of Natal between January 1998 and March 2000. This work is part of an ongoing research project investigating the design and development of a novel material handling system for flexible manufacturing environments.

C V Lindsay

To my Father and Mother,

"Your unquestionable love and support
is the inspiration
in my life."

ABSTRACT

Advanced material handling systems' impact on flexible manufacturing systems (FMS) have increased the efficiency and work rate over conventional manufacturing assemblies. The interaction of automated guided vehicles (AGVs), roller conveyors and conveyor belts with robots and machine tools forms highly sophisticated assembly operations.

Whilst material handling in FMS today is conventionally used to transport assembly units from one work station to another, it does not take an active role in the manufacturing process. With manufacturers implementing more advanced manufacturing principles to perform agile manufacturing, there is a growing need to implement "smarter" material handling systems that would perform essential, integral roles in the assembly process.

This research outlines the development of a cordless linear synchronous motor (CLSM) material handling system. The CLSM incorporates a permanent magnet courier that moves without tether restrictions on an integrated reverse air bearing system which eliminates friction. The CLSM provides a material handling system with enhanced travel, flexibility and accuracy. The CLSM material handling system is designed to integrate with overhead manipulators and part feeders to form a comprehensive flexible manufacturing system.

This research covers the 2-D finite element modeling (FEM) used to determine the CLSM's optimal parameters. The development of the motor windings design and construction, together with the control system for the CLSM, is also covered. The CLSM novel air bearing system is outlined and compared to other conventional linear bearing systems. The possible impact of the CLSM on current manufacturing systems is explored to determine the validity of the research project and possible further research opportunities.

ACKNOWLEDGMENTS

This work presented in this thesis was carried out under the supervision of Prof. Bright of the School of Mechanical Engineering and Prof Hippner of the School of Electrical Engineering at the University of Natal. I wish to thank Prof. Bright and Prof. Hippner for their enthusiastic supervision and support of this project. Their continual support was an inspiration for me to strive for quality.

I also wish to thank :

* To my family for their love and support through my years of study.

* To my girlfriend, Kim Meyer, for all her love. To my friends for their support and friendship through the years.

* To my colleagues, Mr J Potgieter, Mr J Mayor, Mr N S Tlale for their friendship and support. Special thank you to Mr J Potgieter for his assistance in helping develop the control software.

* Mr Ben Foster and staff of the Mechanical Engineering Workshop. Special thank you to Mr Mike Smith for his technical expertise and assistance in the construction of the project.

* Mr Tony Roos of the Electrical Engineering Workshop whose practical advice and assistance was extremely helpful.

* Nina Gould for her invaluable language assistance.

* The National Research Foundation (NRF) and the University of Natal, for their financial support.

TABLE OF CONTENTS

Preface . . . i
Dedication . . . ii
Abstract . . . ii
Acknowledgments . . . iv
List of Figures . . . xi
List of Tables . . . xix
List of Symbols and Abbreviations . . . xx

CHAPTER 1. INTRODUCTION

1. INTRODUCTION . . . 1
1.1 PROJECT BACKGROUND AND OBJECTIVES . . . 2
1.2 NEW CONTRIBUTIONS . . . 3
1.2.1 ADVANCED MANUFACTURING TECHNOLOGY DEVELOPMENT . . . 3
1.3 RESEARCH PUBLICATIONS . . . 4
1.4 THESIS LAYOUT . . . 5

CHAPTER 2. MATERIAL HANDLING ENGINEERING

2.1 HISTORY OF MATERIAL HANDLING . . . 8
2.1.1 GENERAL MATERIAL HANDLING SYSTEMS . . . 8
2.2 MATERIAL HANDLING IN THE AUTOMATED MANUFACTURING SYSTEM . . . 12
2.2.1 ROLLER CONVEYOR SYSTEMS IN THE CIM CONFIGURATION . . . 15
2.2.2 AUTOMATED GUIDED VEHICLES . . . 16
2.2.3 AUTOMATED STORAGE AND RETRIEVAL SYSTEMS . . . 22
2.2.4 ROBOTS . . . 24
2.3 ADVANCED MANUFACTURING MATERIAL HANDLING SYSTEMS 29

CHAPTER 3. LINEAR MOTOR THEORY

3 LINEAR MOTOR TECHNOLOGY 33
3.1 INTRODUCTION 33
3.2 LINEAR INDUCTION MOTOR 34
3.2.1 LIM DESIGN AND OPERATION 34
3.2.2 LIM APPLICATIONS IN MATERIAL HANDLING SYSTEMS 40
3.3 LINEAR SYNCHRONOUS MOTORS 43
3.3.1 LSM TOPOLOGIES 44
3.3.1.1 LSM ARMATURE 45
3.3.1.2 LSM EXCITATION SYSTEMS 50
3.3.2 SPECIAL TYPES OF LSMs 53
3.3.2.1 TUBULAR LSM 53
3.3.2.2 LINEAR STEPPER MOTORS 54
3.3.3 LSM APPLICATIONS IN MATERIAL HANDLING SYSTEMS 56
3.3.4 LSM OPERATION 61
3.3.4.1BASIC MODEL 62
3.4 PERMANENT MAGNET TECHNOLOGY 67

CHAPTER 4. LINEAR SYNCHRONOUS MOTOR ANALYSIS AND DESIGN

4.1 INTRODUCTION 73
4.2 FINITE ELEMENT ANALYSIS AND DESIGN 73
4.2 1 THEORY OF MAGNETOSTATIC FIELD SIMULATION 74
4.3 ANORAD'S BRUSHLESS LINEAR DC SERVOMOTOR 76
4.3.1 LEB-S-2-S FINITE ELEMENT ANALYSIS 76
4.4 FINITE ELEMENT ANALYSIS OF LINEAR SYNCHRONOUS MOTOR 81
4.4.1 2D FINITE ELEMENT MODEL SETUP 81
4.4.2 GEOMETRIC MODEL 83
4.4.3 PARAMETRIC ANALYSIS 83
4.4.4 MATERIAL SETUP 84

4.4.5 BOUNDARY CONDITIONS 86
4.4.6 SOURCES 90
4.4.7 EXECUTIVE PARAMETERS 90
4.4.8 SOLUTION OPTIONS AND MESH REFINEMENT 91
4.5 KINEMATIC AND FORCE ANALYSIS 92
4.6 FINITE ELEMENT MODEL DESIGN 95
4.6.1 PERMANENT MAGNET ANALYSIS 96
4.6.2 BACKIRON ANALYSIS 101
4.6.3 ARMATURE PLATEN ANALYSIS 102
4.6.4 THRUST RIPPLE ANALYSIS 105
4.6.5 FINAL FINITE ELEMENT MODEL DESIGN 109
4.6.6 EFFECTIVE MOTOR LENGTH 112
4.6.7 WINDING CALCULATIONS 114
4.6.8 DESIGN SUMMARY 117

CHAPTER 5. BEARING TECHNOLOGY
5.1 INTRODUCTION 119
5.2 MAGNETIC BEARINGS 119
5.2.1 PERMANENT MAGNET LEVITATION 120
5.2.2 ELECTROMAGNETIC LEVITATION 121
5.3 MECHANICAL BEARINGS 123
5.4 AIR BEARINGS 126
5.4.1 PRINCIPLE OF OPERATION 127
5.4.2 AIR BEARING DESIGN 129
5.4.3 REVERSE AIR BEARING DESIGN THEORY 130
5.4.3.1 GENERAL EQUATIONS 130
5.4.3.2 PLATEN BASE DESIGN 133

CHAPTER 6. CONSTRUCTION

6.1 INTRODUCTION . . . 136

6.2 LSM CONSTRUCTION . . . 137

6.2.1 COURIER . . . 137

6.2.2 PLATEN CONSTRUCTION . . . 138

6.2.2.1 FRAME . . . 138

6.2.2.2 WINDINGS . . . 138

6.3 REVERSE AIR BEARING CONSTRUCTION . . . 140

6.4 STAND DESIGN AND ASSEMBLY . . . 143

CHAPTER 7. CONTROL

7.1 INTRODUCTION . . . 146

7.2 POSITION FEEDBACK DEVICES . . . 146

7.2.1 LASER MEASUREMENT SYSTEMS . . . 147

7.2.2 MAGNETIC SENSORS . . . 149

7.2.3 ULTRASONIC SENSORS . . . 150

7.2.4 OPTICAL AIR BEARING SENSOR . . . 153

7.2.5 MAGNETRACK[1] POSITION SENSOR . . . 155

7.3 CONTROLLERS . . . 156

7.3.1 ANORADS M-SERV CONTROLLER . . . 158

7.3.2 KOLLMORGEN'S SERVOSTAR CD AMPLIFIER . . . 160

7.3.3 DELTA TAU PMAC2 CONTROLLER . . . 161

7.3.4 YASKAWA INVERTER . . . 162

7.3.4.1 INVERTER SETUP . . . 163

7.3.5 DATA ACQUISITION CARD . . . 168

7.4 ELECTRONIC CONTROL HARDWARE DEVELOPMENT AND COMMISSIONING . . . 170

7.4.1 PC30GA WIRING . . . 170

7.4.2 AIR BEARING CONTROL CIRCUITRY . . . 171

7.4.3 INVERTER CONTROL CIRCUITRY . . . 172

7.5 SOFTWARE CONTROL DEVELOPMENT . . . 173
7.5.1 LABVIEW GRAPHICAL PROGRAMMING . . . 173
7.5.2 FRONT PANEL . . . 173
7.5.3 REVERSE AIR BEARING CONTROL . . . 175
7.5.4 CORDLESS LINEAR MOTOR CONTROL . . . 177

CHAPTER 8. CORDLESS LINEAR SYNCHRONOUS MOTOR MATERIAL HANDLING SYSTEM TESTING
8.1 CLSM TEST . . . 181
8.1.1 BACKIRON SATURATION ANALYSIS . . . 181
8.1.2 ARMATURE PLATEN ANALYSIS . . . 182
8.1.3 PERFORMANCE ANALYSIS . . . 183
8.1.3.1 PROTOTYPE PHYSICAL DIFFERENCES . . . 184
8.1.3.2 CLSM TEST . . . 185
8.2 AIR BEARING TEST . . . 189
8.3 POSITIONING . . . 191

CHAPTER 9. CLSM MHS APPLICATIONS AND CIM INTEGRATION
9.1 INTRODUCTION . . . 192
9.2 MANUFACTURING APPLICATIONS . . . 192
9.2.1 ASSEMBLY SYSTEMS . . . 192
9.2.2 FACTORY-WIDE TRANSPORTATION SYSTEMS . . . 197
9.3 CIM INTEGRATION . . . 198

CHAPTER 10. DISCUSSION
10.1 CLSM MHS ANALYSIS . . . 201
10.1.1 POSITION FEEDBACK SENSOR . . . 201
10.1.1.1 INVERTER . . . 202
10.1.1.2 SENSOR SIGNAL CONDITIONING . . . 202

10.1.1.3 PHYSICAL SETUP . . . 203
10.1.2 INVERTER ANALOG INPUT . . . 204
10.1.3 AIR BEARING SYSTEM . . . 205
10.2 FUTURE RESEARCH OPPORTUNITIES . . . 207

CHAPTER 11. CONCLUSION . . . 208

REFERENCES . . . 209
LIST OF SUPPLIERS . . . 218
APPENDICES
Appendix A PERMANENT MAGNET DATA
Appendix B :Anorads LEB-S Brushless Linear Motor Series
Appendix C :COIL DESIGN AND MANUFACTURE DATA
Appendix D :CLSM MHS DESIGN AND ASSEMBLY DRAWINGS
Appendix E : ANALOG ULTRASONIC SENSOR
Appendix F :SLOTTED OPTICAL SWITCH TECHNICAL DATA
Appendix G :YASKAWA VS MINI J7 COMPACT INVERTER
Appendix H :PC30GA DATA ACQUISITION BOARD
Appendix I :CLSM MHS WIRING DIAGRAMS
Appendix J :LABVIEW GRAPHICAL PROGRAMS
Appendix K :PUBLICATIONS

LIST OF FIGURES

Figure 2.1: A material handler carrying rocks to the building site for the Great Wall of China . . . 9
Figure 2.2: The movement of materials by cargo (ship), freight (train), shipment (truck) and freight(plane) . . . 10
Figure 2.3: Corrugates being moved along by powered roller conveyors . . . 11
Figure 2.4: Mine ore being transported to the production house . . . 12
Figure 2.5: A forklift truck stacking a pallet of corrugates . . . 12
Figure 2.6: Breakdown of time spent by an average part in assembly . . . 13
Figure 2.7: The Manufacturing Cell at the Mechatronics and Robotics Research Laboratory . . . 14
Figure 2.8 : Graphical representation of the variations in the workpiece's position and orientation on the roller conveyor . . . 16
Figure 2.9: Driverless train with trailers being used in the manufacture of automobiles . . . 17
Figure 2.10: Forklift AGV in operation . . . 17
Figure 2.11: Unit load AGV used in the construction of a automobile engine . . . 18
Figure 2.12: Wire guided system using the magnetic field produced by the guide wire to steer the vehicle along a path . . . 18
Figure 2.13: The AGV interacting with the CIM cell. The optical guidance system developed for the AGV . . . 20
Figure 2.14: The AGV performing a docking procedure with the CIM cell to deliver a workpiece for assembly . . . 21
Figure 2.15: The S/R machine and the racking system which forms the AS/RS . . . 23
Figure 2.16: The Unimate PUMA 500 series robot . . . 24
Figure 2.17 : The four basic robot configurations . . . 25
Figure 2.18: The SCARA robot . . . 26
Figure 2.19: The six primary axes of robot movement . . . 26
Figure 2.20: Work volumes of various robots; (a) polar, (b) cylindrical, (c) rectangular. . . . 27

Figure 2.21: A robot interfaced to a machine tools and conveyors to load and unload incoming and outgoing work pieces in a machining center 28
Figure 2.22: A minifactory consisting of an x, y planar robot courier interacting with an overhead manipulator 31

Figure 3.1: Developing a linear motor 33
Figure 3.2: (a)Single sided and (b)double sided linear induction motor 34
Figure 3.3: Topologies of LIM (a) longitudinal-flux (b) transverse-flux 35
Figure 3.4: A flat LIM being propelled, suspended and stabilized 36
Figure 3.5: Primary windings; (a) single-layer,(b),(c) double-layer 37
Figure 3.6: A single-sided, short primary, LIM with cage secondary 38
Figure 3.7: Machine tool with a single-sided LIM 41
Figure 3.8 A single-sided LIM used in a separator 42
Figure 3.9: The Transrapid 07 magnetic levitation train 43
Figure 3.10: (a)Heteropolar (b) Homopolar linear synchronous motors 44
Figure 3.11: (a) Ironless motor, (b) Ironcore motor 45
Figure 3.12: Iron-core laminated stack using (1) bolts and (2) pressing angle bars. ... 46
Figure 3.13: Armature slots of iron-core LSM: (a) semi-open, (b) open 47
Figure 3.14: Flat double-sided PM LSM with moving air core armature 47
Figure 3.15: Anorad's balanced PM LSM, LEB-S-2-S 48
Figure 3.16: (a)Single-layer lap winding,(b) side view of a three phase armature with single-layer lap winding 49
Figure 3.17: (a) Double-layer lap winding, (b) Single-layer wave winding 50
Figure 3.18: Single sided flat PM LSM with (a) surface PMs, (b) buried PMs 51
Figure 3.19: Skewed PM arrangements in flat LSM (a) single row,(b) double row and (c) Hexagaonal arrangement 52
Figure 3.20: The development of a tubular linear synchronous motor 53
Figure 3.21: Schematic of a tubular LSM with Halbach magnetic array 54
Figure 3.22: The underside of the Normag4XY 1302-02 planar linear motor 55
Figure 3.23: Basic HLSM operation 56
Figure 3.24: Anorad's Microglide™ FP720 dual axis positioning stage 57

Figure 3.25: Horizontal factory transportation system with moving short armature LSM and long PM reaction rail. 1-armature, 2-PMs, 3-carrier, 4-guiderail. ... 58

Figure 3.26: Comparison of positioning systems with leadscrew and linear motors. ... 59

Figure 3.27: Basic linear motor model showing how force is created 62

Figure 3.28: Basic model of a permanent magnet linear motor 62

Figure 3.29 : Relative reaction rail positions of the motor model 64

Figure 3.30: A two phase model 65

Figure 3.31: Force generated due to two phases 65

Figure 3.32: *B-H* Hysteresis Loop of a hard permanent magnet material 68

Figure 3.33: Typical demagnetization and energy-product curves of a magnet showing the operating point line 69

Figure 3.34: Demagnetization characteristics of Alnico, ferrite, ceramic and rare-earth magnets 71

Figure 4.1: Anorad's balanced PM LSM 76

Figure 4.2: Geometric model generated to analyze the LEB-S-2-S motor 77

Figure 4.3 : Magnetic flux density distribution in the middle of the air gap between the two permanent magnet assemblies 77

Figure 4.4: Magnetic flux lines generated by the PM assembly 77

Figure 4.5: Magnetic flux density distribution with the currents in the windings set to a maximum 78

Figure 4.6: Thrust developed vs instantaneous phase angle (<$>0) of the current phasor for a fixed position of the moving coil assembly 79

Figure 4.7: The thrust developed vs position of the moving coil assembly for a frozen position of the current phasor (0=150°) 79

Figure 4.8: Thrust developed with phase adjustments in the windings. Values adopted from [Hippner et al] 80

Figure 4.9 : The Maxwell 2D Field Simulator Main Menu 82

Figure 4.10: Geometric model of the armature platen showing the assignment of notation to the coil set. The positive signs represent current flowing into the page and negative signs for current flowing out of the page, for each of the three

phases . . . 83
Figure 4.11: Geometric model setup with variable constraints for parametric analysis. 84
Figure 4.12: The B-H curve of nonlinear 1010 steel . . . 85
Figure 4.13: Boundary Conditions assigned to a model in a magnetostatic problem. . . 88
Figure 4.14: (a)Odd symmetry boundary,(b) Even symmetry boundary . . . 89
Figure 4.15: Boundary conditions assigned to the geometric model . . . 89
Figure 4.16: Initial mesh used in the finite element analysis . . . 92
Figure 4.17: Velocity vs time curve for a manufacturing task . . . 93
Figure 4.18: Geometric models setup by parametric analysis . . . 96
Figure 4.19: Thrust per meter developed by individual magnets . . . 97
Figure 4.20: Geometric models setup for the parametric analysis . . . 98
Figure 4.21: Thrust development per meter for PM assembly combinations . . . 98
Figure 4.22: Thrust developed for a complete 8-pole PM assembly versus the summation of the thrust developed by 8 individual magnets . . . 99
Figure 4.23: Thrust and normal force per meter vs air gap variations . . . 100
Figure 4:24: Thrust versus per meter air gap for varying for different PM depths ... 100
Figure 4.25: Normal force per meter versus air gap length for different PM depths. . 100
Figure 4.26: Thrust per meter developed for varying magnetic widths . . . 101
Figure 4.27: Normal force per meter developed for varying magnetic widths . . . 101
Figure 4.28: Thrust and normal force per meter versus varying backiron thicknesses. 102
Figure 4.29: Armature platen geometry . . . 102
Figure 4.30: Thrust and normal force per meter for increasing coil depth . . . 103
Figure 4.31: Thrust per meter developed for increasing coil width . . . 104
Figure 4.32: Thrust per meter for different mover positions for increasing coil spacings . . . 105
Figure 4.33: Normal force per meter for different mover positions for increasing coil spacings . . . 105
Figure 4.34: Manual mesh refinement by adding points to an existing mesh . . . 107
Figure 4.35: Manual mesh refinement . . . 108
Figure 4.36: Thrust per meter developed comparing mesh refinements . . . 108
Figure 4.37: Normal force per meter developed comparing mesh refinements . . . 108

Figure 4.38: Magnetic flux lines in a cross-section of the motor 109

Figure 4.39: Magnetic flux density distribution (calculated) in the air gap below the PM assembly 110

Figure 4.40: Determination of the zero position of the courier 110

Figure 4.41: Thrust curve vs phase angle ϕ_0 to determine the optimum value of ϕ_0 . . 111

Figure 4.42: Thrust per meter developed for increasing ampere-turns 112

Figure 4.43: Thrust and normal force per meter for different courier positions 112

Figure 4.44: Final thrust and normal force developed for the finite motor length. ... 113

Figure 4.45 : Magnetic flux density distribution at 250 ampere turns 114

Figure 4.46: Thrust comparison for increased coil depth from 7.8 mm to 12 mm. ... 116

Figure 4.47: Schematic diagram of proposed LSM showing the dimensional notation 118

Figure 5.1: Proposed magnetic levitation using PMs to levitate and stabilize the courier as it moves down the platen track 120

Figure 5.2: (a)Sectional view of a levitation track, (b) Overall view of the wafer handling system 122

Figure 5.3: Point and line contacts and deformations for ball and roller bearings. .. 123

Figure 5.4: Recirculating roller bearing carriage and linear guideway.[INA] 124

Figure 5.5: Recirculating ball bearing carriage and linear guideway 124

Figure 5.6 : (a)Track roller guidance system, (b) shaft guidance system 125

Figure 5.7: Mechanical bearing system proposal using shaft guided linear ball bearings 125

Figure 5.8: Aerostatic and aerodynamic gas bearing 126

Figure 5.9: Externally pressurized air bearing notation and pressure distribution. .. 128

Figure 5.10: Reverse air bearing testing system using direct line supply concept. ... 129

Figure 5.11: Flow of a gas between two parallel plates 130

Figure 5.12: Platen orifice design and pressure distribution under the courier 134

Figure 6.1: Overview of the prototype material handling system 136
Figure 6.2: Permanent magnet courier with carrier platform 137
Figure 6.3: The coil former used to wind the armature coils 139
Figure 6.4: A coil being wound on the lathe using the former 139
Figure 6.5: Armature platen under construction. 139
Figure 6.6: Y-connection used to wire the armature platen compared to a A-connection 140
Figure 6.7: The direct air lines into the frame base for each bearing pad 141
Figure 6.8: One side of the side air bearing which supplied air to the vicinity of the courier as it traveled down the platen 141
Figure 6.9: Air manifold to supply air to each orifice in the platen bearing pad 142
Figure 6.10: Solenoid valves and pressure regulator supplying air to the requirethanifolds. 143
Figure 6.11: Stand with air manifolds positioned below their respective bearing pads 144
Figure 6.12: Exploded view of the material handling system assembly 144
Figure 6.13: Material handling system with cordless courier and integrated reverse air bearing armature platen 145

Figure 7.1: Laser measurement system applied to the material handling system. ... 148
Figure 7.2: Magnetic encoder with magneto-resistive sensors 150
Figure 7.3: (a)Ultrasonic sensor used for position feedback of the courier 152
Figure 7.3: (b) Ultrasonic sensor perspex target mounted on the courier 152
Figure 7.4: Slotted optical switch layout along the platen switched by the *'winged'* courier 154
Figure 7.5: The air bearing pad activation system showing the courier cutting a optical switch 154
Figure 7.6: Control circuit developed for optical switches 155
Figure 7.7: (a) Block diagram of a open loop voltage-frequency control of a PM LSM, (b) closed loop control of.position, velocity and current of a PM LSM 158
Figure 7.8 (a): Anorad's M-Serv digital servo controller, (b) Kollmorgen's Servostar

CD Amplifier . . . 159
Figure 7.9: PMAC2 PC based motion control card . . . 161
Figure 7.10: Semipower PowerBlock PWM drive . . . 162
Figure 7.11: Proposed PMAC2 control system for the CLSM . . . 162
Figure 7.12: Yaskawa VS mini J7 inverter . . . 164
Figure 7.13: V/f pattern set for the CLSM inverter . . . 165
Figure 7.14 : Automatic output voltage scaling for constant speed operation . . . 166
Figure 7.15: Frequency reference by analog input . . . 166
Figure 7.16: PC30GA data acquisition board . . . 169
Figure 7.17: PC30GA wiring distribution board . . . 170
Figure 7.18: (a) Simple relay switching circuit,(b) transistor switching circuit implemented . . . 171
Figure 7.19: Relay switching boards for air bearing and inverter control . . . 172
Figure 7.20: Front page developed for the CLSM MHS control . . . 174
Figure 7.21: Port C configuration . . . 175
Figure 7.22: True case air bearing control for a forward traveling courier . . . 176
Figure 7.23: False case air bearing control for reverse traveling courier . . . 176
Figure 7.24: CLSM control using the comparison between the courier's current and target position . . . 178
Figure 7.25: Run forward inverter control . . . 179
Figure 7.26: Run reverse inverter control . . . 179
Figure 7.27: Frequency reference for input voltage . . . 180
Figure 7.28: Overview of control system implemented . . . 180

Figure 8.1: Geometric model showing assigned boundary conditions . . . 181
Figure 8.2 : Magnetic flux density distribution, currents in the windings set to a maximum of 2.5 Amps . . . 182
Figure 8.3 : B-H curve for the courier's backiron (1013 steel) showing flux density levels . . . 182
Figure 8.4: Magnetic flux density in the armature platen. Ia=l .25 amps, Ib=l .25, Ic=-2.5 amps . . . 183

Figure 8.5: (a) Finite element model coil shape (b) actual coil shape 184
Figure 8.6: Thrust generation for increases in the air gap length from 3 mm and 4 mm. 185
Figure 8.7: Static thrust for different positions of the mover. Ia=0.86 amps, Ib=0.86 amps, Ic=0 Amps 186
Figure 8.8: Thrust comparison between finite element analysis model and the prototype. Currents adjusted to give maximum thrust at each position. Im = lAmp 187
Figure 8.9: Reverse air bearing system being tested with the courier carrying a 3Kg load 189
Figure 8.10: Film thrust and actual load for an increasing bearing load 190

Figure 9.1: CLSM MHS in-line assembly system 193
Figure 9.2: Top view of a pick and place assembly operation 194
Figure 9.3: Complete in-line assembly system with multiple assembly stations and couriers 195
Figure 9.4: Four DOF overhead manipulator 196
Figure 9.5: Commercial planar motors with assembly head interacting with the CLSM MHS to create a 5-DOF system. 197
Figure 9.6: Factory wide CLSM MHS connecting multiple machine centers together with robot material handlers 198
Figure 9.7: MR^2L CIM cell with integrated CLSM MHS 199
Figure 9.8: MR^2G CIM Cell control system architecture 200

LIST OF TABLES

Table 4.1: Material properties of Grade 35 NdFeB magnets . . . 86

Table 4.2: Motion profile of the courier . . . 93

Table 4.3: Summary of forces experienced by the courier . . . 94

Table 4.4: Summary of results obtained for the 7RNG series of motor design . . . 106

Table 4.5: Winding Results for armature coil development . . . 116

Table 8.1: Summary of thrust results for the finite element model and the physical model . . . 187

LIST OF SYMBOLS AND ABBREVIATIONS

LIST OF SYMBOLS

Ace : is acceleration of the courier

A^ : conductor area.

A^ : total conductor area.

A,: specified coil area.

A-T : ampere-turns.

$A_2(x,y)$: the z-component of the magnetic vector potential.

B : magnetic flux density

B_g: air gap flux density

B_T: remanence

Cd : coil depth

Cw : coil width

d_{cu} : diameter of conductor

F: linear force

F_a: Attractive force

F_d: thrust or force developed

F_f: frictional force

H : magnetic field intensity

H_c : coercivity

I_s: the total slot current

i_s: current per turn

$J_z(x,y)$: the d.c. current density field.

j : current density

kp: packing factor

L : motor's effective length,

M_c: Courier Mass

M,,,: is the moving mass of the courier with load

N : number of turns

N_m : the number of magnetic pole faces

n_{s}: number of turns per slot

Oe : Oersted -units for magnetic field intensity

PC : permeance coefficient

P_d: power developed

s : slip in a linear induction motor.

T : telsa-units for magnetic flux density

t: time

v : courier speed

v_m: velocity of motor

v_s: synchronous speed

x : x-axis of cartesian coordinate system.

y : y-axis of cartesian coordinate system.

z : z-axis of cartesian coordinate system.

0 : angle of rotation about z-axis

u_r: the relative permeability of each material.

u_o: the permeability of free space.

\x : coefficient of friction

V : vector operator 'dell'

x : magnetic pole pitch of the courier

SUBSCRIPTS

d : developed

m : motor

s: synchronous

z : rotation around the z axis.

ABBREVIATIONS

a.c. alternating current

AGV : automatic guided vehicle

AS/RS : automatic storage and retrieval system

CIM : computer integrated manufacturing

CLSM : cordless linear synchronous motor

CMM : coordinate measuring machine

CNC : computer numerically controlled

CSI :current-source inverter

DC or d.c. : direct current

DOF : degrees of freedom

EMF : electromotive force

FEM : finite element model

FMS : flexible manufacturing system

LDR : light dependent resistor

LIM : linear induction motor

LSM : linear synchronous motor

MHS : material handling system

MMF : magnetomotive force

MLDT : magnetic linear displacement transformers

MR^2G : mechatonics and robotics research group

ORIS : object recognition and inspection system

P&D : pick up and deposit

PLC : programmable logic controller

PM : permanent magnet

PUMA : programmable universal machine for assembly

PWM : pulse-width modulation

SCARA : selective compliance assembly robot arm

S/R : storage/retrieval

VSI: voltage-source inverter

1. INTRODUCTION

Technological advances in manufacturing in the latter half of the 20^{th} century have facilitated the growing global trend towards customization as opposed to bulk manufacturing. However, with increasing diversity in the product base, production volumes have grown continually. Increased customer involvement in the manufacturing process, along with increased global competition, has compelled industry to create cost effective, flexible, diverse manufacturing systems capable of producing a wide range of products.

There have been technological advances in computer numerically controlled (CNC) milling machines. On-site inspection of the manufacturing process has been facilitated by the inclusion of co-ordinate measuring machines (CMM) and object recognition inspection systems (ORIS). The development of automated storage and retrieval systems (ASRS) has aided in the storage and inventory of products in the manufacturing environment. The automation of material movement between work cells has borne the development of the automated guided vehicle (AGV). Individually these systems have aided in the evolution of a disjointed manufacturing environment into an advanced flexible manufacturing system, capable of handling a large diverse customer product base.

A fundamental problem with advanced manufacturing systems is that the individual components (such as robots, milling machines, part feeders, conveyor systems etc.) are generally designed as stand alone devices. Information shared between these assembly units has been limited and often reserved for high level information systems. With technology now exploring the bounds of Internet Manufacturing and Virtual Reality Manufacturing, manufacturing systems are undergoing an information revolution, increasing the intelligence of base components such as sensors, actuators, part feeders, and robotic systems. This "bottom-ups" evolution is increasing the information being shared between the manufacturing cell's, individual components and upper hierarchy.

Whilst there has been significant advancement in sensors, actuators and robotic systems etc, material handling systems have lacked the privilege of the same technological advancement. Conveyor belts, roller conveyors, lead screws and AGVs' are conventionally used to transport production units from one work station to another and have not played an integral roll in the manufacturing process. They have lacked the intelligence to complement the manufacturing cells assembly units.

The development of linear motors and their ever increasing inclusion in the manufacturing environment have shown that they posses the ability to evolve the material handling function into an intelligent integral role player.

1.1 PROJECT BACKGROUND AND OBJECTIVES

The scope of this research covers the field of advanced material handling systems and its possible impact on manufacturing systems. Presented in outline is the development of a linear motor material handling system which integrates into manufacturing assemblies and is capable of interacting with assembly and subassembly units to increase flexibility, efficiency and accuracy.

Specific objectives include;

1) The investigation of current material handling systems and their impact on the manufacturing environment.

2) The conceptualization, design and development of an advanced material handling system capable of moving without tether restrictions.

3) The investigation of current bearing systems and the designing of a suitable bearing system to facilitate the new tether-less design material handling system.

4) The development of the required power electronics to control and operate the material handling system.

5) The selection of a suitable control feedback system to complement the motor's performance whilst maintaining the tether-less design.

6) The development of an operating system for easy operation and system integration into current advanced manufacturing systems.

1.2 NEW CONTRIBUTIONS

This research contributes to the ongoing development in linear synchronous motors and their applications in the manufacturing environment through the combination of the motor's topology and unconventional bearing system. The combination of the motor's topology and bearing system make the system unique when compared to other current motor designs and there applications. Mechatronic principles have been applied in the design of the cordless linear motor material handling system. The philosophy of mechatronics ensures equal rating to the component parts and identifies the interrelation between each of the sub-systems and the composite whole. The integration of contributing technologies such as electrical and electronic engineering, mechanical engineering and computer based technologies has assisted in the synergetic operation of the individual components in the material handling system.

1.2.1 ADVANCED MANUFACTURING TECHNOLOGY DEVELOPMENT

This thesis details the development of the CLSM material handling system which should be capable of performing advanced assembly processes through enhanced travel, flexibility and accuracy. The unique design can give accurate positions of assembly units when interacting with overhead manipulators such as robots, glue dispensers, part feeders etc. The increased intelligence allows direct interaction in the assembly process for increased accuracy. Robots with fewer degrees of freedom will be able to interact with the material handling system to form a highly intelligent and sophisticated assembly process capable of assembling a wide product base. Traditional contact bearing technologies have been eliminated. The tether-less courier runs on a reverse air bearing, allowing ultra-smooth motion and complete freedom of travel.

1.3 RESEARCH PUBLICATIONS

The following papers have been published in either local or international conference proceedings and journals:

1. *"Cordless Linear Motor Material Handling System for Computer Integrated Manufacturing"*, M. Hippner, C. Lindsay, G. Bright, Proceedings of the 5th International Conference on Computer Integrated Manufacturing (ICCIM), Singapore, 28 - 30 March 2000.

2. *"Advanced Material Handling System for Computer Integrated Manufacturing."*, C. Lindsay, M. Hippner, G. Bright, Journal of Robotics and Computer Integrated Manufacturing, 2000.

3. *"Reverse Air Bearing Levitation for a Moving Magnet Linear Motor Material Handling System"*, C. Lindsay, M. Hippner, G. Bright, Materials Handling Today, July, 2000.

4. *"Intelligent Material Handling System for Advanced Electronic Component Inspections"*, C. Lindsay, N.S. Tlale, G. Bright, The 11th International DAAAM Symposium: Intelligent Manufacturing and Automation: Man-Machine-Nature, Croatia, 19-21 October 2000.

5. *"Integrated Reverse Air Bearing Levitation System for a Moving Magnet Linear Motor Material Handling System"*, C. Lindsay, M. Hippner, G. Bright, The 6th International Conference on Control, Automation, Robotics and Vision (ICARCV),Singapore, 5-8

December 2000.

6. *"OptimisedMaterials Handling using Cordless Linear Synchronous Motors.*", C. Lindsay, M. Hippner, G. Bright, The 17th International Conference on CAD/CAM, Robotics and Factories of the Future, Durban, South Africa, 10-12 July 2001

1.4 THESIS LAYOUT

The layout of this thesis is based on the literature survey undertaken into related subjects and manufacturing trends, and into the design, construction and testing of the cordless linear motor material handling system. The results of the literature survey are presented in Chapters two and three. Chapters four to eight present the design, construction and testing of the prototype. Chapters nine to ten explore the applications and integration of such a system into the manufacturing environment, the problems which presented themselves and their solutions and future research opportunities.

Chapter 2 introduces material handling engineering and the impact material handling has had on manufacturing. The six generations of material handling systems are presented covering material handling from the manual generation to the highly advanced systems beginning to be implement in advanced manufacturing environments today. The advantages and disadvantages of material handling systems in their specific environments are explored.

Chapter 3 outlines linear motor technology namely linear induction motors (LIMs) and linear synchronous motors (LSMs). The different topologies and applications of both types of linear motors are explored outlining the advantages and disadvantages of each. The basic fundamentals into how thrust is developed in LSMs is presented. A brief insight into permanent magnet technology development is described. Common magnetic materials used in permanent magnet linear motors, highlighting their suitability for certain applications, are outlined.

Chapter 4 presents the design and analysis of the LSM using the finite element method. A kinematic analysis is undertaken to determine the required forces to complete a manufacturing task. The motor's parameters and physical dimension are determined from the finite element model. Design variations and the influence of varying parameters on the motor's performance are analyzed. The motor's final thrust and normal force development are presented together with a summary of the design specifications.

Chapter 5 explores bearing technologies. Bearing systems such as magnetic, mechanical and air are presented. Proposals for the LSM are outlined. A novel air bearing system is designed for the material handling system. The theory of the reverse air bearing system is presented and applied to the implementation of the bearing system.

Chapter 6 covers the design and construction of the cordless LSM material handling system prototype. The construction of the PM courier and armature platen are explained. A novel coil making method is developed and implemented to create the required armature coils. The construction of the reverse air bearing system and its integration into the armature platen, to create a frictionless bearing system, is presented.

Chapter 7 details the literature survey into the different types of position feedback systems used with linear motor control. A non contact position sensor is used to complement the cordless design feature of the courier. A study into control systems and the selection of a suitable controller are presented. The development of a graphical user interface and software program for the optimal control of the PM LSM and reverse air bearing system is outlined.

Chapter 8 presents the results obtained from testing the motor. The results obtained are compared to the results from the finite element model to validate the accuracy of the computer simulation. The air bearing system designed and implemented is tested. The positioning of the courier is also tested.

Chapter 9 explores the possible applications of the cordless linear motor material handling system and the integration of such a system into a CIM cell The information architecture and system setup into a CIM cell is covered, focusing on advantages and disadvantages the system would have.

Chapter 10 discusses the problems which presented themselves and the solutions which were explored and implemented. Further research opportunities are outlined to develop the system's conceptual and tested ideas into a more advanced system.

2 MATERIAL HANDLING ENGINEERING

Despite the development of material handling systems from the manual lifting and moving of material by early man to the fully automated systems seen today, the essence of material handling has remained unchanged. The movement, storage, and control of materials has led to the development of a large array of material handling equipment.

The Industrial Revolution, which occurred during the late eighteenth and early nineteenth centuries, saw the beginning of the factory system. This system led to an increase in material requirements. As global manufacturing enterprises developed, so did several traits of material handling systems. Material handling engineering involves the art and science of using the right method to provide the right amount of material at the right place, at the right time, in the right sequence, in the right position, in the right condition, and at the right cost. [White],

Material handling systems may be classified as external and internal systems. External systems describe those systems which link the factory to outside markets, such as trains. Internal systems describe material handling functions within the factory system. The history of material handling engineering and the impact of material handling systems are explored. The movement of materials within manufacturing cells are investigated together with advanced systems now beginning to find merit within manufacturing environments.

2.1 HISTORY OF MATERIAL HANDLING

2.1.1 GENERAL MATERIAL HANDLING SYSTEMS

The first genera/ion of material handling began as a manual operation in which men were employed to lift, carry, stack and count. From the early biblical times which describe the storage and distribution of grain along the Nile River to the supplying of the Roman Army on their conquering crusades across Europe to the Chinese Emperor employing material handlers to build the Great Wall of China, (depicted in figure 2.1) manual material handling systems are still present in modern industries and our every day lives. Manual material handling has remained a popular method due to the fact that human beings are highly flexible. Special consideration needs to be given to manual material handling operations such as ergonomics and safety aspects for the worker and the material.

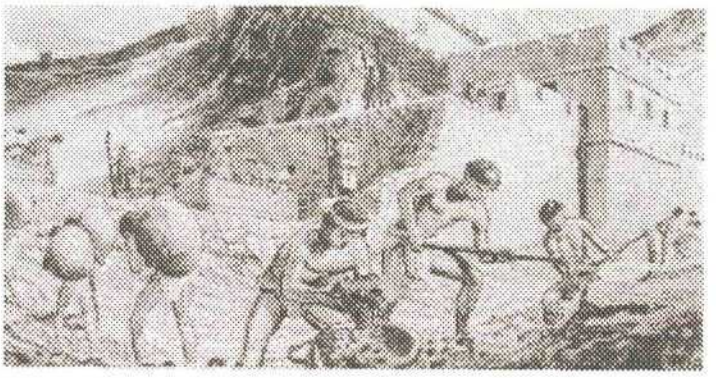

Figure 2.1: A material handler carrying rocks to the building site for the Great Wall of China.[Firth]

The *second generation* of material handling became known as the mechanical generation. Man began to invent structures and mechanisms to help surpass his own strength, reach and speed to obtain more efficient methods of material handling. Four major external material handling inventions have had an enormous impact on the global market by linking foreign countries. These are the movement of materials by ship, train, automobile and plane. The shipping of cargo has developed into the most extensively used means of importing and exporting of materials. The distribution of materials by rail, especially for bulk materials, also had a significant impact on industry. This cheap and easy form of moving material became very popular in the sugar, coal and grain industries. Transporting by rail was very popular in early twentieth century but has seen a decline in popularity in favour of transportation by road. The invention of the automobile had a significant effect on the role of material handling and modern industry. The shipment of raw materials and finished goods by road vastly increased the market areas of businesses and sourcing capabilities for raw materials. [Miller_l] Shipment by road allowed more flexibility. It grew in popularity as road structures linked more cities and towns. Another popular method of material movement is by plane. With the ability to cover large distances in a short space of time, planes been used extensively for transporting materials. Figure 2.2 shows examples of the four major external types of material handling methods.

Figure 2.2: The movement of materials by cargo (ship), freight (train), shipment (truck) and freight (plane). [Milier_l]

Investigation of internal material handling systems which developed in the manufacturing environment showed that material handling plays an important roll in the manufacturing environment. Material handling systems cut across plant sections and departmental boundaries and are often seen as the integrating agent in the manufacturing environment.

The invention of the conveyor system to transport both bulk and unit size materials led to it becoming an integral role player in the factory system. The two main types of conveyors are roller conveyors and belt conveyors. A roller conveyor consists of a series of tubes or rollers that are perpendicular to the direction of travel. Roller conveyors can either be powered to move objects along a path or free to use gravity to cause the load to travel from a higher elevation to a lower one. Powered roller conveyors have the tubes linked by chain or belt and are driven by motor, whereas free conveyors only require a sufficient slope to overcome rolling friction. Powered roller conveyors are used extensively in the manufacturing environment to transport corrugates as shown here in figure 2.3

Figure 2.3: Corrugates being moved along by powered roller conveyors.

Belt conveyors are found in two main forms, namely flat belts for unit loads and troughed belts for bulk materials. They are made of a continuous material belt tensioned over powered rollers at each end. Belt conveyors are best suited for applications where materials need to be elevated from a lower point to a higher point. Belt conveyors are used extensively in the mining industry to transport ore from the mine pit to the production house as shown in Figure 2.4.

The invention of the forklift truck came through the need to move palletized material quickly and efficiently. Obtaining the status of "workhorse" of the material handling industry, the forklift truck is used to load, unload trucks and move and stack palletized goods. The forklift truck's versatile design and mobility makes it suitable for a vast array of material handling requirements. Forklift trucks are found in three general classes, namely electric, diesel and gas. Selection of a forklift truck is based on lifting capacity (the total mass able to be lifted), the mast height (the height to which the load can be elevated), fork size(critical for determining the size of the load) and the powerplant (electric, diesel or gas). Selecting the powerplant is largely dependent on the type of environment in which the forklift will operate. The fork system can be replaced with different lifting mechanisms to handle different types of loads, such as metal drums. Figure 2.5 shows a forklift truck in action. The forklifts[1] high degree of mobility allows them to operate effectively in confined spaces. The ability to turn in narrow isles and stack large loads has made the forklift truck an integral part of manufacturing assembly and warehouse distribution systems.

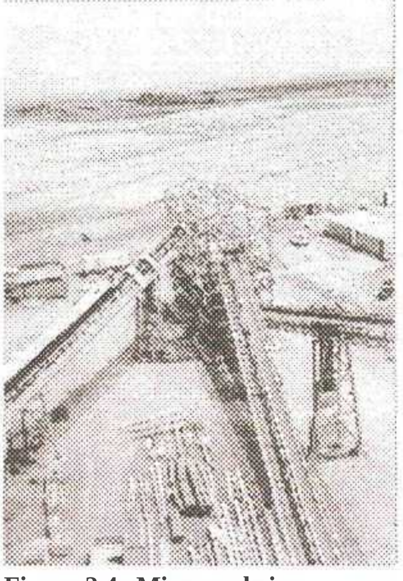

Figure 2.4: Mine ore being transported to the production house.[Materials]

Figure 2.5: A forklift truck stacking a pallet of corrugates.

2.2 MATERIAL HANDLING IN THE AUTOMATED MANUFACTURING SYSTEM

In the design of flexible manufacturing systems or manufacturing cells, the movement and transferring of materials is regarded as the base structure to the design of any plant layout. The interlinking of machine centres through the chosen material handling system is based on the working rule of : "the best material handling is the least material handling". This is best achieved by the optimal arrangement of machine centers and equipment, with consideration to ergonomics, minimizing the distance and trying to obtain a line of flight between machine centers. [Pemberton]

Time studies in material handling functions within the manufacturing cell showed that the work piece spends 95% -98% held in storage or in transit, whilst only 2% - 5% of the time in assembly. [Allegri] The function of material handling is a non value adding entity to the product, however it accounts for 30 % - 50% of the cost. [Allegri] The key objective in manufacturing is to get the right materials and parts to the right machines at the right time. If materials arrive too soon, backed up excess inventory occurs. Arriving too late, and work schedules are delayed, machines stand idle. Figure 2.6 shows the breakdown of the time spent by an average part in the assembly process. [Luggen]

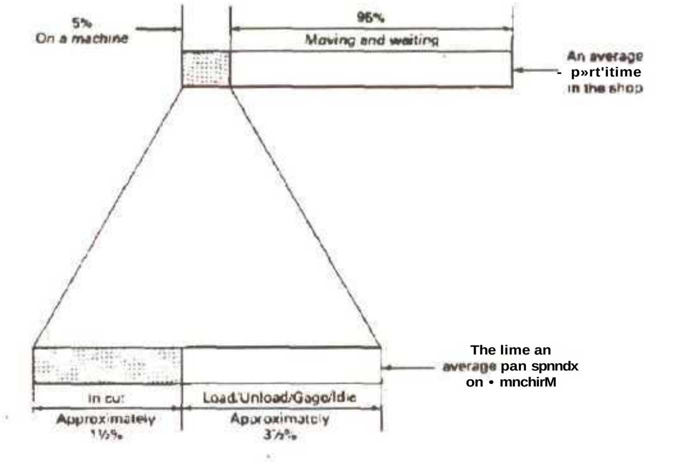

Figure 2.6: Breakdown of time spent by an average part in assembly. [Luggen]

Figure 2.6 shows the significant role material handling has in the automated manufacturing system. The choice of material handling equipment is critical to the success of the entire assembly process. The transfer of materials within the manufacturing system can be defined as:

(1) Continuous transfer systems

(2) Synchronous transfer systems

(3) Asynchronous transfer systems.

The transfer system implemented depends on the type of assembly operation. Continuous transfer systems consists of the work piece and the assembly tool heads moving together. Synchronous transfer systems involve all the work pieces moving together, whereas in asynchronous transfer systems the work pieces only move once the assembly operation is completed. Once the best transfer system has been determined for the manufacturing cell, the best material handling system can be implemented to complement the transfer system and the assembly process.

The Mechatronics and Robotics Research Group (MR^2G) at the University of Natal's School of Mechanical Engineering has developed a manufacturing cell. Investigating the material handling functions within the manufacturing cell, together with other material handling equipment employed in flexible manufacturing systems, revealed that it is the primary component which combines each of the individual manufacturing cell operations. The choice of material handling system is critical to the successful operation of the manufacturing cell as an integrated system. Figure 2.7 shows an overview of the manufacturing cell.

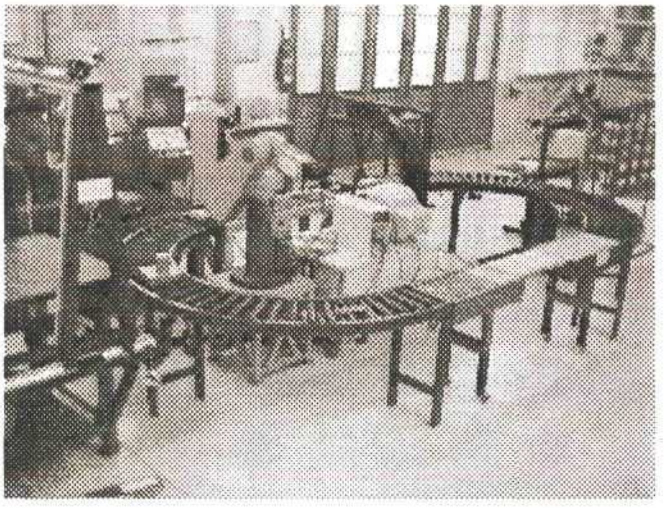

Figure 2.7: The Manufacturing Cell at the Mechatronics and Robotics Research Laboratory.

The manufacturing cell consists of a Heidenhain CNC milling machine, an Object Recognition and Inspection System (ORIS), a Coordinate Measuring Machine (CMM), two PUMA robots, an Automatic Storage and Retrieval System (AS/RS), an Automatic Guided Vehicle (AGV) and a powered roller conveyor system with AGV docking station.

The material handling equipment in the manufacturing cell spans both second and third generations of material handling systems. The *third generation* of material handling is known as the automated generation. AS/RS, AGVs and barcode scanners have become the main components of an automated material handling system. The automatic generation also introduced the robot into material handling, first seen in palletizing and packing and later becoming involved in the actual assembly process, such as welding. [Fuller]

2.2.1 ROLLER CONVEYOR SYSTEMS IN THE CIM CONFIGURATION

The primary material handling system in the manufacturing cell is the continuous roller conveyor system. Although roller conveyors have already been covered, an investigation into their function in the manufacturing cell reveals their advantages and disadvantages. The primary function of the roller conveyor is to transport the work pieces from one assembly stage to the next, such as from the milling machine to the CMM for inspection. One of the current disadvantages of the roller conveyor system is its lack of intelligence in term of the information it supplies to the rest of the manufacturing cells components. The lack of feedback information in terms of the work piece's speed and position, results in errors occurring during transfer operations. At present there are optical sensors to detect the entry and exiting of a work piece onto a section of the roller conveyor. However information on the workpiece between these points is based on the calculated speed of the roller conveyors. This is often inaccurate due to work pieces slipping on start and stop procedures. There are also no position sensors to determine the lateral or y position (see Figure 2.8) of the work piece on the roller conveyor or if the work piece has been skewed. This lack of information or intelligence of the roller conveyor system requires that other material handling systems, such as robots, are required to be fitted with advanced sensors such as vision system to successfully determine the correct position and orientation of the workpiece. There are also no barcode scanners, so material tracking of a workpiece is not possible. Figure 2.8 depicts graphically the problems involved due to the lack of feedback information.

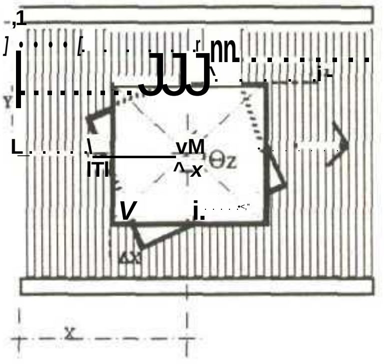

Figure 2.8: Graphical representation of the variations in the workpiece's position and orientation on the roller conveyor.

2.2.2 AUTOMATED GUIDED VEHICLE

AGVs were invented in the United States in the early nineteen forties but were first used after World War II as driverless tractors. [Pence] Since then, with the rapid development in computer technology, AGVs have evolved into highly intelligent, mobile and robust members of manufacturing systems. Defined by the Materials Handling Institute of America as "battery-powered driverless vehicles that can be programmed for path selection and positioning and are equipped to follow a changeable or expandable guide-path."[Luggen] Computer technology has allowed AGVs to become bi-directional, traveling on both closed and multiple loop paths. AGVs also handle traffic control and queuing in multiple-vehicle systems. They allow for material tracking as well. Driven by the type of application and environment in which the material needs to be moved, many different types of AGVs have been developed. Common types of AGVs include:

1) Towing
2) Pallet trucks
3) Unit load

A towing AGV is commonly called a "driverless train" and consists of a towing vehicle that pulls one or more trailers to form a train. Driverless trains are used in applications where heavy payloads need to be moved over large distances. They are common in warehouses and factories. Figure 2.9 shows a driverless train AGV in action.

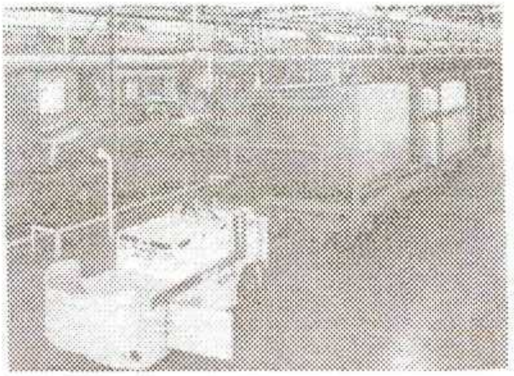

Figure 2.9: Driverless train with trailers being used in the manufacture of automobiles. [Groover]

AGV pallet trucks are used to move palletized loads along predetermined routes. A more advanced version of the pallet truck is the forklift AGV. The forklift AGV is finding popularity in modern warehousing systems as it reduces direct labor costs and employs greater control. [Groover] Figure 2 10 shows an example of a forklift AGV.

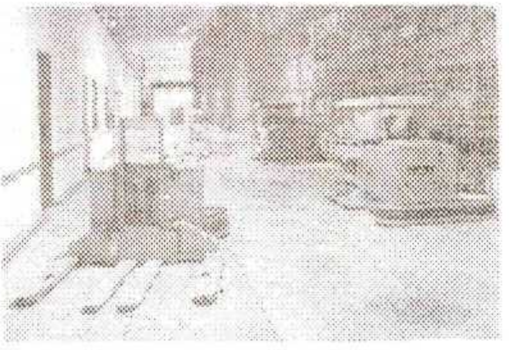

Figure 2.10: Forklift AGV in operation. [Groover]

AGV unit load carriers are used to move single loads from one station to another. They are often equipped with powered rollers, moving belts and mechanized lifting platforms for automatic loading and unloading of units. There are two types of unit load AGVs seen in industry today: light load AGVs and assembly AGVs. These are relatively small, using less space compared to normal AGVs and are designed to take small parts or sub-assemblies to workstations. Assembly line AGVs are designed to carry partially completed subassemblies through a sequence of assembly workstations to build the product as shown in Figure 2.11.

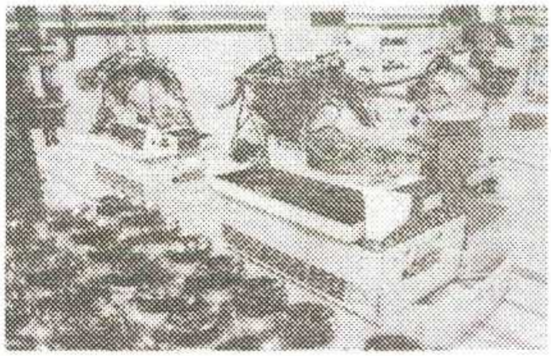

Figure 2.11: Unit load AGV used in the construction of a automobile engine. [Groover]

An AGV guidance system allows for the AGV to follow a predetermined path. Guidance systems used include tow-line, wire guided, inertial guidance, infra-red, laser, optical and teach type. Tow-line guidance systems were the first type of AGV guide system to be used and consist of a chain or cable which pulled the vehicle along. [Groover] One of the most popular guidance systems used is the wire guided system. Wire is embedded into the floor and a low voltage, low current signal is applied, creating a magnetic field. Coils are mounted on the underside of the vehicle, each side of the guide wire. As the vehicle moves the intensity of the magnetic field induces a voltage in the coils. Comparing the differences between the voltage allows the steering mechanism to adjust and keep the induced voltages equal and the vehicle on track. Figure 2.12 show how a guide wire system operates.

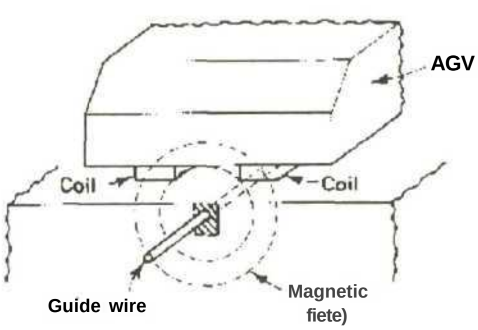

Figure 2.12: Wire guided system using the magnetic field produced by the guide wire to steer the vehicle along a path. [Groover]

Because wire guided systems are permanent fixtures there are problems associated with them. A great deal of planning is required to obtain the best path before the wire is laid. Inertial guidance systems involve using an onboard microprocessor to steer the vehicle on a pre-programmed path using ultrasonic sensors for obstacle detection and gyroscope for directional change. Infra-red guidance systems use infra-red light transmitted from the vehicle and reflected from strategically placed reflectors on walls or the roof to determine the vehicle's position and direction of travel. Laser guidance systems use wall mounted bar-coded reflectors. Using the information on the bar-code gives the AGVs' position.[Manda]

Another commonly used guidance system is optical. Photosensors track strips on the assembly floor. [GrooverJThe strip can be taped, sprayed or painted on the floor. This allows for greater flexibility as the pathway can be easily changed should there be alterations to the plant layout. Strip guidance paths are useful in environments where electrical noise would interfere with a wire guidance system. Strip paths must be maintained, free from dirt and scratches. Teach type guidance systems involve "walking through" the desired pathway, teaching the AGVs the new path.

Other functions which must be considered when implementing an AGV system is traffic cbntrol and system management. Traffic control and safety is important when two or more AGVs are used in the same assembly process. This is achieved by using on-board sensors and zone blocking. Using sensors, such as ultrasonic or optical sensors, to detect the presence of another AGV or obstruction prevents AGVs from colliding with each other or with other obstacles. Zone control is also used to eliminate AGV collisions. Guide paths are separated into zones. If one vehicle is in a specific zone, no other vehicle can enter. Almost all commercially operating AGVs are fitted with an emergency bumper with limit switches, which stops the AGV immediately when activated. System management deals with the dispatching and co-ordinating of an AGVs activities. Extensive research has been undertaken to optimize AGV path planning and work station interaction procedures. [Manda]. In FMS different assembly operations are required for different work pieces. The new routing and work interaction procedures for the specified job is downloaded from the FMSs' central control system to the AGVs sub-control system.

The AGV developed for the CIM cell at the Mechatronics and Robotics Research Laboratory is categorized as a unit load AGV. The wheels used on the AGV are of mecanum type. This consists of a steel rim with wooden rollers mounted around the circumference at an angle of 45 degrees to the wheel's axle, allowing for multidirectional movement. [Bright] Each wheel is driven independently by 12V DC motors. The AGV employs an optical guidance system which uses light dependent resistors (LDRs) to detect the light intensity from the floor. Black tape is used to lay the pathway. Figure 2.13 shows the AGV in operation with a close-up of the optical sensor. [Khan]

Figure 2.13: (a) The AGV interacting with the CIM cell. (b)The optical guidance system developed for the AGV.

The AGV is able to interact with the CIM cell. Using its variable height platform, it delivers and receives work pieces. The AGV moves sideways, integrating its platform with the roller conveyors of the CIM cell. The platform is lowered and the workpiece is deposited onto the roller conveyor. [Khan] The AGV has an emergency bumper to prevent damage to other equipment. The AGV control system uses Labview, a Windows-based graphical programming language, interfaced to a PC30GA I/O board. Information received by the optical guidance system is processed by the on-board computer. The voltage to the four independent motors is adjusted to obtain the desired direction and speed. Figure 2.14 shows the AGV performing a docking procedure with the CIM cell.

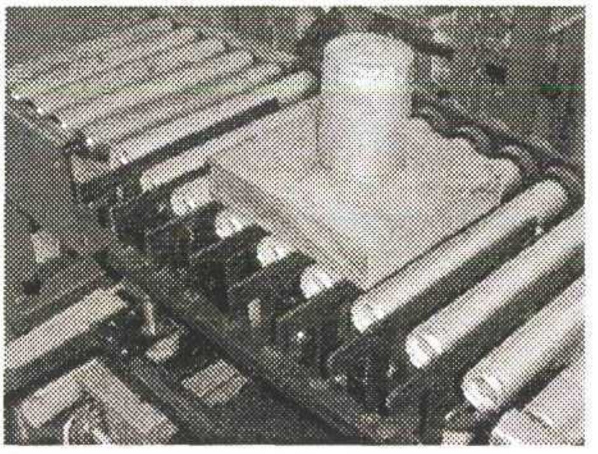

Figure 2.14: The AGV performing a docking procedure with the CIM cell to deliver a workpiece for assembly.

The advantage of the guidance system is its flexibility. The guidance strip can be easily changed by replacing the tape to map out a new guide path. The disadvantage of the current AGV system is the lack of information the AGV can share with the rest of the CIM cell. The AGV is currently a stand alone system, unable to give the CIM cell information on its position and speed. The AGV also has no material tracking facility and therefor it is unable to identify different types of work pieces. The AGV is continually under development with more features being added each year. It is envisaged that the AGV will be developed with enough intelligence to compliment the CIM cell.

AGVs can be highly integrated components of FMS and CIM cells. However, careful consideration must be made when integrating AGVs into a manufacturing system. Determining the number, speed and size of AGV required to successfully automate the material handling function is often a complex procedure. Research undertaken by Ilic' explored problems in determining congestion, contention and scheduling policies of an AGV system in FMS. [Ilic'] AGV systems are complex and require planning and maintenance, whereas a simple mechanical or manual material handling system may be all that is required.

2.2.3 AUTOMATIC STORAGE AND RETRIEVAL SYSTEMS

AS/RS were first pioneered in the nineteen fifties. The growing demand for storage space and the rising cost of land and warehousing space led to the development of high rise, high density storage and retrieval systems. Automated inventory-handling systems consisted of tall, vertical storage racks, narrow aisles and an automated storage and retrieval system. AS/RS, mostly found in warehouses, track incoming material and components, store parts, tools and fixtures and then retrieve them when necessary.

Some major advantages of AS/RSs are:

- improved inventory management and control
- reduced loss or misplacement of parts and tools
- flexibility in handling a wide range of loads
- reduced labor costs
- accurate inventory and load location.

The performance of an AS/RS system is rated by its storage capacity, system throughput, utilization and uptime reliability. The storage capacity is the total maximum number of individual loads that can be stored. It depends on the size and number of racks installed relative to the size of the loads. System throughput is defined by the number of loads per hour the AS/RS can store and retrieve. The utilization of an AS/RS is the percentage of the time that the system is in use compared to the total time available. Uptime reliability of an AS/RS is critical to throughput of a system. Mechanical or electrical faults resulting in down time leads to machines standing idle and delays in production. [Allergri]

The most common AS/RS system is the unit load AS/RS. This is a large automated system designed to handle unit loads on pallets or containers. Each isle is serviced by a storage/retrieval (S/R) machine which delivers the loads to pickup-and-deposit (P&D)stations. Variations of the unit load AS/RS are the miniload AS/RS, man-on-board AS/RS, automated item retrieval system and deep-lane AS/RS. [Groover, Luggen]. Miniload AS/RSs are used to handle small loads that are contained in bins within the storage system. The bin is delivered to the P&D station, where the desired part is removed from the bin. The bin is then returned to its location in the system. Automated item retrieval systems are designed to retrieve and store items in single-file lanes and not in bins. The supply of each item is normally replenished from the rear of the retrieval system. Deep-lane AS/RS are high density unit load storage systems used for the retrieval and storage of large quantities of items of similar type. Multiple items are stored in a single rack in line. A S/R machine retrieves the items from the front while another S/R machine is loading items from the rear. This permits for a first-in/first out inventory control system to be implemented. AS/RS are also utilized in the manufacturing environment on a smaller scale. A small AS/RS has been developed to store parts and incomplete assembly work pieces as part of the CIM cell developed by MR^2G. The S/R machine consists of a gantry system with a mounted carrier head. The carrier head is fitted with extendable forks for the storage and retrieval of mini pallets. The role of the AS/RS will be to place parts or work pieces onto the conveyor system when requested by the main computer of the CIM cell. The AS/RS is also capable of placing parts onto the AGV. This would then perform a docking operation with the conveyor system. Figure 2.15 shows the AS/RS developed to store parts and work pieces for the CIM cell.

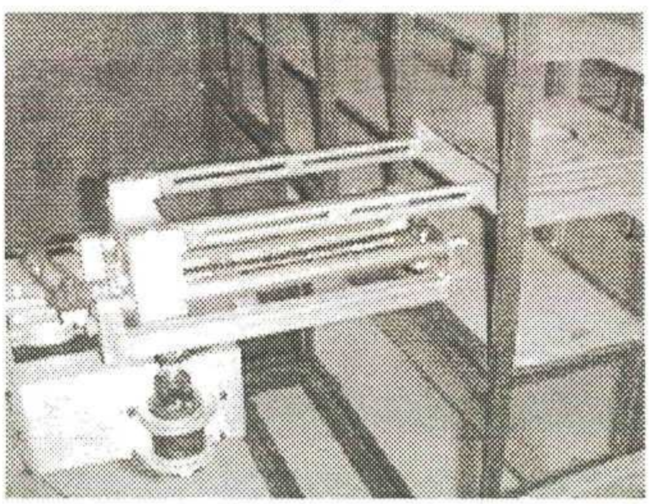

Figure 2.15: The S/R machine and the racking system which forms the AS/RS

Still under development, the AS/RS is currently a stand alone device and has no means of communicating with the CIM cells' other components. The AS/RS also lacks the ability to track materials. A bar code system is currently being researched which will allow the AS/RS to scan and track individual parts as they are stored in the racking system for later retrieval.

AS/RSs have had a significant impact on the inventory and control of parts and materials in the automated manufacturing environment. By installing AS/RSs, companies have found that they can now interface other equipment such as robots, AGVs and conveyors to AS/RSs, thus helping to increase the productivity and success of a FMS.

2.2.4 ROBOTS

The industrial robot is one of the most important developments in the history of automation technology. The vast applications in which robots are utilized today were not envisaged by the earlier pioneers in the 1950s. The development of the microprocessor released the vast potential of robotic capability. In 1962, Joseph Engelberger and George Devol established the Unimation Company. Within a short space of time robots found themselves being quickly applied to material handling operations. The first Unimation robot to be installed was at Ford Motor Company for unloading a die-casting machine. Unimation then developed a Programmable Universal Machine for Assembly (PUMA). The PUMA robot has evolved to become a world renown name. Figure 2.16 shows the Unimate PUMA 500 Robot.

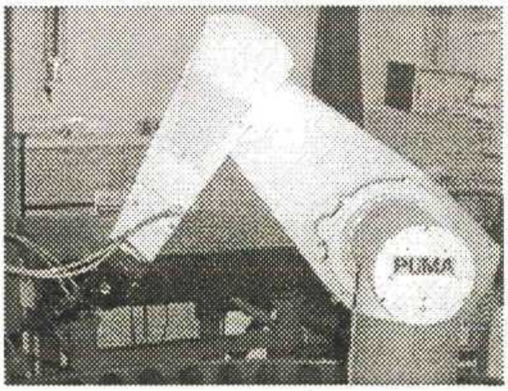

Figure 2.16: The Unimate PUMA 500 series robot.

The implementation of a robot into a FMS or CIM cell is based on the application the robot is to automate and the function it is to perform. These criteria determine the robot's anatomy. The robot anatomy is concerned with the physical construction of the body, arm, and wrist of a machine. The relative movements between the various components of the body, arm, and wrist are provided by a series of joints. Robots are available in a number of configurations. Common configurations are: (as shown in the schematic diagram Figure 2.17.) Polar configurations, Cylindrical configurations, Cartesian configurations, Jointed-arm configurations. [Groover et al]

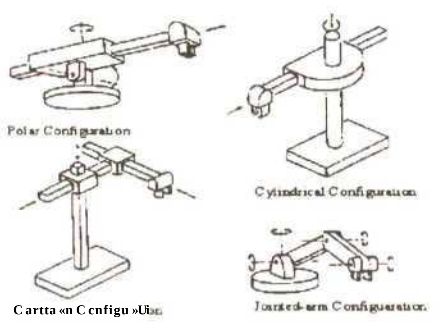

Figure 2.17 : The four basic robot configurations. [Groover et al]

The polar configuration uses a telescopic arm that can be raised or lowered about a horizontal pivot mounted on a base. The joints provided the robot with the ability to move within a spherical space. The cylindrical configuration robot uses a vertical column and a slide which moves up and down the column. The robot creates a cylindrical work space. The Cartesian coordinate robot uses three perpendicular slides to create x, y and z axes. The robot operates in a rectangular envelope. The jointed-arm robot is similar to a human arm, consisting of a shoulder, upper arm, elbow, forearm and wrist. The most common industrial robot which uses the latter configuration is the Selective Compliance Assembly Robot Arm or SCARA shown in figure 2.18. The SCARA robot became one of the first robots to perform in 'pick and place' assembly operations. [Groover et al]

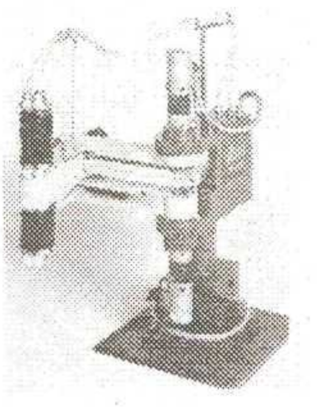

Figure 2.18: The SCARA robot. [Salant]

The motion of a robot is dependent on the degrees of freedom (DOF)which its arm, body and wrist have. Industrial robots usually have 4-6 DOF. A robot's motions are made possible by powered joints. Each joint is connected by a link. In a link-joint-link chain the proximal (link closest to the base) is referred to as the input link. The distal link is referred to as the output link. Industrial robots utilize a number of joints, namely; linear, rotational, twisting and revolving joints. Combinations of these joints allow robots to perform advanced material handling and assembly tasks. [Rehg] Figure 2.19 show a schematic of 6-DOF of an industrial robot.

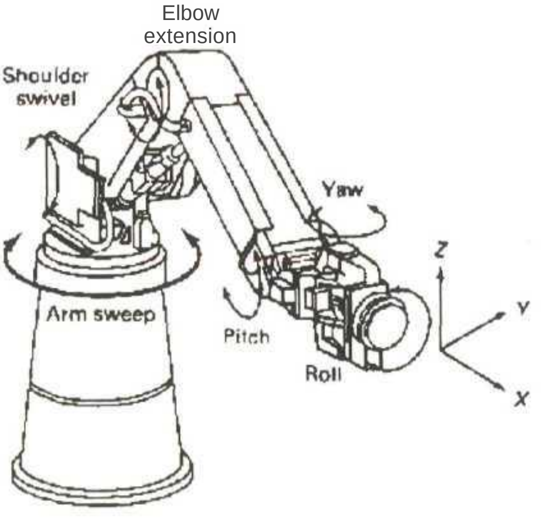

Figure 2.19: The six primary axes of robot movement. (Rehg]

The configuration of a robot's components, through its joints and links, defines the robot's work volume. The work volume is defined as the space within which the robot can manipulate its wrist end. The work volume is determined by:

- the robot's physical configurations,
- the size of the body, arm, and wrist components,
- the limits of the robot's joint movements.

A work volume is important for defining the operating space of a robot. This is critical in determining the positions of machine centers and safety zones with which the robot will interact. The work volumes of various robots are shown in Figure 2.20.

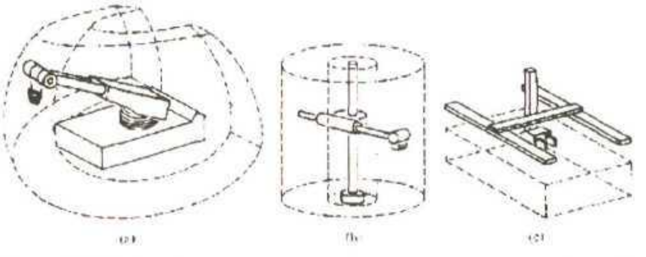

Figure 2.20: Work volumes of various robots; (a) polar, (b) cylindrical, (c) rectangular. [Groover et al]

Depending on the type of application for which the robot is being used, the wrist is fitted with the required end-effector. The end-effector allows the robot to pick up and transport different types of work pieces or perform specific functions such as welding or spray painting. Industrial robots are powered by three types of drive systems. Theses drive systems include:

- Hydraulic
- Electric
- Pneumatic

The two most common popular drive systems used are hydraulic or electrical systems. The choice of drive system is dependent on the power, speed and accuracy required to perform the operation. Hydraulic drive systems are favored for high power and speed applications, whereas electrical drives are best suited for high precision and repeatability. Robots are implemented in manufacturing environments which are hostile, strenuous, repetitive or dull and where economic pressure to perform is high. In this type of environment human beings would often fail. The primary function of robots in FMS and cells is to load and unload parts and tools from machine centres and to interact with conveyor systems. Figure 2.21 shows a schematic example of a FMS with a central robot.

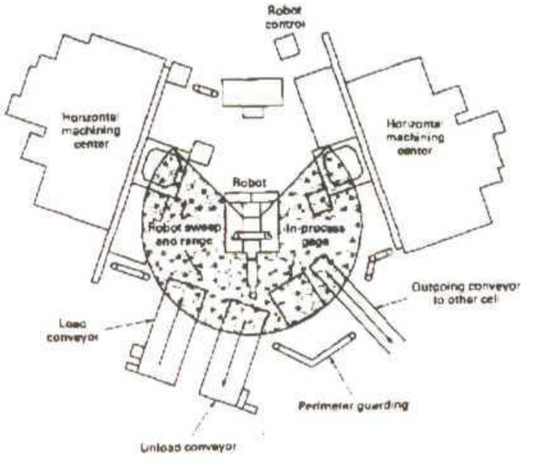

Figure 2.21: A robot interfaced to a machine tools and conveyors to load and unload incoming and outgoing work pieces in a machining center. [Luggen]

A Unimate PUMA robot has been modified to a PC-based robotic system, eliminating the dedicated controller for the CIM cell in the Mechatronics and Robotics Research Laboratory.[Potgieter] This open software architecture has increased the robot's flexibility in terms of set-up and programming functionality. The PUMA robot is now configured, programmed and controlled using a graphical programming environment called Labview. The robot's functions in the CIM cell include interacting with the conveyor system to transport parts to the CMM for inspection and loading work pieces onto the CNC milling machine for machining. Due to the lack of feedback information for the conveyor system, the robot requires additional sensory systems for part recognition and orientation. An intelligent generic gripper has been developed for the PC- based robotic system to help grasp a wide range of parts. [Tlale] The industrial robot continues to be an important element in automated manufacturing and has epitomized the automated material handling generation. Robotics are finding increasing acceptance in the manufacturing environment and are being implemented in more diverse applications.

2.3 ADVANCED MANUFACTURING MATERIAL HANDLING SYSTEMS

The *fourth generation* of material handling was labeled as the integrated material handling generation. The development of automated material handling systems saw them implemented as stand alone systems. Manufacturing systems began to evolve to match the pace of the growing global market. Material handling engineers began to integrate the individual systems such as AGVs, conveyors, AS/RS and robots under a central control system. Linking the individual systems under a central control system allowed for greater planning and control. The flow of information between the central control system and the subsystems, together with information flow between each subsystem, allowed for optimal material handling sequences to be selected together with the best available material handling equipment to perform the task. This allowed once dedicated material handling systems to become "flexible", with the central control system selecting a material handling system to perform a task depending on its availability, the material to be transported and the path planned. The primary focus shifted from hardware specifications to software performance. The open software based architecture allowed for different docking procedures, machine interfacing and route planning to be downloaded to the chosen material handling system in real-time.

Together with the increase in information flow between the manufacturing subsystems, the tracking of materials became an important aspect of a material handling system. Strategically placed bar-code scanners allowed for an inventory of "in-process" materials. In an advanced manufacturing system, this allowed advanced planning and co-ordinating of the material handling systems to be performed.

The fifth generation of material handling systems saw the material handling systems of earlier generations developed a step further. The intelligent material handling generation saw the introduction of artificial intelligence into material handling systems. Driverless forklift trucks were capable of performing complicated tasks like the automatic loading and unloading of trucks. Material handling systems became more intelligent due to advances in computer systems and the synergetic integration of smart sensors. Material handling systems were now able to adapt to varying conditions with in the manufacturing environment.[Pence] Advances in electrical machine technology saw linear motors gaining in popularity in the manufacturing environment. Demands for greater accuracy, repeatability and precision led to linear motors replacing leadscrew and rack and pinion drives and being applied more widely in material handling engineering. Material handling systems became integrated into the assembly process. They processed intelligence and offered the accuracy required to complement advanced manufacturing assemblies. This is clearly demonstrated in the handling of silicon wafers in the production of microprocessors. [Hwang et al]

The sixth generation of material handling systems which advanced manufacturing systems are currently beginning to explore, is being coined as the regeneration. Intelligent integrated information-based material handling systems are synergetically evolving all aspects of manufacturing into complete integrated functions. In the Microdynamics Systems Laboratory at Carnegie Mellon University a new Architecture for Agile Assembly (AAA), which supports the creation of miniature assembly factories or "minifactories", is currently being developed. [Hollis et all] Conventional assembly processes usually incorporate a 4-DOF pick-n-place robot such as the SCARA robot and a conveyor system. Although the SCARA has a proven record, it falls short in a number of areas when applied to assembly processes which require high degrees of accuracy and precision. SCARA's limitations are as follows:

- large motion ranges are required to access part feeders
- a heavy robot arm is used to handle small, light, delicate parts
- high accelerations are needed for pick-n-place cycles to sustain high throughput

- serial kinematic linkage with relatively flexible joints leads to positioning inaccuracies

AAA incorporates planar linear motors on passive steel platens taking the role of "couriers", interacting with overhead manipulators, to form a precise manufacturing assembly [Quaid et al1]. The dual axis planar linear motors, which run on frictionless air bearings, act as material handling devices, accurately positioning themselves below the 2-DOF overhead manipulators, such as a glue dispensers, to create a highly accurate 4-DOF assembly process. This allows robots with fewer degrees of freedom to interact with the couriers, resulting in cooperative part placement. Figure 2.22 shows a schematic representation of a minifactory.

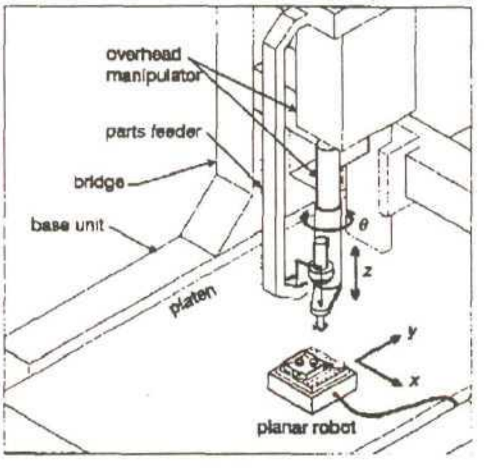

Figure 2.22: A minifactory consisting of an x, y planar robot courier interacting with an overhead manipulator. [Quaid et al1]

The movement of the couriers is restricted by two main features namely, the size of the platen and the tether supplying power to the motor. The complete minifactory incorporates a number of platen modules with multiple couriers interacting with the overhead manipulators. During an assembly process, work pieces are required to be transferred from one courier to another. This is due to the modular platen design, the platen boundaries and the tether length restriction. In order to avoid tether crossings, advanced motion planning is required when multiple couriers are operating on the same platen. Tetherless couriers would eliminate these problems but would create new problems, such as having to supply power to the motor and air for the bearing by some other means without detracting from the motors performance. The possibility of creating continuous modular platens, which will allow the couriers to flow easily over the platen intersection, is also being researched. [Quaid et al_2]

The minifactory concept illustrates the impact advanced, intelligent integrated material handling systems have on manufacturing assemblies. No longer just responsible for transporting the workpiece to the assembly process, material handling systems are complementing the overall assembly process by interacting directly with the assembly subsystems. The information supplied to the overhead manipulators by the couriers, giving their exact position, allows for accurate cooperative part placement.

Material handling system design is being driven by the information technology age and by increased demand for greater accuracy during assembly processes. Manual material handling has remained popular but where value was once placed on a worker's physical strength, emphasis is now placed on a worker's mental capabilities and adaptability. The invention of mechanisms and machines to aid and then replace man to match the advances in manufacturing has transformed material handling into a system integrator, linking departmental divisions. The development of automated systems with increasing intelligence has moved material handling technology from a separate module in the assembly process to an integrated intelligent value-added asset. As material handling systems take a greater role in the manufacturing process, the rate and precision with which complex parts can be assembled will increase.

This study has shown that the material handling systems being utilized in the MR^{2}G CIM cell lack the intelligence to complement the overall CIM cell capabilities. It highlights the need for a material handling system capable of integrating with the assembly process. The system must be capable of performing highly accurate positioning and assembly operations whilst sharing information and still maintaining flexibility both in setup and in travel.

3 LINEAR MOTOR TECHNOLOGY

3.1 INTRODUCTION

Electric motor technology has experienced continual research and development since its invention in the early nineteenth century. Electric motors are the most popular machines of everyday life, with new types of machines being researched and developed for increasing applications. New developments in electrical machine technology have been stimulated by advances in material engineering such as rare earth magnets and super conductors. The development of gearless drives has been advanced by the technological advances in electric motor control, the impact of power electronics and the demand for greater speed and torque. [Gieras et al]

One form of electrical machine which has seen extensive development is the linear motor. Linear motors can drive a linear motion load without intermediate gears, screws, pulleys and belts. A linear motor is developed by virtually slicing a rotary electric motor through a plane perpendicular to its rotational axis and rolling it out flat as shown in figure 3.1. Instead of producing torque like a conventional rotary motor, the linear motor produces linear force or propulsion force. Theoretically all categories of rotary machines may be developed into linear motors.

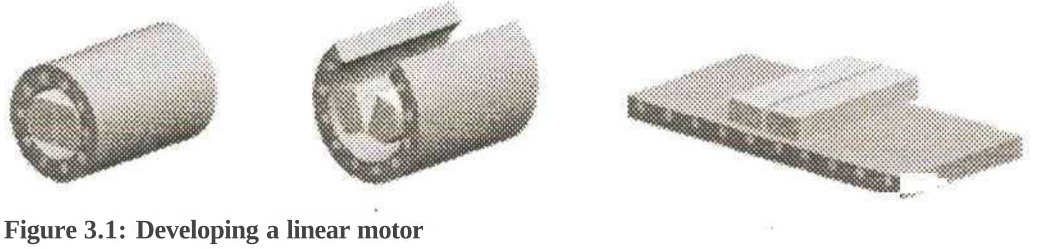

Figure 3.1: Developing a linear motor

The essential difference between a linear motor and a rotary motor is the difference in the air gap. A linear motor has an open ended air gap with an entry end and an exit end, whilst a rotary motor has a closed air gap. Two main types of linear motors have been developed, the linear induction motor (LIM) and the linear synchronous motor(LSM).

3.2 LINEAR INDUCTION MOTOR

3.2.1 LIM DESIGN AND OPERATION

A LIM is basically a rotating squirrel cage induction motor opened out flat. The primary and the secondary in a LIM correspond to the stator and the rotor of a rotating induction motor. The primary consists of a magnetic core with three-phase windings and the secondary may consist of a metal sheet or a three-phase winding wound around a magnetic core. A LIM may be single sided or double sided as shown in Figure 3.2.

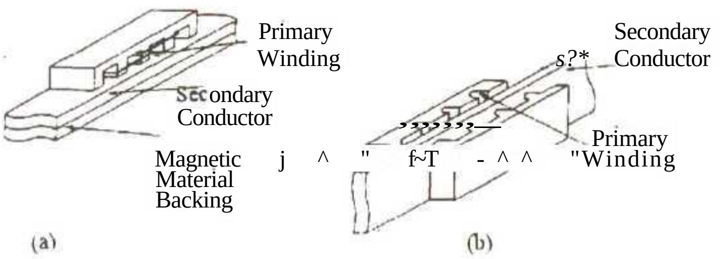

Figure 3.2: (a)Single sided and (b)double sided linear induction motor. [Hippner]

When a supply voltage is applied to the primary windings, the magnetic field produced in the air gap region travels at synchronous speed. If the primary is held stationary, the interaction of the magnetic field with the induced currents in the secondary exerts a thrust on the secondary to move in the same direction as the traveling magnetic field. If however, the secondary is held stationary and the primary is free to move, the primary will move in the direction opposite to that of the magnetic field. Thus two forms of LIM topologies are found, namely the long primary, short moving secondary and the short moving primary, long secondary. Selecting which topology is best is dependent on the type of application and the cost. Compared to a single-sided LIM, a two-sided, double excited LIM produces a larger propulsion force. However due to the balanced nature of the motors design, the attractive forces are eliminated. Theoretically, assuming they have the same dimensions, a double-sided excitation system in comparison with a single-sided excitation system has twice the air gap magnetic flux density, thus producing four times greater thrust [Gieras]. LIM can be constructed with longitudinal magnetic flux and transverse magnetic flux. In longitudinal magnetic flux motors the lines of magnetic flux lie in the plane parallel to the direction of the travelling magnetic field. In transverse magnetic flux motors the lines of magnetic flux are perpendicular to the direction of the travelling field. Figure 3.3 shows the current and magnetic flux planes for the different LIM topologies.

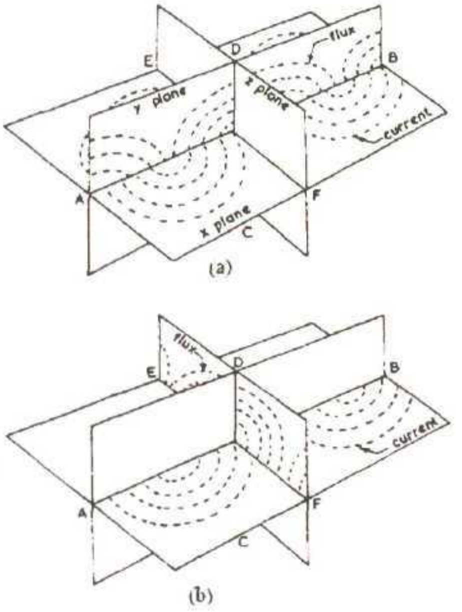

Figure 3.3: Topologies of LIM (a) longitudinal-flux (b) transverse-flux. [Laithwaite et all)

Line AB represents the direction of motion of the traveling field and the moving secondary. In longitudinal flux motors, the magnetic circuit lies in the y-plane while the electric circuit lies fundamentally in the x-plane. The dotted lines show the flux and current lines. Electromagnetic action takes place between the components of flux parallel to CD and components of current parallel to EF. Leaving the electric circuit in the x-plane and changing the plane of the magnetic circuit from y to z, results in a tranverse-flux LIM [Laithwaite et all]. The main advantage of a transverse-flux machine with a large pole pitch is the reduction in the primary's size and weight. The flux density in each tooth in a transverse-flux machine is self-contained and independent of the pole pitch, whereas the flux densities in a longitudinal-flux machine supplement each other and are dependent on the pole-pitch. Thus, the size of the primary core is greater in longitudinal-flux designed machines A flat, single-sided LIM with transverse-flux can produce thrust and electrodynamic suspension. Figure 3.4 shows a flat LIM with transverse-flux and a non-ferromagnetic secondary which is propelled, suspended and stabilized electro-dynamically.

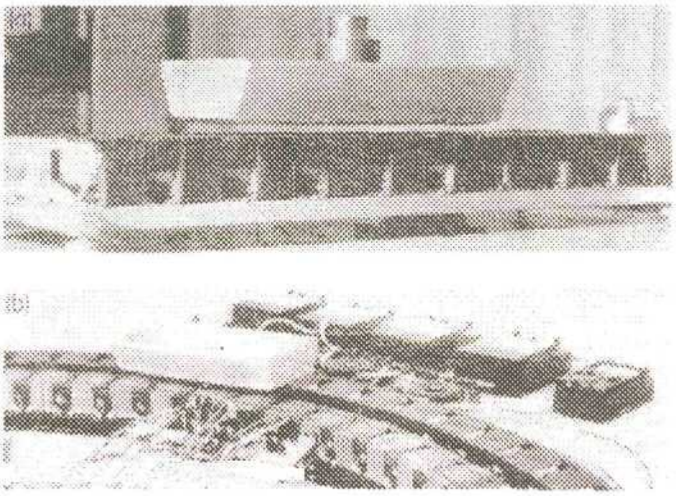

Figure 3.4: A flat LIM being propelled, suspended and stabilized.|Gieras]

LIMs can be classed, according to their geometry, into the following groups;

- with moveable primary or moveable secondary,
- single-sided and double sided,
- flat and tubular,
- with short primary and short secondary,
- with longitudinal and transverse magnetic flux.

The short-primary LIM is common as it is less expensive than a long-primary LIM because construction of the primary is much more complicated than the construction of a secondary. The primary winding of the LIM is essentially the same as its rotating counterpart, consisting of copper conductors. The primary windings can be located in slots or on salient poles. Windings are wound in either single -layer or double-layer configuration. A single-layer winding, as shown in Figure 3.5(a), requires the core to be increased to twice the thickness of a corresponding rotating motor, in order to provide a magnetic path for a greater amount of core flux [Yamamura]. If double-layer winding is adopted, it is possible to have coils in all the slots as shown in figure 3.5(b). However, problems of arranging the conductors at each end arise. When the rotating motor is cut and flattened out, the end connections of the primary coils are also severed. If these severed coils are omitted from the resulting LIM, the primary winding configuration shown in figure 3.5(c) is obtained. A double winding layer is obtained, except for the first and last poles which are single-layered. The flux is the same as its rotating motor counterpart and therefore the primary core is the same thickness.

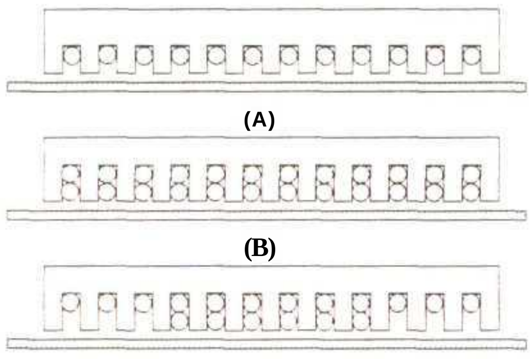

(A)

(B)

(C)

Figure 3.5: Primary windings; (a) single-layer,(b),(c) double-layer.

The LIM secondary is usually made of a metallic sheet. This is usually a homogeneous, nonmagnetic, conductive, sheet. However, LIM secondaries are often constructed of layers of several kinds of metallic sheets, for example an iron sheet sandwiched between two copper or aluminum sheet. Double-layer secondaries consist of an aluminum layer over a solid or laminated steel core. Single-sided LIM with cage (ladder) secondaries, shown in Figure 3.6, can produce higher thrust generation and efficiency than double-layer secondaries. A smaller air gap reduces the magnetizing current and therefore reduces the input power, allowing for a smaller drive to be utilized. The disadvantage of a cage secondary is the high cost of manufacture compared to double-layer secondaries [Gieras]. The secondary completes the path for the motor's magnetic flux and electric current.

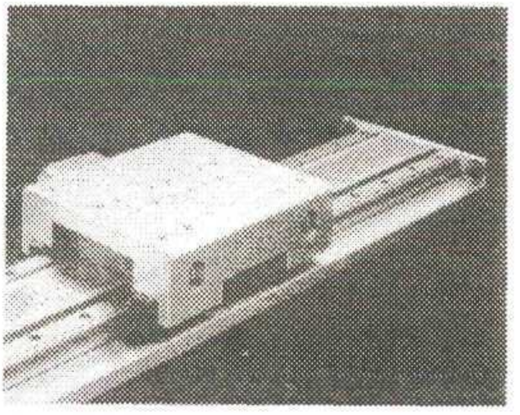

Figure 3.6: A single-sided, short primary, LIM with cage secondary. [Gieras]

The control of LIM is performed by using variable-frequency converters or velocity control. Variable-frequency converters act as an interface between the supply and the LIM. Variable-frequency converters are able to control the LIM by: (a)adjusting the frequency according to the desired output velocity, (b)adjusting the output voltage to maintain a constant air gap flux density in the constant force region and (c)supplying a rated current on a continuous basis at any frequency. The converter is based on the type of rectifier and inverter used, namely:

- pulse-width modulated (PWM) voltage-source inverter (VSI) with a diode rectifier
- square-wave VSI with a thyristor rectifier,
- current-source inverter (CSI).

The most common control method is using a PWM inverter which controls the frequency and the voltage output. The inverter switch control signals are generated by comparing three sinusoidal control voltages with a triangular waveform. Employing velocity control, an inverter-fed LIM can be controlled by varying the input frequency or input voltage, or varying both while keeping the air gap magnetic flux constant. Increasing the frequency will increase the speed of the motor whilst an increase in the voltage will result in an increase in the magnetic flux in the air gap. By varying the voltage and frequency together, velocity control allows the motor to operate at velocities below and above the rated velocities. In order to develop thrust, the LIM secondary must run at a speed less than the MMF synchronous speed. Similar to a rotary induction motor, the slip (s) in a LIM is defined as;

$$5 = \frac{[illegible]}{[illegible]} \qquad (3.1)$$

where v_m is the velocity of the motor and v_s is the synchronous speed. The thrust developed, F_d is;

$$F< = \frac{P*}{Vm} \qquad (3.2)$$

where Pd is the power developed.

LIMs suffer adverse effects due to the open ended air gap. The open magnetic circuit causes longitudinal end effects which change the magnetic field in the air gap. If the LIM secondary is travelling from left to tight, the leading edge is called the entry end and the trailing edge is called the exit end. The magnetic flux density at the entry end of the secondary is weakened, whilst the magnetic flux density at the exit end is increased, adversely affecting the motor's performance. The longitudinal end effects in high-speed and low-speed LIM differ, with end effects having a greater impact on the motors performance when travelling at higher speeds. The faster the motor travels, the further into the air gap the longitudinal end effects extend. The longitudinal end effects appear as,

- non-uniform, velocity-dependent magnetic flux density distribution in the air gap and non-uniform eddy currents in the secondary,
- unbalanced phase currents,
- erroneous braking forces.

Extensive research has been undertaken to identify and quantify longitudinal end effects and possible solutions to eliminate them in high-speed LIMs [Yamamura]. End effects can be classified into static and dynamic. Static end effects occur because of the asymmetric geometry of the primary. In this case the mutual inductances of the phase windings are not equal to one another. This results in asymmetric flux distribution in the air gap and unequal induced voltages in the phase windings. The dynamic end effects occur as a result of the relative motion of the primary with respect to the secondary. As the primary moves over the secondary, a new secondary conductor is brought under the leading edge of the primary, while another secondary conductor is leaving the trailing edge of the primary. The conductor coming under the leading edge opposes the magnetic flux in the air gap, while the conductor leaving the trailing edge tries to sustain the flux. This results in a distorted flux distribution. The exit-end effect, which travels in the same direction as the normal traveling wave, diminishes extremely quickly resulting in minimal effect on the motor's performance. The entry-end effect is minimized by using compensated windings at the start of the primary windings.

3.2.2 LIM APPLICATIONS IN MATERIAL HANDLING SYSTEMS

Applications of LIMs are found in transportation, industrial machines, control systems, robotics and appliances. LIMs have found extensive applications in industrial transportation systems such as material-supply-cars used in airports, pallet transportation, belt conveyors and bulk material handling systems. LIMs have also impacted on manufacturing processes such as machine tools, presses, mills, separators and automated manufacturing systems. Figure3.7 shows a machine tool with a single-sided LIM. The implementation of LIMs, in place of lead screws in machines tools, have increased their accuracy, repeatability and contouring profile capabilities.

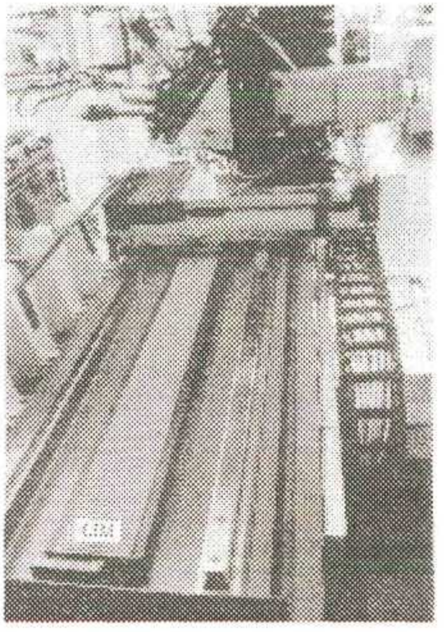

Figure3.7: Machine tool with a single-sided LIM. [Gieras]

LIMs have been used to develop belt conveyors where the secondary (a continuous copper belt) forms the conveyor to transport materials. The use of LIMs has been proposed for the conveyance of aluminum cans in a high-speed transportation and production line. The aluminum cans are levitated and propelled by the same excitation force. [Nysschin et al] A transverse flux LIM, incorporating lift and propulsion, has been developed for non-contact conveying of steel plates [Hayashira et al]. LIMs have replaced pneumatic and conveyor belt systems in many production assembly lines in the food and beverage and car manufacturing industries. The implementation of LIMs in elevators has offered increased safety to passengers, reduced energy consumption, decreased maintenance and increased reliability. Ropeless elevators using LIMs are also being implemented as solutions to transportation systems in high-rise buildings and proposed for a new hoisting technology in the mining industry. [Cruise et al_3] A further industrial application of a single-sided LIM is in separators to remove impurities from materials. Raw material, such as aluminum and copper, is fed over LIMs which attract and remove impurities as illustrated in Figure 3.8.

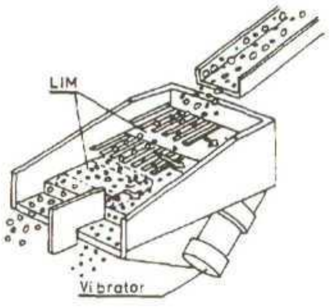

Figure 3.8 : A single-sided LIM used in a separator. [Gieras]

LIMs have been used in many applications other than in material handling systems. The 'Electropult', invented in 1945, could develop an initial thrust of 75 600N and accelerate a mass of 5000 kg to a speed of 185 km/h in 4.2s.[Laithwaite et al_2] The Electropult was the pioneer for the modern catapult systems employed on aircraft carriers today. High-speed LIMs have been used extensively in the development of high-speed transportation systems. Magnetically suspended vehicles have reached speeds of 500 km/h for example Germany's Transrapid 07 magnetic levitation train shown in Figure 3.9. Canada has implemented the Intermediate Capacity Transportation System (ICTS) in Toronto. Similar transportation systems have been implemented in Tokyo and Osaka, Japan. LIMs have being implemented in a vast array of applications over the years. However, research into LIMs has decreased since it peaked in the 1970s. Emphasis has shifted to the research and development of brushless permanent magnet linear motors, namely linear synchronous, brushless dc linear motors and linear stepper motors. This shift in emphasis has been driven by recent advances in permanent magnet materials and power electronics. LIMs have seen a decline in implementation in favor of these more advanced and efficient motors.

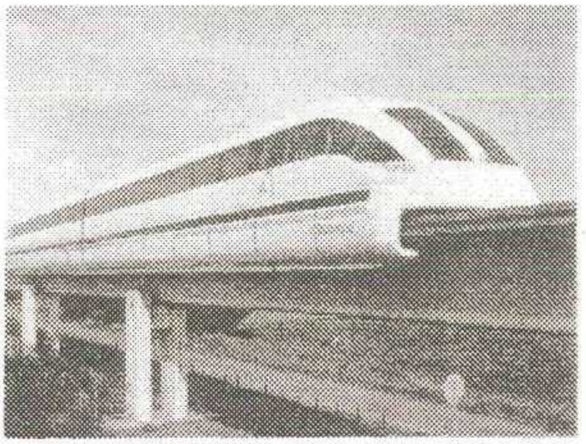

Figure 3.9: The Transrapid 07 magnetic levitation train.[Gieras]

3.3 LINEAR SYNCHRONOUS MOTORS

Traditional a.c polyphase synchronous motors are motors with d.c electromagnetic excitation. For economic reasons the linear version of a conventional synchronous motor proved unsuitable when applied to high speed ground transport systems. Research undertaken to overcome the unsuitability of a traditional LSM led to the development of two short primary transverse flux LSMs. Heteropolar and homopolar LSMs, shown in Figure 3.10, consisted of a passive track with secondary d.c windings located on the primary.[Balchin et al]. The secondary consisted of mild steel poles which led to a reduction in end effects.

Advances in permanent magnet (PM) technology led to the development of the PM brushless motor. PM brushless motors can be classified into rotary motors and linear motors. Developments in power semiconductor technology have led to growing interest in these motors. PM brushless linear motors have found growing applications in the automation industry.

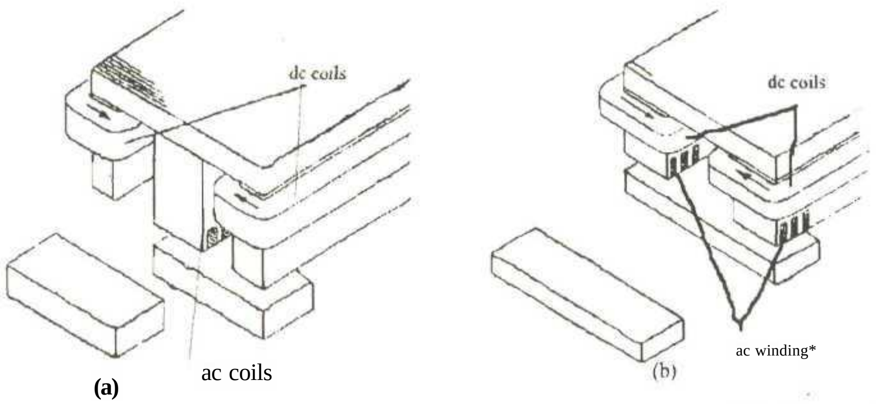

Figure3.10: (a)Heteropolar (b) Homopolar linear synchronous motors.|Balchin et all

PM brushless linear motors can be divided into two groups:

- PM LSM with no position feedback, where the input current waveform is sinusoidal, producing a traveling magnetic field,
- PM d.c linear brushless motor(LBM) with position feedback, in which the input current waveform is trapezoidal or rectangular and is precisely synchronized with the speed and position of the moving part.[Basak et al _1].

The physical construction of the two types of motors is identical and varies only in their control methodologies. The mechanical motion of a LSM is in synchronism with the magnetic field, such that the mechanical speed is the same as the speed of the travelling magnetic field.

3.3.1 LSM TOPOLOGIES

LSM topologies are similar to that of LIM, being constructed either as long primary, short secondary or short primary long secondary type motors. The terminology used for LSMs differ from that of LIMs. The part producing the traveling magnetic field is described as the armature or forcer. The part providing the constant magnetic flux is called the field excitation system, or reaction rail. LSM are classified according to whether they are:

- flat(planar) or tubular (cylindrical),
- single sided or double sided,
- slotted or slotless,
- iron-cored or air-cored,
- transverse flux or longitudinal flux. [Gieras et al]

The most common and commercially available form of LSM is the flat linear motor. Tubular LSMs with PM cores have found increasing applications in industry, replacing pneumatic and hydraulic cylinders for short stroke applications. [Sul et al]

3.3.1.1 LSM ARMATURE

The polyphase armature winding can either be iron-cored or air-cored. An iron-core motor consists of coils wound on steel laminations to maximize thrust generation. An air-core or ironless motor consists of coils wound without a core of steel laminations. This reduces the attractive force between the armature and the PM excitation system, but also produces less thrust. Figure 3.11 shows an iron-core motor with a single sided PM track and an ironless motor with a double sided PM track.

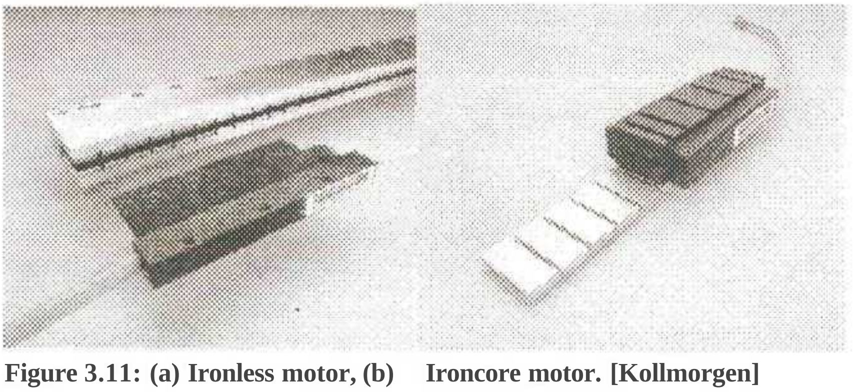

Figure 3.11: (a) Ironless motor, (b) Ironcore motor. [Kollmorgen]

Iron-core armatures are made from laminated ferromagnetic cores which increase the propagation of electromagnetic waves. Typically the laminations are 0.5-0.6 mm thick and are stacked together to form the armature stack. Slotted armatures are created by cutting slots into the stack. The laminations are created *en mass* by either a stamping press or laser cutting machine. The magnet flux occurs in each lamination and is uniformly distributed throughout the laminated stack. A slotted laminated armature stack consists of a backiron and teeth, shown in Figure 3.12.The polyphase windings are distributed into the slots to complete the armature development.

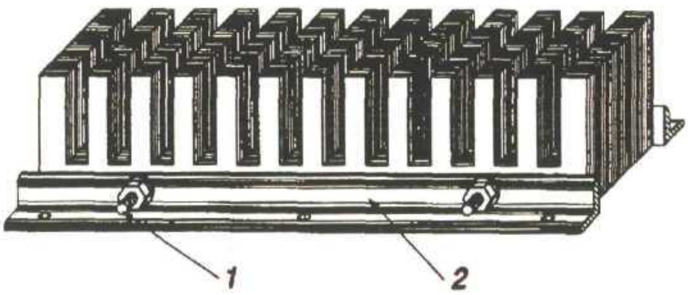

Figure 3.12: Iron-core laminated stack using (1) bolts and (2) pressing angle bars.jGieras et al]

Iron-core LSMs suffer from a parasitic force called thrust ripple. The main cause of thrust ripple is cogging thrust. Cogging thrust is caused by the interaction between the excitation flux and the varying permeance (flux penetrating capability) of the armature core. When the magnet is aligned with the maximum amount of armature iron teeth, the reluctance (resistance) seen by the magnetic flux is at a minimum, thus giving the maximum inductance. If the magnet is moved slightly the reluctance increases, because more air appears in the flux path between the magnet and the armature backiron. A force is developed which pushes the magnet back into alignment to try and maintain a minimum reluctance. Thus cogging thrust attempts to maximize the magnetic flux crossing the air gap from the PM reaction rail to the armature. Another cause of thrust ripple is the detent force. The detent force in a PM LSM arises out of the attractive force between the slotted nature of the armature and the PM reaction rail. This results in a sinusoidal disturbance in the motion of the mover. [Bodika et all] Detent forces are present when no current is flowing in the windings. Cogging thrust is the same type of force but is a result of the currents in the armature coils. Since both forces are due to the presence of the steel core within the motor, the terms "detent force" and cogging thrust" are often incorrectly interchanged in literature when LSM parasitic forces are being describing. To reduce thrust ripple, armature slots are designed semi-closed by designing shoed teeth. In open slot designs the effective air gap length is equal to the distance from the reaction rail surface to the armature backiron. This gives rise to large reluctance variations. By using shoed teeth, the air gap appears to have a uniform permeability as a function of position, resulting in a reduced cogging thrust. Figure 3.13 shows the different teeth designs on a slotted iron-core armature.

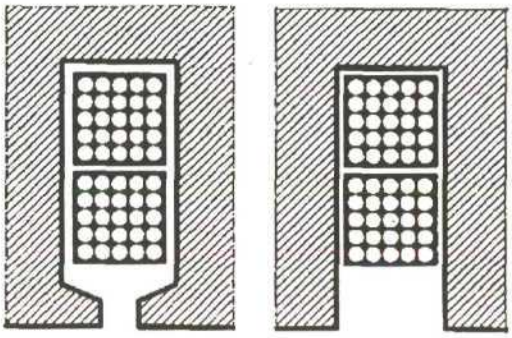

Figure 3.13: Armature slots of iron-core LSM: (a) semi-open, (b) open.[Gieras et al]

A method of eliminating cogging thrust is to design an air-core armature. Air-core armatures are commonly referred to as core-less armatures due to the fact that they have no ferromagnetic stack. Core-less armatures can be constructed as slotted or slotless armatures. In slotless designs, the windings are wound without an armature stack and are embedded in an epoxy core. Figure 3.14 shows a double sided PM LBM with a moving, slotless, air-core armature which is manufactured by Trilogy Systems, USA.[Trilogy_l]

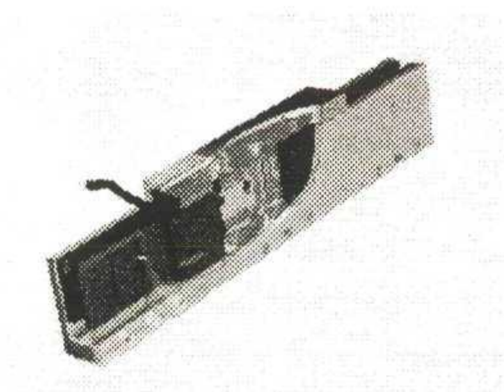

Figure 3.14: Flat double-sided PM LSM with moving air core armature.[Trilogy_2)

Anorad Corporation developed the first balanced PM synchronous motor called the Anoline Brushless Linear DC Servomotor. [Anoradl] A schematic drawing is shown in Figure 3.15. The motor consists of a stationary double sided PM excitation system mounted on a backiron and a short moving armature. The armature consists of non overlapping coils placed side by side in an epoxy core. The armature is placed in the air gap between the two PM rails. The epoxy core armature effects zero cogging thrust, resulting in smoother motion. [Hippner et al] The double sided PM reaction rail eliminates any normal attractive force between the PMs and the armature. At a higher input frequency, air-core LSMs can achieve higher efficiencies than slotted iron-core LSMs. Disadvantages of air-core LSMs are that they require more PM material and produce less thrust than their iron-core counterparts.

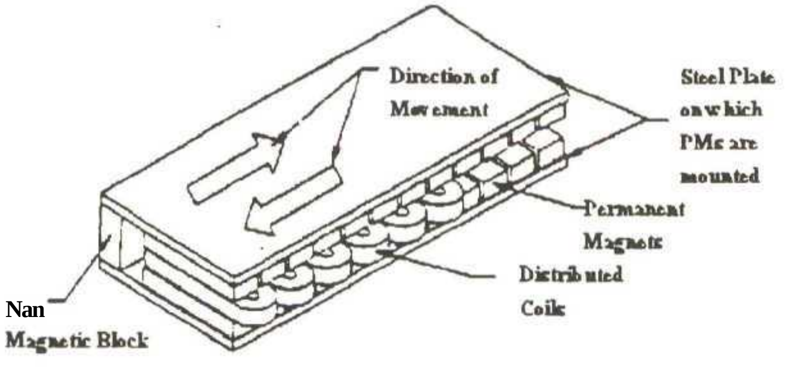

Figure 3.15: Anorad's balanced PM LSM, LEB-S-2-S. [Anorad_2]

Slotted air-core armature frames are constructed from nonmagnetic, non metallic materials such as tufnol or epoxy. The open slots are milled from the material or the air-core armature frame is created by casting. A slotted air-core armature is created to help develop a frame onto which the polyphase windings can be mounted to create a rigid armature. In long distance applications long disjointed armatures have been developed. The discontinuous arranged system is used to maintain momentum of the moving object by re-accelerating the PM reaction rail every few meters. [Seki et al] The discontinuous arranged primary system has been proposed for applications such as' mining-ore transportation and baggage material handling systems in large airport facilities.

The final development of the LSM armature is the polyphase windings. In the development of phase windings it is important to define the relative terms. A turn is defined as two conductors exposed to the air gap flux. One turn is composed of a single wire making a loop so that both ends of the turn meet. A coil of a single phase is composed of one or more series connected turns all linked to the same flux. Multiple turns through the same pair of slots make one coil. All the coils form a single phase that interacts with the flux of a single magnet. This is called a group. The total number of groups of a motor is equal to the product of the number of phases and the number of rotor poles. Three main types of winding approaches are utilized when winding a slotted iron-core, namely;

- single-layer lap winding,
- double-layer lap winding,
- single-layer wave winding. [Hanselman]

A single-layer lap winding is shown in Figure 3.16(a). The winding is single-layered because each slot contains only one coil. The coil is a lap winding because each coil is made from multiple turns, with each turn overlapping the proceeding one. The phase winding is completed by connecting the individual coils in series. To develop a three phase armature, the addition of other phases results in the coils being distributed in the iron-core as shown in Figure 3.16(b).

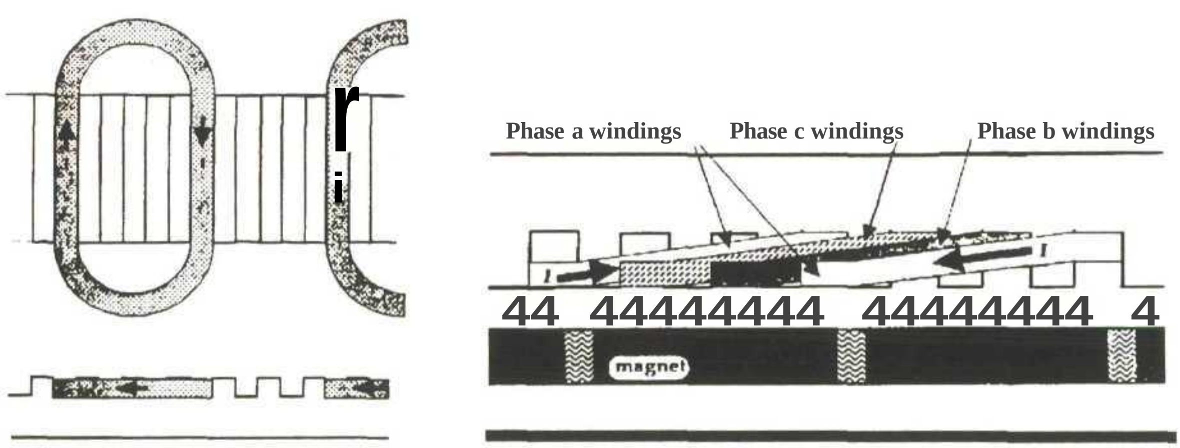

(a) **(b)**

Figure 3.16 :(a)Single-layer lap winding, (b) side view of a three phase armature with single-layer lap winding. [Hanselman]

In double-layer lap winding, a slot carries two coils of the same phase. These carry current in opposite directions as shown in Figure 3.17(a). The coils are constructed from multiple turns, with each turn lapped on top of each other. The third method used to wind iron-core armatures is the single-layer wave winding. The winding is composed of a single multiple-turn coil that snakes its way alternately back and forth through the slots of a single phase, as shown inFigure3.17(b).

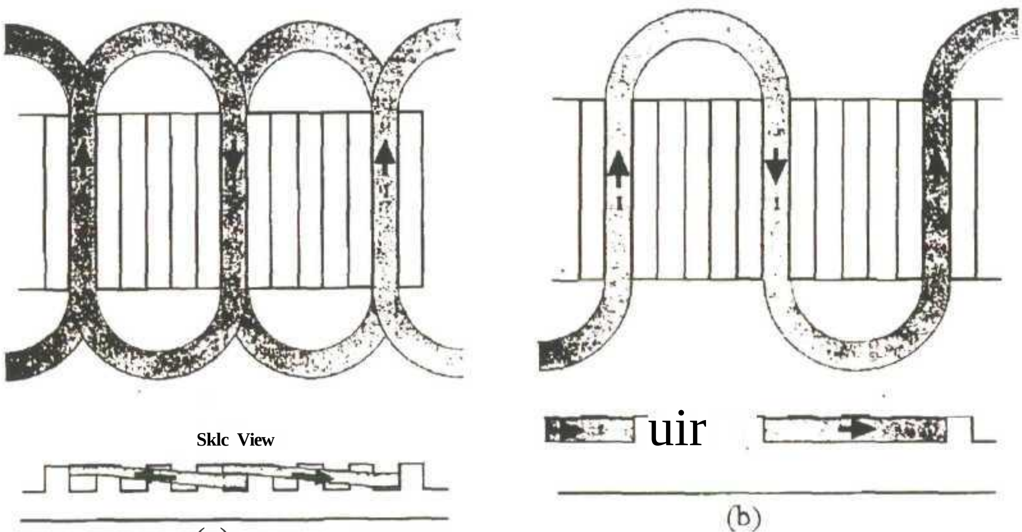

(a)

Figure 3.17: (a) Double-layer lap winding, (b) Single-layer wave winding.[Hanselman]

A different winding approach is applied when dealing with slot-less armature designs. Coils are developed as lap windings similar to single-layer lap windings. However the coils are non-overlapping and are placed side by side in the epoxy core. This form of winding is utilized in Anorad's Anoline Brushless Linear Motor as shown in Figure 3.15.

3.3.1.2 LSM EXCITATION SYSTEMS

LSM which operate on the principle of a traveling magnetic field can be developed using the following excitation systems;

- PMs in the reaction rail,
- PMs in the armature, creating a passive reaction rail,
- Electromagnetic excitation systems incorporating windings,
- Superconducting excitation systems,
- Passive reaction rail with saliency.

The use of PMs in the reaction rail in LSMs creates an active reaction rail. Active reaction rails are developed either by mounting PMs on the surface of a ferromagnetic yoke or backiron, as shown in Figure3.18(a), or by using buried PMs as shown in Figure3.18(b). Surface mounted PMs, with alternating polarity, are magnetized in the normal direction of the traveling magnetic field. The backiron is used to help link the flux path between the magnet poles. Buried PMs are magnetized in the direction of the traveling magnetic field The yoke is a non-ferromagnetic material such as aluminum. [Jeans et a11]

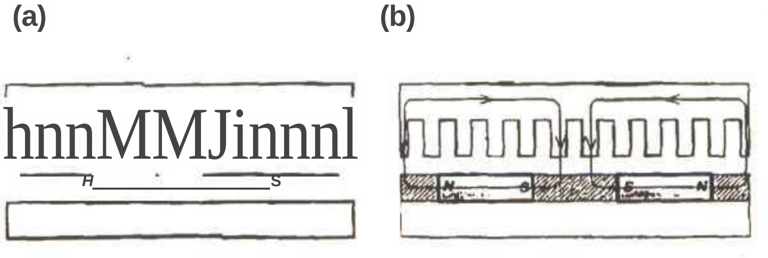

Figure3.18: Single sided flat PM LSM with (a) surface PMs, (b) buried PMs.|Gieras et al]

Active reaction rails can be constructed using a combination of the above two assemblies to create a Halbach magnetic array. A Halbach magnetic array sets up a magnetizing vector which rotates as a function of the position along the reaction rail. The array creates a stronger magnetic flux density and sinusoidally varying flux lines. Active reaction rails are fitted with a damper such as a rotary synchronous motor. When the speed is different from the synchronous speed, electric currents are induced in the damper. The damper also allows for asynchronous starting by reducing oscillations and helping return the motor to synchronous speed.[Sanada et al] Research into aluminum sheet dampers has shown that the performance in PM LSM is increased. [Jeans et al_2] Reduction of thrust ripple in iron-core slotted motors can also be achieved by making modifications to the PM reaction rail by skewing the magnets. [Trilogyl] Figure 3.19(a) and (b) shows the possible PM arrangements to help reduce thrust ripple. The skew is approximately equal to one tooth pitch of the armature core. Anorad Corporation have developed a hexagonal assembly of PMs for thrust ripple reduction shown in Figure 3.19(c).The symmetry axes of the PMs are perpendicular to the direction of motion. [Anorad_2]

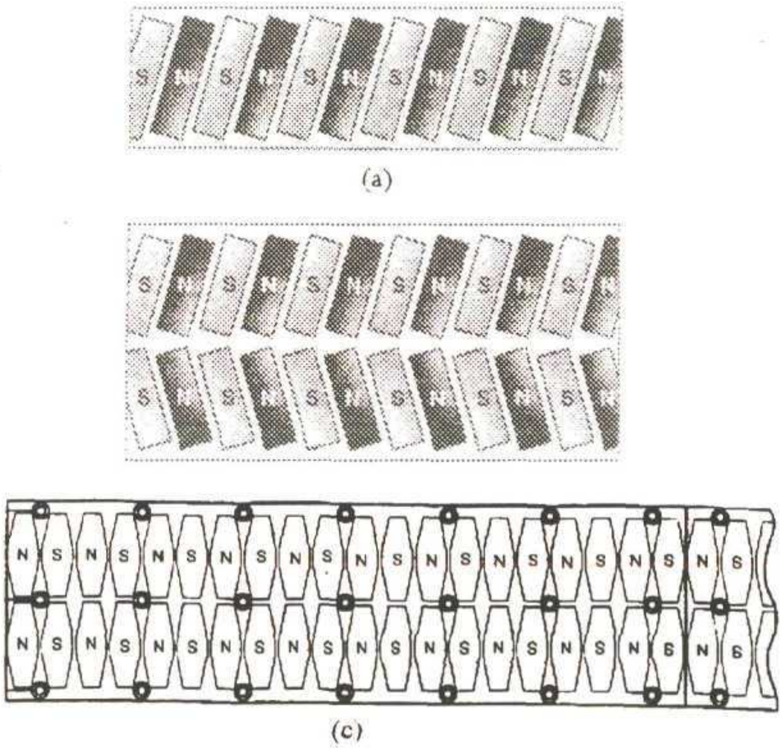

Figure 3.19: Skewed PM arrangements in flat LSM (a) single row,(b) double row and (c) Hexagaonal arrangement

A passive reaction rail LSM is a cheaper option when compared to **an active reaction rail** LSM. A passive reaction rail is constructed by applying PMs to the short armature thus reducing the reaction rail to a simple ferromagnetic plate. The PMs in the armature magnetize the long reaction rail, thus creating magnetic poles. LSM employing an electromagnetic excitation system (instead of using PMs) has poles made of solid or laminated steel, with d.c field windings to create electromagnetic poles. The poles are mounted on a ferromagnetic rail. To create the maximum amount of thrust, a slotted iron core armature is used with this type of reaction rail. Superconducting excitation systems in LSMs are used to replace the electromagnets with ferromagnetic cores. Since the superconducting coils produce an extremely large magnetic flux density, there is no need for ferromagnetic poles. The machine becomes an air-core motor. A variable reluctance LSM consists of poles similar to those employed in electromagnet excitation systems but with no d.c winding. In order to produce more thrust, the ferromagnetic poles are replaced by steel laminations embedded in epoxy, creating greater magnetic flux.

3.3.2 SPECIAL TYPES OF LSMs

3.3.2.1 TUBULAR LSM

An alternative to the flat LSM is the tubular LSM. By rolling a flat LSM around the axis parallel to the direction of the traveling magnetic field, a tubular LSM is obtained as shown in Figure 3.20. A tubular LSM may either consist of a movable internal PM excitation system, called the slider, and a stationary external slotted armature, or of a moveable internal armature and a stationary external PM excitation system. [Lequence] Tubular LSMs have been developed to replace hydraulic and pneumatic cylinders and for implementation as direct-drive linear actuators in machine tool applications, robot links and end affectors. Tubular PM LSMs, when compared to hydraulic and pneumatic cylinders, offer higher maximum speed, reduced power loss, greater positional accuracy and no mechanical backlash.

Figure 3.20: The development of a tubular linear synchronous motor.

Figure 3.21 shows a schematic of a tubular PM LSM, which utilizes a Halbach magnetic array in the slider for reduced thrust ripple. [Kim et al] The tubular motor consists of a stationary armature slider and moving Halbach magnetic array. Tubular LSMs, like flat LSMs, also experience thrust ripple. Based on software commutation, methods for thrust ripple reduction have been developed. By modeling changes in the reluctance and the mmf according to the mover's position and by using feed- forward control, thrust ripple is minimized.[Sul et al]

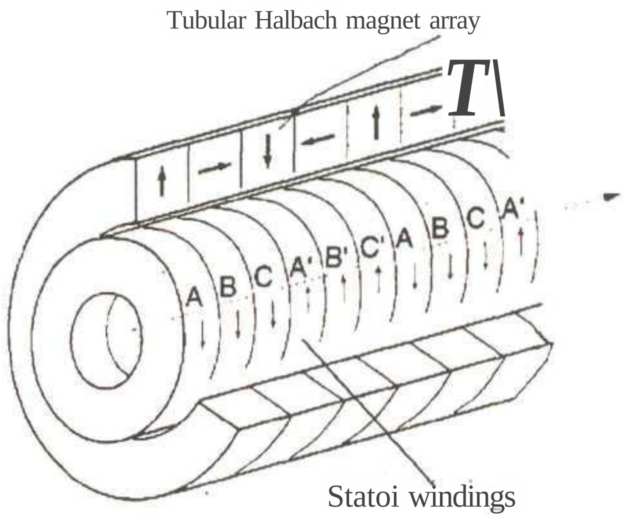

Figure 3.21: Schematic of a tubular LSM with Halbach magnetic array.[Kim et al]

3.3.2.2 LINEAR STEPPER MOTORS

The first successful linear stepper motor was the Sawyer linear motor, developed in 1969. [Hinds et al] Improvements in design have since led to the commercially available hybrid linear stepper motor (HLSM). The HLSM consists of a moving forcer and a stationary variable reluctance platen. The forcer consists of a double set of two actuators mounted orthogonally to generate balanced forces. Two actuators are designated to the x-axis movement and two to the y-axis movement. Each of the four actuators consists of a stack of steel laminations, PMs and two coils. The PM flux closes its path through the electromagnets, the air gap and the platen. Figure 3.22 shows the underside of the forcer of the Normag 4XY1302-2 planar linear motor produced by Northern Magnetics. [Normag] Each actuator has fine teeth etched into the underside. The passive steel platen stator is etched with a two dimensional array of square teeth to produce a waffle iron pattern. The platen is filled with epoxy and planarized to create an air bearing surface. The forcer is magnetically attracted to the platen surface. An air bearing, supplied through a tether into four holes in the forcer, separates the forcer and platen.

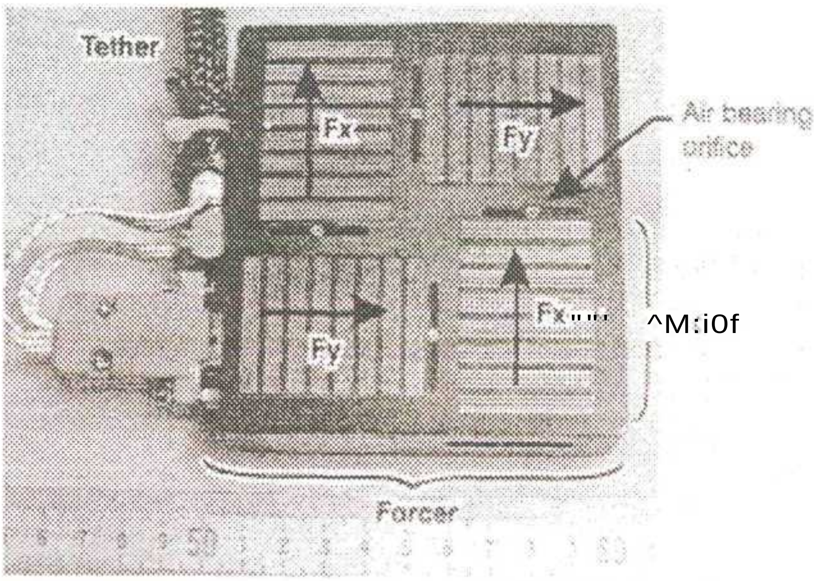

Figure 3.22:The underside of the Normag 4XY1302-02 planar linear motor.|Quaid et al_2)

The motor operates on a flux steering principle, with the coil currents acting to switch the PM flux from one set of poles to another. The poles with the most flux tend to align themselves with the platen teeth. Activating the poles in the correct sequence results in the stepping motion. The interaction between the flux created by the current in the coils and the PM flux results in a force being produced. Figure 3.23 shows the basic operation of a HLSM.

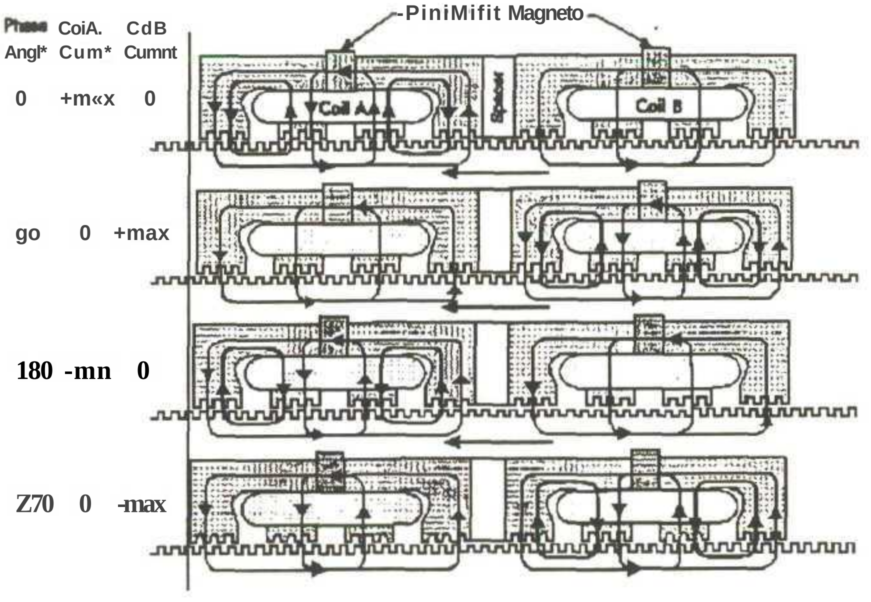

Figure 3.23: Basic HLSM operation (Quaid et al_2].

While offering many practical applications, the performance of current commercially available HLSMs is limited by their open-loop stepping operation. At high speeds the motor loses synchrony and the forcer is also susceptible to unanticipated external forces. This results in steps being missed which cannot be corrected by the open-loop control system. HLSMs are therefore run below maximum operating range in order to ensure that the motor remains in synchronism and does not miss steps. Research is being done to develop position sensors which optimize the performance of planar linear motors [Brenneman et al] HLSM have experienced increasing attention due to their ability to achieve high positioning resolution. They are being implemented into vision systems, with the forcer carrying cameras, and precision assembly systems. HLSM have also being applied to industrial sewing machines, CMM , packaging systems, pick 'n place, printer heads and x-y plotters.

3.3.3 LSM APPLICATIONS IN MATERIAL HANDLING SYSTEMS

LSMs have been developed for high speed magnetically levitated transportation systems, factory and building transportation and industrial automation systems. LSMs have provided the greatest benefits in material handling systems within manufacturing environments. Positioning Stages have dramatically increased in positioning accuracy and repeatability with the replacement of leadscrews with LSMs. Increases in planar accuracy requirements has led to LSMs together with air bearing technology combining to create dual-axis positioning stages capable of a planar accuracy of ±5nm over 4 inches of travel. [Lynch] Anorad's Microglide FP720 is shown in Figure 3.24 indicating the balanced LSM positions. The LSMs allow for 720 mm of travel in both planes. Superior smoothness in travel is achieved with the integration of an air bearing system using a granite base as a reference plane[Anorad_2].Typical uses include CMMs, visual inspection systems, electronic assembly, quality assurance and laser cutting.

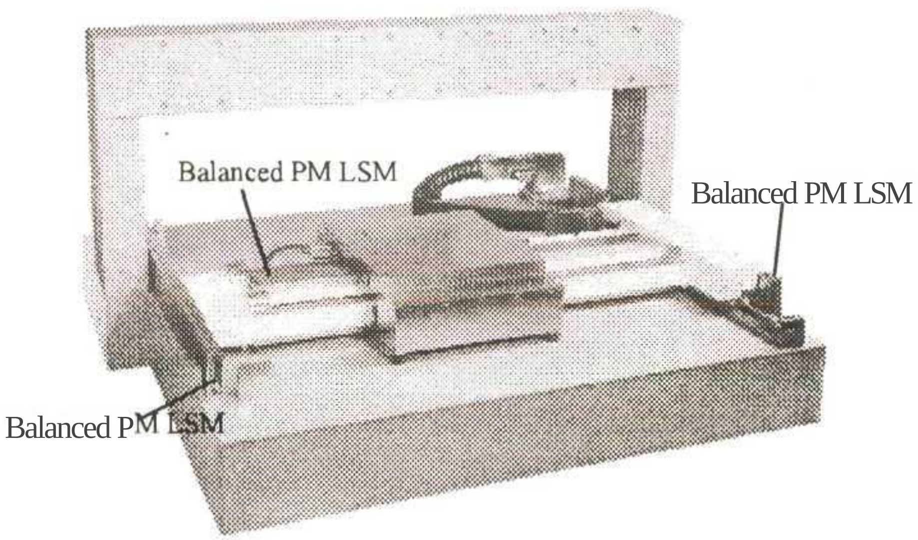

Figure 3.24: Anorad's Microglide™ FP720 dual axis positioning stage. [Anorad_2]

The travel of positioning stages is limited to the bearing table. The implementation of LSMs as factory transportation systems has met the growing need to move materials, containers and tools quickly and efficiently. Figure 3.25 shows an example of a horizontal factory transportation system, which consists of a long PM reaction rail and a moving armature. The disadvantage of this type of system is that the travel of the armature is restricted by the tether supplying power. The alternative design is to employ a stationary long armature and a short moving PM reaction rail. Complete linear transportation lines can be implemented to transfer materials through factory sections and assembly operations. [MagneMotion]

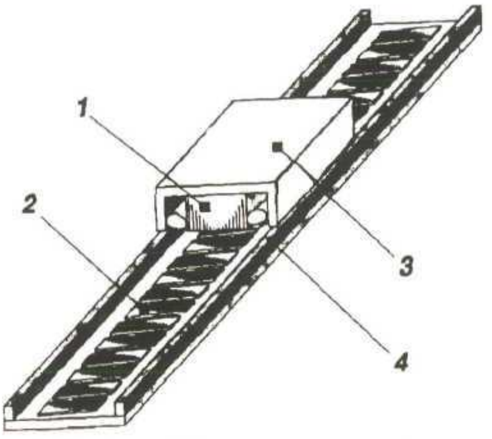

Figure 3.25: Horizontal factor}' transportation system with moving short armature LSM and long PM reaction rail. 1-armature, 2-PMs, 3-carrier, 4-guiderail.[Gieras et al]

LSMs have found applications in manufacturing processes. Applications such as casting, moulding, machining and welding have seen LSMs replace the traditional hydraulic actuators in casting and moulding machines. Where leadscrews are used to achieve accurate positioning, they are susceptible to mechanical backlash and lower resolutions. Figure 3.26 shows a typical linear motor application instead of a traditional leadscrew method. The linear motor-driven positioning system is capable of greater positioning accuracy and resolution and offers greater control and smoother motion. Such systems are used in machine centers such as milling machines, grinders and drill presses. The double-sided long stationary PM excitation rail, with short moving armature linear motor used in Figure 3.26, is restricted in the distance it can travel by the tether supplying power. Reversing the motor's topology by mounting the PM excitation rail on the bottom of the moving plate and mounting the armature on the base, will allow the plate unrestricted travel. Machine centers with LSMs require less maintenance and permit better overall accuracy, especially in contouring applications. In manufacturing plants where clean atmosphere is required, LSMs are replacing hydraulic and pneumatic actuators. In the development of fine pitch flip technology, the die attachment is considered the most critical step. A study performed comparing two flip chip die placement machines, one with a leadscrew and the other with a LSM, revealed that the LSM machine was capable of greater accuracy and repeatability at higher resolutions. [Hwang et al]

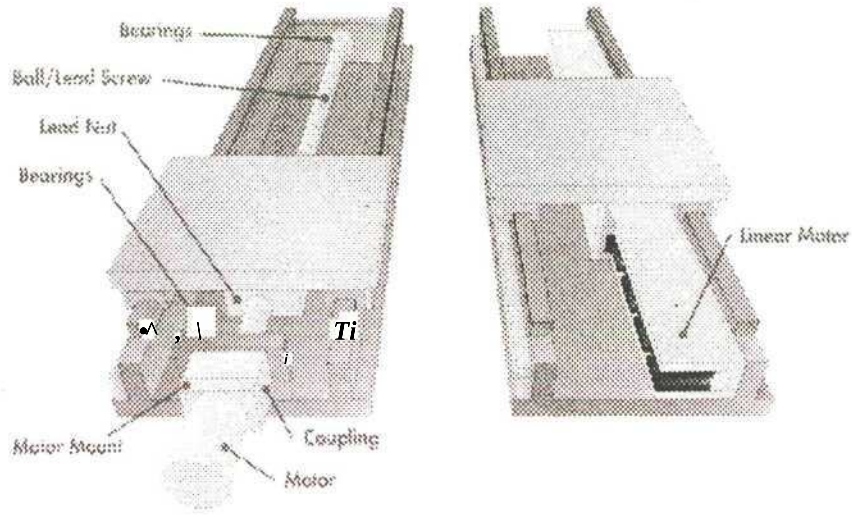

Figure3.26: Comparison of positioning systems with leadscrew and linear motors. [Trilogy_l]

LSMs have also found applications in the transportation of humans. The construction of super high skyscrapers has led to extensive research being undertaken to develop rope-less elevators by applying LSM technology. In South Africa the mining industry has expressed interest in using rope-less hoists in ultra-deep goldmines. Conventional hoisting systems are no longer possible beyond 2800m as the hoisting rope cannot support its own weight. At present sub-vertical shafts are sunk from 2500 m and a roped hoist system is installed underground. The implementation of a PM LSM rope-less hoist is currently being researched. [Landy et al] The efficiency of a rope-less hoist is independent of the depth of the mine shaft but dependent on the thrust-to-weight ratio and the motor thrust. The proposed hoisting system consists of PMs on the hoisting cage and a slotted iron-core armature mounted on the mine shaft walls.

High speed transportation systems employing LSM have received the most attention, as they offer alternative solutions to current transportation systems which impact environmentally and are slow, inefficient and uneconomical. Maglev transportation systems offer a clean, highly efficient and environmentally friendly alternative. Two major maglev systems which have been developed are the Transrapid System in Germany and the Yamanashi Maglev Test Line in Japan. Both systems are examples of the two different maglev technologies which have been developed since the 1970s, namely electromagnetic (ELM) levitation and electrodynamic (ELD) levitation. ELM utilizes attractive forces of electromagnets with a controlled air gap and ELD utilizes repulsive forces and superconductivity. [Gieras et al].

The decision to develop an integrated material handling system, capable of performing accurate positioning assembly tasks, led to linear motors being investigated. The investigation revealed their advantages over traditional linear motion technologies. Investigation of the different types of linear motors, namely LIM and LSM, showed that LSMs are best suited for a material handling system. The topology and construction of LSMs revealed that a single sided, air-core, long armature with a short moving PM excitation rail would offer the best performance in terms of thrust production and smoothness of motion, due to non existent thrust ripple. Utilizing an air-core armature would reduce the attraction between the armature and the PMs. The two sections would still be attracted to each other due to the selection of a single-sided design.

Incorporating the long stationary armature design would allow the proposed material handling system the required flexibility. As a PM excitation rail is to be used, no tether would be required to the moving part. Advances in PM technology have allowed PMs to develop enough magnetic flux for thrust generation to create efficient PM LSMs. Further study was done into the theory of PM LSM, focusing on the generation of thrust. Since PM materials play a major part in the development of the proposed LSM, further research into PM technology was undertaken.

3.3.4 LSM OPERATION

The theoretical analysis of PM LSMs often evolves from developing a theoretical model based on salient pole synchronous machines, utilizing d-axis and q-axis synchronous reaction. This analysis often develops to an advanced theoretical level, based on a good theoretical knowledge of traditional rotary synchronous machines and brushless motors. The degree of mathematical knowledge associated with such theoretical models frequently exceeds the capabilities of the reader. Factory engineers, maintenance personnel and students (especially from other engineering disciplines) are often daunted by such theoretical analyses. Numerous literature is available for an in-depth and theoretical development of LSM principles [Miller, Gierasetal].

The development of computer-aided analysis and design packages have allowed complex electro-mechanical devices to be designed without a *deep* theoretical knowledge of the device. Finite element method allows for parameters to be altered and modeled optimizing the device's design. The proposed motor was designed using the finite element method. An understanding of how thrust was generated and how varying parameters would effect the motors performance was gained. By disregarding the complex mathematical theory and focusing on the quantitative design parameters which contributed to the motors performance, a complete design could be created. Figure 3.27 shows a schematic of a basic linear motor. The coil assembly encapsulates copper windings within a core material (eg. epoxy, steel). The copper windings conduct current (I). The magnet assembly consists of PMs mounted with alternating polarity on a steel plate, which generates magnetic flux density (B). In simple terms, when the current and the flux density interact, force(F) is generated in the direction shown. According to the right hand rule the force can simply be expressed as:

$$F = I x B \qquad (3.3)$$

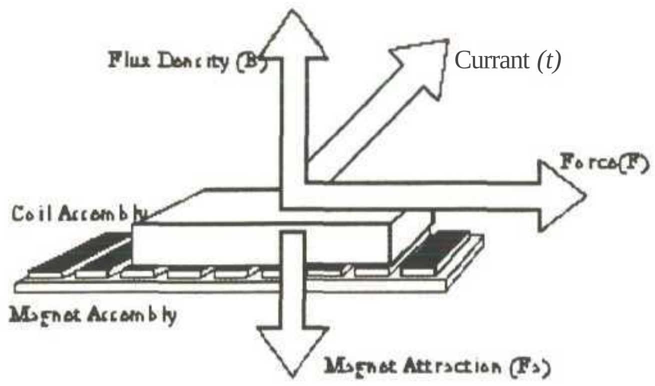

Figure 3.27: Basic linear motor model showing how force is created.

3.3.4.1 BASIC MODEL

Figure 3.28 shows a cross-sectional view of a basic linear motor model The structure shown is assumed to repeat indefinitely in both directions. In figure 3.28, the PM reaction rail is composed of surface mounted PMs alternating in polarity, separated by nonmagnetic spacers (such as air). The PMs are attached to a ferromagnetic backiron. The armature is composed of a ferromagnetic backiron with slots containing the windings of one phase. The slot pitch is such that there is one slot per magnet, or one slot per pole per phase. The purpose of the backirons is to provide a path for the magnetic flux as illustrated in the figure. x_p is the magnetic pole pitch, $T_m$is the magnet width, $x_f$is the magnet spacer width, l_m is the magnet depth and g is the air gap length.

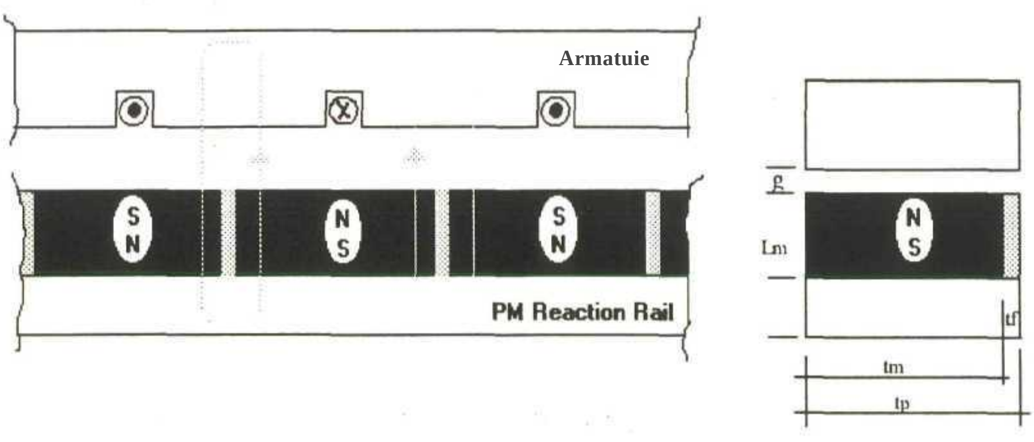

Figure 3.28: Basic model of a permanent magnet linear motor.

The flux from each magnet splits equally and couples with the two magnets adjacent to it. The flux linkage(A) of the magnets and the armature winding is a function of the PM reaction rail's position. In Figure 3.29(a), the magnetic flux linking the coil is at a negative maximum value. The flux is at a maximum because the flux from an entire magnet face is passing through the coil, but is negative because it is opposite in direction to the flux created by the current in the coil. In Figure 3.29(b) the flux linkage is zero as no net magnetic flux is linked by the coil, since half the flux travels in an opposite direction through the coil. In figure 3.29(c) the flux linkage is once again a maximum, but it is positive. The flux is positive because the direction of the flux is the same as that of the flux created by the current in the coil. For reaction rail positions between these points, the flux linkage varies approximately linearly. The period of the flux linkage is defined as the electrical period of the motor. The physical distance is equal to two pole pitches, t_p. The electrical distance is 2rc, and therefore one pole pitch is equal to *n* electrical radians.

The primary significance of flux linkage is that it induces a voltage in the armature winding as the flux linkage varies with time. This voltage is termed the back emf voltage. The back emf is determined by the product of velocity and the rate of change in the flux linkage with respect to position. In Figure 3.29 (a), current flowing in the coil produces a magnetic field directed away from the air gap according to the right hand rule. Thus a magnetic south pole is created on the surface of the armature. The PM on the left of the reaction rail is therefore attracted to the magnetic south pole, generating a positive force and moving the reaction rail to position shown in Figure 3.29(b). For the position shown in Figure 3.29(c), the armature and the reaction rail are aligned and the force generated is zero. Zero force positions are referred to as detent positions. [Hanselman]

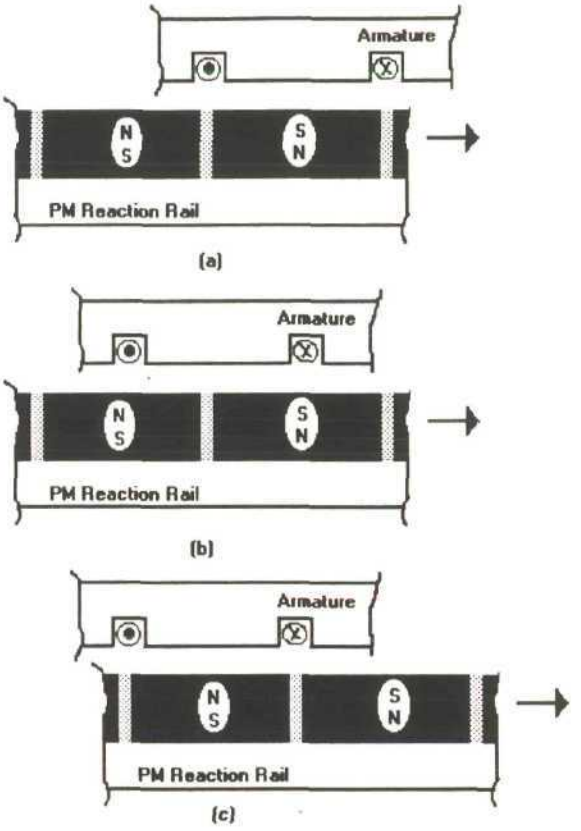

Figure 3.29 : Relative reaction rail positions of the motor model.

Due to periodic detent positions, it.is not possible to produce smooth motion. To generate constant motion with unidirectional force, additional current carrying slots are required such as those shown in Figure 3.30. The figure shows two phases in the motor section, with additional slots placed halfway between the original slots. Constant force can be created by applying current to which ever phase winding is not at or near a detent position. Unidirectional motion can be achieved by applying negative current to the appropriate coil. The force generated by a two phase motor is shown in Figure 3.31.

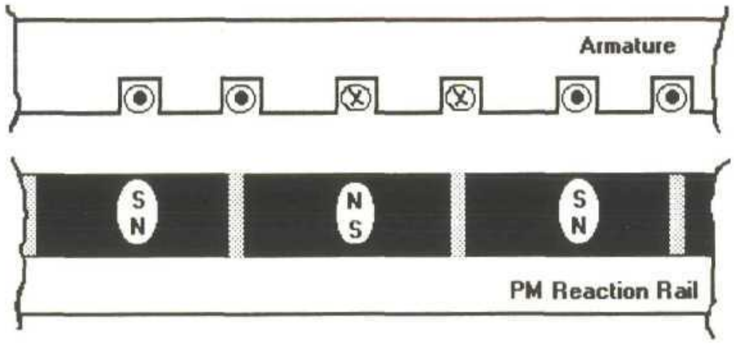

Figure 3.30: A two phase model

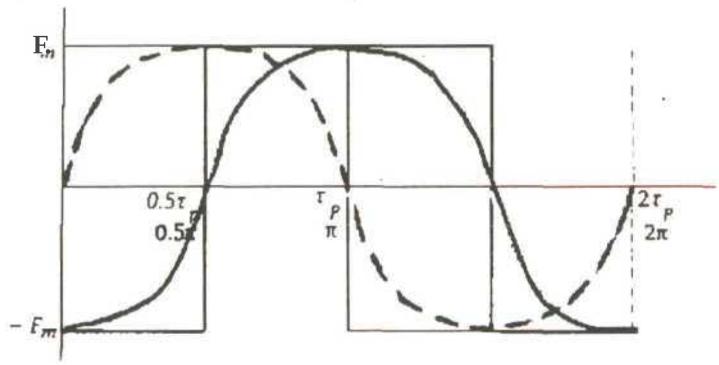

Figure 3.31: Force generated due to two phases. [Hanselman)

Therefore the force equation can be better expressed as;

$$F = NmBgLL. \qquad (3.4)$$

where N_m is the number of magnetic pole faces,

B_g is the air gap flux density,

L is the motor's effective length,

I. is the total slot current.

The significance of each term is explored separately. If the air gap flux density (B_g) is increased then the amount offeree is increased. The flux density is limited by the ability of the iron-core teeth to pass the flux without becoming saturated. An increase in the magnetic **flux density** requires the use of a magnet with a higher remanence. An increase in **the** magnetic flux density can be achieved by increasing the magnet length or decreasing the air gap length. However, decreasing the air gap length results in an increase in the cogging force. The active motor length (L) can be increased to increase the force produced. However, disadvantages include an increase in the mass and volume of the motor. Increasing L also requires longer slots and hence an increase in the armature resistance. The active motor length is therefore chosen as the minimum value required to meet a required force specification. Increasing the number of magnetic poles (N_m) increases the force generated by the motor. By increasing N_m whilst maintaining a fixed area requires decreasing the magnet widths. This results in an increase in the amount of magnetic leakage flux thus decreasing the air gap flux density. Another advantage of increasing N_m is that the backirons thicknesses decrease since less magnetic flux is passed to the back iron. The slot current (I_s) is the product of the number of turns per slot (n,) and the current per turn (i_s) Increasing *i*\ increases the inductance making the motor more difficult to drive However, an increase in n, allows for less conductor current to be used, decreasing the winding losses. Increasing n, whilst keeping the current per turn constant will increase the force generated but will require larger slots. Increasing the slot current while keeping n_s constant increases the current density and armature winding loses. Thus there is a conflict between a high air gap flux density and a high slot current. If the current increases, more slot area is required to maintain constant resistive loss resulting in the maximum flux density decreasing. The magnetic flux density decreases as the slot width increases because magnetic saturation limits the flux carrying capacity of the teeth as the teeth decrease in size. Since the force generated is a product of the flux density and the slot current a trade-off is required. [Hanselman] Information gained from the above quantitative analysis was used to design the proposed linear motor material handling system using the finite element method.

3.4 PERMANENT MAGNET TECHNOLOGY

The rapid development of new permanent magnet (PM) materials have increased their use in the design of d.c and synchronous machines. In all machines using PMs it is desirable that the magnetic material have the following characteristics:

(a) large residual flux density so that the magnet provides the needed flux
(b) large coercivity so that the magnet cannot be demagnitized by stray magnetic fields.

PM characteristics are best described by developing their *B-H* loop or 'hysteresis loop'. A typical *B-H* curve of a PM is shown in figure 3.32. The x-axis measures the magnetizing force or field intensity, //, in the material. The field intensity is measured in units of Oersted, (Oe) or Ampere-turns/meter,(A/m). The y-axis is the magnetic flux density, *B*, in the material and is measured in Telsa (T). An un-magnetized sample has $B=0$ and $H=0$. If the sample is subjected to a magnetic field, such as that produced by an electromagnet, then *B* and *H* will follow the curve OA and become initially magnetized. If the electromagnet is turned off, the magnet relaxes along AB. Where the line crosses the y-axis (at *H=Q),* the flux density is called the remanence, B_T. The remanence is the maximum magnetic flux density retained by the magnet at a specific temperature after being magnetized to saturation. If current is applied in the opposite direction, the magnet operating point follows the curve from B through the second quadrant to point C. Where the curve crosses the x-axis to give $B=0$, the corresponding magnetizing force, $-H_c$, is called coercivity. If the external electomagnet is turned off, the magnet relaxes along the line CD. The magnet is now magnetized in the opposite direction and the magnetic flux density is set to $-B_T$. To create negative flux density from D, a positive $//_c$ must be applied.[Miller]

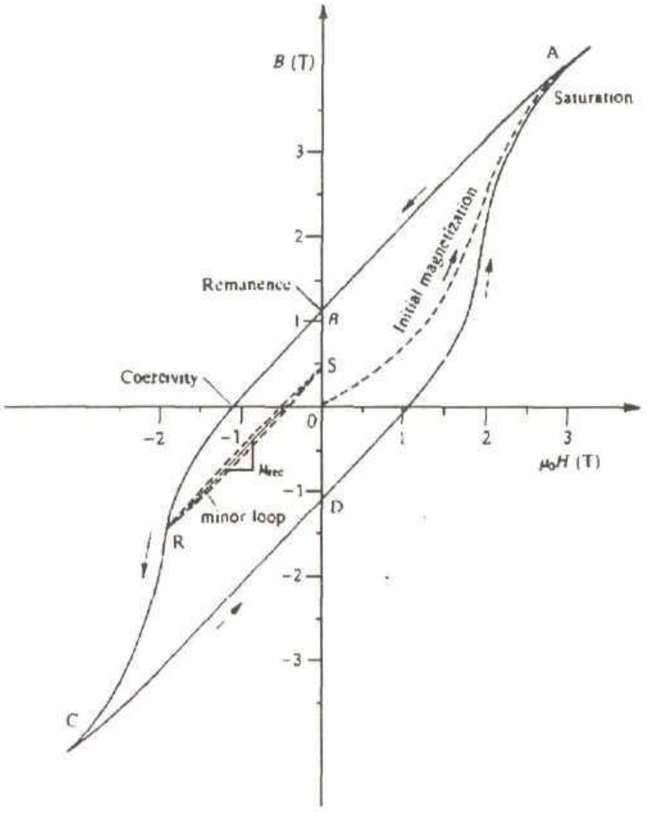

Figure 3.32: ***B-H*** **Hysteresis Loop of a hard permanent magnet material.) Miller]**

If the magnet is negatively magnetized starting at point B, and switched off at R, the operating point of the magnet recoils along RS and the flux density decreases to S. If the external negative magnetic field is reapplied, the operating point returns along SR. The line RS is referred to as the relative permeability of the magnet. An ideal permanent magnet has a flat-topped wide hysteresis curve so that residual magnetism remains at a high level when the applied field is removed. Thus a large enclosed area of the hysteresis loop is a characteristic of a strong PM. The basis for evaluating a PM is obtained by studying the second quadrant of the hysteresis loop which is called the demagnetization curve. In the process of designing a magnetic circuit, it is essential that PMs be operated where they can supply the maximum energy. The energy density of a magnet is expressed as the area of the hysteresis loop. The product *(BxH)* of magnetic flux density B and magnetic field intensity H is called the energy product. To determine the operating point of a PM, the maximum energy product,(BxH)max, is first calculated by reading off the B and H values from a typical energy product curve (quadrant 1) which results in a maximum BxH value. This is shown as the as the knee of the curve in quadrant one in Figure 3.33. Extending a horizontal line from this point into the second quadrant to intersect the demagnetization curve determines the PM optimal operating point. The magnetic operating line is defined as the line which extends the origin through the operating point, as shown in Figure 3.33. The energy available in the air gap is at a maximum when the point of operation corresponds to the maximum energy product of the magnet. [Miller] The magnitude of the slope of the operating line is the permeance coefficient (PC). Thus operating at remanence yields a PC of infinity, operating at coercivity yields a PC of zero.

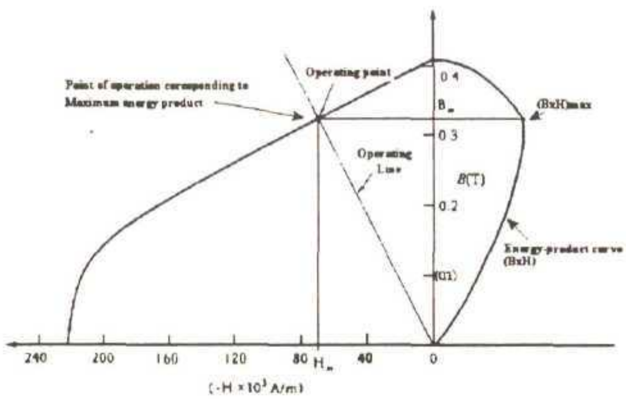

(b)

Figure 3.33: Typical demagnetization and energy-product curves of a magnet showing the operating point line.[Miller]

Two factors in particular affect the operating point of the magnet; the air gap length and operating temperature. Increasing the length of the air gap results in the slope of the operation line decreasing and the operating point moving down the demagnetizing curve. If the operating line drops below the 'knee' of the demagnetization curve, then the recoil line will be parallel but lower than the original recoil line. This results in the magnet recoiling to lower *B* and *H* values. Less magnetic flux density results in lower forces being produced by the motor. A rise in temperature alters the hysteresis loop, causing the demagnetizing curve to shrink towards the origin. As the temperature increases, the flux available from the magnet decreases, thus decreasing the force generated by the motor. [Hanselman] Exposing a magnet to sufficiently high temperatures for prolonged periods produces metallurgical changes. These changes may impair the ability of the material to be re-magnetized. The Curie temperature is the temperature at which all magnetism is reduced to zero. When a magnet has been raised above the Curie temperature, it is possible to re-magnetize the magnet provided no metallurgic changes have occurred. When the temperature change is limited in scale, the losses are reversible and are approximately linear. Thus temperature coefficients for remanence and coercivity are used. They are expressed in percentages per degree Celcius, (%/°C).

Alnico was the fist type of PM to be used in electric machinery Alnico was succeeded by Ferrite, Ceramic, Rare-Earth/Cobalt magnets and more recently by Neodymium-Iron-Boron (NdFeB). PMs can be classified as 'hard' or 'soft'. A hard PM material is one in which the hysteresis loop in the second quadrant is straight, ie: a linear demagnetization curve. This is a characteristic of rare-earth/cobalt, NdFeB and most ceramic PMs. Since the demagnetizing curve is linear, the recoil line is coincident with the second quadrant curve.'Soft' PMs are those whose demagnetization curves exhibit a 'knee' in the second quadrant. Alnico magnets are an example of soft PM. Figure 3.34 shows the demagnetizing characteristics of these permanent magnets. The physical characteristics and the advantages and disadvantages of these magnets, when applied to electrical machines, will now be described. More specific data on certain magnets is listed in Appendix A.

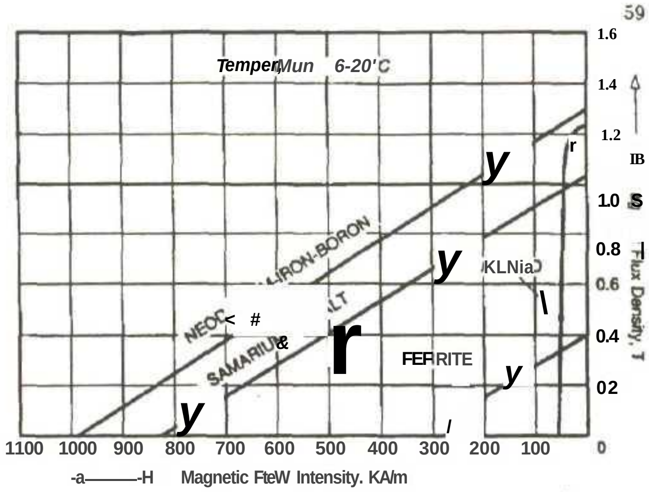

Figure 3.34: Demagnetization characteristics of Alnico, ferrite, ceramic and rare-earth magnets.|Gieras et al]

-Alnico: The physical composition of Alnico is Aluminum (AJ), Nickel (Ni), Cobalt (Co) and iron (Fe). Alnico magnets have high remanence with excellent mechanical and thermal properties. This makes them suitable for high temperature operating motors. The temperature at which significant metallurgic changes develop, is lower than the Curie temperature. Alnico is capable of operating at temperatures up to 520°C , with a temperature coefficient, B_t of 0.02 %/°C. Disadvantages of Alnico its low coercive force and its non-linear demagnetizing curve. Alnico magnets are limited by the extent to which they can withstand demagnetization fields . It is easy both to magnetize and demagnetize them. Alnico magnets dominated the electrical machines industry from the 1940s to the late 1960s when ferrite magnets began to replaced them. [Parker]

- ***Ferrite I Ceramic:*** Ferrite magnets are commonly described as Ceramic magnets. Ferrite magnets are produced by powder metallurgy. Two common ferrite magnets are barium and strontium ferrite magnets. They possess a higher coercive force than that of Alnico but have a lower remanent flux density. Strontium has a higher coercive force than barium. The temperature coefficients are relatively high, with B_r equal to 0.20 %/°C and H_c to 0.27 %/°C. Ferrite magnets are capable of operating at temperatures of up to 400°C. In ferrite magnets metallurgic changes due to temperature effects occur below the Curie temperature. The advantage of this is that ferrite magnets can be safely demagnetized for handling and finishing purposes by heating them above the Curie temperature. A further advantage of ferrite magnets is their relatively low cost. Barium ferrite PMs are commonly used in small d.c motors used for fans, pumps and windscreen wipers.

- ***Cobalt:*** The first generation of rare-earth magnets was based on the composition of samarium-cobalt (SmCo) which produced a hard magnetic material with a high energy product. The advantages of SmCo are its high remanent flux density, high coercive force and low temperature coefficient. The temperature coefficients for B_r are 0.03 %/°C and $//_c$ 0.14 %/°C. This makes them suitable for high temperature operation up to 330 °C. Physical metallurgic changes occur below the Curie temperature. Because SmCo is limited in supply it is expensive.

- *NdFeB:* Due to the availability of Nd and iron, NdFeB PMs are cheaper than SmCo magnets. NdFeB magnets are the second generation of rare-earth magnets. According to their manufacturing process, NdFeB PMs are classed as sintered PMs and bonded PMs. At room temperature NdFeB PMs have the highest energy product of all commercially available PMs. [Parker] High remanence and coercivity values allow for reduced motor frame sizes for the same output. Due to a coercive temperature coefficient of 0.70 %/°C, the demagnetization curve is highly temperature dependent. The maximum operating temperature is limited to 170°C. A further disadvantage is the fact that NdFeB PMs are susceptible to corrosion. NdFeB PMs are often coated in either zinc (Zn), Nickel (Ni) or resin to prevent corrosion. The physical and magnetic characteristics of NdFeB sintered and bonded PMs are available in Appendix A.

The information gained about permanent magnets has shown that NdFeB PMs are best suited for the proposed motor. This is due to the large amount of magnetic flux density which NdFeB PMs can offer, thus maximizing the force a motor can produce. Agents were identified to source further information on NdFeB PMs. This information is available in Appendix A.

4 LINEAR SYNCHRONOUS MOTOR ANALYSIS AND DESIGN

4.1 INTRODUCTION

The design of a short moving magnet, long armature LSM is proposed. A Finite Element Simulation Package, Maxwell™, developed by Ansoft, was used to design the proposed motor [Ansoft1]. A kinematic analysis was undertaken to determine the required material handling specifications, such as the amount of thrust required to perform specific manufacturing tasks. The results from the finite element analysis were used to construct the physical prototype.

4.2 FINITE ELEMENT ANALYSIS AND DESIGN

The Maxwell 2D Field Simulator is an interactive software package for analysing electric and magnetic fields in structures. The field patterns can be analysed by modeling the cross section of an object. Finite element analysis facilitates the solution of large scale complex electromagnetic field problems by modeling the whole or part of the device. Maxwell™ allows for the simulation of Electrostatic and Magnetostatic fields in models to be computed. Models can be developed in either two dimensions (2D) or three dimensions (3D). The electrostatic field simulator computes static electric fields arising from potential differences and charge distributions. The magnetostatic field simulator computes static fields arising from DC currents and other sources, such as permanent magnets and external magnetic fields. Magnetic fields in linear and non-linear material can be simulated. [Ansoft1] The term 'static' implies that the time rate of change is slow. Field parameters are determined by using Maxwell's equations. The differential and integral forms of Maxwell's equations made electrostatic and magnetostatic solutions a discipline which is (chiefly) mathematically orientated. With the development of computers and the increased ability to do vast computational analyses, commercially available FEM packages have become the preferred method of design and analysis of electro-magnetic machines [Hoole et al]. 2D magnetostatic field simulation was chosen to design the proposed motor.

4.2 1 THEORY OF MAGNETOSTATIC FIELD SIMULATION

The objective of the 2D magnetostatic field simulation is to determine the magnetic field intensity, H, through the surface of a plane using Ampere's law. This can then be used to compute the magnetic flux density and other useful design parameters. Ampere's circuit law, which is only valid in the absence of time varying fields, states that 'the line integral of a static magnetic field taken around a closed path must equal the current enclosed by a path.'[Meijer] Ampere's law is expressed as :

$$V \; x \; // = J \qquad (4.1)$$

where: H is the magnetic field intensity,

J is the current density,

V is the vector operator 'dell'.

The magnetic field intensity can be expressed in terms of magnetic flux density as:

$$H = \frac{B}{0} \qquad (4.2)$$

where : B is the magnetic flux density,

$\backslash i_r$ is the relative permeability of each material,

H_o is the permeability of free space.

Thus Equation 4.1 can be expresses as:

$$\nabla \times \left(\frac{B}{\mu_r \mu_0}\right) = J \qquad (4.3)$$

In magnetostatic field simulation, the magnetic field intensity, H, cannot be determined directly. The field simulation first solves for the magnetic vector potential, A. The current density, J, is assumed to only have a z-component with current flowing parallel to the z-axis. This results in A only having a z-component as well. Both quantities can therefore be treated as scalars. The magnetostatic field equation solves for A using the field equation using the field equation:

$$J_z(x,y) = \nabla \times \left(\frac{1}{\mu_r \mu_0}\right) \cdot (\nabla \times A_z(x,y)) \qquad (4.4)$$

where: $A_z(x,y)$ is the z-component of the magnetic vector potential,

$J_z(x,y)$ is the DC current density field.

Since the current density J and the vector potential, A, are treated as scalar, Equation 4.4 can be simplified to:

$$J = \nabla \times \left(\frac{1}{\ }\right)(\nabla \times A) \qquad (4.5)$$

The magnetic flux density, B, can then be expressed in terms of the vector potential, A:

$$B = \nabla \times A \qquad (4.6)$$

The magnetostatic field simulator determines the vector potential through a defined plane of the model. Once A has been calculated, then the magnetic field intensity and density can easily be computed and used to determine other required system parameters such as inductance, force, torque, admittance, impedance and flux linkage.

4.3 ANORAD'S BRUSHLESS LINEAR DC SERVOMOTOR

To become familiar with finite element analysis and PM LSM design techniques, Anorad's Brushless Linear DC Servomotor, LEB-S-2-S, of which a schematic drawing is shown in Figure 4.1, was simulated and analysed as a reference model.

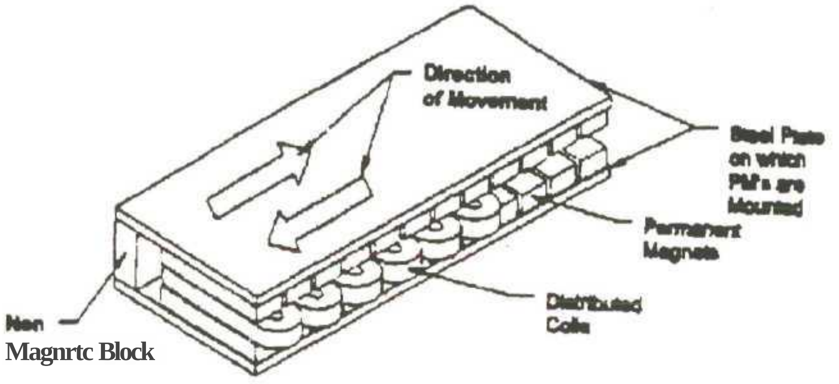

Figure 4.1: Anorad's balanced PM LSM. [Hippner et al]

Anorad manufactures both epoxy core and steel core brushless servo motors. The LEB-S series forms part of the epoxy core motor series. The numeration, 2, in LEB-S-2-S denotes the number of coil sets. A maximum of eight coil sets are commercially available. The last term S, denotes a series connection of the coil sets. Details of the motor's specifications are available in Appendix B.

4.3.1 LEB-S-2-S FINITE ELEMENT ANALYSIS

A 2D finite element model was developed by the candidate to analyze the parameters of the LEB-S-2-S motor. Figure 4.2 shows the geometric model setup. The model consists of two parallel steel plates (backirons) with alternating PMs mounted on the internal surface. The three phase moving coil assembly is positioned between the PM assemblies.

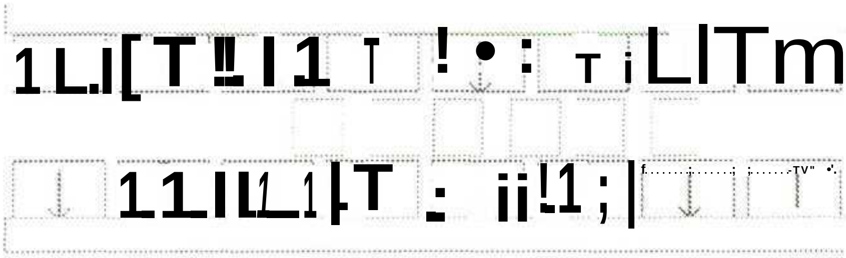

Figure 4.2: Geometric model generated to analyse the LEB-S-2-S motor.

The magnetic flux density distribution in the air gap generated by the PM assemblies is sinusoidal, with a magnitude of 0.5 Telsa (T). Figure 4.3 displays the magnetic flux density distribution in the air gap.

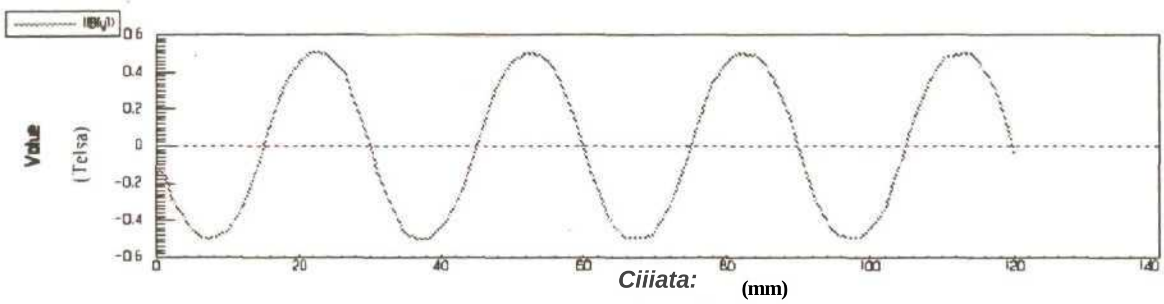

Figure 4.3 : Magnetic flux density distribution in the middle of the air gap between the two permanent magnet assemblies.

The magnetic flux lines of the motor are shown in Figure 4.4. The flux pattern generated by the PM assembly is regular with a distinct repetitive pattern. The flux line shows the reason for the steel backiron. The backirons allow the flux path to be closed, concentrating the magnetic flux towards the air gap.

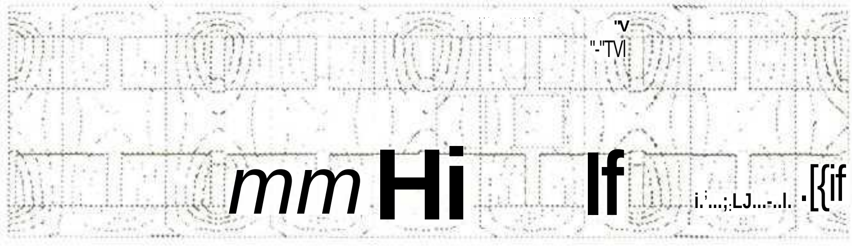

Figure 4.4: Magnetic flux lines generated by the PM assembly.

The backirons are subject to saturation. Figure 4.5 shows a plot of the magnetic flux density distribution with current adjusted to a maximum of 500 Ampere-turns. The highest values of the flux density appear in the backirons in between the PMs. The backirons are saturated if the values of magnetic flux density fall above the 'knee' of the B-H curve. The magnetic flux density in the backirons was below the saturation level.

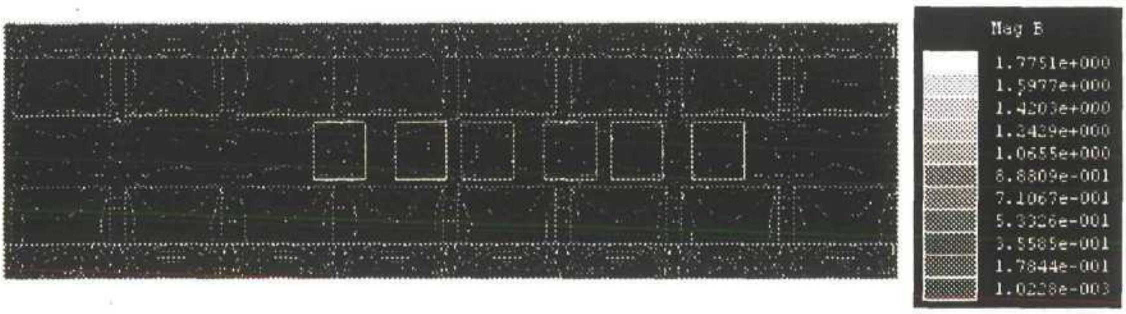

Figure 4.5: Magnetic flux density distribution with the currents in the windings set to a maximum.

When a symmetrical three-phase system of currents is applied to the winding a force between the PM assemblies and the coil assembly is generated. Due to the symmetrical design and positioning of the coils in the air gap, the y and z-components of the force become non-existent. The x-component of the force developed by the motor is termed the thrust. The development of the thrust depends on the position of the windings with respect to the PM assemblies and the phase shift of the currents in the windings [Hippner et al]. The values of the currents are defined as:

$$I_a = I_m \sin(\phi_0 + \theta) \quad (4.7)$$

$$I_b = I_m \sin(\phi_0 + \theta - 120°) \quad (4.8)$$

$$I_c = I_m \sin(\phi_0 + \theta + 120°) \quad (4.9)$$

Where: ϕ_0 is phase angle in degrees with respect to the starting position of phase A;

θ is the phase shift in degrees.

For $\phi_0 = 60°$ and $\theta = 0°$, the thrust developed varies sinusoidally. The 'zero position' or starting position of the motor is the position of the moving coil assembly when the thrust generated is zero. If the coil assembly is held in the zero position and the phase angle ϕ_0 is increased to 150°, the maximum value of thrust is produced. [Hippner et al] Figure 4.6 shows the thrust developed versus the instantaneous angle of the current phasor for a fixed position of the moving coil assembly. If the coil assembly is allowed to move from the zero position whilst the current is kept constant, the thrust developed varies almost sinusoidally. Figure 4.7 shows the thrust developed versus the position of the moving coil assembly for a frozen position of the current phasor.

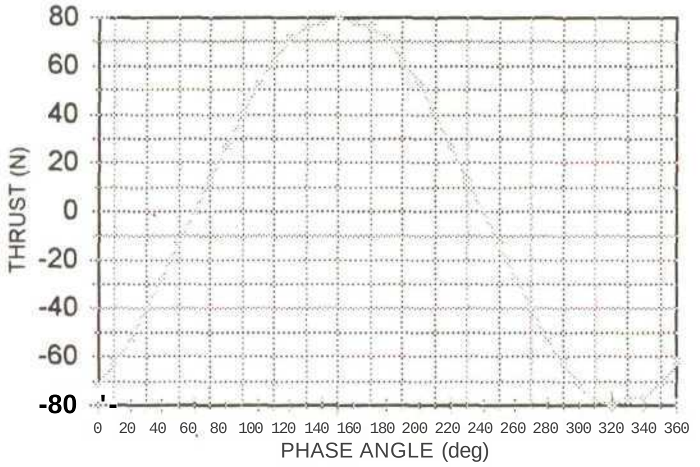

Figure 4.6: Thrust developed vs instantaneous phase angle (<j)0) of the current phasor for a fixed position of the moving coil assembly.

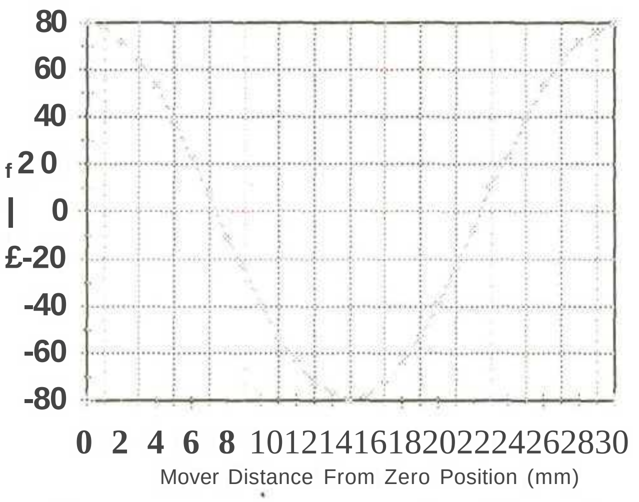

Figure 4.7: The thrust developed vs position of the moving coil assembly for a frozen position of the current phasor (6=150°)

For each position of the moving coil assembly there is an optimum value of the phase shift, 0, resulting in the maximum thrust being developed. The relationship between the phase shift and the position of the moving coil assembly is given by:

$$0 = \frac{x}{\tau_m} \times 360 \qquad (4.10)$$

where: x is equal to the coil assembly position as it moves from the zero position.

t_m is the magnet pitch.

This relationship is linear and has a period equal to two magnetic pitches [Hippner et al]. For each position of the coil assembly, as it moves down between the PM tracks, the phase currents are adjusted by continually substituting the results of equation 4.10 into the phase current (Equations 4.7- 4.9). This results in the maximum possible thrust being generated for each position of the mover as shown in Figure 4.8. The thrust ripple is minimal due to the coreless armature design and the optimization of the magnet pitch to coil span ratio. A more comprehensive investigation into the thrust development and thrust ripple of the LEB-S-2-S motor can found in [Hippner et al].

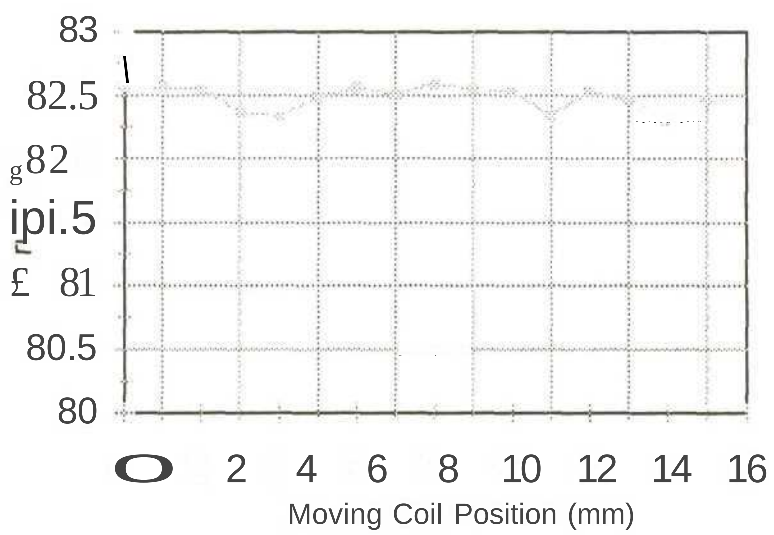

Figure 4.8: Thrust developed with phase adjustments in the windings. Values adopted from [Hippner et al].

A finite element analysis has been performed on a balanced PM linear synchronous motor. Finite element design techniques have been learnt by creating a finite element model of the motor. The stationary double-sided PM assembly excitation rail and moving armature motor is in contrast to the single-sided, moving PM and long stationary armature linear motor which was proposed. By removing the lower PM assembly, reducing the upper PM assembly to a suitable moveable size and extending coil set infinitely to create an armature platen, a possible design for the proposed linear motor material handling system can be envisaged.

4.4 FINITE ELEMENT ANALYSIS OF LINEAR SYNCHRONOUS MOTOR

The proposed linear motor design was based on the operating principle used to develop thrust in Anorad's brushless PM motor. By eliminating one of the PM tracks, the proposed motor was no longer balanced and an attractive force existed between the armature and the PM assembly. The moving PM assembly was termed the *'courier^* and the continuous armature was termed the *'platen'*. A detailed 2D finite element design and simulation was undertaken, highlighting how the model was constructed and analysed to arrive at the final design. A detailed analysis of the individual parameters affecting the motor's performance was undertaken.

4.4.1 2D FINITE ELEMENT MODEL SETUP

When developing a 2D finite element model, a basic framework needs to be followed in order to create a realistic simulation of the desired motor. The model must be defined geometrically in either cartesian (XY plane) or axisymmetric (RZ plane) coordinates. Once the geometric model has been defined, objects which are identical are grouped. The individual elements which define the model are assigned material characteristics and properties. Sources of voltage and current are then assigned to the model, together with boundary conditions. The boundary conditions allow the behavior of magnetic fields on the inside surface or edges of the drawing space to be modelled. Quantities, such as force, torque and flux linkage, can be computed for objects or groups of objects by defining the executive parameters. Once the boundary conditions have been defined, the finite element mesh is generated and optimized. With the mesh defined, the nominal solution can be computed. A parametric analysis can be performed which allows the simulation of design variations using a single model. A post processing is undertaken to plot common field quantities and calculate field. The implementation of the finite element simulation allows multiple design variations to be undertaken to optimize the motor's design [Ansoft1]. Figure 4.9 shows the Maxwell 2D Field Simulator Menu which is the framework for developing a finite element model.

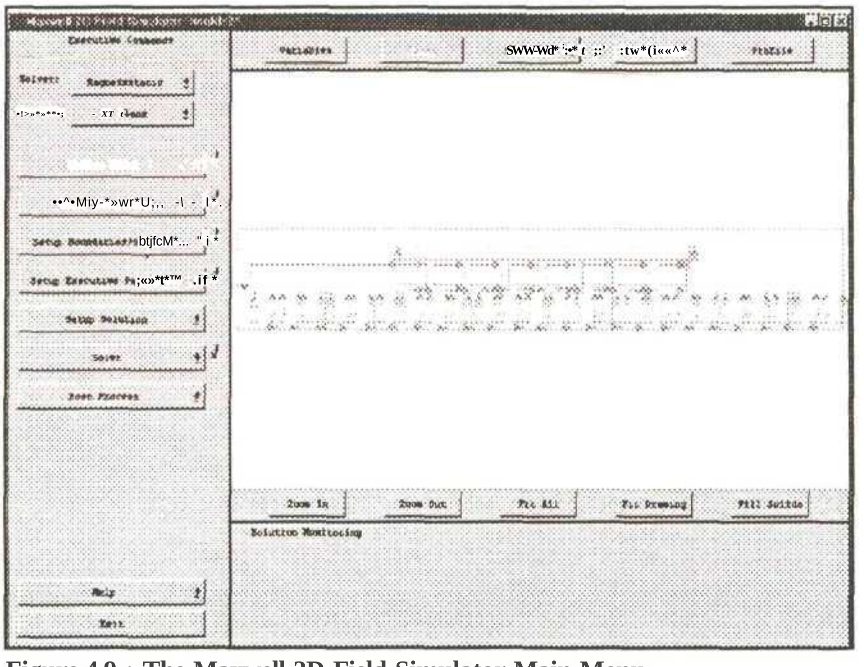

Figure 4.9 : The Maxwell 2D Field Simulator Main Menu.

To successfully develop a model each section is performed in sequence. The geometric model has to be defined before the materials can be assigned to the model. Once a section has been completed, it is ticked off, as shown in Figure 4.9. This allows the next section to be performed. The reason for developing the 2D finite element design and simulation were to:

- investigate the effect of varying model parameters on the motor's thrust and normal force development such as magnet thickness and width,

- reduce the thrust ripple by optimizing the magnet pitch to coil-span ratio,
- determine the final thrust developed by the simulated motor,
- use the final optimal model dimensions to create a physical prototype,
- determine the required ampere turns and current density to produce the desired thrust.

4.4.2 GEOMETRIC MODEL

The 2D cross sectional geometric model consists of a moving PM courier and a three phase armature platen (see Figure 4.11). The PM courier consists of the backiron with PMs mounted under the base of the backiron. The armature platen is geometrical modelled as a set of non overlapping rectangular coils. Each coil set consists of three phases, phase A, phase B and phase C, represented by six rectangles with two rectangles assigned per phase. The coil sets are aligned side by side to form the armature platen. The first rectangle for each phase in a coil set is positive, due to current flowing into the page. The second rectangle is negative, as current flows out of the page. Figure 4.10 shows a section of the armature platen layout.

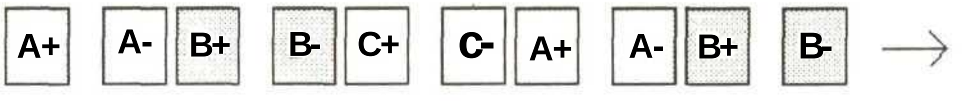

Figure 4.10 : Geometric model of the armature platen showing the assignment of notation to the coil set. The positive signs represent current flowing into the page and negative signs represent current flowing out of the page, for each of the three phases.

4.4.3 PARAMETRIC ANALYSIS

A parametric analysis allows the simulation of design variations using a single model. The parametric analysis identifies the basic design parameters that are to be varied during the simulation. Variables, such as geometric dimensions, can be changed to model the effect of changing model parameters. Parametric analysis allows for solutions to be obtained for a range of values by setting up the model and computing a solution for each variation of the nominal problem. To perform a parametric analysis, the nominal model must first be developed. The nominal model is the 'static' design simulation. By adding dimensional constraints and geometrical variants to the nominal problem, a parametric analysis can be performed. Each variant of the nominal model is known as a 'parametric setup'. Each parametric setup is a new nominal problem resulting from the dimensional variations. Results obtained from each parametric setup can be compared to determine how each design change affects the model's performance [Ansoft_2]. The following items were identified as design variants:

(1) backiron thickness,

(2) overall courier position,

(3) permanent magnet thickness,

(4) permanent magnet width,

(5) permanent magnet pitch,

(6) Coil thickness,

(7) Coil width,

(8) Coil pitch

Figure 4.11 shows the geometric model of the proposed motor with the geometric constraints and variants required to perform a parametric analysis of the motor.

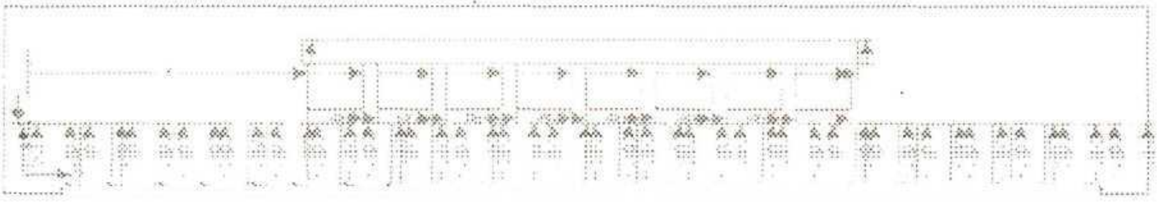

Figure 4.11: Geometric model setup with variable constraints for parametric analysis.

4.4.4 MATERIAL SETUP

Objects in the model were assigned specific materials from the material database. The model background represents the space surrounding the model and is assigned a default material such as a vacuum. The material database consists of a group of predefined materials that may be assigned to individual objects in the model. Materials can be added to the material database. The following materials were assigned to the model components:

Armature Platen - the coils in the armature platen were assigned a conductive material, copper, from the material database.

Backiron - the courier's backiron was assigned 1010 Steel. Since 1010 Steel has a permeability that varies with the flux density, it is considered to be a nonlinear material. A B-H curve is therefore required to describe the material's nonlinear behavior. The B-H curve is shown in Figure 4.12 The nonlinear characteristics of 1010 Steel were added to the material database and assigned to the backiron.

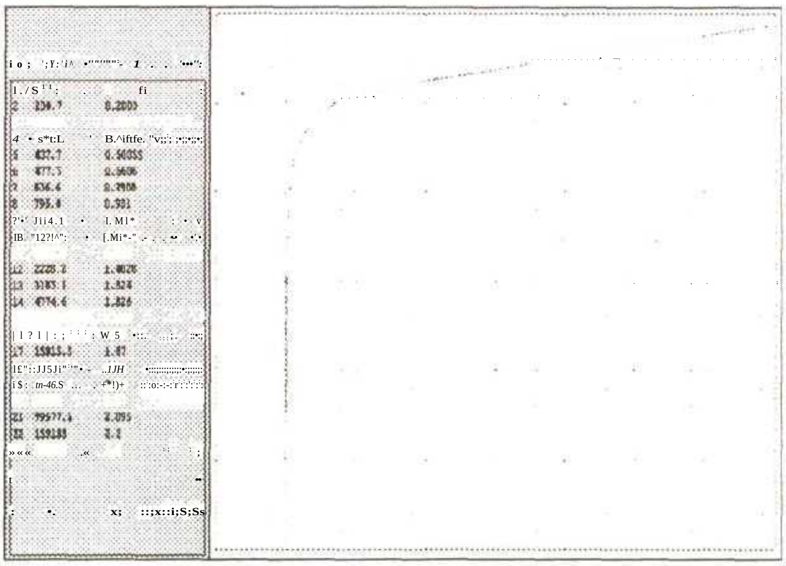

Figure 4.12: The B-H curve of nonlinear 1010 steel

Permanent Magnets - the PMs of courier were assigned NdFeB permanent magnet material. The material properties of Grade 35 NdFeB (NeFe35) magnets were obtained from the material data listed in Appendix A and entered into the material database.

The following material properties were assigned to NeFe35 in the material database.

Material Property	Value	Unit
Relative Permeability (Mu)	1.0997785406	
Magnetic Coercivity (He)	-8.9e+005	ampere/ meter
Magnetic Retentivity (Br)	1.23	telsa
Magnetization (Mp)	978802.901134	ampere/ meter

Table 4.1: Material properties of Grade 35 NdFeB magnets.

The PM assembly of the courier required the magnets to be setup with alternating polarity. Vector properties were assigned to each magnet to define individual alternating magnetic poles.

4.4.5 BOUNDARY CONDITIONS

Magnetostatic boundary conditions define the behavior of the magnetic field at the object's interfaces or edges of the problem region. To achieve accurate simulations the correct assignment of boundary conditions is critical. Boundary conditions can be used to:

- Identify structures that are magnetically isolated.
- Set the magnetic potential at a surface of an object to a constant value or a function of position to define the magnetic field on that surface.
- Simulate the field patterns that would exist in a structure while modeling part of it. Thus planes of symmetry where magnetic fields are either tangential to or normal to the surface can be defined [Ansoftl].

The following boundary conditions can be assigned to a finite element model:

Default(Neumann), Value, Balloon and Symmetry boundaries. Default boundary conditions for the magnetostatic models are set to Neumann or natural boundaries. All outside edges are defined as a Neumann boundary where the tangential component of H is zero, forcing the magnetic field to be perpendicular to the boundary as shown on the upper surface of the structure in Figure 4.13. All object interfaces are defined as natural boundaries, where the tangential component of H and the normal component of B are continuous across the object surface.

Value boundaries are used to set the magnetic vector potential, A^ to a constant value on a boundary. If A_z is constant along a horizontal boundary, the partial derivative of A_z with respect to zero will be zero. The flux density, B, will therefore have an x-component only and be tangential to the boundary. If \ is constant along a vertical boundary, the partial derivative of A^ with respect to y will be zero. The flux density will therefore have a y-component only and be tangential to the boundary. Thus as a general rule, the magnetic field will be tangential to any boundary on which A_z has been set to a constant [Ansoftl], Examples of value boundaries are shown in Figure 4.13. Balloon boundaries model the region outside the drawing space as being 'infinite', thus isolating the model from other sources of current or magnetic fields. By studying the flux lines along a boundary line, a clear indication may be obtained as to whether it is a balloon boundary or not. If the flux lines are neither tangential nor horizontal then the boundary can be assigned as a balloon boundary, as shown on the bottom of Figure 4.13.

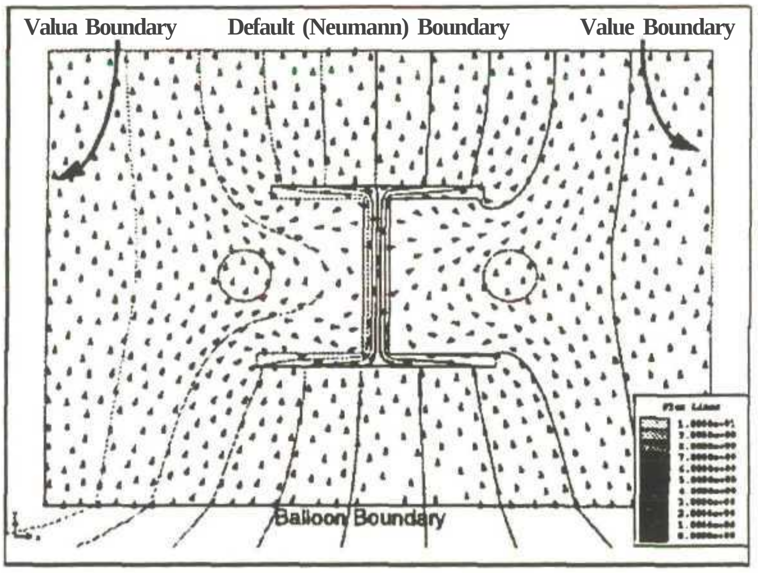

Figure 4.13: Boundary Conditions assigned to a model in a magnetostatic problem.[Asoft_3|

A symmetry boundary models a plane of symmetry in a model. This type of boundary is used when only part of a model is developed to save on computing resources. An example of using symmetry is to model only one quarter of an electric motor. Results obtained from the quarter simulation can be extended to the whole motor. Two types of symmetry boundaries are defined for magnetostatic simulation: Odd and Even symmetry. Odd symmetry boundaries are assigned if the signs (positive or negative) of all currents on one side of a symmetry plane are opposite to those on the other side, such as shown in Figure 4.14a. The magnetic field is tangential to an odd boundary. Even symmetry boundary models a structure in which the signs of the currents on the one side of a symmetry plane are the same as those on the other side. The magnetic field is perpendicular to this type of boundary as shown in Figure 4.14b. Boundary conditions were assigned to the proposed linear motor model by examining the flux patterns generated by the model

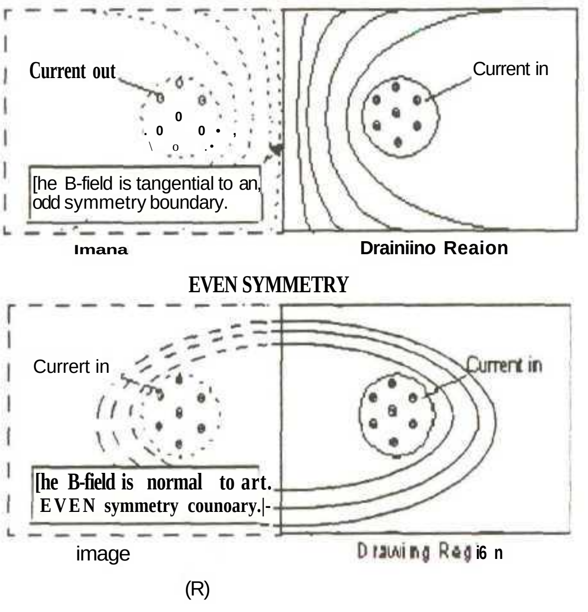

Figure 4.14: (a) Odd symmetry boundary,(b) Even symmetry boundary[Ansoft_3]

The following boundary conditions were applied to the finite element model:

Vertical Left Right Boundaries- The vertical boundaries were assigned odd symmetry boundaries. Since only a section of the armature platen is modelled, additional coil sets can be imagined to the left and right of the modelled platen. Thus an odd boundary situation is established.

Top and Bottom Boundaries- Both boundaries were assigned Value Boundaries with a vector potential, A = 0, due to the flux lines being tangential to both surfaces [Mizuno et al]. Figure 4.15 graphically shows the boundary assignments.

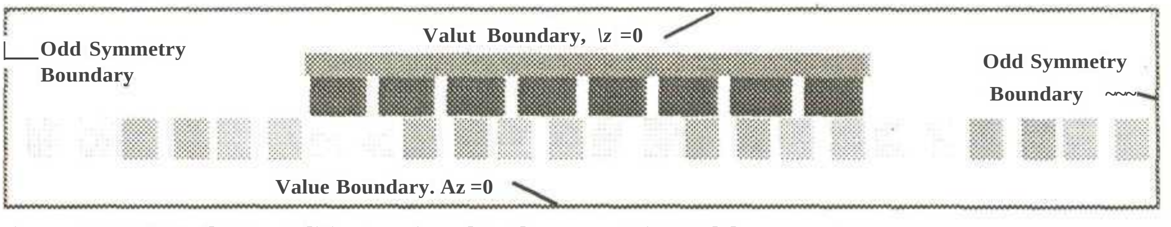

Figure 4.15: Boundary conditions assigned to the geometric model.

4.4.6 SOURCES

Sources define how charges, voltages or currents are distributed on edges or solid objects in a model. Two types of sources could be assigned to the model. They were:

- Solid sources used to model distributions of currents, charge or voltage on objects.
- Sheet sources used to model edge voltages, charge sheets or current sheets.

A solid source, such as a current source, specifies the DC current flowing in a conductor. The current source can be set as a total current or a current density flowing in the object. The current in each phase was defined as a functional current source. The sinusoidal current sources allowed the simulation of a three phase current source. Current sources I_a, I_b and I_c represented the current flowing into the page and I_{an}, I_{bn} and I_{cn} represented the current flowing out of the page(refer to Figure 4.10). For the finite element design, I_m is the ampere turns (amps x the number of turns) per coil. The functional current sources assigned were:

$$I_a = I_m Sin(\phi_0 + \theta) \quad (4.11)$$

$$I_{an} = -I_m Sin(\phi_0 + \theta) \quad (4.12)$$

$$I_b = I_m Sin(\phi_0 + \theta - 120^\circ) \quad (4.13)$$

$$I_{bn} = -I_m Sin(\phi_0 + \theta - 120^\circ) \quad (4.14)$$

$$I_c = I_m Sin(\phi_0 + \theta + 120^\circ) \quad (4.15)$$

$$I_{cn} = -I_m Sin(\phi_0 + \theta + 120^\circ) \quad (4.16)$$

4.4.7 EXECUTIVE PARAMETERS

The executive parameter is used to indicate which quantities are to be computed. The main executive parameters available are:

Matrix- requires that the capacitance, inductance, impedance, admittance or conductance matrix be computed.

Force- Requires that the net force on an object or group of objects be computed.

Torque- Requires that the net torque on an object or group of objects be computed.

Flux Linkage- Requires that the flux linkage be computed across a specified line[Ansoft_l],

The main aim of the simulation was to determine the thrust developed by the model. Since the selected topology of the motor requires the courier to move over the length of the platen, the **net** force developed on the backiron and the PMs constituting the courier was to be computed.

4.4.8 SOLUTION OPTIONS AND MESH REFINEMENT

The Maxwell 2D Field Simulator divides the problem region into many triangles to form a finite element mesh. The magnetic fields are computed at the nodes (vertices) of the triangles. If the mesh is too large, the field inside the triangles cannot be interpolated accurately from the nodal values. The optimal mesh for a structure is one which contains enough triangles to represent the field solution accurately. Figure 4.16 shows the initial mesh setup used to compute the field solutions. The solver residual is a normalized measure of how closely each field solution can satisfy the electromagnetic field equation being solved. Each time a field solution is computed, the solution is plugged back into the field equation. If the correct answer is achieved, the residual will be zero. If the solution is incorrect, there is a non-zero residual and a correction factor is added. The solution process continues until the residual is less than the specified residual values. For magnetostatic problems that contain linear **and** non-linear materials there is a Linear and Non-linear residual value that must be specified. The values specified were:

Linear residual : 0.0001

Non-linear residual: 5e-007

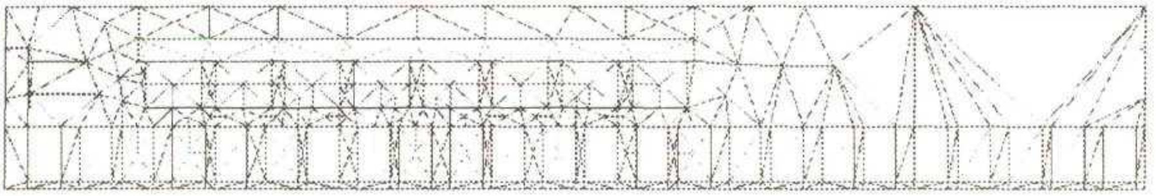

Figure 4.16: Initial mesh used in the finite element analysis.

Once the solution options had been specified, the finite element model was ready for parametric analysis to be performed.

4.5 KINEMATIC AND FORCE ANALYSIS

A kinematic and force analysis was performed to determine what thrust was required to perform specific manufacturing tasks. The manufacturing task used in the kinematic analysis was a simple pick and place procedure. The courier moves to a specified position and dwells for a specified time whilst a part is placed on the courier. The following estimations and assumptions were made:

Courier Mass : 30 N (T3 kg)
Load Mass : 20N(*2kg)
Attractive Force: 50 N

The total courier weight is therefore estimated as 100 N. The velocity profile was assumed by considering a typical operation the material handling system may have to perform. The initial quantitative values were based on desirable speeds for a given travel of 250 mm. Consider the velocity versus time curve shown in Figure 4.17. The courier accelerates from the home position to a velocity of 300 mm/s in 40 mm, (Phase 1), then travels at a constant velocity for 125 mm, (Phase 2). The courier decelerates to standstill in 85 mm (Phase 3) and dwells for 3seconds (Phase 4) for a total travel of 250 mm.

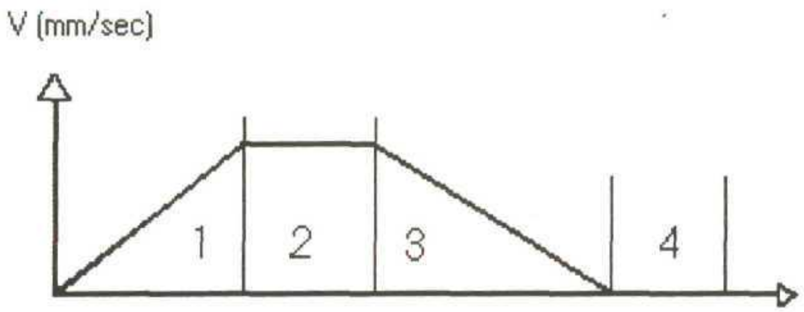

Figure 4.17: Velocity vs time curve for a manufacturing task

The accelerations and times are calculated for each phase and are summarized in Table 4.2 to complete the motion profile of the courier.

Positioning Phase Variable	**Units**	**Phase 1**	**Phase 2**	**Phase 3**	**Phase 4**
X (displacement)	mm	40	125	85	0
V (velocity)	mm/sec	0-300	300	300-0	0
A (acceleration)	mm/sec^2	1125	**0**	529.4	0
T (time)	sec	0.26	0.41	0.56	3

Table 4.2: Motion profile of the courier.

Once the kinematic analysis was completed, the forces experienced by the courier as it completed the manufacturing task were calculated. The coefficient of friction was estimated to be u= 0.008. Thus the factional force (F_f) can be calculated as:

$$F_f = [Mc + Fa] \times \mu$$

$$F_f = [50 + 50] \text{ x } 0.008 = -8N \quad \text{(4.17)}$$

where : M_c is the total weight of the courier;

F_a is the total attractive force.

The inertia force *(F,)* for each phase is calculated from:

$$F_t = M_m x Acc \qquad (4.18)$$

where : M,,, is the total moving weight (total combined weight of courier and load)

Ace is the acceleration of the courier.

An external force acting on the courier is assumed in phase 4 whilst an assembly procedure is performed. The forces experienced by the courier are summarized in Table 4.3. The continuous force, peak force and duty cycle can be calculated using the information presented in Table 4.3. The required peak force is calculated by taking the maximum force experienced by the courier during the manufacturing process.

Force	Phase 1	Phase 2	Phase 2	Phase 3
Friction (N)	-8	-8	-8	**-8**
Inertia (N)	-5.74	0	-2.701	**0**
Resistance (N)	0	0	0	**-10**
Total (Absolute)	13.74	8	10.7	**18**

Table 4.3: Summary of forces experienced by the courier.

From Table 4.3 the peak force must be greater than 18 N. For design purposes, the peak force is set to be approximately 20 N. The continuous force is therefore calculated at:

$$F_c = \sqrt{\frac{F_{t1}^{\,2} \times T_1 + F_{t2}^{\,2} \times T_2 + .. + F_{tn}^2 \times t_n}{\sum_{i=1}^{n} T_i}} = l.SN \qquad (4.19)$$

where : F_{ti} = total force for the position phase

T_i = time taken in each phase.

From the above kinematic and force analysis, a rough estimate was obtained of the force required by the proposed linear motor material handling system. Using the finite element analysis, the motor is designed to produce a thrust approximately equal to the calculated peak force.

4.6 FINITE ELEMENT MODEL DESIGN

The aim of the finite element design was to create a model which generated sufficient thrust with minimal thrust ripple and a reduced attractive force. Individual motor parameters were identified in order to analyze their varying effect on the motor's performance. The parameters identified were the courier's PM and backiron dimensions and the platen coil dimensions. To ensure minimal thrust ripple, the magnet pitch to armature coil-span ratio was optimized. Once the motor's optimal two-dimensional specifications and dimensions had been determined, the motor's effective length was calculated to achieve the motor's required thrust development. The dimensions to construct a physical prototype were taken from the final finite element model.

The finite element design was undertaken in two main divisions. The courier design involved studying the effect of varying the PMs and backiron dimensions, whilst keeping the armature platen dimensions constant. The platen design involved varying the platen dimensions and current specifications, whilst keeping the courier's dimensions constant. Although the courier design and platen design are closely related in the development of thrust by the motor, they are initially dealt with independently to determine their individual effects on the motor's performance. The relationship between the courier design and the armature design are then investigated as a whole and the effect on the generation of thrust and normal force, developed by the motor design, is studied.

4.6.1 PERMANENT MAGNET ANALYSIS

A permanent magnet analysis was undertaken to show how each PM and combinations of PMs contributed to the development of thrust and the normal attractive force. The effect of increasing the magnet depths and widths on the motor's thrust and normal force, was also modelled. Determining the effect of each magnet and the combinations of PMs to develop a PM assembly gave a better understanding of how these trends would affect the motor's performance. The magnets' original dimensions were set equal to Anorad's LEB-S-2-S motor dimensions. The PM depth and width were set at 7 mm and 12 mm respectively. The magnet pitch was set to 15 mm. Figure 4.18 shows the finite element model setup using parametric analysis to set up the finite element model for each analysis to be performed. The current sources were set to a constant value to eliminate the effect of varying current sources on thrust development. The backiron thickness was kept constant for each geometric model.

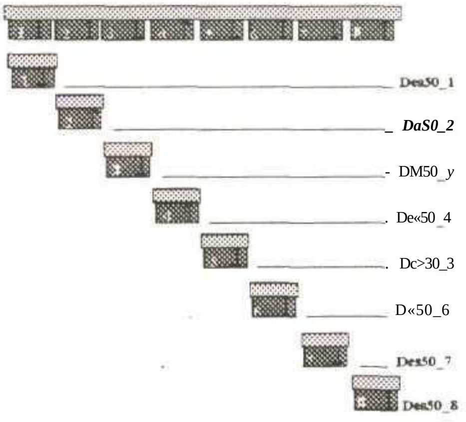

Figure 4.18: Geometric models setup by parametric analysis.

The results obtained from the parametric analysis showed the thrust per meter developed by each individual magnet in the courier, as they are swept along the armature platen, is highly regular and sinusoidal. Comparing the thrust curves generated by the individual models showed that the thrust peaks are shifted to the right. For magnets one to four the thrust curves shift to the right by 5mm increments. The thrust curves generated for magnets five to eight, mapped the thrust curves generated by the first four magnets with the same phase shift. The results of the finite element models are shown in Figure 4.19. The resultant thrust curve from combining the first four magnets to create a PM assembly would be the same as the thrust curve developed by combining the last four magnets. This indicated that the magnetic assembly was best suited as sets of four PMs.

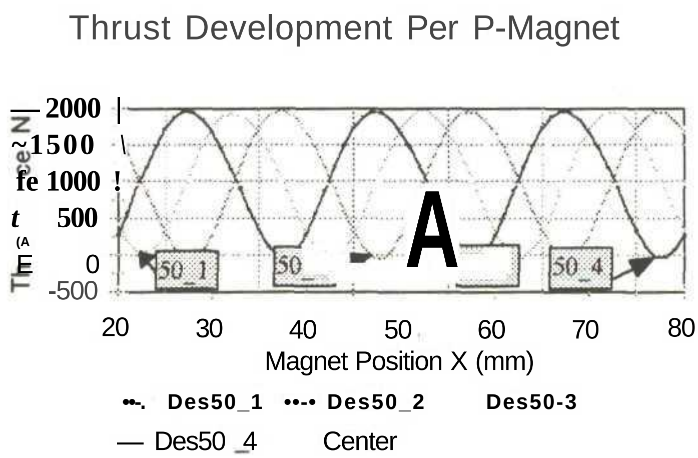

Figure 4.19 : Thrust per meter developed by individual magnets.

The results above led to combinations of PMs been modeled. Additional magnets were added to the PM assembly to study the effect on the thrust development. Figure 4.20 shows the geometric models setup by the parametric analysis. The results obtained showed the thrust developed increased with the number of PMs being added whilst shifting towards the right. The thrust also displayed significant fluctuations until four PM had been added to the magnetic assembly. The thrust curve developed by a PM assembly with four PMs showed significant reduction in the thrust fluctuations. This is proved by adding a fifth PM to the PM assembly. The thrust developed exhibited increased thrust fluctuations as shown in Figure 4.21.

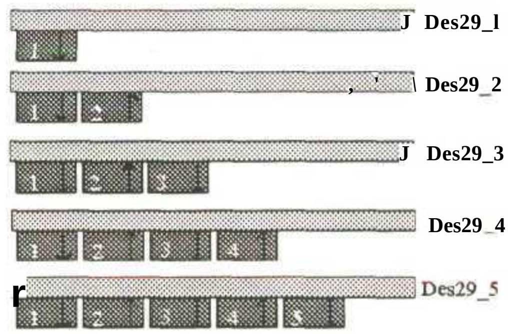

Figure 4.20: Geometric models setup for the parametric analysis.

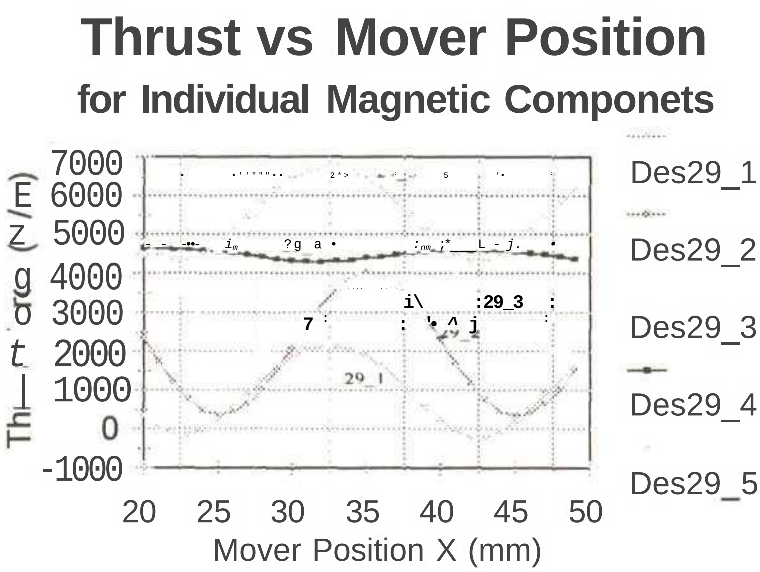

Figure 4.21: Thrust development per meter for PM assembly combinations.

The above results showed the courier could be designed with a PM assembly in sets of four. Taking into consideration cost, weight and the total thrust required, a courier which consisted of two set of four magnets was considered for further research. The summation of the thrust developed by eight individual PMs was compared to the thrust developed by a complete courier consisting of eight magnets. The results, shown in Figure 4.22, show a significant difference in the amount of thrust developed, with an increase in thrust fluctuations in the complete courier. The differences in the thrust curves can be attributed to the interaction of the PMs with each other and the generation of magnetic flux loops. Research into the magnets' effect on thrust development and fluctuations was undertaken.

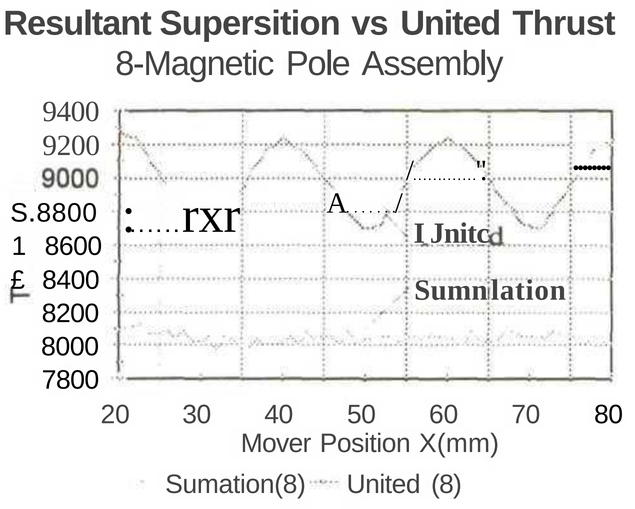

Figure4.22: Thrust developed for a complete 8-pole PM assembly versus the summation of the thrust developed by 8 individual magnets

Maintaining the magnetic pitch and width of the PMs in the courier, the effect of increasing the PM thickness on the thrust and normal force was modeled. The effect of a varying air gap length on the development of thrust and the normal force was also investigated. The courier was held in a stationary position and the currents in the armature were set to a constant value. This ensured that the results were not influenced by varying currents or different courier position. The parametric analysis varied the air gap length and calculated the forces developed by the motor. The results, shown in Figure 4.23, show the thrust declining significantly with an increasing air gap length, whilst the normal force shows minimal variation.

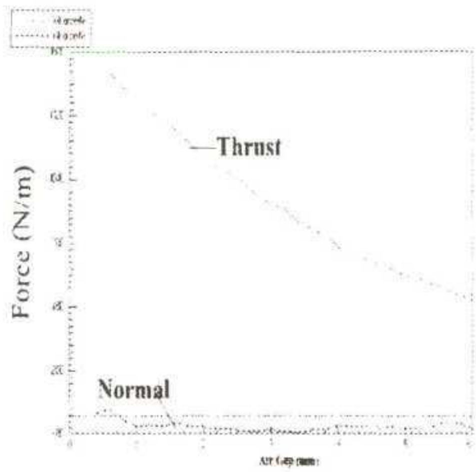

Figure 4.23: Thrust and normal force per meter vs air gap variations.

Since smooth air bearing surfaces were required between the courier and the armature platen, an air gap length of 3 mm was chosen for further investigation. The 3 mm air gap would allow for two bearing surfaces, such a sheets of polycarbonate, to be inserted in between the PMs and the armature coils. The effect of increasing the PM depth on the thrust and normal force development, for different air gap lengths, is shown in Figure 4.24 and Figure 4.25. The thrust increases with a increasing magnetic depth, from 3 mm to 7 mm, but maintains the rate of decline for an increasing air gap length. A PM depth of 7 mm generates the most thrust whilst developing the smallest and most stable attractive normal force for an increasing air gap length.

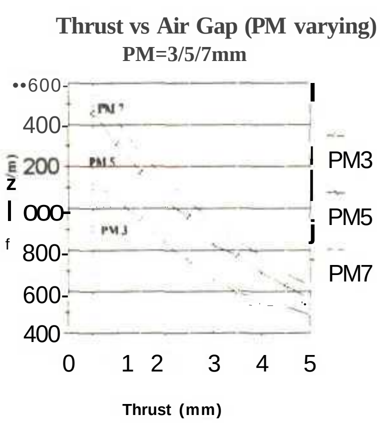

Figure 4:24: Thrust versus per meter air gap for varying for different PM depths

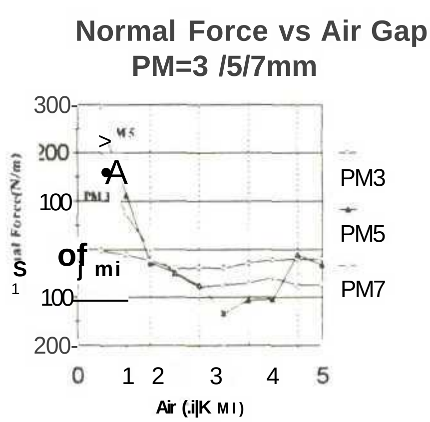

Figure 4.25: Normal force per meter versus air gap length for different PM depths.

The effect on the thrust and normal force for different magnetic widths, whilst maintaining the magnetic pitch ,t_m, equal to 15 mm, was also investigated. The magnet width was varied from 12 mm to the maximum of 15 mm. The results, shown in Figure 4.26, see the thrust increasing up to a width of 14 mm but decreasing as the magnet width approaches a maximum of 15 mm. From these results it would seem advantageous to increase the magnet width to 13 mm. However, the normal force increases with an increasing magnet width (shown in Figure 4.27). Further research was undertaken to study the effect of the magnet width in more detail, considering the magnet pitch to coil pitch ratio.

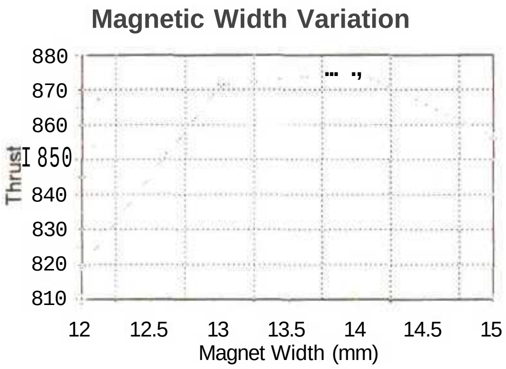

Figure 4.26: Thrust per meter developed for varying magnetic widths.

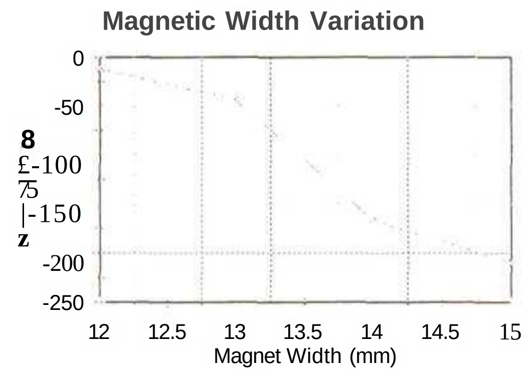

Figure 4.27: Normal force per meter developed for varying magnetic widths.

4.6.2 BACKIRON ANALYSIS

The function of the backiron is to provide a path for the magnetic flux. Since the backiron is made from steel it is subject to saturation. The thickness of the backiron is critical for ensuring that the flux has sufficient area to pass and that the backiron does not become saturated. The effect of various backiron thicknesses on the development of thrust and normal force was investigated. The thrust developed was relatively constant for backiron thicknesses greater than 4 mm. The normal force showed minimal variation for an increasing backiron thickness as shown in Figure 4.28. A backiron thickness of 5 mm was chosen for further design analysis. The overall design criteria when determining the backiron thickness was saturation. The saturation was determined in the final designs to verify the chosen backiron thickness.

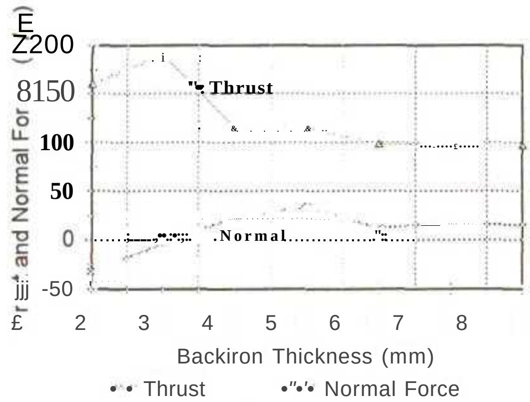

Figure 4.28: Thrust and normal force per meter versus varying backiron thicknesses.

4.6.3 ARMATURE PLATEN ANALYSIS

The original armature design was based on Anorad's LEB-S-2-S motor. The coil pitch was set to 20 mm. The coil width (CW) was set to 7 mm, leaving the distance between the insides of a coil (C3) set at 4 mm and the space between each coil (C4) at 2mm. The coil depth (Cd) was set at 7mm. (refer to Figure 4.29).

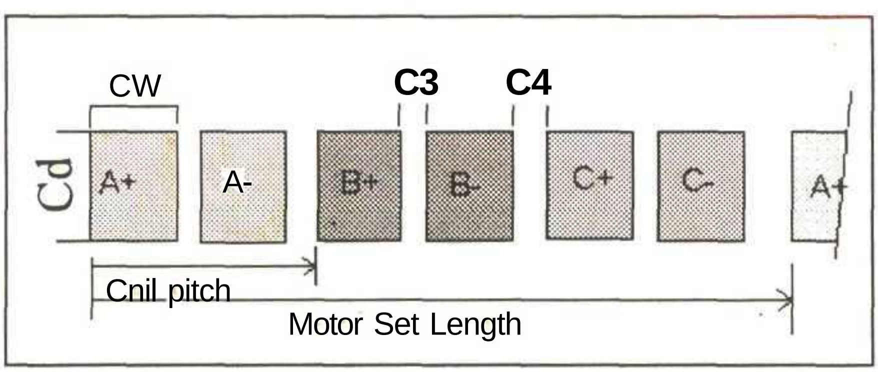

Figure 4.29: Armature platen geometry.

Provided the current is kept constant, variations in the coil dimensions will effect the current density. Increase in the current density increases the thrust and normal force developed by the motor. Thus, provided the current is kept constant, increasing the ceil depth will result in lower values of current density, reduced thrust and normal force. Figure 4.30 shows the results of increasing the coil depth of the armature platen. The coil depth is also dependent on the capability of physically wiring the desired number of turns into the specified space. The loss of thrust due to an increase in the coil depth can be compensated by increasing the magnet depth or increasing the current in each coil.

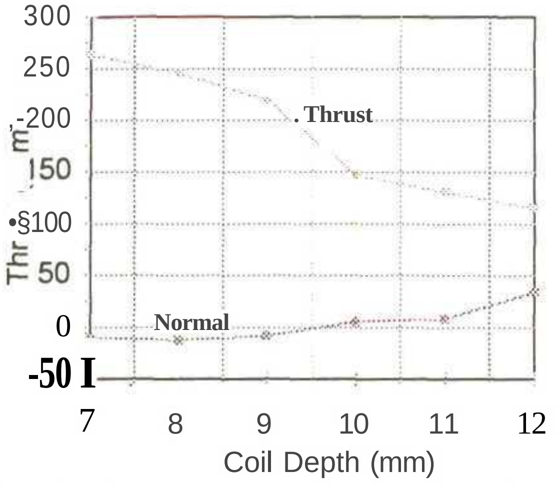

Figure 4.30:Thrust and normal force per meter for increasing coil depth.

Investigating the forces developed for increasing coil width, while keeping the coil pitch constant, revealed that the thrust decreased significantly. While keeping the ampere turns constant the coil width was varied from 6 mm to 8 mm. The thrust curves shown in Figure 4.31 revealed that a decreasing current density had no effect on the thrust fluctuations. The normal force developed under the same conditions revealed that it decreased for an increasing coil width and had no effect on the normal force variations as the courier moved over the armature platen. Although a low normal force was desired, a lower thrust would have to be accepted. A trade off to achieve the best solution resulted in the coil width being set to 7 mm.

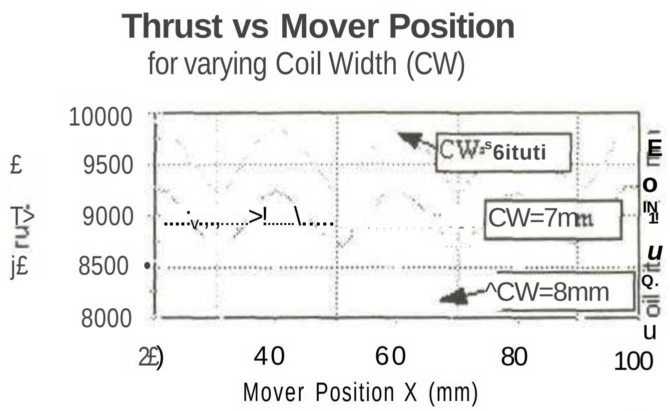

Figure 4.31: Thrust per meter developed for increasing coil width.

While maintaining the coil pitch and setting the coil width to 7 mm, the spacings C3 and C4 were varied to model the effect on the motor's performance. A parametric analysis was used to model the varying platen dimensions. The values for C3 and C4 were varied from 0 mm to 6 mm. Thus when C3 was set to a maximum of 6 mm, C4 was set to 0 mm, leaving no space between each coil. C4 was increased incrementally to 6 mm, whilst reducing C3 to 0 mm. The results depicted in Figure 4.32 and 4.33, show that the overall thrust decreased for an increasing space between the coils but had no effect on the thrust and normal force fluctuations. The largest magnitude of thrust was achieved by setting C4 =0 mm. The normal force, however, varies in magnitude for increasing coil spacings. The lowest normal force was achieved by setting C4 =4 mm. Thus a trade-off resulting in the optimum normal force to thrust ratio was achieved by setting C3 = 4 mm and C4 = 2 mm which was used in the final model.

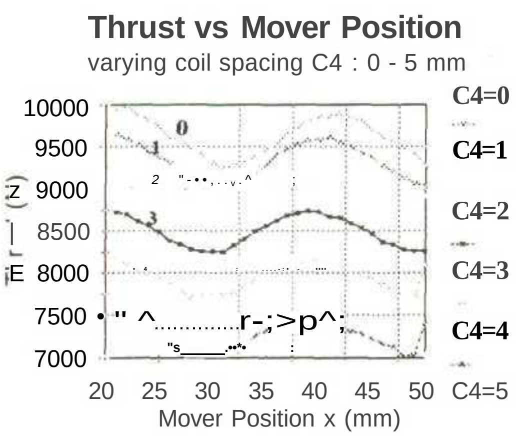

Figure 4.32: Thrust per meter for different mover positions for increasing coil spacings.

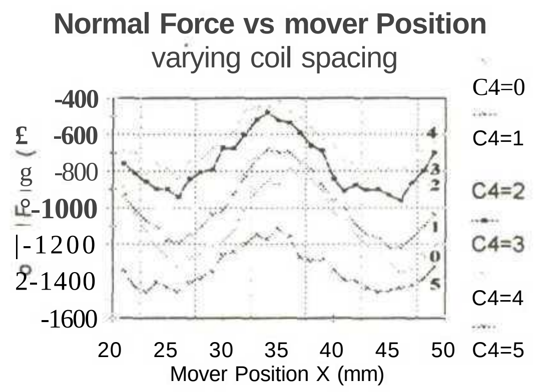

Figure 4.33: Normal force per meter for different mover positions for increasing coil spacings.

4.6.4 THRUST RIPPLE ANALYSIS

The PM thickness and width, coil depth and width and courier backiron have shown minimal effect on the thrust fluctuation which has been a characteristic of the thrust and normal curves generated by the finite element model. These parameters are termed static variations, affecting only the magnitude of the forces being developed. The coil pitch and magnet pitch have been kept constant while analysing the static design parameters. A reduction of the thrust fluctuations was investigated by modelling various magnetic and coil pitch lengths, while keeping the magnet pitch /coil pitch ratio constant. The original magnet pitch/coil pitch ratio was set to 1.333. Maintaining the magnet pitch/coil pitch ratio ensured that four magnets of alternating polarity cover one set of coils. This constituted a motor set. The motor set lengths were varied from 60 mm to 72 mm Table 4.4 shows a summary of the results obtained. The 7RNG implies that a coil width of 7mm is set with the space between the magnets increased from 1 mm to 3 mm for different motor set lengths.

The thrust variation averaged about 3% for the different motor set lengths. The increase in thrust was due to the increase in the magnet width, resulting in more magnetic material being exposed to the air gap.

DESIGN	Mae Pitch	Coil Pitch	Max (N/m)	MinfN/m)	Ranee(N)	Average	%Dev
7RNG_1_48	12 mm	16mm	6461.63	6082.24	379.99	6271.94	3.0
7RNG_1_60	15 mm	20 mm	9704.14	9157.64	546.50	9430.89	2.9
7RNG_1_72	18mm	24 mm	12149.50	11399.30	750.20	11774.40	3.2
7RNG_2_.60	15 mm	20 mm	9233.48	8694.08	546.70	8960.13	3.1
7RNG_2_72	18mm	24 mm	11817.10	11044.40	772.70	11430.75	3.4
7RNG_3_.60	15mm	20 mm	8528.86	8029.07	493.50	8279.11	2.9
7RNG_3_72	18mm	24 mm	11293.40	10590.10	703.30	10941.75	3.2

Table 4.4: Summary of results obtained for the 7RNG series of motor design.

The results obtained from the magnetic pitch/coil pitch ratio analysis showed no positive impact on the reduction of the thrust variation. The thrust curves generated displayed a thrust variation which was sinusoidal. Further analyses into thrust variations were modelled by varying the magnetic pitch/coil pitch ratio. Results obtained showed no effect on reducing the thrust variation generated by the motor. The thrust curves developed were unpredictable, with no periodic variation and large, rapid deviations. The results obtained from the finite element models for thrust variation analysis, showed that no significant advantage was gained by varying the magnetic pitch to coil pitch ratio or by varying the motor set length. Thus the magnetic pitch and coil pitch were kept at 15 mm and 20 mm respectively, keeping the ratio at 1.333.

A possible influence on the thrust variations by the finite element mesh was analysed. The *initial mesh* created by the 2D field simulator was very coarse initially. During the solution process, the adaptive refinement process increases the density of the mesh in areas of high error energy. It does not however adequately refine the mesh in areas of low energy. There was no reason to refine the mesh in areas where the magnetic field does not change rapidly. Where the magnetic field varies dramatically, such as in the air gap, or where flux is channeled through narrow areas, a mesh containing one or two triangles in that area proves to be inadequate. Manual refinement of the mesh in these areas helped the adaptive procedure to compute more accurate results. To obtain better results, the mesh over the magnetic assembly needed to be refined to a finer mesh. Figure 4.16 shows the initial mesh used to model the motor. Note the coarse mesh generated in the PM assembly area. A higher resolution is required to obtain a more accurate solution. There are three ways to refine the mesh, namely:

Point: Adds points to the mesh at the triangles where you click the mouse. These become the vertices of the new triangles.

Area: Refines the mesh within a defined rectangle.

Object: Refines a mesh within a selected object.

Two methods for adding points to a mesh are available:

Circumcircle: The point is added at the center of a circle whose circumference is defined by the vertices of the triangle, as shown below.

Centroid: The point is added at the center of the triangle. Both methods are shown in Figure 4.34 .

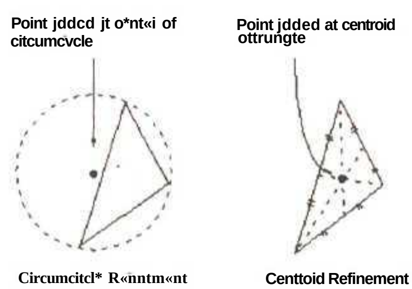

Figure 4.34: Manual mesh refinement by adding points to an existing mesh.

Circumcircle refinement produces triangles with lower aspect ratios (the ratio of the base of a triangle to its height) than centroid refinement. The triangles added using circumcircle method have sides which are nearly equal. The computational error in such triangles is generally lower than in "skinny" triangles with two long sides. To refine a mesh by area, the rectangle is defined in the selected area and the target number of triangles within the rectangle is specified. A method of adding points to the mesh must also be selected, either circumcircle or centroid. To refine the mesh within certain objects, either the desired number of triangles in each object or the minimum area of each triangle needs to be specified. Since the area of concern is the magnetic assembly, the number of triangles in each magnet and the backiron were doubled. The backiron was refined to 100 triangles and each magnet to 50 triangles. The mesh in the air gap was also refined by defining the area and increasing the number of triangles. Figure 4.35 shows the refined mesh which was used to model the motor's performance.

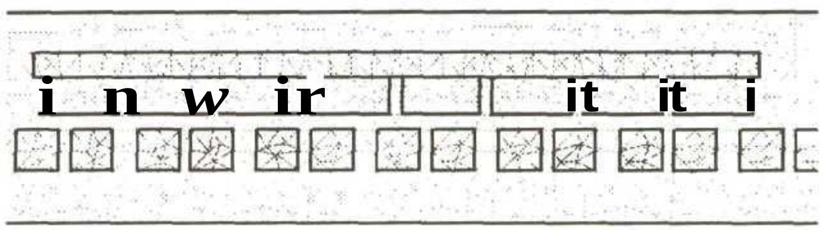

Figure 4.35: Manual mesh refinement

The refinement of the mesh is only valid for the "nominal" setup and is not valid for the parametric analysis model setup. Because the model's geometry changes for each setup, the initial mesh (Figure 4.16) is recreated for each step of the parametric analysis. In order to study the effect of modelling with a refined mesh on the thrust fluctuations, the motor was set up at various positions and the nominal solution was found using the refined mesh. The solution was then compared to the solution obtained from the parametric analysis for the same positions. The results from using the manual mesh refinement compared to the parametric analysis results are shown in figures 4.36 and 4.37.

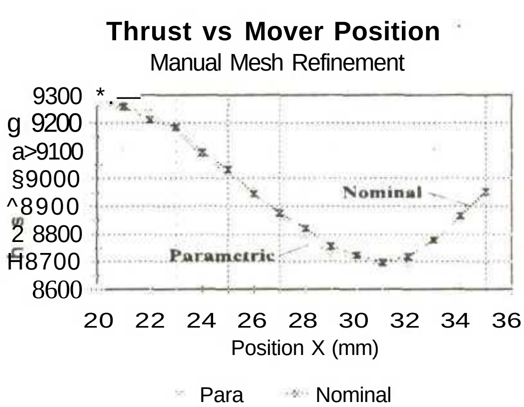

Figure 4.36: Thrust per meter developed comparing mesh refinements

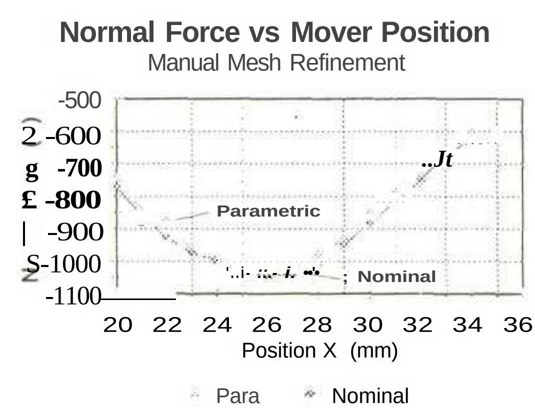

Figure 4.37: Normal force per meter developed comparing mesh refinements.

The nominal results using the refined mesh gave a better, more consistent curve compared to the initial mesh. The manual mesh refinement presents no solution to the periodic fluctuations in the thrust. The thrust variations developed by the motor had to be accepted as part of the motor's performance. A possible cause for the thrust variations was the single-sided design, which resulted in the unbalanced nature of the motor. This results in the magnetic flux being concentrated on only one side of the armature platen, with no regulated flux pattern set up by having a second set of PMs and backiron, as in Anorad's balanced LEB-S motor.

4.6.5 FINAL FINITE ELEMENT MODEL DESIGN

The geometric model was setup with the dimensions set to the optimum values determined by the analyses performed on the individual parameters. The courier, consisting of eight PMs with alternating polarity and a steel backiron, was positioned 3 mm above the armature platen. The magnet dimensions were set with a pitch of 15 mm, with magnet depth and width of 10 mm and 12 mm respectively. The coil pitch was set at 20 mm with a coil depth and width of 7 and 7.8 mm respectively. A finite element analysis was performed to determine the flux patterns and densities in the single-sided model. Figure 4.38 shows the flux lines setup by the PM assembly in the courier. The closed loop configuration of the flux lines was a indication that the alternating PM pole orientation was set up correctly.

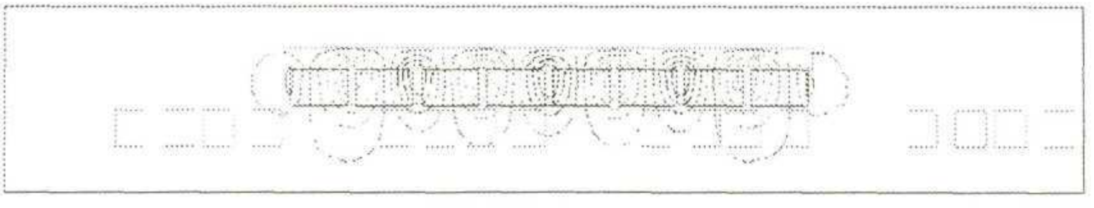

Figure 4.38: Magnetic flux lines in a cross-section of the motor.

The magnetic flux density distribution in the air gap is shown in Figure 4.39. The magnitude of the flux density is approximately 0.3 T, a reasonable value for a coreless motor and a reduced amount of PM material when compared to Anorads LEB-S-2-S motor.

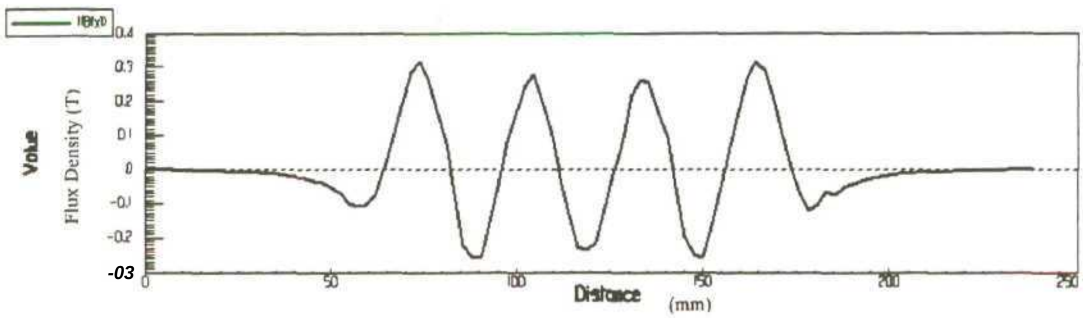

Figure 4.39: Magnetic flux density distribution (calculated) in the air gap below the PM assembly.

To determine the zero position of the motor, the currents in the three phase armature windings were *'frozen in time'* at a particular phase angle with respect to the starting position of Phase A. The currents were set by adjusting ϕ_0=60° and θ=0°. A parametric analysis was performed by varying the courier's position over the armature platen. Figure 4.40 shows the thrust produced by the motor. The zero position is determined by the position of the courier when zero thrust is produced. From Figure 4.40 the zero position was determined to be 20 mm. The thrust curve also shows that a zero position occurs every 30 mm, at x = 50 mm, 80 mm and 110 mm etc. Holding the courier in the zero position and adjusting the phase angle ϕ_0 from 0-360° whilst keeping θ =0°, the optimum value for ϕ_0 (developing the maximum amount of thrust) was determined. See Figure 4.41. A value of ϕ_0=330° was determined.

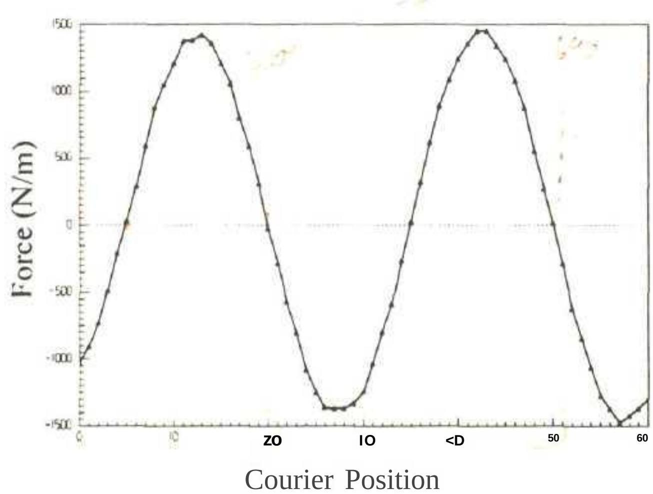

Figure 4.40: Determination of the zero position of the courier.

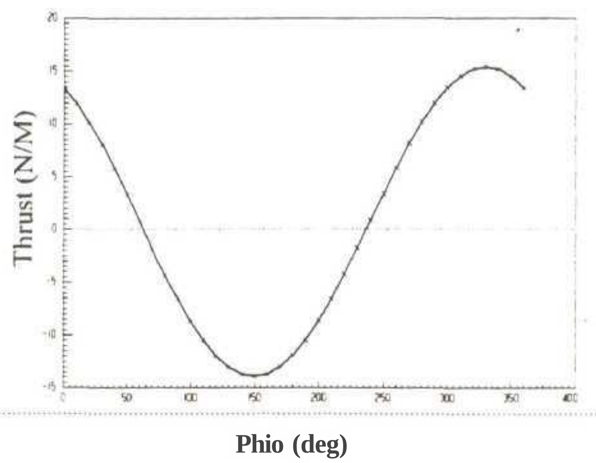

Figure 4.41: Thrust curve vs phase angle 4>$_0$ to determine the optimum value of 4>$_0$.

By adjusting the phase angle Φ_0 =330° the maximum thrust is generated in the zero position. If the courier is advanced from the zero position whilst maintaining 6 =0°, the thrust generated will vary sinusoidally. To maintain maximum thrust as the courier advances from the zero position, there exists an optimum theta value for each position of the courier. To determine the relationship between the theta and the courier's position, the courier was placed in a number of positions along the platen. In each position, the value for theta producing the greatest thrust, was determined. Using the theta values calculated, the linear relationship between 6 and the courier's position was determined as:

$$0 = 360\left(1 - \frac{x}{2l_m}\right) \qquad (4.20)$$

where x = mover distance from the zero position
and t_m = magnet pitch.

The expression for 6 shows that the period is equal to two magnetic pitches. The amount of ampere-turns required to create the calculated peak force (section 4.5) was determined by holding the courier stationary and adjusting the ampere-turns. Figure 4.42 shows the thrust per meter developed for increasing ampere-turns. Setting ^ equal to 250 ampere-turns, the final thrust and normal force per meter developed are shown in Figure 4.43.

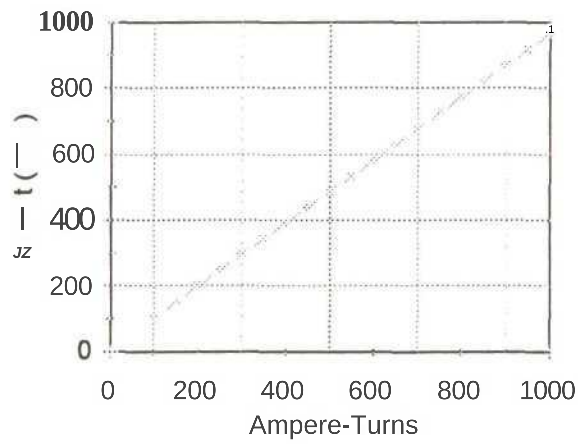

Figure 4.42: Thrust per meter developed for increasing ampere-turns.

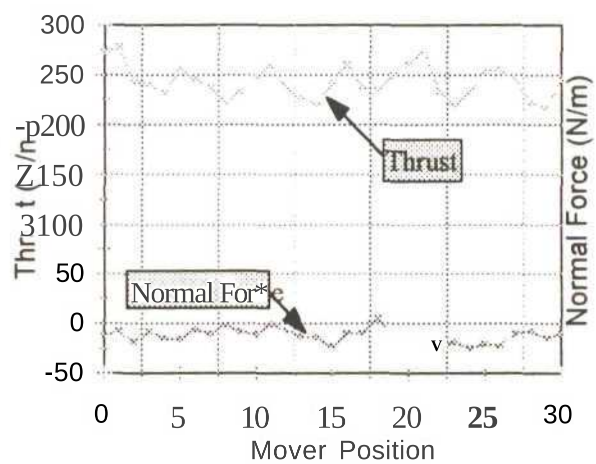

Figure 4.43: Thrust and normal force per meter for different courier positions

4.6.6 EFFECTIVE MOTOR LENGTH

The results obtained from 2D finite element analysis are per unit length. To determine the motor's final thrust and normal force development, the results shown in Figure 4.43 had to be multiplied by the motor's effective length. The motor's effective length is determined by :

$$\textit{Thrust / meter} \times \textit{effectivelength} = \textit{PeakForce} \quad (4.21)$$

The thrust per meter was determined by taking the average of the thrust values from the final model. An average of 240.47 N/m was obtained. The required peak force of approximately 20 N was calculated from the kinematic analysis performed in Section 4.5. The motor's effective length was set to *1=118 mm.* Once the motor's effective length had been determined, the final thrust and normal force curves could be plotted as shown in Figure 4.44.

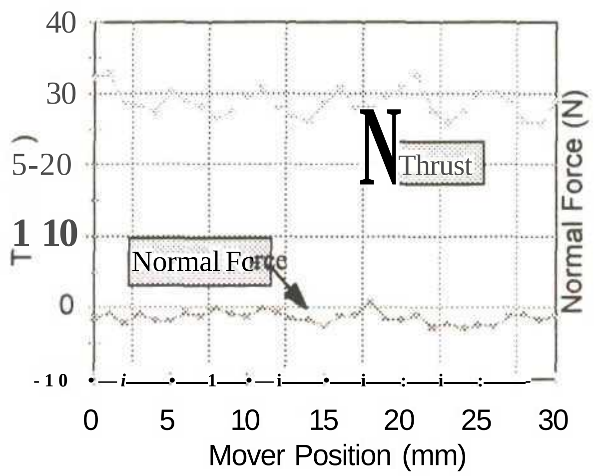

Figure 4.44: Final thrust and normal force developed for the finite motor length.

The effective length of 118 mm resulted in the motor developing an average thrust of 27.97 N which is higher than the calculated peak force. A larger thrust was chosen to counter any losses in thrust due to possible differences between the finite element model and the physical prototype. The magnetic flux density in the backiron was plotted to determine if the backiron was saturated. Figure 4.45 shows a plot of the magnetic flux density at a maximum of 250 ampere-turns. The flux density is at a maximum in the backiron between the PMs. The maximum flux density value of 1.7269 T was below the 'knee' of the 1010 Steel B-H curve, indicating that the backiron was not saturated and a 5 mm thickness was sufficient.

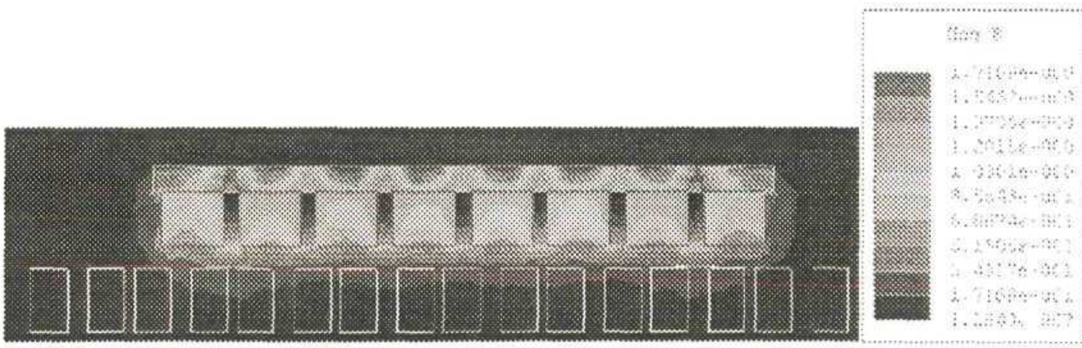

Figure 4.45 : Magnetic flux density distribution at 250 ampere turns

4.6.7 WINDING CALCULATIONS

The results obtained from the finite element model design determined that 250 ampere-turns (A-T) were required to produce the desired thrust. To determine the number of turns per coil and the current per turn, the current density and packing factor had to be calculated. A relatively low current density was required to eliminate the need for forced cooling of the armature platen. The specified coil area, A_t, is calculated by:

$$A_t = CW \times Cd \qquad (4.22)$$

where: CW is the coil width.
Cd is the coil depth.

The total conductor area (A_{cu}) is determined by the product of the conductor area (A_{cond}) and the number of turns (N) in the coil. It is expressed as:

$$A_{cu} = N \times A_{cond} \qquad (4.23)$$

Since neither the conductor area nor the number of turns are known, estimations of the packing factor were determined. The packing factor (k_p) is an indication as to how well the coils are packed into the specified area and is calculated as the ratio of the total conductor area to the specified coil area:

$$k_p = 4 \wedge \qquad (4.24)$$

Initial estimates of the packing factor were made by assuming that the specified coil area was a square whose sides were equal to the diameter of the total conductor area, d_{cu} Thus an initial value for the packing factor was:

$$k_p = \frac{\frac{\pi}{4} d_{cu}^2}{d_{cu}^2} = \frac{\pi}{4} = 0.785 \qquad (4.25)$$

The initial packing factor was used to calculate the total conductor area and hence the conductor area, A ^ , and the number of turns through iteration. A spread sheet was used to calculate possible solutions to the above equations. The results are presented in Appendix C. The diameter of the conductor was selected from data sheets for commercially available copper wire which matched the calculated conductor area. The copper wire data sheets are available in Appendix C. The current density (j) is calculated by:

$$j = \frac{\{A- \quad T)l \quad N}{\;''_{cond}} \qquad (4.26)$$

The results obtained for the iterations performed using the above equations are presented in Table 4.5.

Ampere-turns	250 Ampere-turns
Number of turns	100
Current	2.5 Amps
Conductor Diameter	0.71 mm
Current Density	6.314 Amp/mm^2

Table 4.S: Winding Results for armature coil development.

The specified coil area proved to be too small to physically wind and fit 100 turns. The depth, Cd, of the specified coil area had to be increased to 12 mm to accommodate the required number of turns instead of reducing the conductor diameter, which would result in an increased current density. Increasing the current density would result in a need for forced cooling of the armature. The increase in the coil depth was remodeled on the finite element model. The reduction in thrust compared to the original thrust obtained is demonstrated in Figure 4.46.

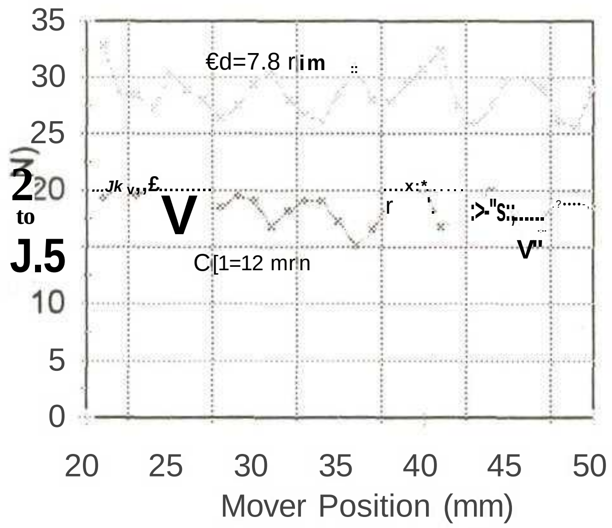

Figure 4.46: Thrust comparison for increased coil depth from 7.8 mm to 12 mm.

The increase in the coil depth resulted in the thrust decreasing to an average of 18 .072 N. The reduction in the thrust was accepted, as it was relatively close to the magnitude of the desired peak force calculated in section 4.5. The coil width and pitch were kept the same and the decreasing in the thrust was accepted as a compromise for an increase coil depth, Cd. This also insured that forced cooling would not be required.

4.6.8 DESIGN SUMMARY

The finite element results presented determined the motor's design parameters. The parameters were used to create a physical prototype. A summary of the results determined from the finite element model is presented below. Figure 4.47 show a schematic of the proposed LSM for the material handling system.

Physical Dimensions

Conductor Diam[illegible]

Current density

PM Courier	
PM Depth	10 mm
PM Width	12 mm
PM Pitch	15 mm
PM Length	118 mm
Backiron Thickness	5 mm
Armature Platen	
Coil Depth	12 mm
Coil Width	7 mm
Coil Pitch	20 mm
Coil Spacing (C3)	2 mm
Coil Spread (C4)	4 mm

Coil Specifications

Number of Turns	100
Conductor Current	2.5 Amps

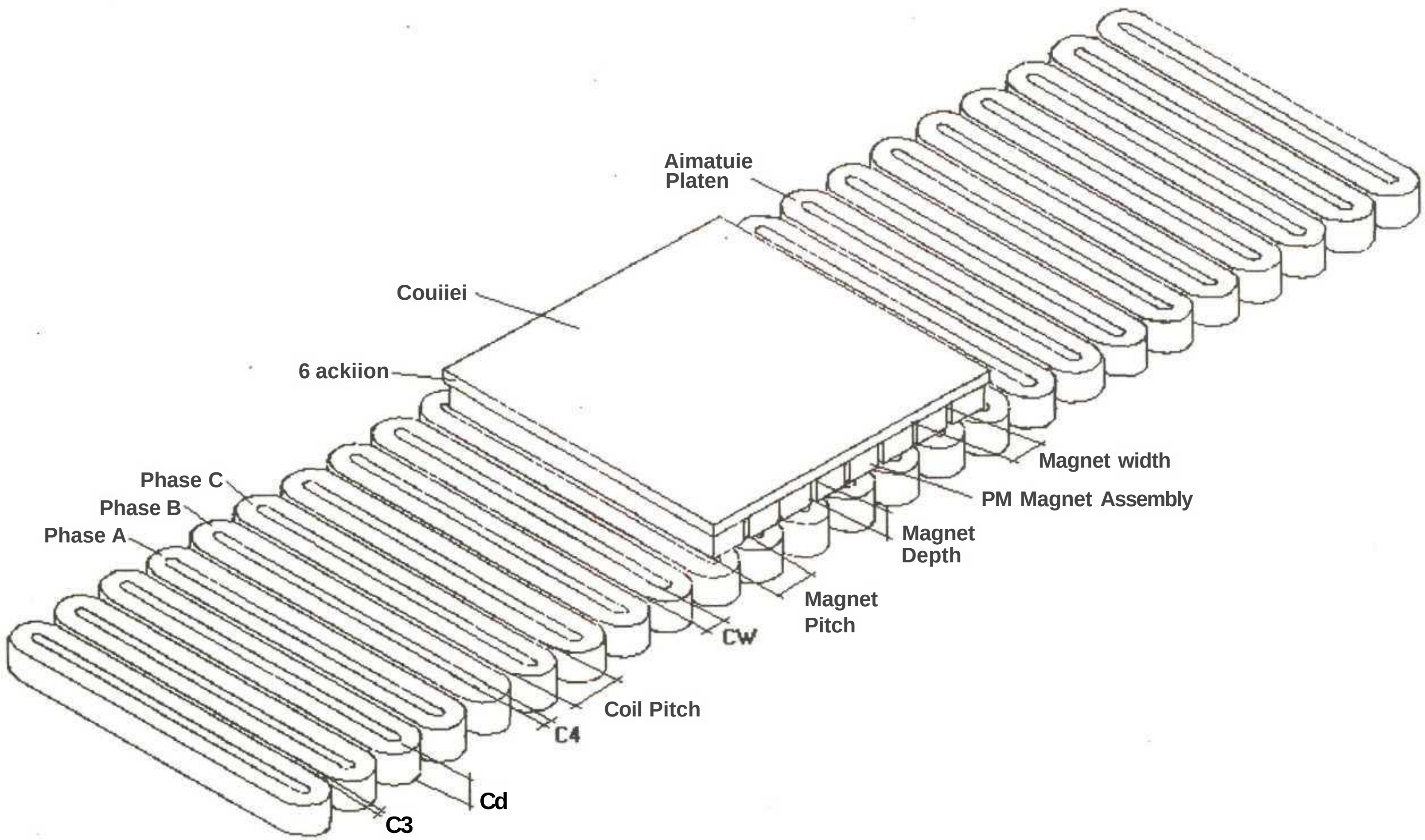

Figure 4.47: Schematic diagram of proposed LSM showing the dimensional notation

5. BEARING TECHNOLOGY

5.1 INTRODUCTION

The unbalanced design of the CLSM material handling system resulted in a normal force existing between the courier and the armature platen. The normal force together with the weight of the courier required the development of a bearing system to be developed. The purpose of the bearing system was to maintain the air gap between the courier and the armature platen, allowing the courier to move with ultra smooth motion. The courier would be free from any tether restrictions and so be able to move over large distances. Three main bearing systems were investigated, namely magnetic, mechanical and air bearing systems. Magnetic bearing systems studied included electromagnetic levitation with permanent and electro magnets and simple but costly permanent magnet bearing systems. Mechanical bearing systems studied embraced linear guidance systems, including ball and roller bearing systems. Air bearing systems studied included aerostatic and aerodynamic air bearing systems. The results obtained from researching the individual bearing systems led to the proposal and design of a unique reverse air bearing system.

5.2 MAGNETIC BEARINGS

Magnetic bearing systems are classified according to the levitation forces by which they operate, namely attractive and repulsive systems. An example of an attractive system is a system which uses PMs as moving components suspended under dc electromagnets which are on a stationary track. [Athert on et al] Examples of a repulsive system are one which uses PMs levitated above a superconductor and one which uses using two PMs with the same poles facing each other.[Williams et al] The physical set up of attractive systems does not make them suitable for many applications, as the design restricts access to the carrier from below. Generally, it is desirable that the carrier travel above the guide tracks for convenient access to the load. For this reason, only repulsive magnetic systems were explored. A proposal using a PM facing PM repulsive systems was investigated and systems with magnetic levitation using permanent magnets and electromagnets were investigated.

5.2.1 PERMANENT MAGNET LEVITATION

Levitation systems using PMs have been uncommon due to the low strength of PMs and their unreliability in high temperature environments. Large PMs were required to achieve sufficient levitation force. Developments in PM technology like rare earth PMs, such as NdFeB PMs, have overcome these problems. When PMs are used in a repulsive levitation system, with the same poles facing each other, the z-axis (levitation height) is stable. However, the x and y axes are unstable. If one magnet is kept stationary on the ground, the other magnet is levitated above it, but it is laterally unstable because of lateral destabilizing forces. In principle there can be no stable levitation between two time-invariant magnetic fields. Figure 5.1 shows a schematic drawing of a proposed PM levitation bearing system which consists of two pairs of PMs on each side of the courier. The horizontal PMs create the repulsive force required to levitate the courier above the platen. The vertical PMs stabilize the courier in the y axis. Stabilization of the PM levitation system in the x axis (the direction of travel) is achieved by controlling the current in the armature. This produces a force on the courier counteracting the de-stabilization force.

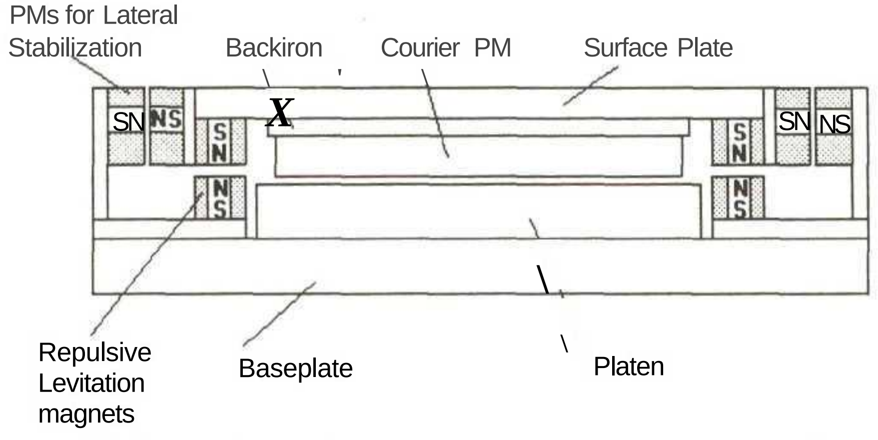

Figure 5.1 :Proposed magnetic levitation using PMs to levitate and stabilize the courier as it moves down the platen track.

The proposed PM levitation system for the CLSM material handling system was reject for the following reasons:

- The lateral de-stabilization in the x-directioh (direction of travel) would result in a need for increased control. The de-stabilization force would vary unpredictably, retarding or assisting the courier's motion. This would decrease the motor's performance.
- There would be varying levitation height for varying loads. The levitation height would increase or decrease as the load changed, resulting in varying air gap lengths, thus affecting the motor's performance.
- Cost. The proposed levitation system would cost approximately R7 000 per meter to manufacture.

5.2.2 ELECTROMAGNETIC LEVITATION

Electromagnetic levitation systems have been designed for high speed transportation systems. [Wang et al, He et al] There has been minimal research into the suitability of their design for factory automation systems. Research into developing stable magnetic levitation systems has been undertaken. Magnetic Bearing Stages have been developed for performing wafer positioning in photolithography. [Hocken et al] If the upper magnet in a PM levitation system is stabilized by additional stabilizers with the introduction of proper feedback control, and the lower magnet is replaced by an electromagnet, a stable repulsive levitation system can be obtained. [Tzeng et al] A new repulsive magnetic levitation system for silicon wafer handling has been developed. The material handling system consists of three subsystems: levitation, stabilization and propulsion. The system uses PMs and air-core electromagnets to levitate the silicon wafer carrier. The carrier has four sets of PMs attached to the base. These PMs are repulsively levitated by four oblong shaped electromagnetic tracks. Due to the lateral instability of repulsive levitation, the" stability of the levitated PMs is regulated by electromagnetic stabilizers. Stabilization coils run the length of the tracks above the levitation coils. Figure 5.2a shows a levitation track consisting of levitation coils, a permanent magnet and stabilization coils. In order to provide velocity and positioning capabilities, an electromagnetic propulsive system is placed in the center of the four levitation tracks. [Bush-Vishniac et al] Figure 5.2b shows an overview of the silicon wafer transportation system. The development of such a levitation system for the CLSM would prove impractical. The control system required is complex with separate controllers required for levitation and stabilization. The number of levitation tracks required to limit the effect of rotational forces on the carrier would make the system bulky and complex. Due to the open track design, the system's applications would be restricted to clean room environments. The advantages of such a system are that the carrier is free from tethers and the non-contact bearing system allows for ultra smooth motion.

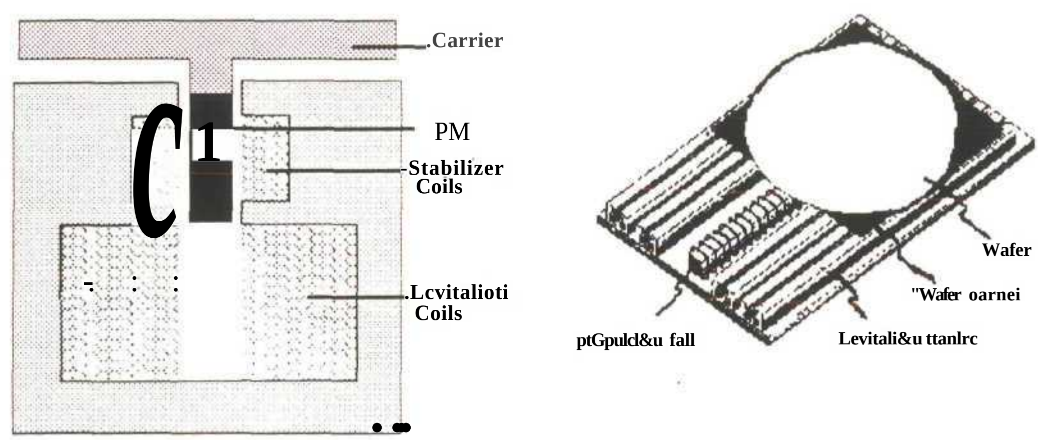

Figure S.2:(a) Sectional view of a levitation track, [Bush-Vishniac et al] **(b) Overall view of the wafer handling system**

Electromagnetic levitation systems in general were excluded as possible bearing systems due to the increased complexity that would be added to the project. Electromagnetic levitation systems are designed for specific applications and require a comprehensive design and analysis to be undertaken to ensure their optimal performance. The effect of electromagnetic fields on the motor's performance would have to be determined. The two systems would possibly have to be isolated and controlled separately. The cost of feedback sensors for levitation height and stability control was also regarded as a negative factor.

5.3 MECHANICAL BEARINGS

The two types of mechanical or contact bearings commonly used are crossed roller bearings and ball bearings. Crossed roller bearings have a line of contact between the roller and the raceway, whereas ball bearings have a point contact between the ball and the raceway.Roller bearings have a greater contact area and can therefore take greater loads. Less surface deformation and wear over the roller surface occurs as the load is distributed more evenly. However, increased contact results in increased friction. Ball bearing systems have a smaller contact area resulting in reduced friction, but limited loading capacity. Figure 5.3 shows the line and point contacts for roller and ball bearing systems and their deformations under load.

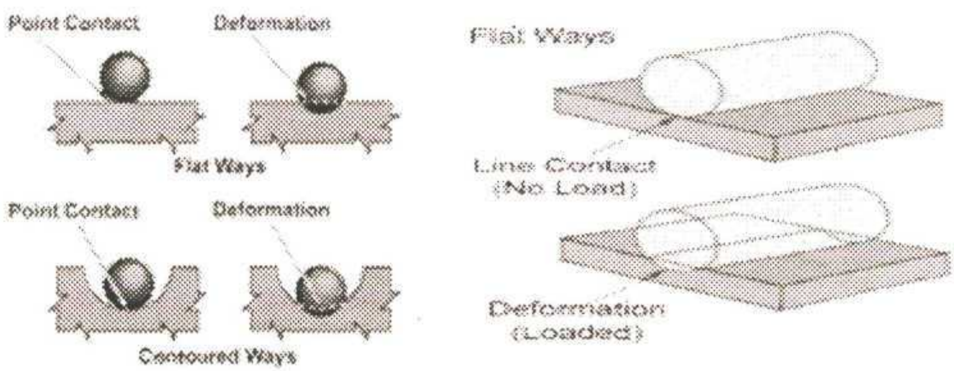

Figure 5.3: Point and line contacts and deformations for ball and roller bearings. [Trilogy_l]

The advantages of contact bearings are high load bearing capabilities ,low maintenance, low friction and less sensitivity to load variations. Disadvantages include friction (when compared to air bearing systems), mechanical wear, increased vibration through ball and roller movement in the raceway and unsuitability for clean room environments. Three main types of linear guidance systems use roller and ball bearing mechanisms: monorail guidance systems, track roller guidance systems and shaft guidance systems.

Monorail guidance systems are designed with either linear recirculating roller bearings or linear recirculating ball bearings in a carriage. The carriage runs on a linear guidance track to create a linear guidance system. Carriages with roller bearings can withstand greater static and dynamic loading when compared to carriages with recirculating ball bearings. [INA] A schematic diagram of a linear recirculating roller bearing and guideway track is shown in Figure 5.4. Linear recirculating ball bearing carriages are used for systems where loads are less and increased positioning accuracy and friction are desired. A schematic diagram of a linear recirculating ball bearing carriage and guideway track is shown in Figure 5.5.

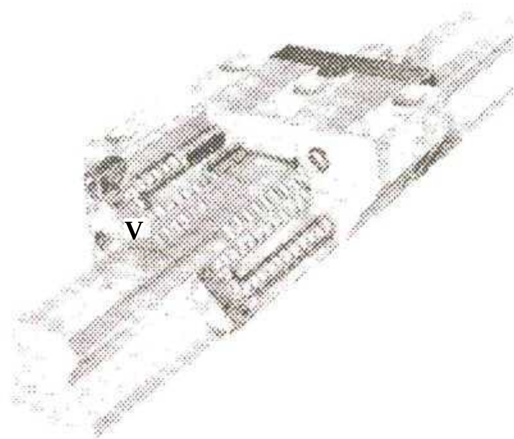

Figure 5.4: Recirculating roller bearing carriage and linear guideway.|INA)

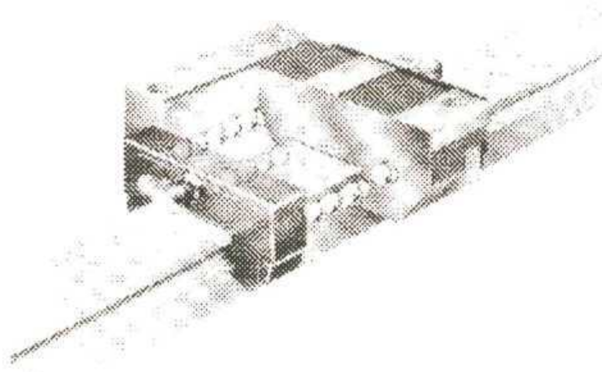

Figure 5.5: Recirculating ball bearing carriage and linear guideway.|EVA]

Track roller guidance systems consist of a guidance track with roundbar mounted on both sides along the track. The carriage consists of four track rollers which run along the roundbar. An advantage of such linear guidance systems is that the carriage is capable of running on curved guideways. Figure 5.6a shows a track roller guidance system. Shaft guidance systems consist of a shaft on a mounted support rail with a linear ball bearing system within a housing. Shaft guidance systems are less costly than monorail and track guidance systems. The reduction in cost is due to the specially machined guidance track being replaced with a steel roundbar. Positioning accuracy is lower than monorail and track guidance systems however. [INA] Figure 5.6b shows an example of a shaft guidance system.

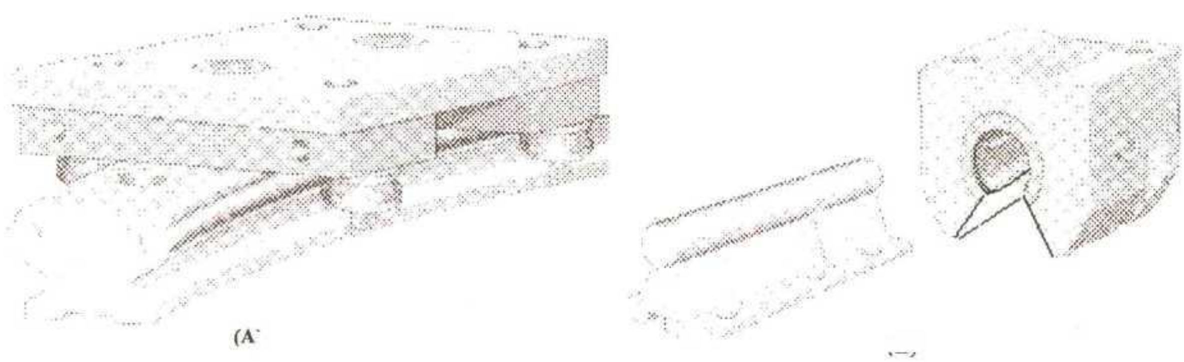

Figure 5.6 :(a) Track roller guidance system, (b) shaft guidance system

A shaft guidance system was proposed as a bearing system for the CLSM material handling system. The proposal consisted of two sets of guidance shafts mounted on a base plate on either side of the stationary armature platen. A carrier plate, attached to the linear bearing housings running on the shafts, carries the PM courier mounted below. Figure 5.7 shows an illustration of the proposed bearing system.

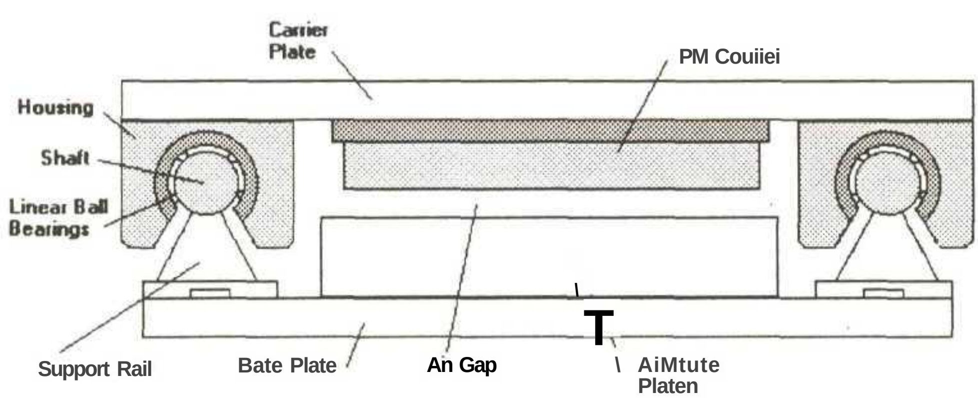

Figure 5.7: Mechanical bearing system proposal using shaft guided linear ball bearings

The advantages of implementing a shaft guidance bearing system are: high bearing load capabilities, the courier is free of tether restrictions, easy to install, low maintenance, off-the-shelf systems and no control system is required. Disadvantages of such a system include: susceptibility to vibrations, friction, reduced positioning accuracy compared to monorail and track guidance systems, unsuitability for clean room environments. The implementation of such a bearing system was a viable option. The simplicity of its design and operation made the system an attractive proposal.

5.4 AIR BEARINGS

Aerodynamic and aerostatic bearing systems, commonly known as air bearings, have a considerable advantage over oil lubricated or hydrodynamic film lubricated bearings. Some inherent advantages are higher precision, increased accuracy, better resolution, clean room compatibility, longer life and improved reliability. There is also minimal heat generation due to zero friction and the operating temperature range is far greater. [Grassam et al] One of the most critical elements is the bearing assembly. There are a number of air bearing types namely steady self-acting bearings, journal bearings, thrust bearings and conical bearings. Aerodynamic bearings rely on the movement of the opposing surfaces to develop the bearing pressure film, whilst aerostatic bearings are commonly referred to as externally pressurised bearings. Figure 5.8 shows the difference between the two types of air bearings.

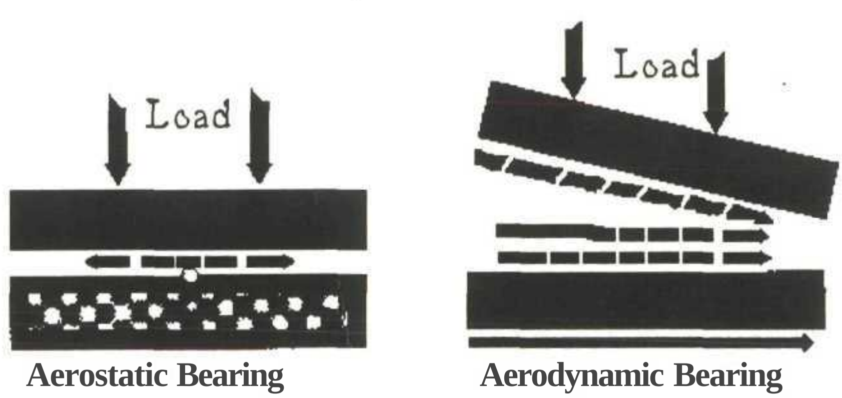

Figure 5.8: Aerostatic and aerodynamic gas bearing.[Dover)

Air bearing systems have become more prominent in linear motor applications. This is due to their having the advantage of being non-contact bearing systems. Most air bearing systems used in positioning stages are externally pressurised bearing systems. Thus they require a continuous pressure source and feed line and work by a squeeze film action. An appreciation of the mechanism of squeeze- film action may be obtained by observing the spread of a drop of liquid between two flat glass plates as they are squeezed together. When the clearance between the plates is very small, the speed with which the liquid spreads is far greater than the speed of approach of the glass plates, thus creating a pressurized film between the plates. [Geary] Air bearings are used in X-Y positioning stages, providing ultra smooth motion and positioning capabilities. [Gizal]. The use of air bearings with linear motor positioning stages provide straightness of travel which is unmatched when compared with traditional mechanical bearings. [Townsend] The development of micro-inch accuracy stages has been made possible by frictionless air bearings capable of 0.5um planar accuracy. [Lynch] Air bearings are beginning to replace mechanical bearing systems in actuators and end effectors. The design of multi-degree-of-freedom spherical actuators has been enhanced through the development of air bearings, allowing increased positioning accuracy in fine motion applications. [Ezenekwe et al]

5.4.1 PRINCIPLE OF OPERATION

Figure 5.9 shows the basic structure of an externally pressurized thrust bearing. When the machine is to be operated, the supply pressure(Ps) enters the pocket. The pressure builds up in the pocket until it reaches a pressure (P,) at which it is able to lift the pad clear off the slideway. This action initiates a flow of air through the inflow orifice and the pocket to the pad extremities. Thus a pressure drop occurs from the supply pressure to final escape pressure, usually atmospheric pressure. The land faces are exposed to a pressure difference which is P, at the inner edges and which falls progressively to P_o at the outer edges.

The normal force from the air film resisting the approach of the surfaces results only from the relative motion of the two surfaces in the direction of their common normal. [Geary] The resistance of the air film to flow is proportional to the velocity at which it is caused to flow and to its viscosity. The air flows between the plates only because pressure is created in the film of the fluid. The pressure in the film resists the attempt to squeeze the plates together. Thus it can be said that squeeze film action is a consequence of the extremely rapid motion of the air between the plates.

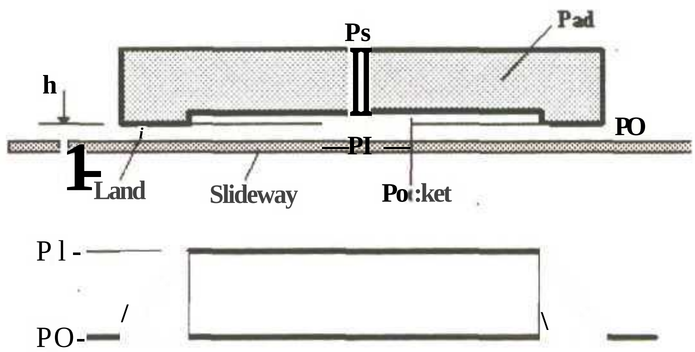

Figure 5.9: Externally pressurized air bearing notation and pressure distribution.

The size of a pocket in an air bearing should be kept to a minimum. If the pocket is too large then the compressibility of the gas enclosed in the pocket results in delays in the response of the steady-state value of the pocket pressure to a sudden change in the clearance height due to load variations. 'Pocket-less' designs are best suited for air bearing applications. In this case the 'pocket' consists of the space immediately under the hole, which occupies no more than a negligible fraction of the bearing area. The air pressure falls progressively all the way from the edge of the hole to the outer edge of the bearing pad. With an increase in the load on the bearing, the pad approaches the slideway thus decreasing the film thickness and increasing the outflow resistance. The inflow resistance increases and therefore the pocket pressure P, will increase to balance the new load. The air bearing is said to have a self regulating action. [Geary]

5.4.2 AIR BEARING DESIGN

The advantages of implementing an air bearing system for the CLSM are increased positioning accuracy, zero friction and ultra smooth travel. A disadvantage of such a system is the tether restriction which would be needed to supply pressurized air to the courier as it moved over the platen. The tether restricts the travelling distance and flexibility of the system. A bearing system which operated without tether restrictions and still managed to carry the bearing load successfully was required. The concept of suppling the air through the platen to the vicinity of the courier as it moves over the platen was researched. The principle was tested by developing a manifold which split the air into separate lines and fed into a pattern of orifices in a perspex plate representing the armature platen. Figure 5.10 shows the experimental setup used to test the reverse air bearing principle. The direct line supply method proved extremely successful with the test model bearing successfully levitating 5.5 kg on 0.5 bar supply. To aid with the generation of smooth, straight travel, the implementation of side bearings was also investigated. The principle of operation is still the same as a normal externally pressurized bearing pad.

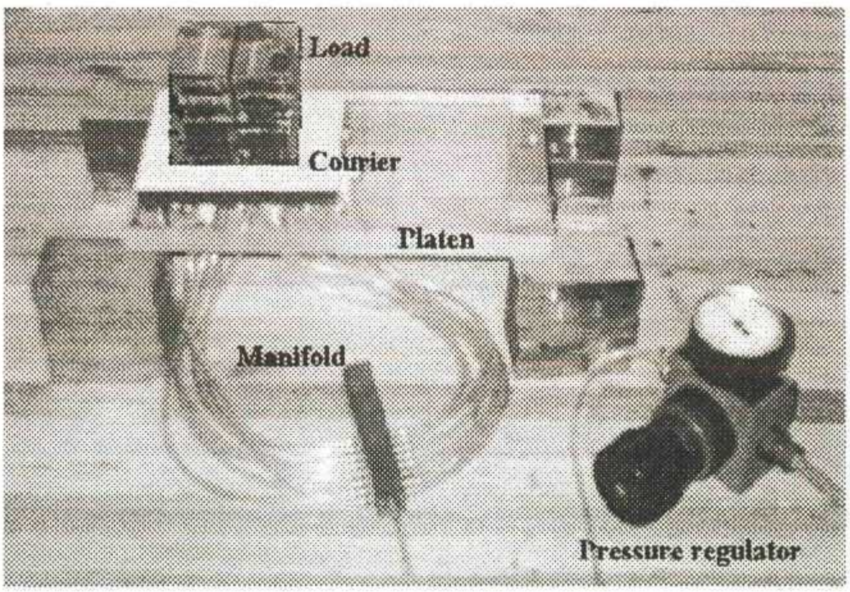

Figure 5.10: Reverse air bearing testing system using direct line supply concept.

The integration of the air supply lines through the armature platen was the critical design factor. The space between the phases, determined by the finite element model, was 2 mm. This was insufficient for the orifices to supply air. The distance inside the coil loops was 4 mm. This space was used to integrate an orifice pattern to supply air to the courier.

5.4.3 REVERSE AIR BEARING DESIGN THEORY

5.4.3.1 GENERAL EQUATIONS

The general equations of motion for fluid between parallel plates, shown in Figure 5.11, with constant viscosity across the film thickness (h) is given by [Constantinescu];

$$\frac{\partial p}{\partial x} = \mu \frac{\partial^2 u}{\partial^2 y} \qquad (5.1)$$

$$\frac{\partial p}{\partial y} = 0 \qquad (5.2)$$

$$\frac{\partial p}{\partial z} = \mu \frac{\partial^2 w}{\partial^2 z} \qquad (5.3)$$

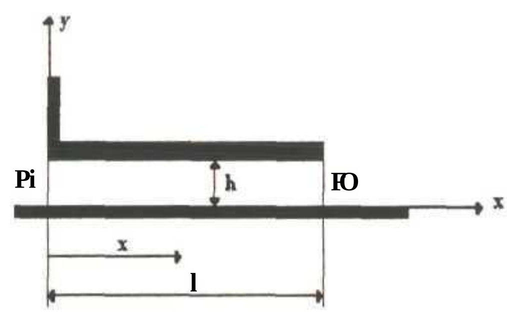

Figure 5.11: Flow of a gas between two parallel plates

If the film thickness is small compared to the length l, the flow will be relatively slow so the temperature can be assumed to be constant at every point. Thus the pressure and the density are connected by the simple relationship ;

$$\frac{p}{\rho} = const \qquad (5.4)$$

From the boundary conditions integrating equation 5.1 yields the velocity profile,

$$« = -±\%(h-y) \quad \text{(5.5)}$$
$$2p \;\; dx$$

Assuming the bearing surfaces are stationary, ie VI = V2 = 0 m/s^2, the equation for continuity is given by;

$$\wedge - \int_0^h \rho u dy = 0 \quad \text{(5.6)}$$
$$ox$$

From the relationship expressed in equation 5.4, we get

$$\partial/\partial x(\rho\, \partial p/\partial x)/\partial x = O \quad \text{(5.7)}$$

Integrating equation 5.7 and applying boundary conditions, yields the pressure distribution in the form of;

$$p^{11} = C_x x + C_2 \quad \text{(5.8)}$$

where C, and C_2 are determined by the boundary conditions (BC);

from BC of x = 0, $p=Px$

$$P?=C_2; \quad \text{(5.8a)}$$

from BC of x-- $l,p= p_0$

$$Po^2 = C_x l + C_2 \quad \text{(5.8b)}$$

thus obtaining;

$$P^2 = P?-(p'-Po^2)x/l \quad \text{(5.9)}$$

or

$$plPo = [Px^2 IPo - iPx^2 IPo^2 - \backslash)xll\backslash^2 \quad (5.10)$$

If $p_,/p_0$ is small, the pressure variation is almost linear as in the case of incompressible flow. Thus it can be assumed that p is constant and equation 5.10 reduces to;

$$P = P\backslash \sim(P\backslash - Po)^x/^1 \quad (5.11)$$

Thus the resulting thrust per unit width is;

$$FA = _0\{V\ A\rangle\&= \backslash\wedge P\%^J P - Po' \quad (5.12)$$

from equation 5.8,

$$2p = C, \frac{dx}{dp} \quad \text{therefore} \frac{dx}{dp} = \frac{\wedge}{C,} \quad (5.12a)$$

substituting equation 5.12a, yields;

$$F_A = \int_{Pl}^{I} \frac{-7T-dp-}{C_l} P_O l = \frac{-\!\!-_2}{^J Pi \sim Po} -jl- Pol \quad (5.13)$$

The resulting thrust is for one side of the bearing only, therefore the total thrust per unit width is expressed as;

$$F_A = \frac{4}{3} \frac{\wedge K\, 2\, l P_O\, l}{P\backslash - Pi} \quad (5.14)$$

The resultant thrust F_A is the force generated for the fluid as it travels over the lands of the air bearing. The total lifting force includes the major load bearing force of the pocket at pressure

P, and the load sustained by the lands.

5.4.3.2 PLATEN BASE DESIGN

The CLSM platen was divided into eight sections to cover the travel distance of the courier. The number, size and pattern of orifices required per section was restricted by the primary coils dimensions and pitch. The total area of the orifices is determined by calculating the vent area,

$$Va = Perm x h \quad (5.15)$$

where Perm is the perimeter of the courier and h is the bearing film thickness. The bearing film thickness was estimated at 150um.The courier dimensions were taken from the finite element model. The courier's overall dimensions were set at 126 mm by 126 mm square. Thus

$$V_A = 0.000189/w^2 \quad (5.16)$$

The total orifice area for each section is taken as two times vent area;

$$A_t = 2xV_A \quad (5.17)$$

The orifice quantity and pattern was chosen as a simple matrix pattern of 18 orifices with 3 rows and 6 columns. Thus the orifice diameter was estimated to be,

$$d_o = \sqrt{\frac{A_t}{ii} \times n} \quad (518)$$

An orifice diameter of 1.63mm was required. Due to the space constraints, the size of the orifice diameter was reduced slightly to 1.5mm. Knowing the load required to be levitated and the courier dimensions, the required pocket pressure (P,) could be calculated by

$$P = W/A \quad \text{(5.19)}$$

Referring to equation 5.13, the total thrust on the courier generated by the film pressure can be expressed as,

$$F_{total} = \left[\frac{2}{3} \frac{(p_1^3 - p_0^3)}{(p_1^2 - p_0^2)} \times l \times b \right] \times 2 + p_1(a \times b) - p_0(2l + a) \times b \quad \text{(5.20)}$$

Although the courier does not have an actual pocket, the area under the bearing's central region develops an almost constant pressure due to the comparatively large number of orifices. The pressure falls to P_o from the outer orifices to the courier's outer edges. It is assumed that the air falls to P_0 only at the courier's leading and trailing edges and that no air escapes on the sides due to the side bearings. Figure 5.12 shows the orifice pattern and constant pressure area. To ensure smooth continuous travel, the orifice pattern is regular and continuous for each platen section. The supply pressure to each section is split by a manifold into the required supply lines per section and fed through the platen.

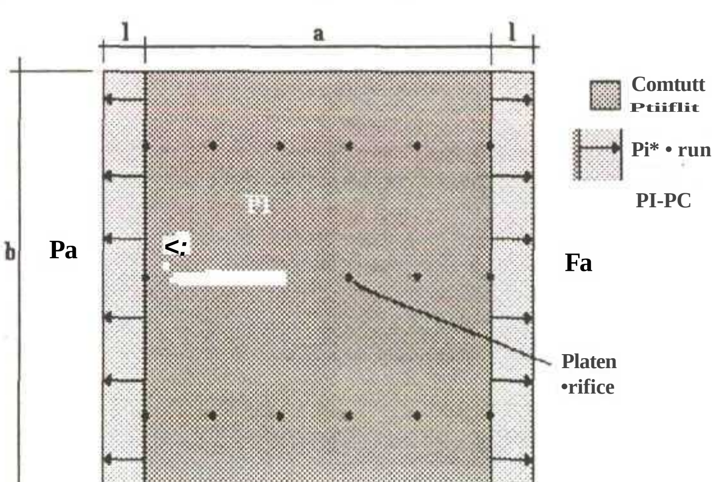

Figure 5.12: Platen orifice design and pressure distribution under the courier.

As the courier moves down the platen, the air is supplied to the corresponding manifold. This feeds air through the platen section and carries the required load. The switching of the air supply to the correct platen section is supplied by connecting each manifold to a solenoid valve. The switching of the corresponding solenoid valve is dependent on the courier's position. This ensures optimal usage of air by not pushing air through the entire length of the platen. Side bearings were also designed to increase the straightness of travel and to counter any lateral forces developed by the CLSM. This provided a complete cushion of air on all three sided of the courier, producing a frictionless bearing system.

The reverse air bearing was chosen as it provided the advantages of a conventional air bearing system but also allowed the courier the freedom to travel over large distances, unrestricted by tethers.

6. CONSTRUCTION

6.1 INTRODUCTION

The dimensions obtained from the finite element model were used to construct a prototype. A prototype consisting of a platen, approximately one meter in length was constructed. The construction of the LSM was categorized into two main sections namely the PM courier and the armature platen. The reverse air bearing system was constructed and integrated into the armature platen. The air manifolds were designed to be suspended on a level frame beneath the length of the platen. The machine and assembly drawings are presented in Appendix C. A schematic overview of the material handling system prototype is shown in Figure 6.1

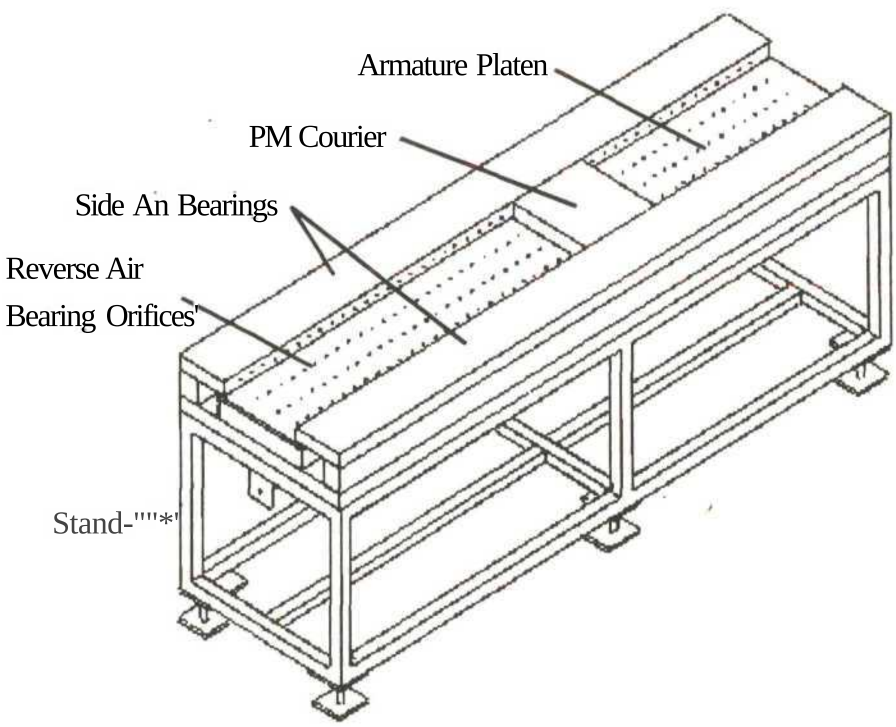

Figure 6.1: Overview of the prototype material handling system.

6.2 LSM CONSTRUCTION

6.2.1 COURIER

The courier was constructed by assembling the NdBFe PMs onto the backiron with alternating poles. The backiron dimensions were calculated to be 120 x 120 mm. This left a 1 mm hangover over the edge of the magnet assembly. The backiron was machined from 1013 Steel as 1010 Steel is not readily available commercially. The machine drawings for the backiron are presented in Appendix D-l. The PM dimensions were taken directly from the finite element model results. Ten Grade N38 NdFeB PMs with a anti-corrosive zinc coating were ordered from Technical and General Distributions. The machine drawings for the PMs are presented in Appendix D-2. The zinc coating was selected to prevent the magnets from oxidizing. The magnets were attached to the backiron. Nonmagnetic spacers (clear polycarbonate) were used to separate the magnets and maintain the magnetic pitch. To create the smooth air bearing surface required on the courier for the reverse air bearing and side bearings, a 1.5 mm polycarbonate plate was used to enclose the courier. The overall courier dimensions were 126 x 126 x 16.5 mm. To separate loads from the PM courier, a platform of perspex was created 30 mm above the backiron. Figure 6.2 shows an overall view of the courier with the platform.

Figure 6.2: Permanent magnet courier with carrier platform.

6.2.2 PLATEN CONSTRUCTION

6.2.2.1 FRAME

A coreless armature was chosen to eliminate cogging thrust. The coils could be placed side by side and sealed in epoxy or slotted into a non-metallic frame to create the armature platen. By sealing the armature coils in epoxy, they would become a 'black box'. Should any fault occur with one of the windings, the entire armature platen would have to be replaced. Since this was an undesirable feature, a non-metallic slotted frame was developed to create the armature platen. Electrical grade tufnol was chosen as suitable material to manufacture the armature frame. The dimensions for the tufhol frame are presented in Appendix D-3. To create the armature frame, slots were milled out of an electrical grade tufnol plate. The frame was used to keep the armature coil pitch constant and maintain the coil spacings. The dimensions of the slot pitch, depth and width were taken from the finite element results for the coils.

6.2.2.2 WINDINGS

The three phase armature windings were wound in the Electrical Engineering Workshop. A custom engineered coil 'former' was developed to create the armature coils. No commercial armature winders for linear motors were available in South Africa, thus a tool for creating the coils to be inserted into the tufnol frame was required. A coil set consisted of three coils for each phase. Fifteen coil sets were required to create an armature platen of 900 mm. Thus 45 coils of 100 turns had to be wound using the former shown in Figure 6.3. The former was designed to be bolted together and the coils wound onto the former using a lathe (as shown in Figure6.4). Once the required 100 turns were wound onto the former to complete the coil, the coil was bound to hold the turns together. The former was then unbolted and the completed coil was removed from the former and inserted into the slotted frame. The former design and assembly drawings are presented in Appendix D-4.

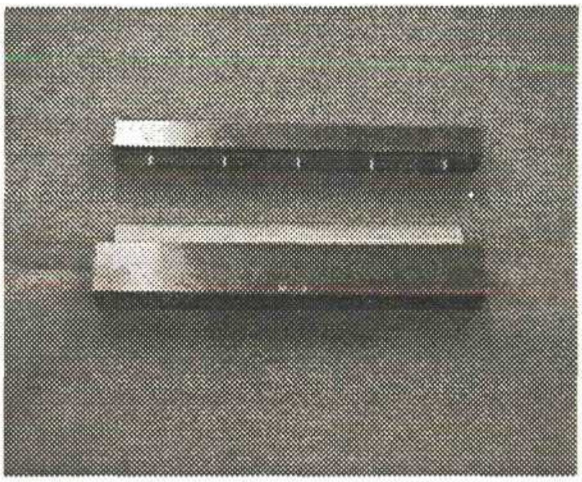

Figure 6.3: The coil former used to wind the armature coils.

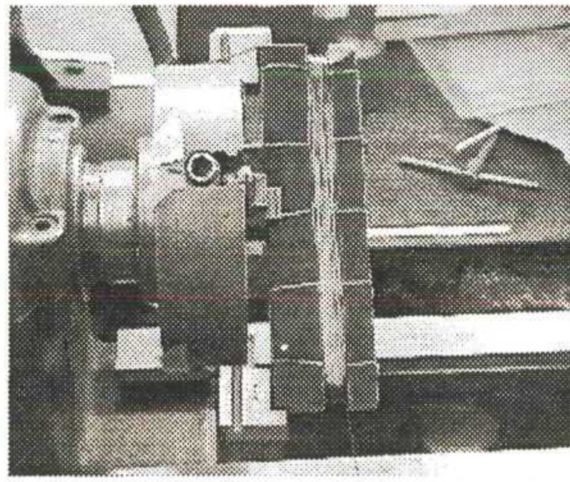

Figure 6.4: A coil being wound on the lathe using the former.

To keep the coils in the slots, nylon ties were used to secure them. Eight holes were drilled along each frame slot and the nylon fed from the bottom, over the coil and out through the frame again. The coil was then pulled and bound into position in the slot. The construction of the armature platen is shown in Figure 6.5.

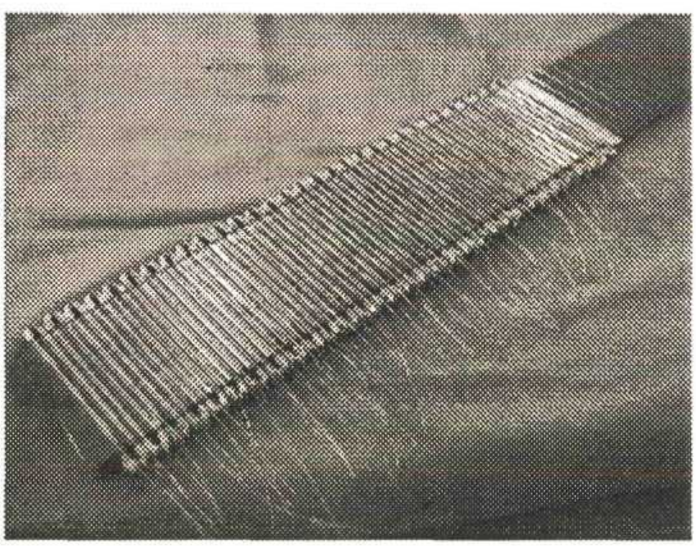

Figure 6.5: Armature platen under construction.

The construction of the armature platen was completed by joining the phases together. The coils of similar phases were joined in series. Thus the first coil was joined to the fourth coil and every third coil thereafter to create the phase A windings. Continuity tests ensured that good electrical connection was obtained between each coil. The total resistance for each phase was measured at 24.2 ohms. The phases were connected in *star* or Y connection form. Thus the phase endings were wired together to match the y-connection shown in Figure 6.6. Due to the balanced load, the neutral point was not connected to ground. Due to undesirable circulating currents in the A and triplen harmonics the delta (A) connection was not used. [Hanselman] Delta connection of phase windings is shown in Figure 6.6. Advantages of Y-connection is the reduction in the number of power electronics required, an absence of triplen harmonics and the fact that each phase contributes equally to the force production. Thus each phase experiences the same losses and the drive electronics can be identical for each phase [Hanselman].

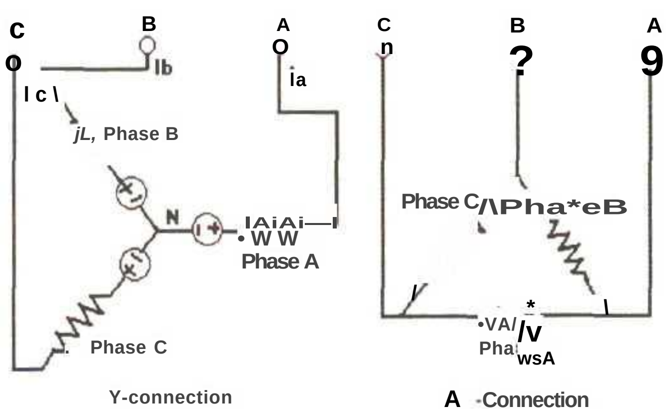

Figure 6.6: Y-connection used to wire the armature platen compared to a A- connection.

6.3 REVERSE AIR BEARING CONSTRUCTION

The air bearing system was developed with the aim of integrating the air bearing into the armature platen, thus ensuring that the courier would remain levitated at all times. The platen was divided into eight bearing pads. Each bearing pad was controlled separately, only working when the courier was travelling over the bearing pad. This ensured optimization of air supply demand and sufficient pressure to the correct bearing pad. The orifice pattern and density was determined by the space between the coils. The space between each phase was 2 mm. This was regarded as too small to drill a 1.5 mm diameter hole. The space between each coil was

4 mm. The orifice density chosen was a simple grid pattern of 3 evenly spaced holes between each coil. Each bearing pad consisted of 6 rows of 3 orifices. To supply air to each orifice in a bearing pad, air pipes were inserted into the base of the tufhol frame, as shown in Figure 6.7.

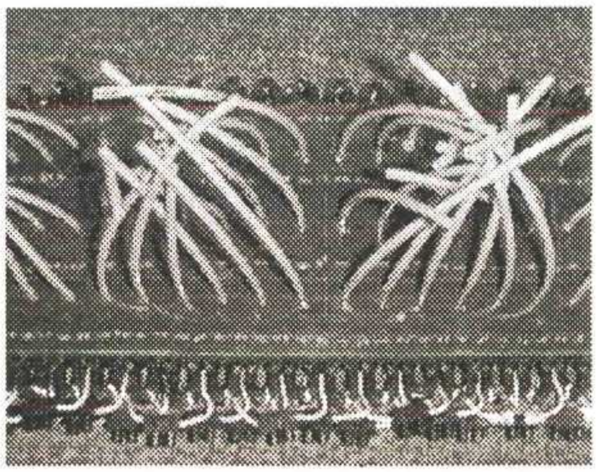

Figure 6.7: The direct air lines into the frame base for each bearing pad.

The side air bearings were constructed from perspex plates and positioned to decrease the possibility of any lateral movement or skewing of the courier. The orifice pattern for the side air bearing was designed as a single row of holes with a pitch of 20 mm to correspond with the orifices in the platen. Thus each bearing pad consisted of 6 side bearing holes on each side to ensure smooth frictionless motion of the courier. A section of a side bearing is shown in Figure 6.8. The assembly drawings for the side bearings are presented in Appendix D-5.

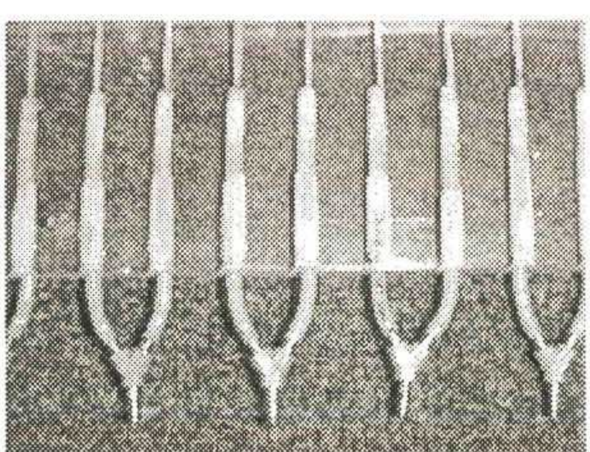

Figure 6.8: One side of the side air bearing which supplied air to the vicinity of the courier as it travelled down the platen.

Air manifolds were manufactured to supply air to each bearing pad. Each direct line from a bearing pad was attached to a manifold outlet pipe. A manifold consisted of twenty four outlet pipes. Eighteen of the outlet pipes were assigned to the reverse air bearing lines from the frame. The remaining six outlet pipes were assigned to the side air bearing lines. The manifolds were manufactured from mild steel square bar. The square bar was machined out and outlet holes drilled into the central hole. Copper tubing was inserted and soldered into the holes to create the outlet pipes. The air lines were inserted onto the copper outlet pipes. The air manifold assembly drawings are presented in Appendix D-6. Figure 6.9 shows a manifold for a bearing pad.

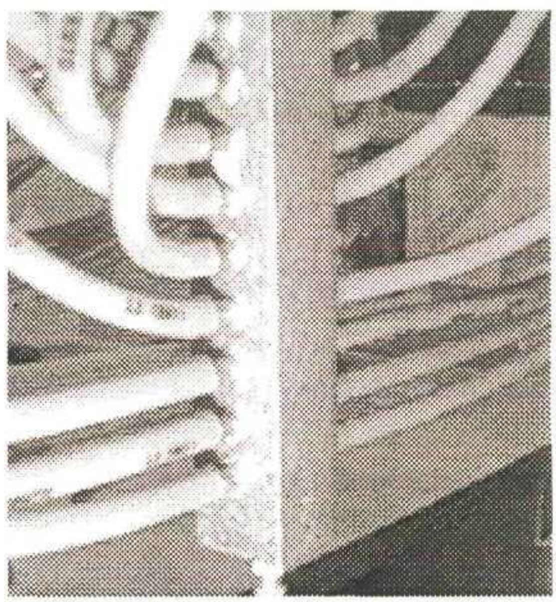

Figure 6.9: Air manifold to supply air to each orifice in the platen bearing pad.

To create the smooth bearing surface required, a 1.5 mm thick polycarbonate plate was placed on top of the platen. The orifices were drilled through the polycarbonate plate to match the orifice pattern in the tufnol frame. The drawings are presented in Appendix D-7. The bearing surface plate on the bottom of the courier and on top of the armature platen were also used to maintain the 3 mm air gap. The air manifolds are supplied with pressurized air from CPV solenoid valves. Each bearing pad is assigned a solenoid valve which is energized only when the courier is present. To regulate the required pressure a pressure regulator was placed between the compressor supply line and the solenoid valves. Figure 6.10 shows eight solenoid valves and the pressure regulator setup. The switching of the solenoid valves is done using the position feedback of the courier.

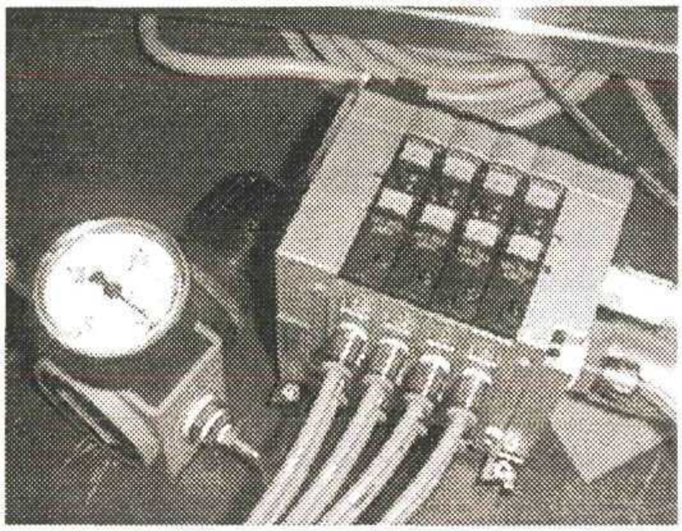

Figure 6.10: Solenoid valves and pressure regulator supplying air to the required manifolds.

6.4 STAND DESIGN AND ASSEMBLY

For the air bearing to operate properly, the bearing surfaces had to be level. A stainless steel stand with adjustable feet was developed. Stainless steel was used for it's non-magnetic properties. The air manifolds were suspended from the frame below the platen. The adjustable feet were used to level the material handling system to ensure the air bearing operated properly. The frame assembly drawings are presented in Appendix D-8. Figure 6.11 shows the stand under construction.

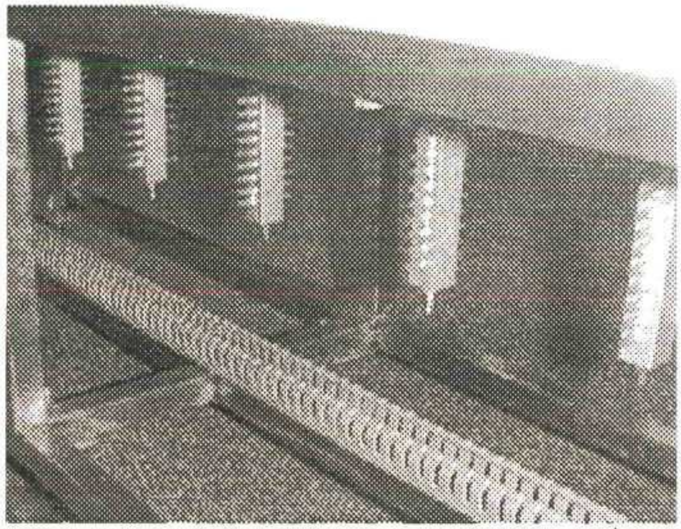

Figure 6.11: Stand with air manifolds positioned below their respective bearing pads.

A polyethylene base plate was bolted to the frame. The platen was attached to the base plate. To create a base for the side bearings to be placed so that they were level with the platen surface, side walls were constructed. The design and assembly drawings are presented in Appendix D-9. Figure 6.12 shows an exploded view of the material handling system assembly.

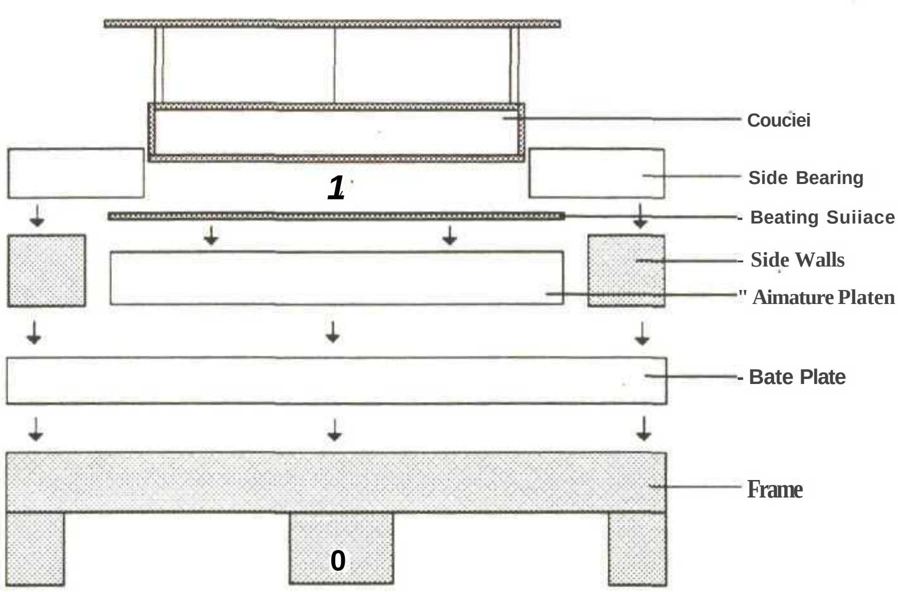

Figure 6.12: Exploded view of the material handling system assembly.

Figure 6.13 shows the final assembly of the cordless linear synchronous motor material handling system with the courier on the platen with the integrated reverse air bearing and side bearing.

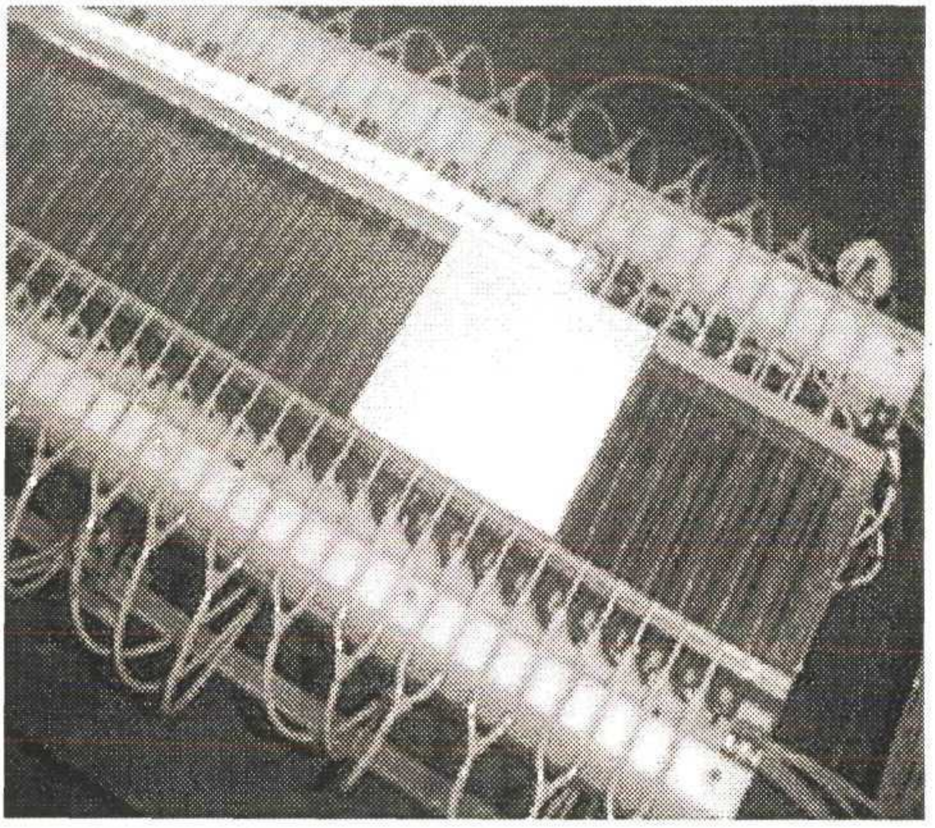

Figure 6.13: Material handling system with cordless courier and integrated reverse air bearing armature platen.

7 CONTROL

7.1 INTRODUCTION

The control of the CLSM MHS was developed in two main streams. The CLSM control system was developed with emphasis on thrust development and the courier's speed and position. The control of the air bearing system was developed to be independent from the varying motor's control variables and any external parameters. The various controllers and system architectures studied are presented, together with the different position feedback systems. A non contact position sensor was required to ensure the courier remained free from tether restrictions. This limited the choice of position feedback systems and dictated which controllers could be used.

The development of the chosen motor control system is outlined, together with the air bearing control system employed to ensure optimal performance of the CLSM MHS. A graphical user interface (GUI) was developed to create a simple operator interface for easy operation of the CLSM MHS. Emphasis was placed on developing a control system architecture which was highly software based. This software based control architecture allows for control variables to be changed easily and for the system to be expanded and integrated into higher control levels. The key design aspect of the chosen controller is the ability to share as much information as possible with other systems. This making integration into a manufacturing system, such as a CIM cell, a simple task.

7.2 POSITION FEEDBACK DEVICES

The tether-less design ensured that the courier was free to travel over large distances. To achieve position feedback on the courier, a non contact position sensor had to be chosen. The three main types of sensor technologies used are; inductive, magnetic and optical. The most common form of position feedback sensor used in industrial applications is the linear optical encoder. Incremental and absolute linear optical encoders were not investigated as a possible position feedback devices due to the tetherless design restriction. Laser technology, which has found increased applications in high performance systems, was explored as a possibility. Linear magnetic encoders were also studied together with ultrasonic sensors to determine their suitability. The position feedback system chosen was based on the ability of the sensor to complement both the courier's tether-less design and the drive system.

7.2.1 LASER MEASUREMENT SYSTEMS

Laser measurement is accomplished using the technique of interferometry. Laser interferometry uses the wavelength of light as a basic unit of measurement. An interferometer measures the distance by counting the number of wavelengths of light that one element moves relative to another. All light rays of laser light have exactly the same wavelength and are in phase with each other.[Renishaw] Figure 7.1 shows a laser measurement application being applied to the CLSM MHS. Referring to Figure 7.1, the laser interferometer system works in this way:

1. The outward laser is split into two beams. One half passes directly through the beamsplitter optic. The second is reflected through 90°.
2. Then both of the beams are reflected through 180° by retro-reflector optics. The high quality retro-reflector optic has the ability to return a laser beam parallel to the entry path.
3. On their return the two reflected laser beams converge to form pulses of constructive and destructive interference.
4. The detector optics within the laser then count these returning pulses. By counting the number of pulses, the change in distance between the two optics can be monitored and the distance determined.

The implementation of a laser measurement position feedback system presented the best possible solution to providing a non contact position feedback device. The courier remains free from any tether restriction. The courier is also free to travel over large distances using the laser positioning system. In addition, the laser measurement systems provide the greatest accuracy and are the accepted positioning feedback device in ultra-high precision X-Y stages. [Lynch] The major disadvantage of the system is the cost. The cost of the laser system, excluding the retro-reflector optics, is in the Rl 5 000 to R20 000 range [Nova]. Due to budget constraints, this makes the implementation of such a system unviable.

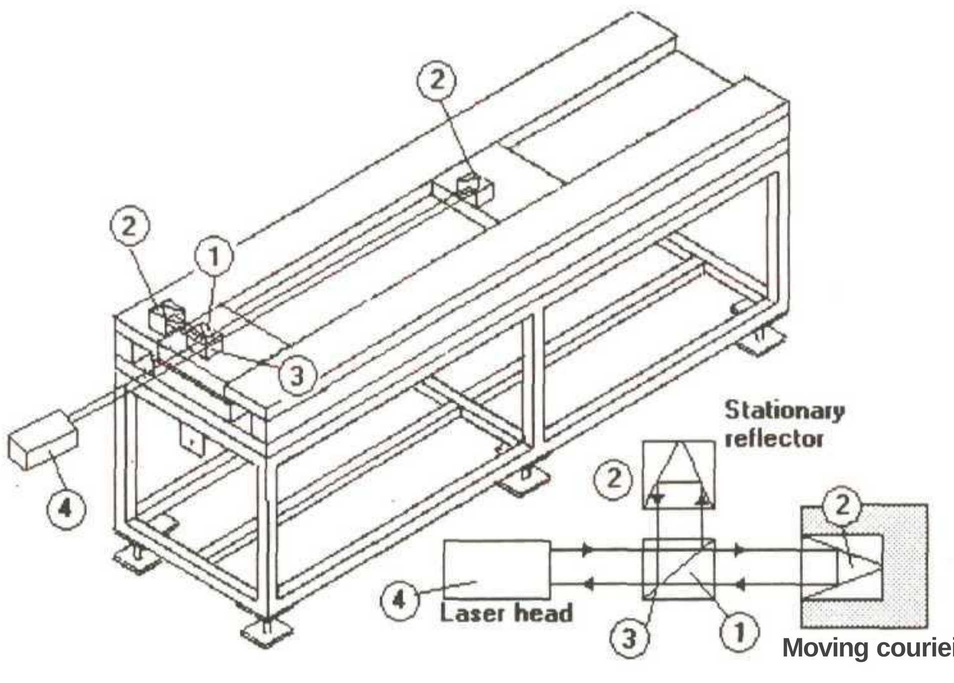

Figure 7.1: Laser measurement system applied to the material handling system.

Laser distance measurement systems with analog outputs were also studied. The DME2000 laser system works by measuring the time it takes for a number of wavelengths of light to reflect off the moving target and be received by the laser. The distance is calculated by halving the total time taken for the laser beam to be rebound back to the receiver. The laser is capable of being reflected off almost any target. The simplicity of its operation makes the system suitable for a larger number of industrial applications than laser interferometry technology.

However the cost of the DME2000 laser measurement system is in excess of R26 000 [Rhomberg],

7.2.2 MAGNETIC SENSORS

Compared to optical sensors, magnetic sensors are characterized by their simplicity, reduced sensitivity to contamination and low cost. Magnetic encoders use magneto-resistive (MR) sensing elements and magnetically salient targets. The MR sensors change their resistance under the influence of the magnetic flux density and are capable of reading densities as low as 0.005T.[Gieras et al] Four sensors are electrically connected to a resistive bridge polarized by a 5Vd,c source as shown in Figure 7.2. The bridge output varies sinusoidally, reflecting changes in sensor resistance. The magnetic salient target is a flexible magnetic strip distributed along the motion track. The strip is made from alternating pole low energy NdFeB PMs mixed with rubber. The two magnetic poles situated below the MR sensing elements affect the sensors in the same way but with opposite polarity. When the alternatively magnetized ruler moves one pole pitch, t, the output signal will complete one cycle. The relative position is determined by counting the number of poles moving through the sensor. The speed can be determined by the frequency at which the poles pass. In linear motors with moving magnetic array, the installation of the magnetic strip is unnecessary. The encoder sensors are located near the surface of the guideway and the magnetic field produced by the PMs is used as the magnetic target. The position feedback system described is used in the Moving Magnet Lightning Motor Series manufactured by Anorad.[Anorad_3].

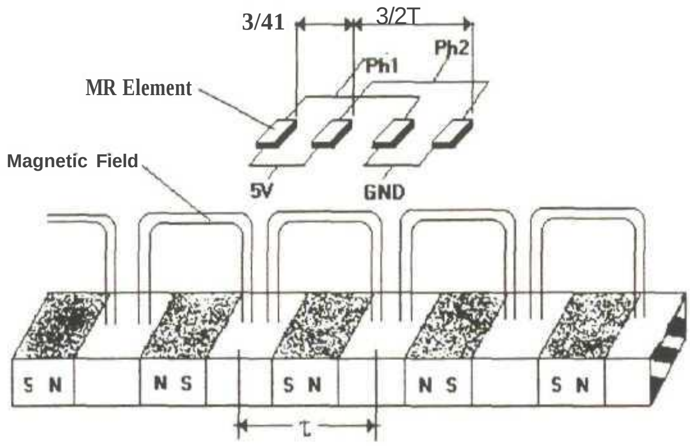

Figure 7.2: Magnetic encoder with magneto-resistive sensors. [Gieras et al]

The implementation of magnetic sensors using the PM courier as the magnetic sensing source was considered. Four-sensor resistivity bridges placed periodically along the armature platen could be used to sense the alternating magnetic field as the courier travelled along the platen track. The spacing between the sensing bridges would ensure a sensing bridge under the courier at all times. The output from the sensors is sent to a multiplier where the signals are interpolated to achieve the required feedback signal for controller compatibility. The implementation of such a position feedback system was not undertaken due to the large amount of data processing and interpolation that would be required. The system would also be an in-house design and manufacture, with no guarantee of reliability or accuracy. Although such a system has been implemented by Anorad, it is not available as a stand alone, commercially available system. The high degree of electronic development required was beyond the scope of the project. The development of such a feedback system should be undertaken as a separate research project.

7.2.3 ULTRASONIC SENSORS

Ultrasonic sensors are widely used in the process control industry. Applications include monitoring material position, transparency or reflectivity and thickness. The ultrasonic sensor uses a remote ultrasonic transducer for displacement measurement applications. A sound wave pitched above the upper limit of human hearing is emitted by the transducer The sound wave travels until the target object is reached. The sound wave rebounds or 'echoes' and is received by the sensor. The distance is determined by halving the time taken for the ultrasonic sound wave to be received. The Q45U ultrasonic sensor range developed by Banner Engineering Corporation[1] is temperature compensated and capable of resolutions up to 0.01 mm. [Banner]. The ultrasonic sensor output can be selected for either a 0-10V voltage or 4-20mA current analog output. The sensor is taught the sensing window range with push button teach mode. The range is automatically scaled to give the correct analog output for varying target distances within the sensing window.

The short range ultrasonic sensor in the Q45U series is capable of sensing an object's distance from 0. lm to 1.4 m. The long range sensor is capable of detecting targets at distances up to 3 m. A short range sensor was chosen as the position feedback device. The sensor was chosen as it provided the following advantages;

- The sensor is a complete non contact sensor allowing the courier to be free from any tether restrictions.
- The sensing windows are easily set with push button teach mode. This allows for different window settings to be changed easily.
- Automatic scaling of the analog output for new sensing windows.
- The analog output type is selectable as a voltage or current output.
- The response time of the sensor is very high.
- The sensor is an off-the-shelf system. This greatly facilitates implementation and commissioning.
- The cost of the ultrasonic sensor (R2500.00), was favorable.

The ultrasonic sensor was chosen as the position feedback device instead of the laser and magnetic systems discussed. The laser system would be susceptible to errors due to lateral movements and vibrations of the courier. This would result in alignment errors between the reflector prism and the laser head. The laser system would also limit the choice of possible drive systems. The drive system would have to be able to accept laser interferometer signals. The magnetic feedback system was rejected because a custom engineered system would have to be developed. The compatibility between the magnetic position feedback system and drive system was also questionable. The signal from a magnetic sensor system would not be directly compatible with most standard drive systems and would require signal conditioning to make them compatible.

Technical information and setup procedures of the ultrasonic sensor are presented in Appendix E. The ultrasonic sensor target material and size was determined by trying various materials such as aluminum and perspex. The minimum target size for maximum sensing distance is 35 mm x 35 mm. The trials revealed that a black perspex plate 55 mm x 55 mm achieved the best results. The results were analyzed according to echo strength, indicated by a red LED. Figure 7.3a show the ultrasonic sensor mounted to a bracket attached to the material handling system frame. Figure 7.3b shows the courier with the ultrasonic sensor target attached.

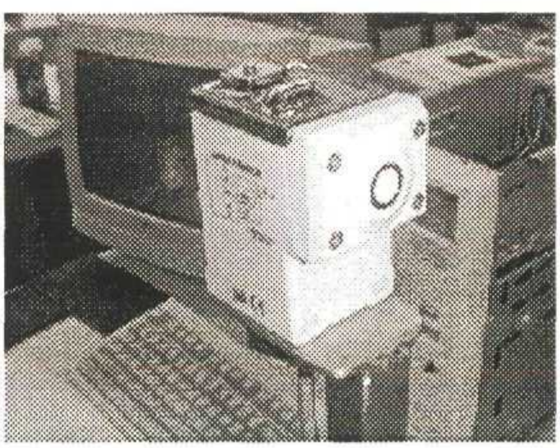

Figure 7.3 (a) Ultrasonic sensor used for position feedback of the courier.

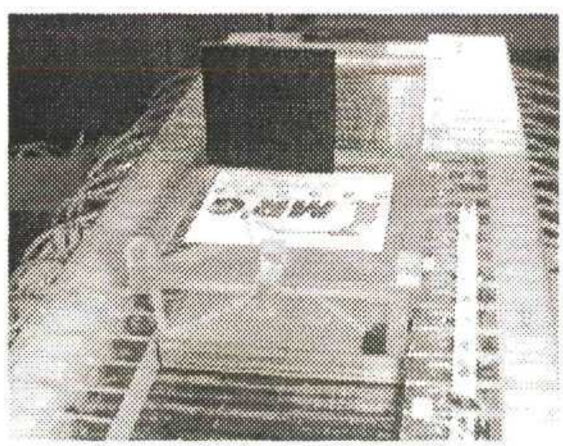

Figure 7.3 (b) Ultrasonic sensor perspex target mounted on the courier.

Using the teach mode the sensing window limits were set. The proximal sensing window limit was set by holding the courier in the zero position and by holding the teach mode button. The analog output was set to OV. The distal sensing window limit was set by moving the courier to the furthermost point the courier could travel on the platen and by holding the teach mode button. The voltage output was automatically set to 10V for the distal sensing window limit. The total distance the courier was capable of travelling was 780 mm. The ultrasonic position feedback system chosen allowed for accurate tracking of the courier. The non contact sensing technology complemented the cordless LSM design.

7.2.4 OPTICAL AIR BEARING SENSOR

The air bearing system implemented required the activation of bearing pads according to the courier's position. Only those bearing pads which were required to levitate the courier were activated along the platen. Knowledge of the position of the courier was only required in certain positions. A separate positioning system-was designed and implemented to determine the courier's position when entering and exiting bearing pad regions along the platen. The air bearing sensor system was designed and implemented before a final decision had been made on the ultrasonic position sensor. Slotted optical switches (H22A) were placed in strategic triggering positions along the length of the platen. The H22A slotted optical switch is a light emitting diode coupled to a silicon photodarlington. Technical data on the slotted optical switch is presented in Appendix F. The courier was fitted with 'wings'. These 'wings' closed the optical switch when they passed through it's slot. The wings were positioned on opposite corners on the leading and trailing edges of the courier. Figure 7.4 shows the layout of the optical switches along the platen. Fifteen slotted optical switches were placed along the platen track.

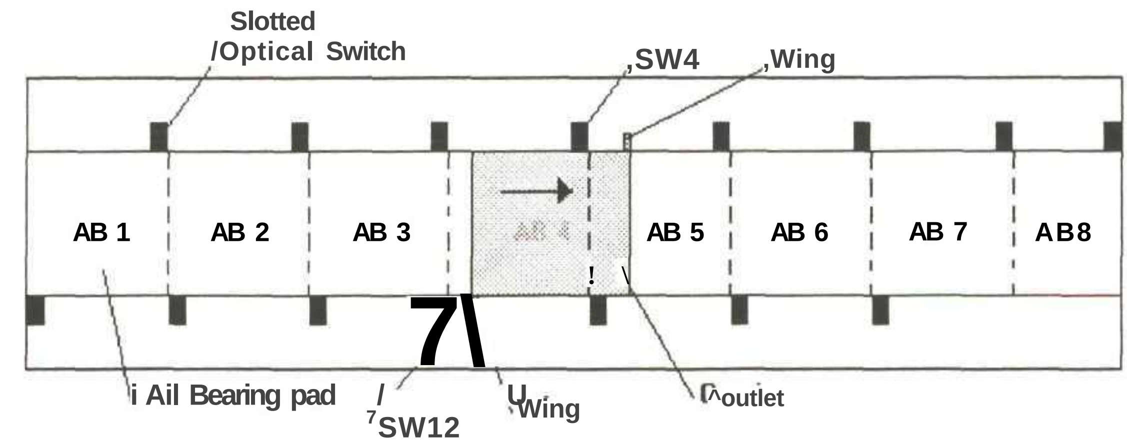

Figure 7.4: Slotted optical switch layout along the platen switched by the *'winged'* courier.

The required bearing pad was activated by the leading edge *wing* cutting the optical switch. As the courier moved off a bearing pad, the *wing* on the trailing edge of the courier turned the air bearing pad off. With air bearing pad four (AB 4) already activated and the courier traveling from left to right, AB 5 is activated by the *wing* on the leading edge cutting the optical switch SW 4. The bearing pad AB 3 is deactivated by the trailing edge *wing* cutting the optical switch SW 12. For the courier moving up and down the platen, the leading edge *wing* is responsible for activating the bearing pads and the trailing edge *wing* is responsible for deactivating the bearing pads. This ensures that air is supplied only to the pads under the courier. Figure 7.5 shows the air bearing position sensor system in action.

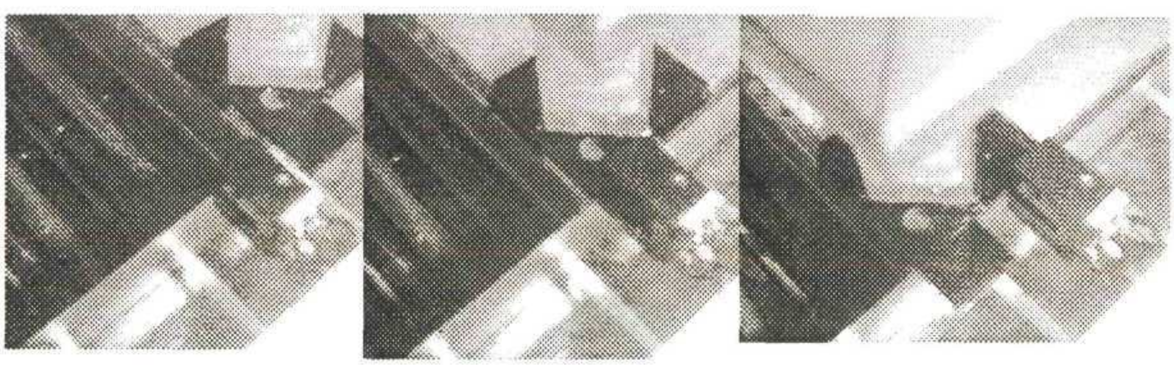

Figure 7.5: The air bearing pad activation system showing the courier cutting a optical switch.

A 5V signal was required when an optical switch was cut. When the switch was *uncut* or open, a OV signal was required. A simple control circuit was designed and developed to create the desired control outputs for the slotted optical switch. The control circuit outputs were sent to a PC-based control card. The details of the PC-based control card are presented in section 7.3.5. The output from the control card was based on the sequence of inputs from the control circuits. The outputs were used to switch the solenoid valves and activate the correct bearing pads. The control circuit designed and developed for each optical switch is shown in Figure 7.6.

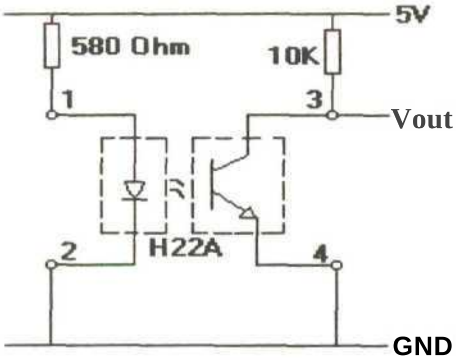

Figure 7.6: Control circuit developed for optical switches

The optical air bearing sensor system proved highly successful without current in the armature windings. The magnetic field generated by the armature windings was strong enough to induce erroneous signals in the control circuits. This caused bearing pads to turn on and off with no logical sequence, resulting in the reverse air bearing being ineffective. Attempts were made to isolate the slotted optical switches' wiring from the magnetic field by housing them in aluminum. With minimal improvement in the stability of the system, it was decided to use the position feedback information from the ultrasonic sensor to control the switching of the air bearing solenoid valves.

7.2.5 MAGNETRACK[T] POSITION SENSOR

The Magnetrack[1] LSM monorail material transport system, developed by MagneMotion, uses a unique position sensing system [MagneMotion]. A wireless transducer, attached to the moving element, induces a signal into the long, stationary, motor winding (armature). This is picked up by the motor control system. The induced signal enables the control system to determine the exact position of the moving element to within a fraction of a millimeter

[Thornton et al]. The position feedback system is currently being designed as a commercialized stand-alone system for material handling, process automation, moving people and amusement rides. The stand-alone system uses a simple phased conductor winding, placed along the track or guideway. The implementation of such a position feedback system would be ideal for the CLSM MHS. The stand-alone non contact positioning system is expected to be commercially available in the year 2001 and should be considered for implementation.

7.3 CONTROLLERS

For a LSM to operate properly the control system must track the position of the moving element accurately in order to properly synchronize the moving field current in the stationary armature. The implementation of a closed loop system would lead to proper synchronization of the LSM, ensuring optimal propulsion. If synchronization is lost or interrupted, the motor slips and loss of propulsion can occur. In an ideal LSM, the windings in the motor armature are configured to yield a sinusoidally shaped Back EMF waveform. The function of the controller is to provide sine wave currents at high frequencies. The phase angle must correspond to the position of the motor and the signal amplitude controls the motor force. This is called sinusoidal commutation even though the windings are permanently connected to a source and the current is not switched but varied instantaneously. In the control of traditional motors, the current is commutated by *switching* the current from one winding to another in the correct direction at the correct time. With sinusoidal commutation, the linear encoder used for position feedback is also used to vary the instantaneous phase of the currents in each winding. Phase finding is required on power-up and then motor phases are incrementally advanced with each encoder pulse to produce smooth motion. Thus the motor's fundamental design is to produce a constant force output when the driving voltage on each phase matches the characteristic Back EMF waveform [Trilogyl].

The choice of position feedback device required that a controller capable of using an analog signal for position feedback. This would achieve closed loop control of the CLSM. Without position feedback the phase angle of the armature currents cannot be adjusted to correspond to the position of the courier and maintain maximum thrust. Further study into the types of control systems architecture was undertaken, together with a look at commercially available controllers.

Control variables are classified into input variables (input voltage, input frequency), output variables (speed, displacement, force) and internal variables(armature current, magnetic flux). Scalar control methods are based on changing only the amplitudes of controllable variables. Scalar control can be implemented in both open and closed loop control systems. Vector orientated control methods change both the amplitudes and phases of the vectors of variables. The vector control is based on the field orientation principle, where the active and reactive currents are decoupled. These in turn determine thrust and magnetic flux respectively [Gieras et al]. Figure 7.7 (a) shows a block diagram of a scalar open loop control system. Compare this to the closed loop vector control system shown in Figure 7.7 (b).

The implementation of a suitable control system lead to (a) the study of commercially available servo controllers based on vector control methods and (b) in-house developed control systems based on scalar control methods. The digital servo controllers developed by the leading linear motor manufacturers, Anorad Corporation and Kollmorgen Motion Technologies, were investigated. A motion control system developed by Delta Tau Data Systems was also explored, together with the implementation of an constant flux inverter based control system. The advantages and disadvantages of each system are presented.

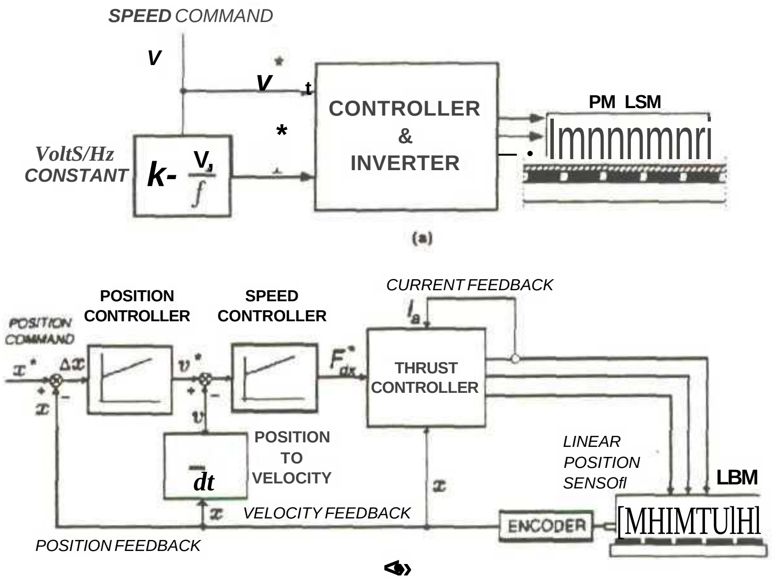

Figure 7.7: (a) Block diagram of a open loop voltage-frequency control of a PM LSM, (b) closed loop control of position, velocity and current of a PM LSM (Gieras et al].

7.3.1 ANORAD'S M-SERV CONTROLLER

Anorad has a wide range of Digital Signal Processor (DSP) based servo controllers which are matched to all their linear motors. The M-Serv digital servo controller, shown in Figure 7.8(a), is a stand-alone unit consisting of an integral digital amplifier and power supply. The M-Serve provides sinusoidal and trapezoidal software commutation at a 20kHz update rate [Anorad_2]. The controller can be easily interfaced to a host computer through the RS-232 port. The host computer monitor is used as the interface to the system. The controller is easily programmed, using the Windows based software tool. Control programs, such as point-to-point moves, are developed, using the ACS programming language (ACSPL) used in all Anorad's controllers. The graphical user interface provides a graphic representation of the position, velocity and current loop response enabling the user to optimize the system tuning parameters easily [Anoradl].

The M-Serv controller incorporates sixteen digital outputs and one analog (* 10V) output for plant interface. The controller also has sixteen digital inputs and one analog (0-5 V) input which is sampled via a 10 bit analog to digital converter. The input and output ports are used to interface external transducers and limit switches to the controller. The controller's encoder input port is configured to accept three channel differential, TTL level, optical encoder or laser interferometer signals. Investigations were made into the compatibility of an analog position feedback device with the M-Serv controller. Enquiries into the possibility of programming the M-Serv controller to read the analog input port as the position feedback signal, revealed that the M-Serv controller was not compatible with analog position feedback devices. This meant that the ultrasonic sensor could not perform the same function as an encoder to commutate the motor. The motor would have to run in an open loop system The implementation of Anorad's M-Serv controller for the CLSM MHS was not undertaken for the following reasons:

- Non- compatibility with analog position feedback devices.
- Anorad is not represented in South Africa. This meant that training and after-sale service would prove difficult. This was a concern with regards to commissioning and programming of the controller.
- The programming language, ACSPL, was an unknown programming language.
- Due to the high exchange rate between the U S A and South Africa, the cost of the M-Serv controller made it unaffordable. The cost of the M-Serv was quoted at US$ 2 225. (R15 575 @ R7.00/US$)

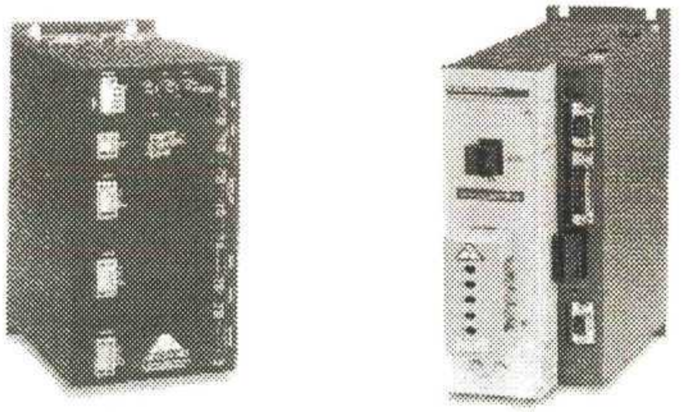

(A) (B)

Figure 7.8(a): Anorad's M-Serv digital servo controller [Anorad_2], (b) Kollmorgen's Servostar CD Amplifier. (Kollmorgen)

7.3.2 KOLLMORGEN'S SERVOSTAR CD AMPLIFIER

Kollmorgen's Servostar CD amplifier is an amplifier and integrated power supply unit. The controller, shown in Figure 7.8(b), is programmed using Kollmorgen's tailored software environment, MotionLink®. The ServoStar CD contains control algorithms such as pole placement, proportional -integral (PI) and pseudo-derivative feed forward (PDFF) to control all types of machines. The stand-alone controller utilizes advanced patented sinewave commutation technology with digital control loops to provide smooth, precise low speed control and high-speed performance. The controller possesses an array of configurable I/O with three digital inputs and one digital output for a variety of customized functions. A separate analog input port is used for commands such as speed and direction. The controller is capable of receiving serial communication from either a PC or PLC for easy integration into the manufacturing system [Kollmorgen].

The ServoStar CD controller, however, is configured to receive only encoder or resolver feedback devices. Thus the analog signal from the ultrasonic sensor would have to be sent to either a data acquisition board or PLC and the motor's speed and direction communicated with the serial port. The control system would then essentially be an open loop system with no variation of the current. Thus all the built-in control algorithms and advanced features would not be utilized. Kollmorgen Motion Technologies has an agent in South Africa, Tio-lec (PTY) Ltd. Tio-lec provided technical information about the ServoStar CD controller. The ServoStar CD range is available with either a 3 Amp or 6 Amp amplifier at costs of R8 301.17 and R9 639.78 respectively [Tio-lec]. Implementation of the ServoStar CD contoller was not effected for the following reasons:

- Non-compatibility with analog position feedback devices.
- The programming language, MotionLink, was an unknown programming language.
- The cost of the ServoStar Cd controller range, although less than Anorad's M-Serv digital controller, was still too high.

- The control algorithms would be wasted without a resolver or encoder feedback device to fully optimize the control features offered.

7.3.3 DELTA TAU PMAC2 CONTROLLER

Delta Tau Data Systems are known as the world leader in multi-axis motion control. Delta Tau Data Systems PMAC2, shown in Figure 7.9, is their latest motion control card. The PC based control card, utilizing DSP technology, is capable of simultaneously controlling from 1 to 8 axes. Since each axis is completely independent, a single PMAC2 motion control card can control a single axis on each of 8 different machines, 8 axes of motion on 1 machine, or any combination in between [Delta Tau_1]. Essentially the PMAC2 is a control card which sends digital pulse width modulation (PWM) signals to a drive (amplifier) such as the PowerBlok drive, shown in Figure 7.10. The PowerBlok is a direct PWM controlled digital servo drive. The PowerBlok is designed to be controlled by a digital PWM servo controller such as the PMAC2 [Semipower].

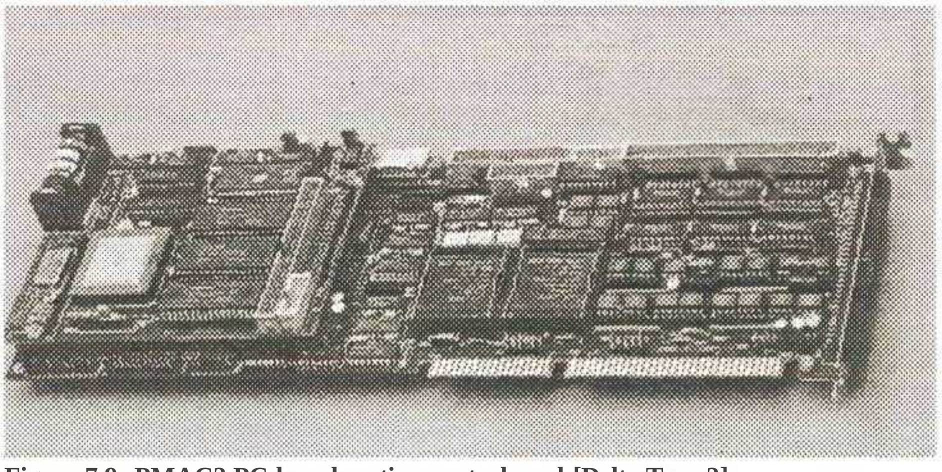

Figure 7.9: PMAC2 PC based motion control card [Delta Tau_2].

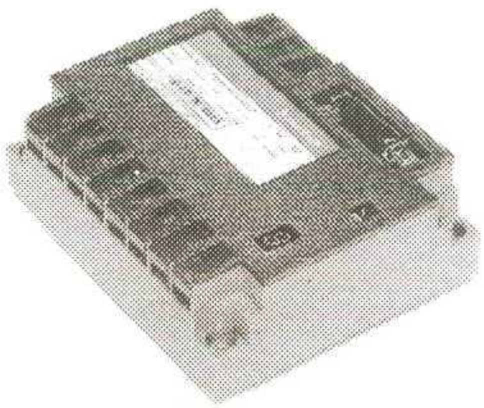

Figure 7.10: Semipower PowerBlock PWM drive[Semipower].

The PMAC2 supports a wide variety of feedback devices, namely; digital quadrature encoder, sinusoidal interpolation, laser interferometer, analog feedback, resolver and magnetic linear displacement transformers (MLDTs). A 16 Bit A/D accessory card is required for the analog feedback signal to be interfaced to the PMAC2 control card. With analog feedback devices supported by the PMAC2 controller, its possible implementation as the control system was considered. The analog position feedback signal can be used to commutate the motor. Figure 7.11 shows the proposed control system. The PC-based PMAC2 control card is connected to the PowerBlok servo drive. The PowerBlok drives the three phase armature. The analog signal from the ultrasonic sensor is connected to the accessory card (ACC28A) which connects to the PMAC2 control card.

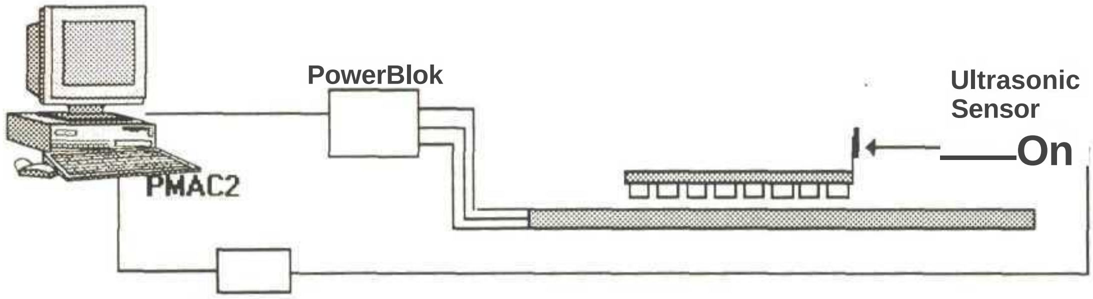

Figure 7.11: Proposed PMAC2 control system for the CLSM.

When the PMAC2 is combined with the PowerBlok drive, the PMAC2 directly and synchronously closes the current, velocity and position loops of the system and outputs the required digital PWM command to the PowerBlok. Semipower have developed a SensorlessServo Indexing Drive. The IndexBlok can position any three phase rotary or linear brushless permanent magnet motor without a sensor. The SensorlessServo technology replaces the physical sensor (e.g :encoders and resolvers) with a software algorithm. The algorithm calculates positional information from current and votage measurements. The position is fed to the PID servo system within the IndexBlok, resulting in a three phase vector drive without the need for a physical sensor on the motor. The IndexBlok allows users to program and select 16 different absolute or relative moves. With RS 485 communication, the number of predefined moves becomes unlimited. The IndexBlok replaces the PowerBlock, allowing for position feedback systems to be eliminated. [Semipower]

The control system was proposed in consultation with Accutech Automation, the Delta Tau Data Systems agents in South Africa. The disadvantage of implementing the proposed system was the cost. The cost of the PMAC2 control card was quoted at R22 000 [Accutech]. A decision was made not to implement the control system as it was decided that the CLSM was a newly developed motor, the parameters of which were not fully understood. To implement such an advanced control system before fully testing and understanding the motor performance characteristics was too great a risk.

7.3.4 YASKAWA INVERTER

The study of commercially available servo controllers has shown that a scalar control system would be best suited for the initial control system of the CLSM. A Scalar control systems has been successfully implemented in the control of a LSM propelled hoist prototype [Landy et al]. The control system is implemented on a personal computer, interfaced to the motor via a digital to analog converter, driving a constant flux inverter and a position encoder. The maximum velocity and final destination are passed to a control algorithm which determines the maximum possible acceleration, the thrust produced by the motor and the point of maximum acceleration and deceleration. The output signal is then mapped to the current position of the mover, utilizing the encoder signal as an output signal reference. The above control method is only applicable to the synchronous machine due to its natural frequency tracking characteristic. The motor is held in position by ensuring that the mmf wave produced by the stator is stationary. This is achieved by applying minimal output frequencies and rapidly toggling the direction of the voltage output [Landy et al].

The implementation of a similar system was proposed for the control of the CLSM. The analog position feedback signal from the ultrasonic sensor would be sent to a PC-based data acquisition board. An inverter would be supplied with the desired speed and direction from the user. The 200V single to three phase VS mini J7 Yaskawa inverter shown in Figure 7.12, was obtained to drive the CLSM. The inverter is supplied by a 200V single-phase power supply and outputs a three phase system to supply the motor.

Figure 7.12: Yaskawa VS mini J7 inverter.[Yaskawa_lJ

7.3.4.1 INVERTER SETUP

The inverter was wired according to the wiring specifications. The three inverter output terminals , U,V,W, were connected to the three phase armature terminals Phase A, Phase B and Phase C respectively. The inverter was configured by setting the inverter's internal registers. The standard wiring specification and constant internal registers and definitions are presented in Appendix G [Yaskawa_2], The inverter was set to operate in a voltage-frequency (V/f) control mode which controls the motor using sine wave PWM. The V/f pattern was defined by setting the internal register constants for maximum output frequency (nOll), maximum voltage (nO12), maximum voltage output frequency (nO13), middle output frequency (nO 14), middle output frequency voltage (nO 15), minimum output frequency (nO 16) and minimum output frequency voltage as shown in Figure 13(a). Since the motor does not have the starting torque problems associated with standard motors, the V/f pattern could be simplified to a linear curve as shown in Figure 13(b). In V/f mode, the VS mini inverter automatically adjusts the voltage during constant speed operation to achieve the required torque. To increase the torque, the gradient of the V/F curve is kept constant but is automatically scaled up in magnitude to give higher voltages for a given frequency, thus maintaining the required speed under a new load as shown in Figure 14.

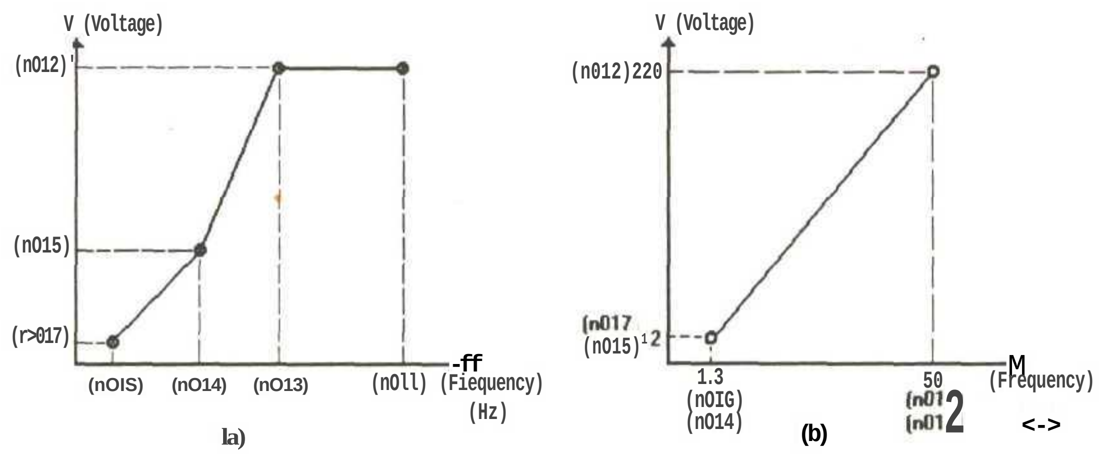

Figure 7.13: V/f pattern set for the CLSM inverter [Yaskawa_2].

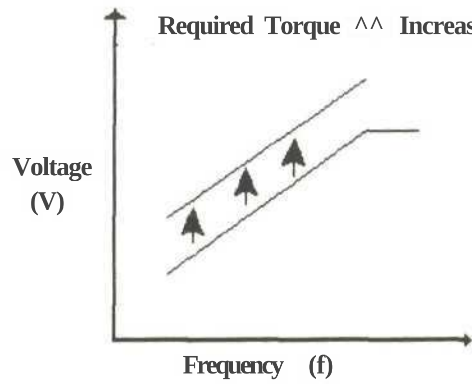

Figure 7.14 : Automatic output voltage scaling for constant speed operation [Yaskawa_2].

The speed at which the motor courier will travel is determined by the frequency of the armature mmf waveform which is determined by the frequency of the a.c. voltages applied to the armature windings. The frequency of the armature mmf waveform was controller by sending an analog signal of 0-1OV to the inverter. The inverter's internal register constants were set to enable the frequency to be set by voltage reference. This allowed the operator to set the desired frequency of the mmf waveform by inputting an analog voltage to the inverter. To provide a frequency reference by analog input through the inverter control terminals, the relationship between the analog input and frequency reference was obtained by setting the frequency reference gain and the frequency reference bias as shown in Figure 7.15.

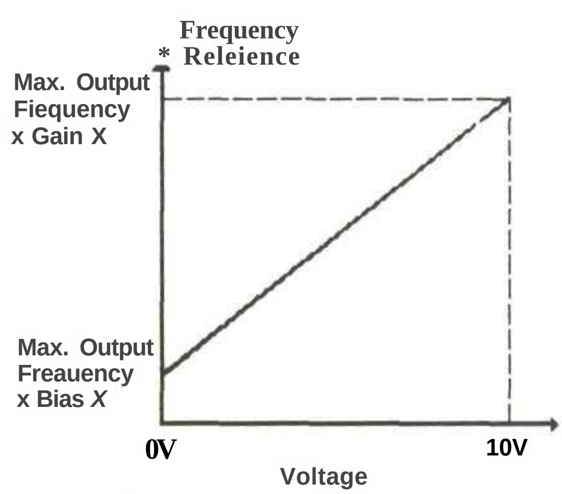

Figure 7.15: Frequency reference by analog input [yaskawa_2].

Since the speed of the courier is equal to the synchronous speed v_s of the traveling magnetic field, the speed of the courier can be calculated as:

$$v = v.v = 2 / r \quad (7.1)$$

Where v is the courier speed

v_s is the synchronous speed waveform

/ is the frequency of the mmf waveform

i is the magnetic pole pitch of the courier

Due to the length of the platen track, the speed of the courier was limited to 150 mm/s. The speed of the courier was restricted to half the speed used in the kinematic analysis outlined in Section 4.5 for initial testing of the motor. From equation 7.1 a maximum frequency of 5Hz was calculated. The maximum speed of the courier for a maximum voltage input of 10V was set as a percentage of the maximum output frequency. The frequency gain was set at 10 % of the maximum frequency output of 50Hz. Thus for a voltage input of 10V by the operator, the courier was set to run at a maximum of 5 Hz. The 300 mm/s used in the kinematic analysis would require the frequency of the mmf waveform to be set to 10 Hz It was decided that this was to fast for the limited length of the platen track. The maximum speed of the courier could be easily changed by simply increasing the frequency gain register in the inverter. The courier's speed for the minimum voltage input of 0V was set to zero by setting the frequency bias to 0%.

The acceleration time (Accel 1) is the time needed for the output frequency to reach 100% for a step voltage input. The acceleration time was set at 5 sec to allow the courier time to gain momentum and to insure the courier traveled smoothly. This acceleration time results in an acceleration below the acceleration time used in the kinematic analysis, but was regarded as sufficient for initial testing of the motor. The deceleration time is the time needed for the frequency to reach 0%. The inverter is capable of implementing two different types of stopping methods by either decelerating the courier to a stop using DC injection or simply allowing the courier to coast to a stop. Deceleration using DC injection was chosen to help achieve positional accuracy of the courier. If the courier was allowed to coast to a stop, the courier would overshoot the target position. The deceleration time was set to 0.5 sec with DC injection been applied immediately before a stop. If the deceleration time is short or the load inertia is large, an overvoltage(O V) fault may occur at deceleration [Yaskawa_2]. The amount of DC injected is set as a percentage of the motor's rated current. The motor's rate current was initially set to 2.5 Amps, equal to the current rating determined by the finite element model. Thus, the DC injection current was set to 50 % of 2.5 Amps.

The setting of the inverter's constant values was adjusted, with farther testing of the motor to optimize its performance. The internal constant values can easily be set using the inverter keypad. The final commissioning of the inverter required the external circuitry to be wired to the inverter.

7.3.5 DATA ACQUISITION CARD

The implementation of a PC based control system required a computer interface and data acquisition platform to interact with the CLSM MHS. A data acquisition board was required to switch the solenoid valves for the air bearing pads according to the position feedback information from the analog sensor. The inverter received run forward and run reverse commands from the control circuit terminals. The data acquisition board would be required to provide the following; 1 (0-10 V) analog output for setting the inverter frequency output (courier speed), 1 (0-10 V) analog input for the ultrasonic position feedback signal, 10 digital outputs for the air bearing solenoid valves and inverter external circuitry.

The PC30 series board developed by Eagle Technology is a low cost, high accuracy analog and digital I/O board. The PC 30 series board allows the board features to be controlled by software. The PC30GA board has a throughput of 100 kHz with 4 digital-to-analog converters (DACS) which produce analog output voltages of-lOV to +10V DC. The board also features

16 single ended or 8 differential analog-to-digital inputs with software programmable gains of 1, 10, 100 and 1000. In single ended input connections, input signals share a common low side, which is analog ground. Differential inputs use two multiplexer switches per channel. The A/D converter measures the difference between the high and low input lines of each channel. Differential input configuration is best suited for eliminating system noise. The board also features 3 digital I/O ports with 8 lines per port, allowing 24 digital I/O lines. The ports can be configured into two digital output ports (16 input lines) and one digital input port (8 lines), or one digital output port and 2 digital input ports. The PC 30GA board has an onboard 16 Bit counter that allows real-time timing applications such as PID control [Eaglel], The card is provided with instrument drivers for graphical programming languages such as Lab View and Visual Basic. Figure 7.16 shows the PC30GA board. The PC30GA board was chosen as the data acquisition card to be implemented, as it provided sufficient analog and digital I/O. It has also been implemented as standard data acquisition hardware for the mechatronic based CIM control strategy in the Mechatronics and Robotics Research Laboratory. The PC30GA hardware specifications, pin configuration and wiring diagrams are presented in Appendix H [Eagle_l].

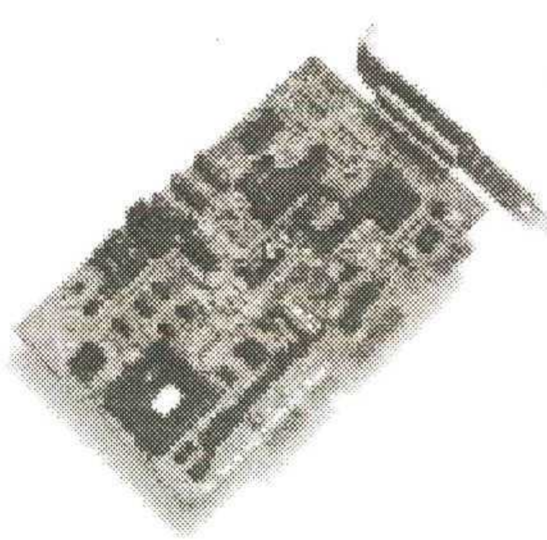

Figure 7.16: PC30GA data acquisition board[Eagle_2].

7.4 ELECTRONIC CONTROL HARDWARE DEVELOPMENT AND COMMISSIONING

7.4.1 PC30GA WIRING

The CLSM MHS is referred to as the *plant,* consisting of the CLSM and the reverse air system. To interface the data acquisition platform to the plant, a special cable was made, allowing data transfer for control to be achieved. The 50 pin female D-type connector on the PC30GA card required a 50 pin male D-type connector to connect to it. A 50 pin male D-type connector was soldered to two 25-core cables. The other end was left open to wire to the plant. The pins were assigned to the PC30GA pin assignments presented in Appendix H. The pin assignments and cable colours for the data transfer cable are presented in Appendix I. Due to the large number of individual cables, a distribution board was created which allowed the PC30GA outputs to be positioned in groups. This allowed for blocks of strip connectors to be used to group the digital ports and analog ports together, enabling easy commissioning and wiring. The distribution board is shown in Figure 7.17 with the detailed wiring diagram presented in Appendix I.

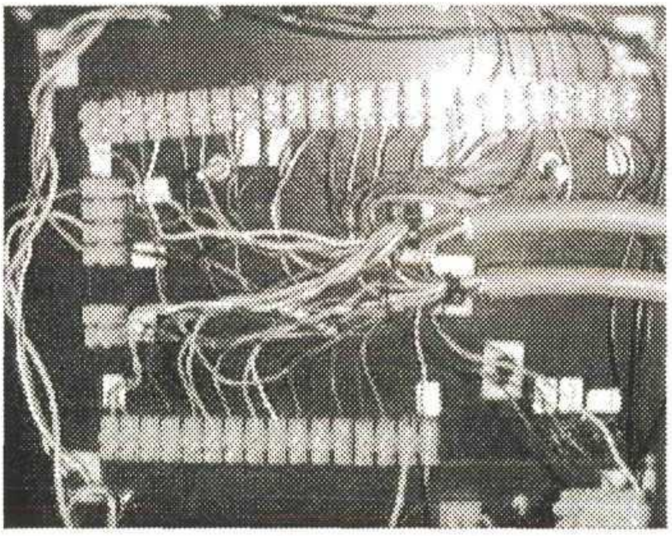

Figure 7.17: PC30GA wiring distribution board.

7.4.2 AIR BEARING CONTROL CIRCUITRY

Port C on the PC30GA card was configured as a digital output port. The 8 digital ports were used to control the air bearing solenoid valves. The PC30GA card is capable of outputting 5 V per digital line. The air bearing solenoid valves required 24V to be energized. A relay switching circuit, shown in Figure 7.18(a), was developed to switch the solenoid valves. The 5Vs from the card energized the 5V DC relay switch, allowing the air bearing solenoid to be energized by a 24V power supply. Initial tests showed that the PC30GA digital output lines had insufficient current source to energize the relays. The digital lines are rated at a maximum 5.5 V with a current source of 1mA. The 5V DC relay required a rated current of 70mA to switch. The relay circuit was redesigned and a simple transistor switching circuit added, as shown in Figure 7.18(b).

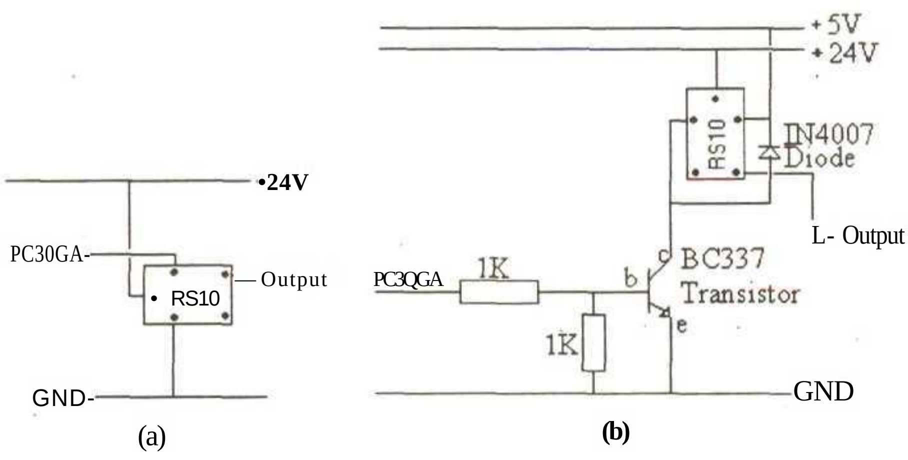

Figure 7.18: (a) Simple relay switching circuit.(b) transistor switching circuit implemented.

When there is no input voltage from the PC30GA card, there is no potential difference across the relay coil. The collector of the transistor is at a potential of approximately 5V. When the input voltage is received from the PC30GA card, the transistor switches, so that a potential difference of 5V is setup across the relay. However, the 5V is now supplied by a DC power supply with sufficient current source to switch the relay. A power supply set at 24V supplied the potential difference with sufficient current to energize the solenoid valves. Three relay boards, consisting of 4 switching circuits each, were developed for the air bearing and inverter control. Figure 7.19 shows the relay boards developed. A detailed wiring diagram for the relay boards is presented in Appendix I.

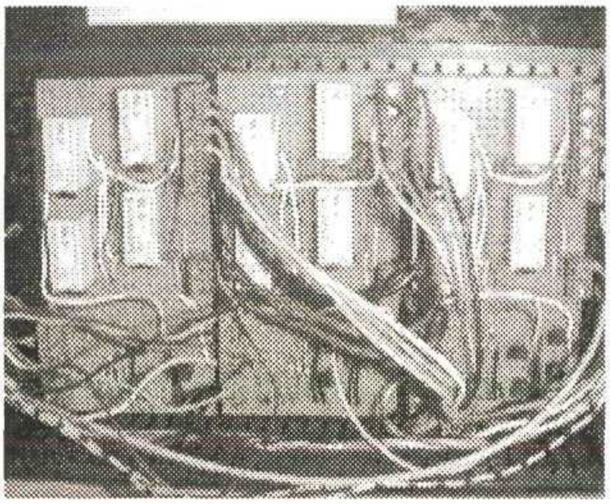

Figure 7.19: Relay switching boards for air bearing and inverter control.

7.4.3 INVERTER CONTROL CIRCUITRY

The inverter's main control circuit terminals were wired to the PC30GA distribution board and the third relay board. A 'run forward' and 'run reverse' command was required from the PC30GA card. Due to the fact that the PC30GA card had insufficient digital outputs, the analog output ports DACl and DAC3 were configured to supply 5V each simulating digital outputs. The inverter's main terminal control switches required 24V to be switched. Since the PC30GA card could only supply 5V with insufficient current, the card's output signal was first used to drive a 5V relay which would switch to supply 24V across the inverter's main control circuit terminals as outline in Section 7.4.2. The third set of relays shown in Figure 7.19 were used for this task. The speed of the motor was determined by the user setting the analog output on the PC30GA card (DACO) to a value between 0-1 OV. The analog output was wired to the voltage reference terminal on the inverter. Setting the analog output to 1 OV would result in the courier running at a maximum of 5Hz. The wiring configuration of the inverter's main supply, linear motor armature and control circuit is presented in Appendix I.

7.5 SOFTWARE CONTROL DEVELOPMENT

7.5.1 LABVIEW GRAPHICAL PROGRAMMING

The Lab View Graphical Programming language is an example of a Windows based language. Lab View is a program development application much like C or Basic The main difference is that Lab View uses a graphical programming language, G. Lab View programs are referred to as virtual instruments (Vis) as they imitate actual instruments. Lab View operates in two panels. The *front panel* is the operator's control screen or graphical user interface (GUI) while the back panel or *diagram window* contains the graphical code. The front panel simulates the panel of a physical instrument. The front panel can contain knobs, push buttons, graphs and other controls and indicators. Using the mouse or keyboard the user can enter data and view the results on the computer screen. The diagram window holds the block diagram of the VI, the graphical source code.The block diagrams are created by *wiring* together objects that send and receive data, perform specific functions and control the flow of execution. Lab View includes libraries for data acquisition, instrumentation control, data analysis, data presentation and data storage. [Lab Viewl] Lab View was used to configure the PC30GA card to receive and transmit data to control the CLSM MHS.

7.5.2 FRONT PANEL

The GUI or front panel developed for the CLSM MHS, shown in Figure 7.20, consists of a graphical display of the controls and indicators required to control the system. The control of the system is based on the continual comparison between the user's entered target value and the current position of the courier as determined by the ultrasonic feedback sensor. The activation of the control system is linked to the air bearing Boolean control button. The button is configured with a 'Switch When Pressed' action. This changes the control value each time the user clicks on it, similar to the action of a light switch. When the air bearing button is 'ON' all I/O are operable. When the button is pressed to the 'OFF' status, all I/O are dropped and the program stops running. The position of the courier is shown using numeric indicators. The numeric indicators give the voltage from the ultrasonic sensor and the corresponding position in millimeters(mm) of the courier. The user can input a desired target position in mm using the rotary numeric control lever. The desired maximum speed of the courier can be set by entering a voltage of between 0-10V. The voltage output drives the frequency reference setup in the inverter to run between 0 and 5 Hz. The comparison between the desired target position and the courier's actual position automatically determines the direction the courier must travel. If the current courier position is less than the target position, the run/forward command is automatically activated, making the magnetomotive force (mmf) wave travel in the forward direction. If the courier position is greater than the target position, the run/reverse command is automatically activated, making the magnetomotive force (mmf) wave travel in the opposite direction. The status of the air bearing is indicated by the digital indicator pads which display the current status of each bearing pad. If a bearing pad is activated, the indicator pad changes to a blue with an 'ON' text description. If a bearing is non-active, the indicator pad is represented in grey with an 'OFF' text description. Thus the user has a highly visual indication of the air bearing status.

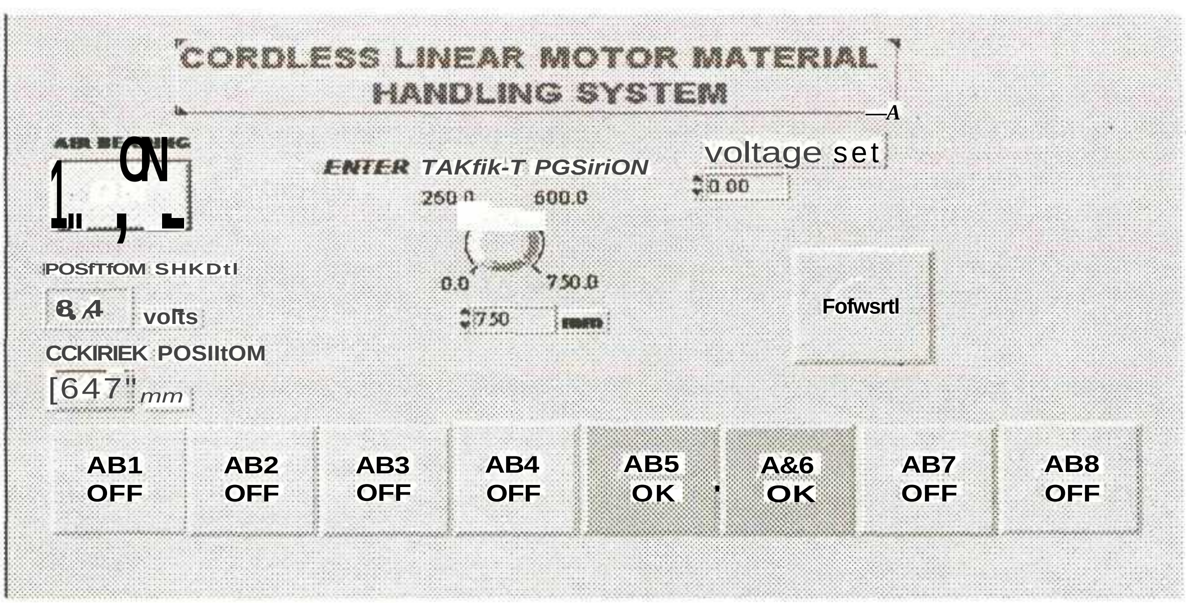

Figure7.20: Front page developed for the CLSM MHS control.

7.5.3 REVERSE AIR BEARING CONTROL

The control of the reverse air bearing system is based on the analog voltage input for the courier's position. The diagram window was used to create the graphical program to control the switching of the solenoid valves. The position feedback voltage is declared a global variable in the program. The air bearing pad is activated by directly addressing the digital output port on the PC30GA card. The port is configured using the LabView software configuration tool. Figure 7.21 shows the digital line output tool used to configure Port C on the PC30GA card as a digital line output port with 8 lines.

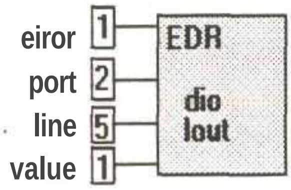

Figure 7.21: Port C configuration

A port value of 2 represents the third port (digital lines 17-24) which is configured as a digital line output port. Each line can be addressed. In Figure 7.21 line 5 is being assigned a value of 1 which results in a 5V output at PC5. Different voltage window limits are assigned to activate a bearing pad, depending on whether the courier is traveling in a forward or reverse direction. True-False Case structures were used to implement the control logic. If the courier was traveling in the forward direction the true case would be relevant and the voltage window limits would control the switching of the air bearing pads. Figure 7.22 shows the true case for the air bearing control.

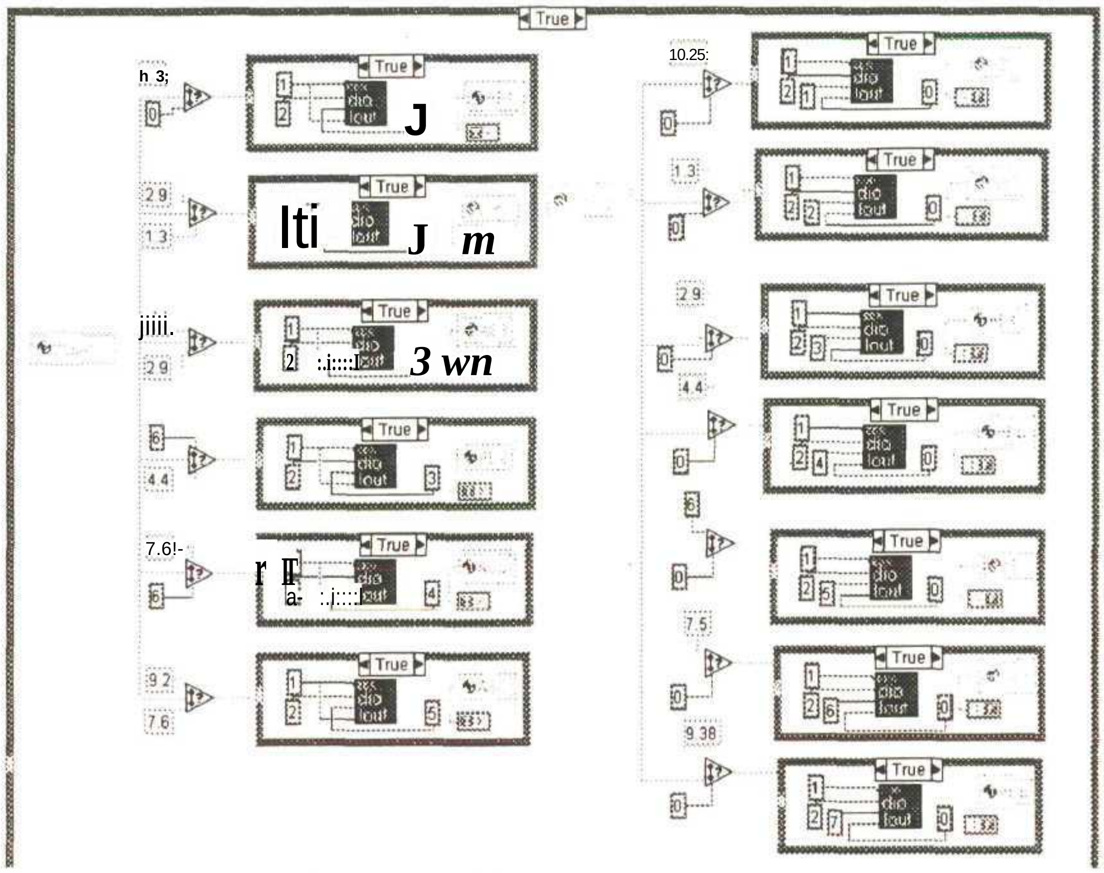

Figure7.22: True case air bearing control for a forward travelling courier.

The control of a bearing pad was done by using a case structure wired to the output of a comparison function. Each bearing pad was designated a voltage window. If the voltage for the courier's position is equal to or greater than the lower limit or less than the upper limit voltage specified for the comparison function, **the true** case is activated and the corresponding air bearing pad is activated. If the position voltage falls outside the voltage window the false case structure is activated and the digital line is set to zero. For example, the activation of air bearing pad four (AB4) will only occur when the position feedback voltage is between 2.7V and 4.3 V. When the courier is traveling in the run reverse mode, the voltage limits on the comparison functions for the air bearing pad control are different, as shown in Figure 7.23. The control of the side bearings was not required as they are fed from the same air manifold delivering air to the corresponding bearing pad.

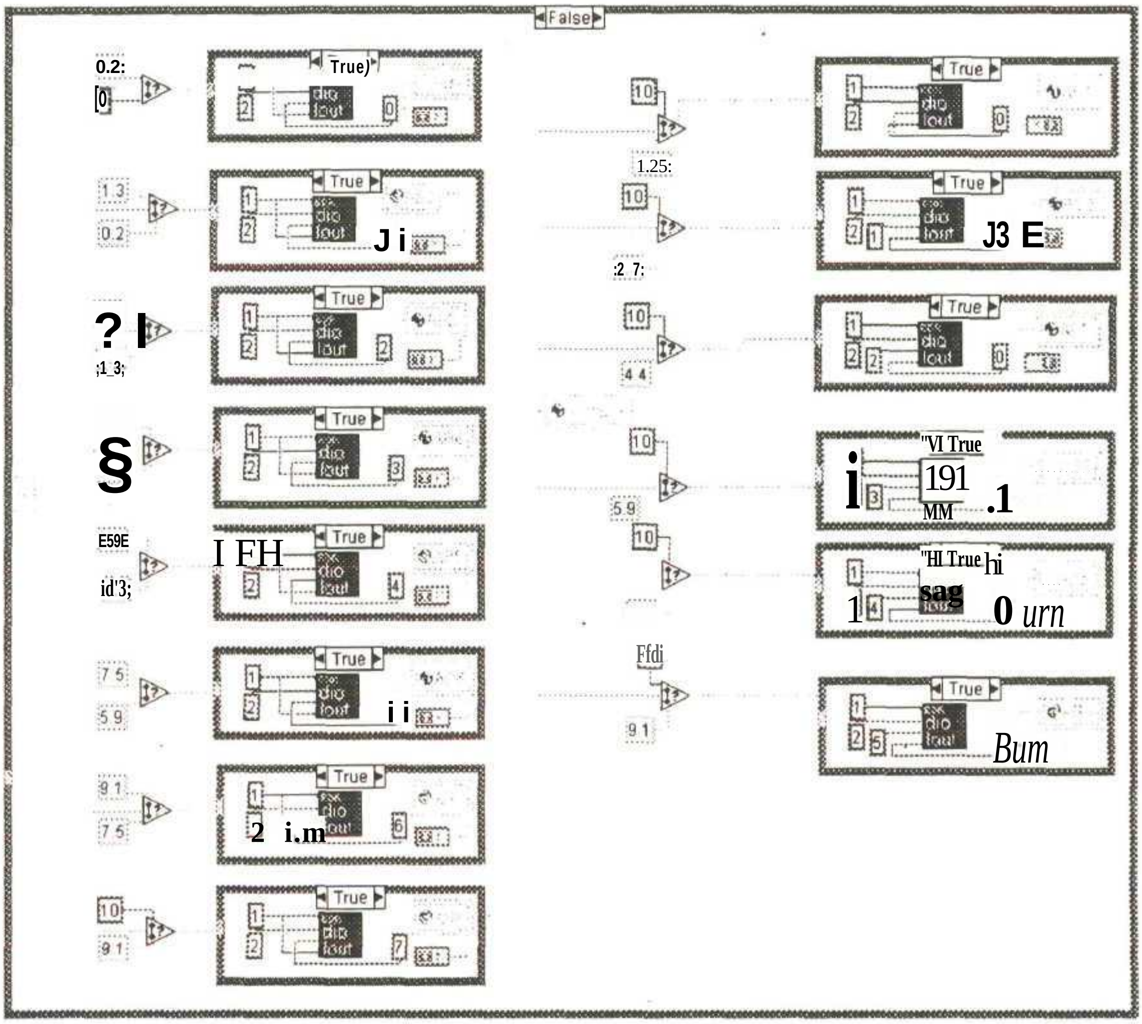

Figure 7.23:False case air bearing control for reverse traveling courier.

7.5.4 CORDLESS LINEAR MOTOR CONTROL

The difference between the target position and the courier position is continually compared and used to control the direction of the courier as shown in Figure 7.24. The position input voltage is multiplied by a scaling factor to give the courier's position in mm. This is seen on the front page by the user. The courier's current position in mm is compared to the target position in mm. The result of the comparison is used to set two case structures, namely the air bearing control and the inverter direction control.

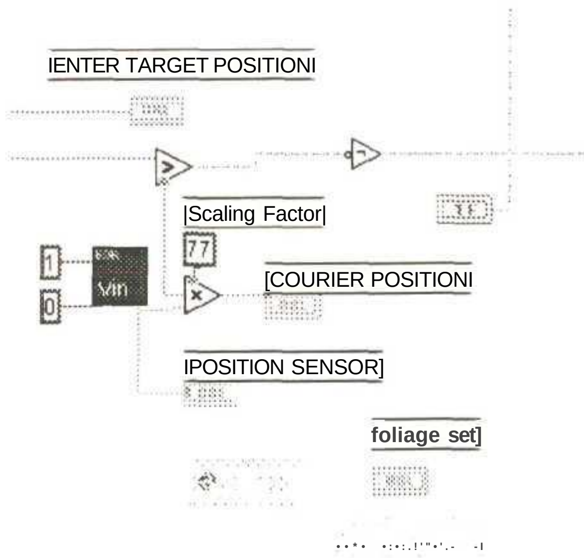

Figure 7.24: CLSM control using the comparison between the courier's current and target position.

When the courier's position is less than the target position, the inverter is run in a forward direction by setting the.output voltage on DAC1 to 5 V and the voltage to DAC3 to OV. When the courier's position is greater than the target position, the inverter is run in a reverse direction by setting the output voltage on DACl to OV and the voltage on DAC3 to 5V.This was achieved by using the result from the position comparitor to change a case structure. The true case structure, shown in Figure 7.25, was used to run the inverter in the forward mode. The false case structure was used for the reverse run mode as shown in Figure 7.26. The voltage input by the user for the selected speed appears in both cases to keep the speed constant and independent of the direction.

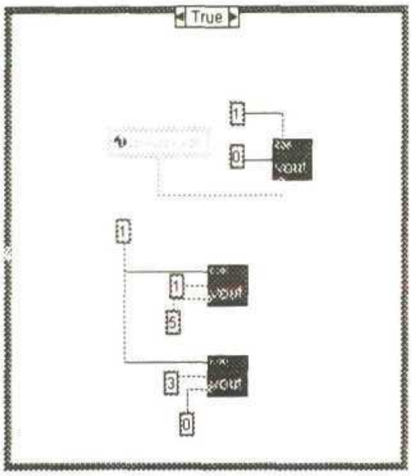

Figure 7.25: Run forward inverter control

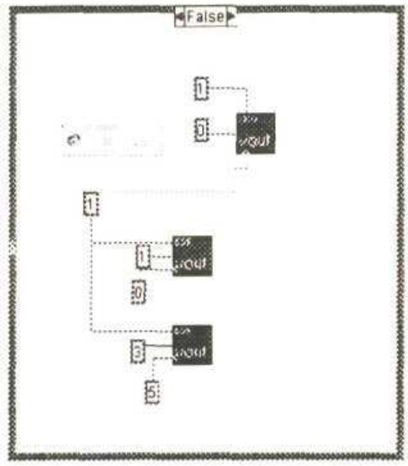

Figure 7.26: Run reverse inverter control

The control system developed allowed for the courier to be in any position along the platen when the system commences. The positioning of the courier was to be achieved by setting the frequency of the mmf wave form to O.lHz and toggling the forward-reverse command. This would set up a stationary mmf wave, holding the courier in position. **This could not be** implemented because the analog output at low voltages was insufficient to drive the inverter. Only when the output voltage reached approximately 2.7 V, would the frequency output of the inverter work. No frequency reference commands for voltage inputs below 2.7V could be received as depicted in Figure 7.27. Thus the courier was controlled in an ON-OFF state. **The** control system was designed to drop all outputs to the system when the courier's position is equal to the target position. The direction and speed command to the inverter are dropped together with the air bearing, which results in the courier dropping onto the platen track. The courier travels at a constant speed until the target position is reached. However, due to it's momentum, the courier passes the target position. As soon as the courier has passed the target position, the mmf wave is automatically reversed and the courier travels back towards the target position. Thus the courier appears to *hunt* for the target position, hovering back and forth. The control system is therefore reactive instead of pro-active.

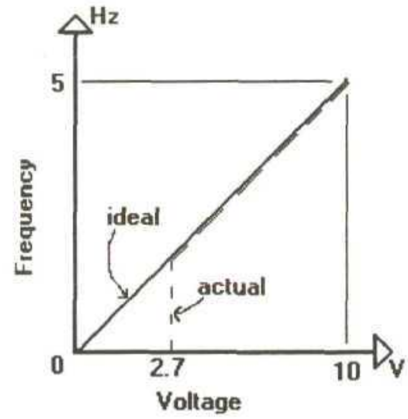

Figure7.27: Frequency reference for input voltage.

The air bearing ON/OFF button on the front page is the logic for a case structure. The control systems discussed above are set within an overall true case structure for the air bearing button being ON. When the air bearing is turned OFF all I/O on the PC30GA card are dropped and **the** system shuts down. This button has the dual function of an emergency button. The complete Lab View program is presented in Appendix J. Figure 7.28 shows a graphical overview of the control system implemented.

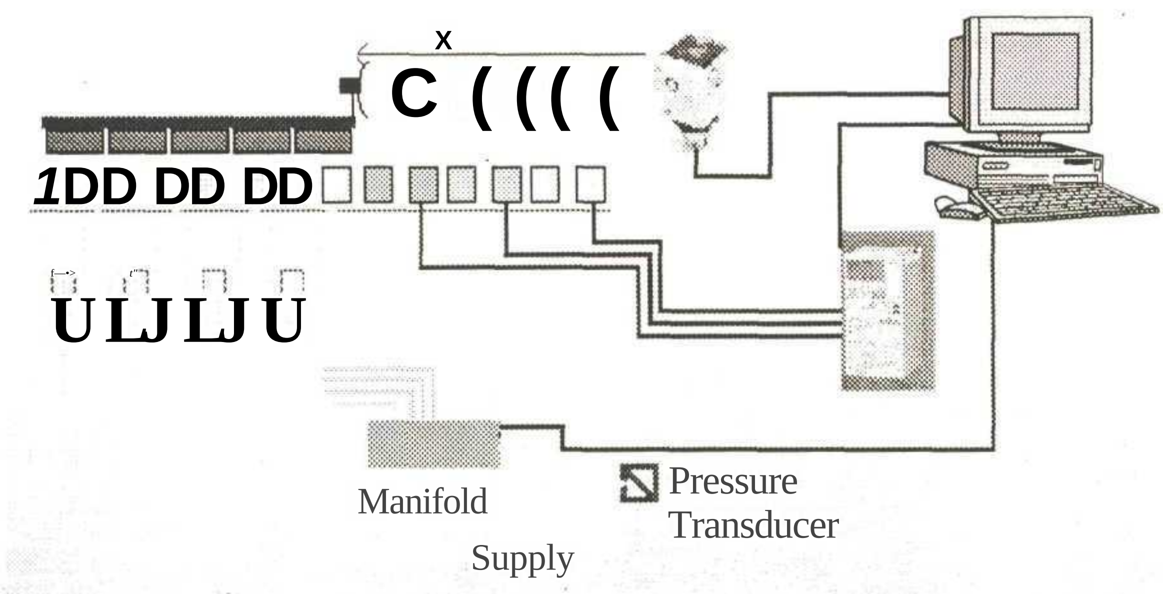

Figure 7.28: Overview of the control system implemented.

8. CORDLESS LINEAR SYNCHRONOUS MOTOR MATERIAL HANDLING SYSTEM TESTING

8.1 CLSM TEST

The CLSM was designed using 2D FEM analysis. The development of the prototype was based on the dimensions determined from the CLSM finite element model. The developed prototype was tested to verify the accuracy of the FEM results. Figure 8.1 shows a summary of the FEM setup used to construct the prototype.

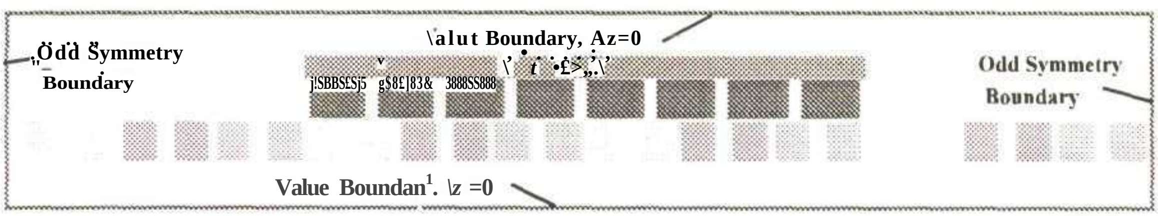

Figure 8.1: Geometric model showing assigned boundary conditions.

8.1.1 BACKIRON SATURATION ANALYSIS

The backiron of the courier is subject to saturation from high magnetic flux densities. Figure 8.2 shows the magnetic flux density distribution in the cross sectional area of the motor with the currents set to a maximum. The highest values of the flux density in the backiron appear between the magnets in the courier. The magnitude of the flux density at these points was determined and plotted on the B-H curve for 1013 steel. Figure 8.3 shows that the results for the flux density fell below the saturation level (knee of the curve). Thus the courier backiron was not saturated when operating at maximum current.

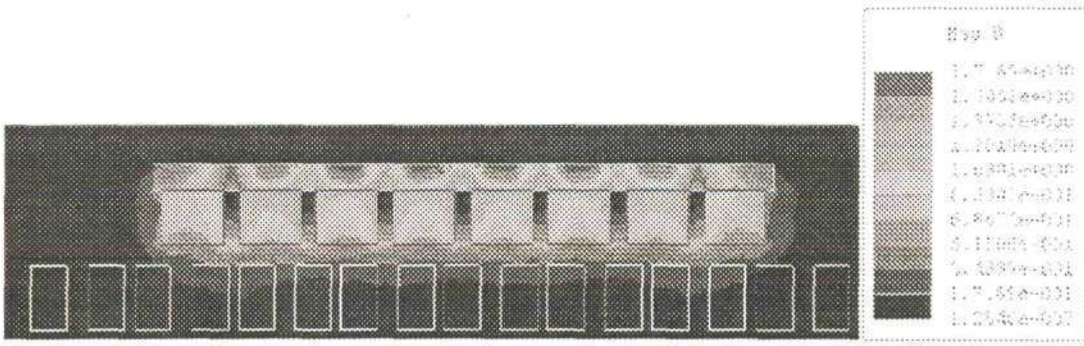

Figure 8.2 : Magnetic flux density distribution, currents in the windings set to a maximum of 2.5 Amps

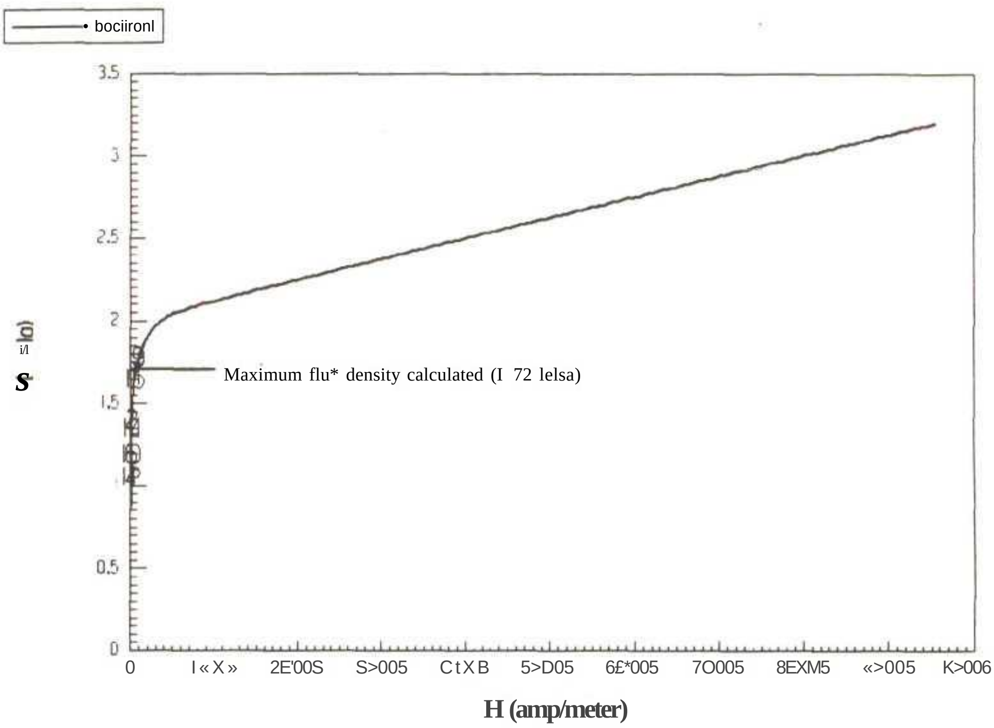

Figure 8.3 : B-H curve for the courier's backiron (1013 steel) showing flux density levels.

8.1.2 ARMATURE PLATEN ANALYSIS

In order to examine the contribution to the magnetic field density in the air gap created by the armature currents alone, the PM assembly was removed from the finite element model. Figure 8.4 shows the magnetic flux density distribution created by the currents in the armature platen. The periodic areas of high magnetic flux density along the platen are due to Phase C being set to a maximum of 2.5 Amps compared to Phase A and B, 1.25 Amps each. The maximum magnitude of the magnetic flux density was calculated to be 1.512e-002 T, considerable less than the magnetic flux densities modeled with the PM courier present.

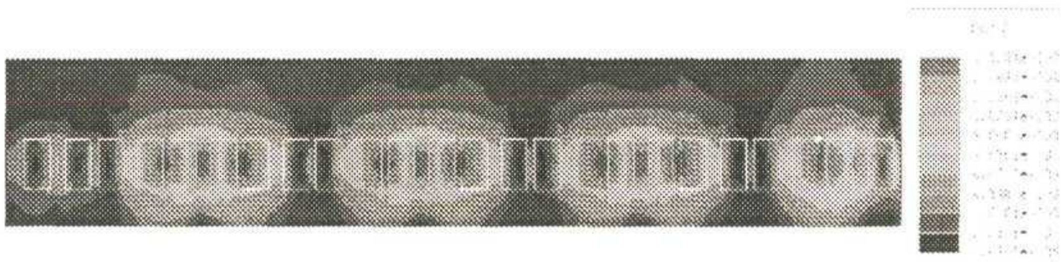

Figure 8.4: Magnetic flux density in the armature platen. Ia=1.25 amps, Ib=1.25, Ic=-2.5 amps

8.1.3 PERFORMANCE ANALYSIS

The performance of the prototype CLSM MHS was tested by measuring the thrust developed by the motor and comparing it to the thrust results obtained from the finite element model. The motor was tested by energizing the armature windings to match the value of the current assigned to the coils in the finite element model for each position of the courier. Because the control system implemented was a scalar control system which did not directly adjust the instantaneous phase angle of the armature currents according to the couriers position, the current in each armature winding was set directly to the required calculated value for the courier's position. The thrust produced was then measured. Each phase was required a separate DC power supply to vary the currents independently. Three 30 V, 5.5 Amp power supplies were setup with ammeters in series for each phase. This allowed the current in each phase to be adjusted to the correct values for each of the courier. Due to the limited voltage supply of 30 V, the motor was modeled at a maximum of 1 Amp. The average resistance per phase was 24.2Q.

8.1.3.1 PROTOTYPE PHYSICAL DIFFERENCES

To accurately compare the thrust developed by the prototype CLSM to the thrust calculated by finite element analysis, any physical dimensions which were different to the finite element model had to be identified. The effect on the motor's thrust production due to the difference between the physical prototype and the finite element model had to be taken into account. The most significant physical difference was in the construction of the armature platen coils. Figure 8.5 shows a comparison between the finite element model armature platen and the physical prototype. The coils were modelled as rectangles with sharp distinctive edges as shown in Figure 8.5 (a). Figure 8.5 (b) shows the actual shape of the coils in the armature platen. The coils are non uniform with rounded edges. The coils do not fill the slots fully. This results in a larger air gap than the 3 mm modeled in the finite element model.

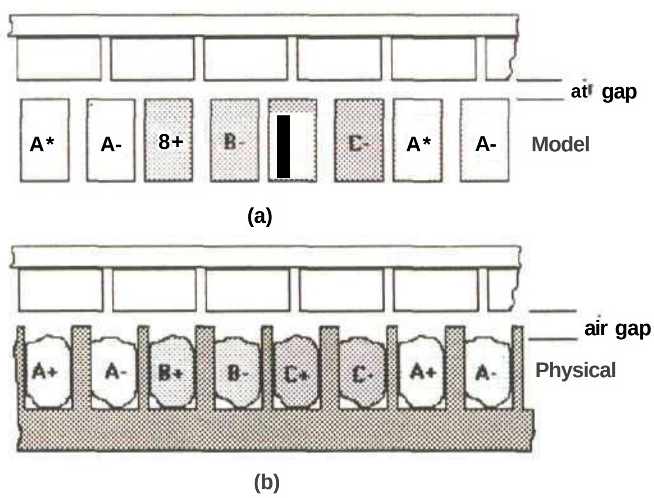

Figure 8.5:(a) Finite element model coil shape (b) actual coil shape.

This increased air gap length results in less thrust being developed by the motor. The effect of an increased air gap on the thrust was shown in Figure 4.23. Measurements were made on the physical prototype to determine the distance from the top of the coils to the top of the tufnol frame. An average distance of lmm was measured. This accounted for an average air gap in the physical prototype of 4mm. Thus, the finite element model was analyzed with an air gap of 4 mm to minimize the difference between the finite element model and the physical prototype. The motor was also modeled at a maximum of 1 Amp, so the results could be easily compared to the test results. Figure 8.6 shows the results for an increased air gap compared to the original air gap of 3 mm.

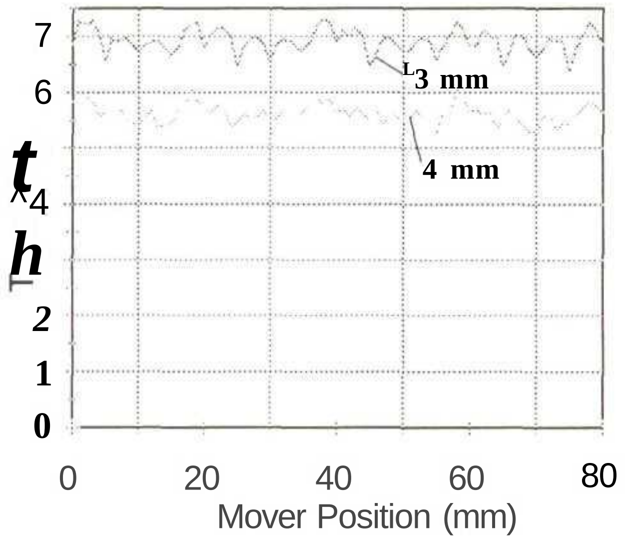

Figure 8.6: Thrust generation for increases in the air gap length from 3 mm and 4 mm.

The thrust developed with an air gap of 3 mm is greater with an average thrust of 6.92 N. On increasing the air gap to 4 mm the average thrust decreased to 5.85 N. The finite element model with an air gap of 4 mm is more representative of the physical prototype. To validate the accuracy of the finite element model, the thrust developed by the motor was compared to the thrust developed by the model.

8.1.3.2 CLSM TEST

The first test performed was to verify the zero position of the motor. The current in each phase was determined by setting <\> =60° and 0 =0°. Phase A was set to 0.86 Amps, Phase B -0.86 Amps and Phase C 0 Amps. Because the mmf waveform was stationary, the courier moved **into** a zero position. The distance measured from the start of the armature platen was 50 mm. The courier was moved to the next zero position along the platen. The distance measured along the platen was 80 mm. This verified the results obtained in Figure 4.40, which showed a zero position occurring every 30 mm. Thus the zero position of 20 mm determined by the finite element model was verified by the physical model. The current in each phase was adjusted to 0.5 Amps, 0.5 Amps and -1.0 Amps for Phase A, B and C respectively. The distance between the zero positions along the platen was measured again at 30 mm. The finite element results plotted in Figure 4.40 are validated by the test results.

To measure the static thrust developed by the motor, the courier was positioned in the zero position, x = 80 mm. To measure the static thrust, a linear scale was attached to the courier. According to the model results shown in Figure 4.40, the maximum static thrust is achieved at approximately 7.5 mm from the zero position. This is one quarter of the static thrust curve. With the currents held constant, the courier was pulled to the left and the thrust developed on the courier measured incrementally. Figure 8.7 shows static thrust measured plotted against calculated static thrust. The results show a good comparison between the finite element model's and the physical motor's static thrust curves. The accuracy of the test was limited by the measuring equipment. The linear Newton scale had a resolution of 0.25N. The distance to the courier was measured using a meter rule along the length of the platen track.

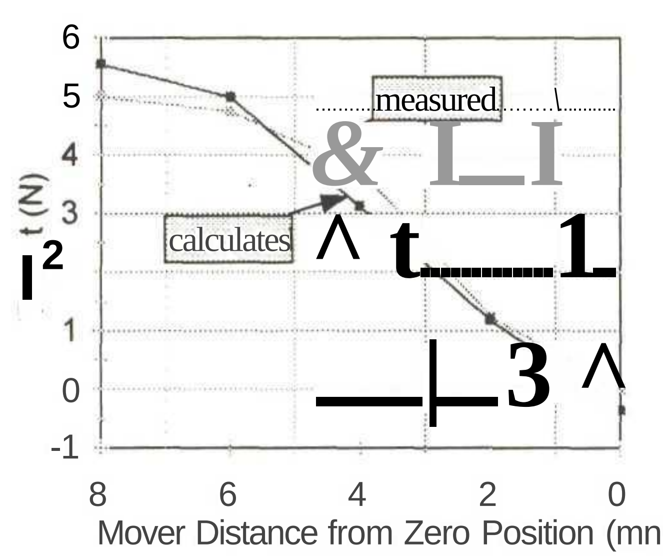

Figure 8.7: Static thrust for different positions of the mover. Ia=0.86 amps, Ib=0.86 amps, Ic=0 Amps.

The courier was advanced by 2mm intervals over two magnetic pitches and the currents in each phase was adjusted to the correct value for that position. The thrust was measured at each point and plotted against the calculated values for thrust determined by the finite element model. The results presented in Figure 8.8 demonstrate a good agreement between the measured and the calculated values of the thrust, proving the usefulness of using finite element analysis to design electro-mechanical systems. The accuracy of the results was restricted by the resolution of the measuring apparatus. A summary of the results is presented in Table 8.1.

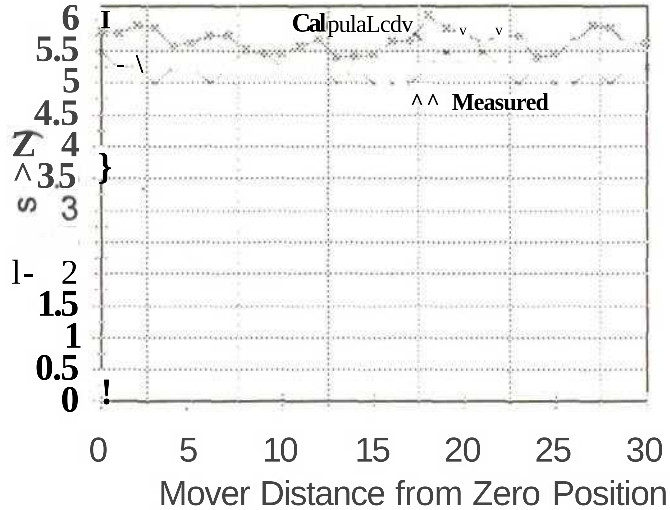

Figure 8.8: Thrust comparison between finite element analysis model and the prototype. Currents adjusted to give maximum thrust at each position. Im = lAmp

	Calculated (N)	Measured (N)
Average Thrust	5.9	5.4
Max Thrust	6.1	5.5
Min Thrust	5.4	5
Range	0.7	0.5
% Difference	8.47	

Table 8.1: Summary of thrust results for the finite element model and the physical model.

The measured values from the prototype were compared to the calculated values from the final finite element model which had an air gap of 4 mm. When the average measured thrust is compared to the average calculated thrust and error of 8.47 % is calculated. The results obtained from the tests performed on the motor are comparative to the finite element model results, justifying FEM as a credible design tool. Reasons for differences between the results obtained can be attributed to:

- The FEM package used was 2D and not 3D, resulting in fringing effects being neglected. Hence fringing along the motor depth (118mm) of the system was excluded. All results obtained from the finite element model were per meter depth. The final thrust production was obtained by multiplying the thrust by the motors effect length.

- The limitation imposed by using a 2D finite element approach, precluded the determination of a skewing force (lateral force).

-Physical differences between the finite model and the physical model. This is particularly relevant when comparing the armature coils. In the finite element model the coils were represented as rectangles with defined edges. In the physical model the coils were not of uniform shape and bunched together in the slot. This could contribute significantly to the thrust variations experienced, as this resulted in a varying coil pitch in the armature platen.

- The experimental apparatus used. A Newton spring scale was used to measure the thrust which had a resolution of 0.25N. Positioning of the courier was done using a meter rule. All these factors contributed to the low resolution and accuracy of the measured test result.

8.2 AIR BEARING TEST

The reverse air bearing test rig developed to test the principle was capable of successfully levitating 5.5 Kg on 0.5 bar. The reverse air bearing system was tested by loading the courier with sample weights of 250 g each. The courier's final mass was measured at 1.9 Kg. The reverse air bearing system was tested by loading the courier with an additional load of 3 Kg as shown in Figure 8.9. The total test load was 4.9 Kg.

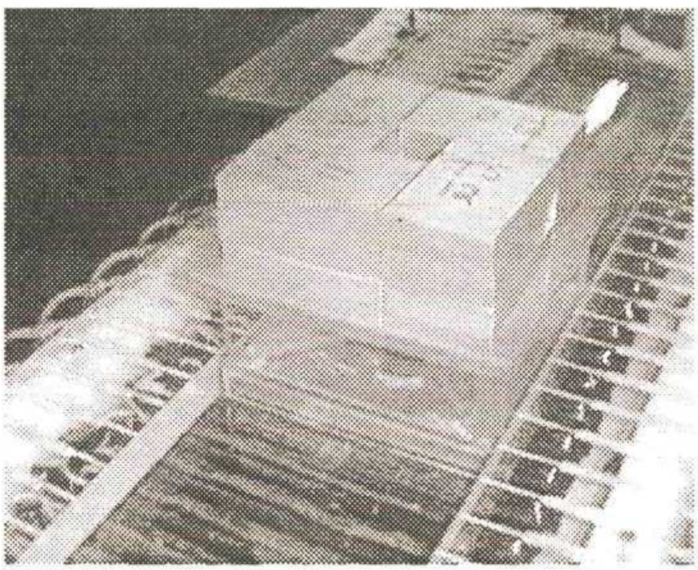

Figure 8.9: Reverse air bearing system being tested with the courier carrying a 3Kg load.

The total load was successfully levitated with a pressure of 1.5 bar. The increase in the required air pressure can be attributed to the following facts:

- the number of outlets on the air manifolds was increased to 24 compared to the 16 outlets used in test rig. The increase in the air manifold outlets was due to the side air bearings being added to the system. This resulted in the pressure having to be distributed to two areas. Consequently less pressure was driven through the armature platen.

- The construction of the armature platen led to significant losses in pressure. The clear polycarbonate sheet, which was attached to the surface of the tufnol frame, was forced off the tufnol frame. This resulted in some air being forced between the sheet and the frame instead of directly through the orifices in the polycarbonate plate. Air was found to flow into the slots and escape out the side. This was the major cause of loss of pressure and air flow to the air bearing system.

Due to the systems dynamics it was not possible to measure the pressure developed under the courier. Equation 5.20 (Chapter 5.4.2.2), was developed to calculate the film thrust developed under the courier. Knowing the courier's mass and the sample weight masses, the film thrust determined by equation 5.20 was compared to the actual load required for increasing bearing load. Figure 8.10 shows that the expression developed for the film thrust differs slightly from the actual load required. Thus it can be said that the mathematical model developed to design the reverse air bearing system was a good representation of the system.

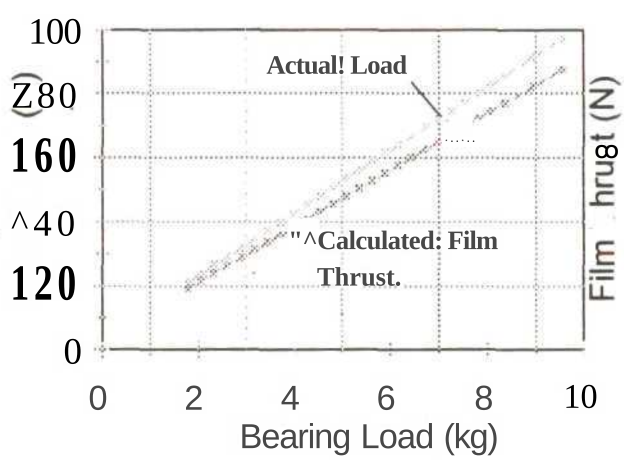

Figure 8.10: Film thrust and actual load for an increasing bearing load

The testing of the reverse air bearing system has proven that its implementation as the chosen bearing system complemented the CLSM design. The courier was levitated on a cushion of air allowing ultra smooth motion as it travelled down the platen track.

8.3 POSITIONING

The ultrasonic sensor was used for position feedback to control both the courier and the reverse air bearing system. Without current in the armature windings, the analog output of the ultrasonic sensor would rise linearly from 0-10V as the courier was moved along the armature platen. With the inverter operating and the coils energized, the analog signal from the ultrasonic sensor would only rise to a maximum of 3.2V as the courier moved down the platen. The analog output signal also became erroneous, giving random, untrue values for the courier's position. This resulted in two major problems arising:

- The air bearing system, which relies on the ultrasonic feedback signal to switch the correct bearing pads on and off, no longer operated properly. Incorrect bearing pads were activated, resulting in the courier sliding along the platen track, instead of levitating on an air bearing film.

- The courier kept moving at the same speed towards the target position, but would move past the target position. This was due to the control system, which used the ultrasonic feedback information to continually compare the current position to the target position. Because the sensor output signal would not rise above 3.2 V, the motor would continue running causing the courier to pass the target position. The control program remained in the run-forward mode as there was no convergence between the courier's current position and the target position.

To test the control system developed, the target position was limited to distances below the corresponding 3.2 V position. However, due to the signal been unstable, no positioning runs could be performed with much accuracy.

9 CLSM MHS APPLICATIONS AND CIM INTEGRATION

9.1 INTRODUCTION

The implementation of the CLSM MHS into manufacturing environments is explored. The advantages and disadvantages of integrating the system into flow-through assembly operations is outlined. Applying the concept of the CLSM MHS to factory-wide material handling functions and factory automation is outlined. The possible integration of the CLSM MHS into the CIM Cell, being developed in the Mechatronics and Robotics Research Laboratory (MR^2L), is explored as a case study. The CIM cell lacks an assembly system capable of performing simple assembly tasks. Two areas are identified for the CLSM MHS to be implemented. The functions of the CLSM MHS in these positions are analyzed and the advantages outlined. The sharing of information between the CIM cell modules and the host CIM host controller is also discussed.

9.2 MANUFACTURING APPLICATIONS

9.2.1 ASSEMBLY SYSTEMS

The driving force behind the CLSM MHS development was the demand for agile precision assembly systems. The interaction of the CLSM MHS with overhead manipulators, to form a comprehensive assembly operation, is the overall vision of intelligent, information based manufacturing systems. Studying other advanced manufacturing systems being developed [Hollis et al_2, Quaid et a11, Sandia] led to a number of possible applications for the CLSM MHS. The ability of the courier's open carrier surface to interact with other subsystems such as robots, glue dispenses, lasers and other overhead manipulators allows for comprehensive assembly systems to be developed. Figure 9.1 shows an in-line assembly system using the CLSM MHS interacting with an overhead manipulator and part feeder. The courier carries the assembly part and positions itself below the overhead manipulator. The ability of the courier to be positioned accurately along the platen track allows the overhead manipulator and courier to perform comprehensive pick-and-place assembly operations. The overhead manipulator has 2-DOF and is capable of rotating (0) to different angular positions and moving vertically (2) to pick'n place.

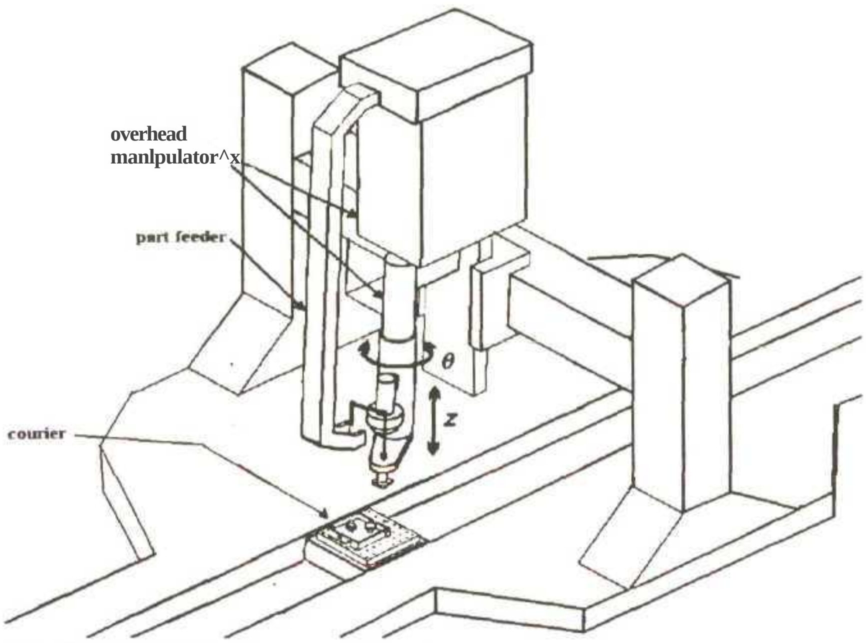

Figure 9.1: CLSM MHS in-line assembly system.

The courier is restricted to 1-DOF. According to the assembly procedure defined, the courier can be accurately positioned at a programmed point. The workpiece is then assembled by the 2-DOF overhead manipulator which selects a part from the part feeder and inserts it into the workpiece. The complete system forms a comprehensive 3-DOF assembly system. The overhead manipulator has a set line-of-action. By sharing the position information with the overhead manipulator controller, the courier positions itself so that the target point is in the line-of-action of the overhead manipulator. Figure 9.2 shows a top view of a pick 'n place assembly operation, with interaction of the workpiece's target point and the manipulators line-of-action. The courier will align the target position on the workpiece with the overhead manipulator's line-of-action for a successful assembly operation to take place.

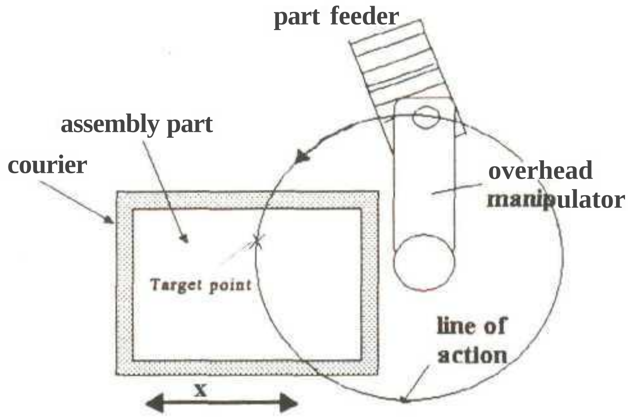

Figure 9.2: Top view of a pick and place assembly operation.

Couriers travelling along a continuous platen track, whilst interacting with a number of overhead manipulators or stations, is envisaged. The couriers cordless design will allow the courier to travel a long distance. The cordless design also allows the platen to carry a number of couriers should it be necessary. The ability of the courier to accurately position itself, enhanced by the air bearing system, allows it to interact with a wide range of assembly systems and part feeders. Figure 9.3 shows a complete in-line assembly system using the CLSM MHS to transport the workpiece. The assembly system is flexible in its design, as the courier can be designed to carry a number of different workpieces. The courier interacts only with those overhead manipulators from which it requires parts. An example of an assembly procedure would be the population of printed circuit boards. A courier carrying an unpopulated printed circuit board for product "A", could interact with every odd assembly station, selecting which components need be assembled. Another courier carrying product "B" for assembly could interact with every even assembly station, thus successfully assembling a different product on the same assembly line. To ensure a synchronized assembly operation, the position information can be used to define 'operating zones' for each courier.

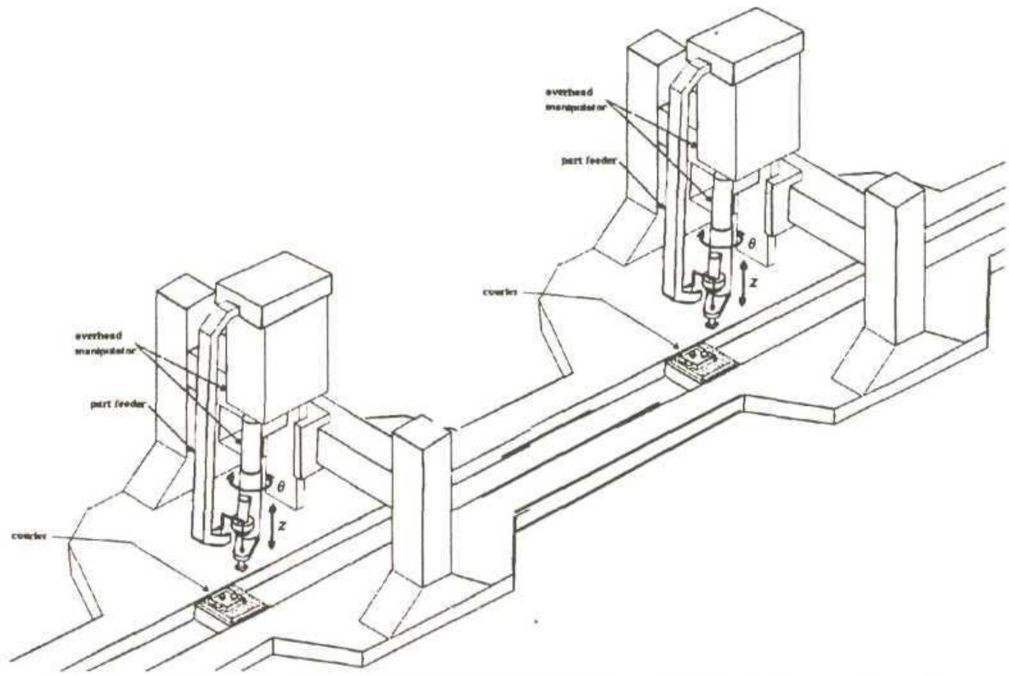

Figure 9.3: Complete in-line assembly system with multiple assembly stations and couriers.

The system described above is presented as an alternative to the 2-DOF planar motors used in the mini-factory described in Chapter 2, Section 2.3 and in [Hollis et al_2].The mini-factory system gives rise to a number of design concerns. The planar motors use open-loop stepping motors and must be driven slower than their peak speeds to avoid missed steps. Position sensors for closed loop control of planar motors are currently being developed [Brennemann et al]. The CLSM MHS has been developed with a position feedback system together with a number of other position feedback systems which may be implemented to suit the proposed application. The planar motors are restricted in their movement by the tether restriction which supplies them with power for the actuators and air for the air bearing system. Present commercial platens are fixed in size and therefore limit the courier's freedom. This requires that the workpiece be transferred from one courier to another at the tether limit or platen edge. The CLSM MHS ensures that the courier is free to travel over large distances without requiring workpiece transfers. A disadvantage of implementing the CLSM MHS in place of the planar motors is the decrease in the overall number of DOF from 4 to 3. However, the lateral (y) movement of the courier is limited by the air side bearings.

The integration of the CLSM MHS with a 4-DOF planar robot suspended from a platen ceiling forms a highly accurate 5-DOF assembly system. Due to the magnetic attraction between the planar motor and the platen table, they can be operated in an inverted position. The planar robot is fitted with a 2-DOF rotational and vertical displacement head to create the 4-DOF overhead manipulator as shown in Figure 9.4. The overhead manipulator is designed for pick and place operations with integrated I/O and on-board vacuum generator. [Robotworld]

Figure 9.4: Four DOF overhead manipulator. [Robotworld]

Combining the overhead manipulator and the CLSM MHS allows for the manufacture of high density electronic component products. The overhead manipulator is able to choose from a number of part feeders to complete a number of assembly operations on a single workpiece carried by the courier. The proposed system is illustrated in Figure 9.5. Since there is no mechanical wear or lubrication required due to both systems running on air bearing systems, the system is ideal for clean room applications.

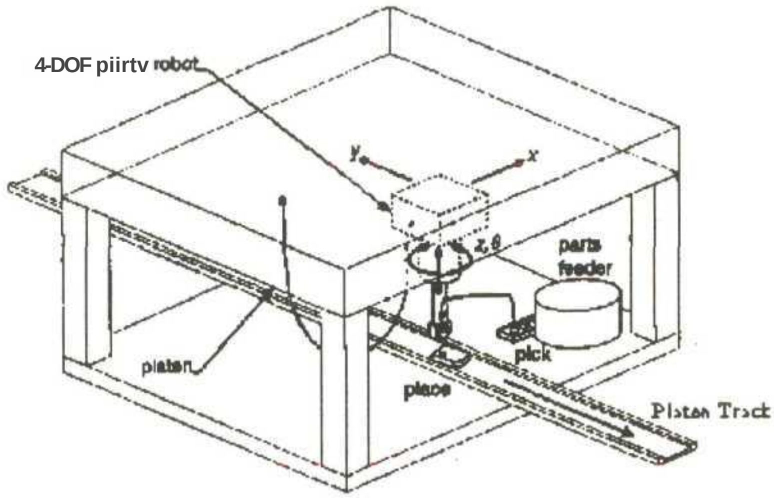

Figure 9.5: Commercial planar motors with assembly head interacting with the CLSM MHS to create a 5-DOF system.

9.2.2 FACTORY-WIDE TRANSPORTATION SYSTEMS

The tether-less courier design allows for objects to be transported over large distances. Due to the natural frequency-tracking characteristic of the motor, the courier can be made to move over large distances without the need of a position feedback device. Small containers, baskets, hand tools, machine tools and bottled liquids are just some of the many materials that can be transported around the factory floor. The transportation of workpieces from machine center to machine center is explored as a possible application. The system consists of two rows of a number of machine centers (MC),incorporating milling and drilling machines, together with two PUMA robots mounted on mechanical linear bearing systems and positioned by balanced PM LSMs. The workpieces are transported between machine centers by a CLSM MHS with a number of couriers. Multiple courier systems are made possible by developing the armature into a number of sections. Only those sections which are required to move the courier are energized. The courier positions the workpiece in front of the machine center. The workpiece is removed from the courier and placed on the machine table for machining. During machining, the courier is free to move to other machining centers to receive completed workpieces that need to be transported to other machine centers. The couriers can also be used to transport machine center tools and materials from an AS/RS. The placement and removal of workpieces, tools and materials from the couriers are shared between the two robots. The system described below is an alternative to the AGV, which is often used to transport materials, tools and workpieces between machine centers. Although AGVs have a high degree of flexibility and range, they are often costly and require significant maintenance. The proposed factory-wide transportation system is free to move over large distances and requires minimal maintenance. However, the system is more dedicated in its path compared to an AGV system. Figure 9.6 shows a graphical illustration of the factory-wide transportation system.

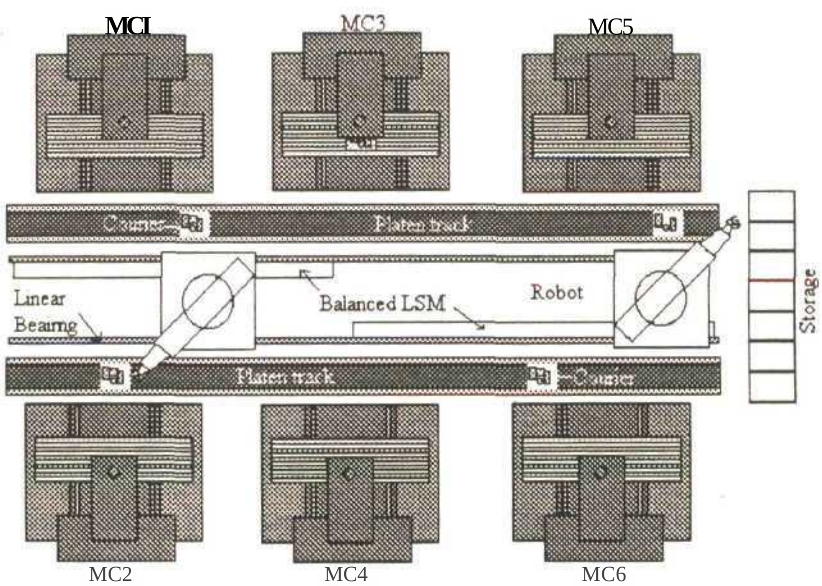

Figure 9.6: Factory wide CLSM MHS connecting multiple machine centers together with robot material handlers.

9.3 CIM INTEGRATION

The integration of the CLSM MHS into the CIM cell at the MR^2L was explored. The components of the CIM cell was discussed in Chapter 2. Two areas in the CIM cell where the inclusion of a CLSM MHS would be advantageous were identified. The addition of the CLSM MHS with an overhead manipulator and part feeder, to perform simple assembly tasks and a

CLSM MHS positioning track is proposed. The flow of information required between the CLSM MHSs and the CIM cell host controller and other CIM elements is identified. Figure 9.7 shows the integration of the CLSM MHSs into the CIM cell. The CLSM MHS in front of the CNC milling machine is used to communicate the position of a workpiece to the PUMA robot and the milling machine. Knowing the position of the workpiece, the PUMA robot can easily pick up the workpiece and place it on the milling machine table. Powered roller conveyors are currently used to transport the workpieces to the milling machine center. They require a number of position sensors and limit switches to position the workpiece. Due to the slipping of the workpiece on the roller conveyor system, the PUMA robot is unsure of the workpiece's exact position and requires extra sensors to successfully grasp it.

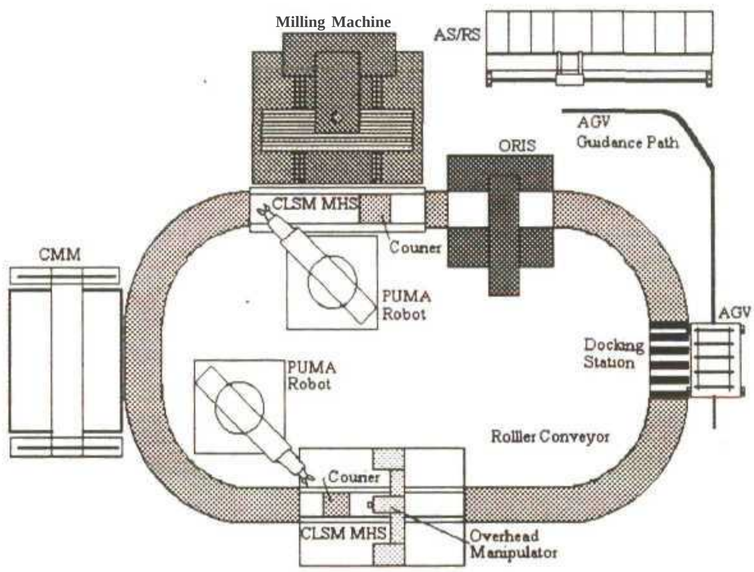

Figure 9.7: MR^{2}L CIM cell with integrated CLSM MHS

The CLSM MHS assembly system is positioned along the length of the oval track. When the courier is in the home position workpieces are placed onto the courier by the second PUMA robot. Parts can be assembled onto the workpiece, as discusses in section 9.2. To transfer the workpiece successfully the PUMA robot requires positional information. The growing trend in industry for in-transit inventory control can be facilitated by the CLSM MHSs. Each CIM module is currently being networked to 'a mainframe controller. By knowing where the couriers are positioned and what workpiece they carry, the host CIM controller can optimize the material flow in the CIM cell between the modules. The control system architecture and flow of information for the CIM cell is illustrated in Figure 9.8. The key aspect to optimal control of the CIM cell is the amount of quality information shared between the CIM modules.

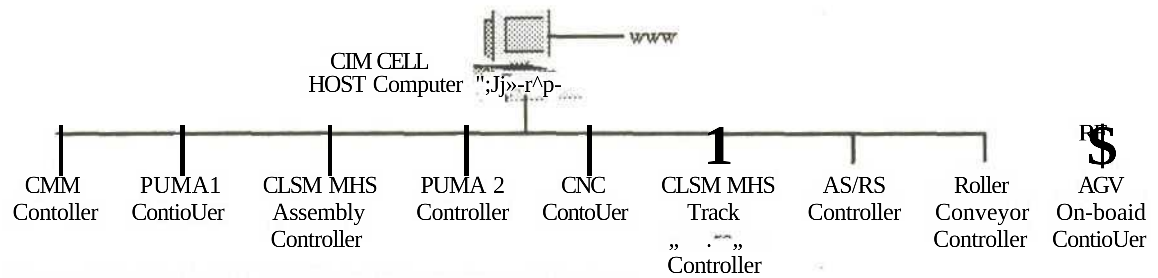

Figure 9.8: MR^{2}G CIM Cell control system architecture.

A number of material handling functions have been proposed for the CLSM MHS. Assembly systems and factory transportation systems are a few of the possible applications. The implementation of the CLSM MHS is also proposed for an advanced electronic component inspection system which is currently being built in the MR^{2}L. The proposed implementation of the CLSM MHS into the MR^{2}G CIM Cell has shown the advantages an intelligent, integrated material handling system in comparison to a traditional roller conveyor system can offer.

10. DISCUSSION

The integration of the moving magnet LSM and the custom engineered air bearing system, presents a number of new alternatives to current material handling systems being implemented in the manufacturing environment. Although moving magnet LSMs are not new, they have found limited applications in industry. The electromagnetic force directly engages the moving courier with no mechanical connection, thus the accuracy of the system depends entirely on the bearing system and feedback control. The reverse air bearing system has given the moving magnet LSM the flexibility and freedom it requires to impact on material handling functions. The bearing system allows the courier to move with ultra-smooth motion, enabling the courier to achieve high positional accuracy. The design, development and commissioning of the CLSM MHS presented challenging problems for which solutions had to be found. The problems which presented themselves and their solutions are discussed.

10.1 CLSM MHS ANALYSIS

10.1.1 POSITION FEEDBACK SENSOR

The ultrasonic sensor implemented as the position feedback device did not perform to acceptable standards. The analog output signal was unstable and peaked at 3.2V out of a 10V range. The courier could not be positioned successfully, neither could the air bearing system be controlled due to the erratic sensor signal. An investigation into establishing the cause of the interference on the ultrasonic sensor was undertaken by looking at the setup of the inverter, the wiring of the ultrasonic sensor to the PC30GA card and the physical setup of the sensor. By identifying the cause of the interference, it was hoped a solution could be found. It was known that the ultrasonic sensor output signal was linear when the inverter was not running.

10.1.1.1 INVERTER

Due to the interference of the analog output of the ultrasonic sensor only being present when the inverter was operating, the inverter was initially targeted as the source of interference. Discussions with Varispeed, the Yaskawa inverter agents, yielded two possible solutions. The first possible solution was to eliminate any input noise from the inverter supply. Two 0.1 p.F capacitors were connected between the Live and Neutral input terminals and the earth terminal on the inverter. The installation of the capacitor filters however made no improvement to the output signal of the ultrasonic sensor. The second possible solution was to install an output noise filter between the inverter and the motor. The output noise filter specifications are presented in Appendix G. The testing of the motor, with the filter installed, found that no improvement in the sensor's output was gained.

A further suggestion was to alter the inverter transistor switching frequency (carrier frequency) to reduce the motor noise. The carrier frequency had been set to the factory setting of 10 kHz. The motor was tested with the carrier frequency lowered to 7.5 k Hz. Since this had no effect on reducing the interference on the ultrasonic sensor, the carrier frequency was lowered to 5 kHz. However, at 5 KHz, the vibrations in the courier's backiron became audible which was undesirable. Due to the altered carrier frequencies having no effect, it was reset to 10 kHz.

Three possible sources of interference from the inverter were identified and tested with no positive result in eliminating the ultrasonic interference. The inverter was eliminated as the source of interference on the ultrasonic sensor

10.1.1.2 SENSOR SIGNAL CONDITIONING

The output of the ultrasonic sensor was rewired from a single ended input to a differential input (see Appendix H) on the PC30GA card to eliminate noise. This had no effect on the ultrasonic output signal. An oscilloscope was placed on the ultrasonic sensor output to view the noise signal. The oscilloscope showed that the sensor output contained significant noise. The noise was drastically reduced by installing a noise filter. However, testing of the motor with the noise filter on the ultrasonic sensor, resulted in no significant reduction in the sensor's output signal stability. With the reduction of the noise not yielding a solution, the problem pointed to a physical source.

10.1.1.3 PHYSICAL SETUP

The physical setup of the ultrasonic sensor was reviewed for possible causes of interference. The sensor was originally mounted on a stainless steel bracket attached to the CLSM frame. The sensor and bracket were held stationary whilst the motor was run. This resulted in a slight increase in the stability of the sensor output signal. Further investigations were done after removing the sensor from the stand and the CLSM stand was placed on rubber dampers. The sensor was mounted on a retort stand placed on the same table as the CLSM MHS. This increased the stability of the signal. However, the output signal was still too unstable. Improvements were gauged by looking at the size of the voltage output and the stability of the signal. Voltages above the previous 3.2V barrier with better stability were achieved. Further analysis of the physical setup revealed that if the sensor and its stand were placed on a table separate from the CLSM MHS, thus isolating them from each other, there was a dramatic improvement in the stability of the sensor output. An explanation for the ultrasonic interference was the vibration generated by the coils. The vibrations created a frequency which fell within the ultrasonic frequency range, thus interfering with the ultrasonic sensor output.

The increase in the output signal stability allowed for the air bearing system to operate effectively enough to levitate the courier. The new physical position of the sensor improved stability of the courier's movement. However, the sensor was still subject to lapses in stability. Thus with the courier positioned in the 7V range, a sudden momentary lapse in the sensor's output to 3V results in the courier suddenly moving forward. This is due to the control program being told that the courier was in a position less than the target position. To prove that the sensor was still being influenced by non audible noise created by the current flowing through the armature, the ultrasonic sensor was rotated 180° to face away from the armature platen. A target was moved within the sensor window limits to test the output. The output signal was very stable, much like when the sensor is operated without the inverter running. As soon as the ultrasonic sensor was rotated to face over the armature platen, the output signal showed a decrease in stability.

Although the stability of the output signal has been greatly improved, tests have shown that an ultrasonic sensor may not be the best suited position feedback device to be used with LSMs. Alternatives were presented in Chapter 7 which could replace the ultrasonic sensor.

10.1.2 INVERTER ANALOG INPUT

The PC30GA analog output used to set the analog input frequency reference on the inverter resulted in the motor's minimum frequency setting to be 1.32 Hz at 2.7 V. No output frequencies were obtained for input voltages below 2.7 V. Measurements taken on the voltage output of the card showed that the voltage was correct. Thus the problem was believed to lie with the inverter. After further discussions with the Yaskawa agents and the Electrical Engineering Workshop Staff, more information was gained as to how the inverter operated. Since the project's commissioning, experience has been gained by frequently operating the inverter and exploring the affects of varying the internal registers. With more information and a better understanding of the inverter, the problem was identified. The initial setup of the inverter's voltage frequency pattern was assigned according to Figure 7.13. The voltage frequency pattern was set to the voltage supply to range from 1.3 Hz to 50 Hz. The minimum output frequency was set to 1.3 Hz for a minimal output frequency voltage of 12 V. The frequency reference by analog input was set (Figure 7.15) by setting the frequency gain and the frequency bias. A 0% bias setting did not result in a 0 Hz output. It is a characteristic of the inverter to reference the inverter's frequency output according to the original voltage frequency pattern. The inverter could not operate for frequencies less than 1.3 Hz, which corresponded to analog voltages less than 2.7 Vs from the PC30GA card. Only when a frequency demand greater than 1.3 Hz (from a analog input of 2.7 V or more) was received, did the inverter begin to operate.

The solution was to determine a new voltage frequency pattern. This was done by adjusting the minimum output frequency and to the minimum value allowed of 0.1 Hz. The minimum frequency voltage output was adjusted to 1 V. Thus, an analog input setting of 1 V would result in an output frequency of 0.1 Hz. Test performed on the motor showed that a frequency output of 0.49 Hz resulted for a 1V input to the inverter. This can be attributed to the mapping of the frequency reference curve to the voltage frequency pattern. The movement of the courier at 0.49 Hz was more consistent compared to running at 1.32 Hz. The reduction in the minimum frequency output resulted in the momentum of the courier decreasing. The overshoot of the courier from the target position therefore decreased. The distance the courier moved either side of the target position was reduced to approximately 3 mm. The inability to run the inverter at 0.1 Hz inhibits the ability of the motor to achieve accurate positioning. To achieve accurate positioning of the courier, a more advanced control system may be required.

10.1.3 AIR BEARING SYSTEM

The performance of the reverse air bearing system developed was inhibited by the loss of pressure through the platen. This was largely due the layered construction of the armature platen. Since more has been learnt about the CLSM and confidence has been gained in operating the motor, the platen can be reconstructed. Reconstruction of the platen would involve removing the polycarbonate sheet attached to the platen frame and filling the entire platen with epoxy. Once the epoxy is cured, the platen surface can be plained to create a smooth air bearing surface. This would eliminate any loss of pressure through the platen, resulting in less orifices being required and greater loads being levitated by less pressure. Thus the same number of solenoid valves can be spread over a larger distance, making the reverse air bearing system more economical. A disadvantage of enclosing the armature platen in epoxy would be that the entire platen would have to be discarded should a coil break.

Cost-wise such a bearing system when compares favourably to a conventional mechanical bearing systems. When compared to a linear recirculating ball bearing carriage and guideway sized to support the same system the following advantages and disadvantages became evident. The cost to develop the air bearing system for the lm platen track was approximately US$700. This cost reduces to approximately US$450/m for each subsequent meter of the platen. The reduction in cost can be attributed to the duplication of roles by assigning several bearing pads along the platen track to the same solenoid valve. To develop the bearing system using a linear ball bearing system would cost approximately US$750 for the first meter. The cost would reduce to approximately US$570/m for subsequent meters. This can be attributed to requiring additional guideway lengths whilst still using the same linear recirculating ball bearing carriage. For a 5m track, the comparable prices of the two bearing systems would be;

Reverse Air Bearing System: US$2550
Linear Ball Bearing System: US$3030

The cost of developing the reverse air bearing system excludes the manufacturing and labor costs. Manufacturing and labor cost include the drilling of the orifices though the platen and inserting of the air lines, and the development of the bearing manifolds for each bearing pad. Although the cost of the reverse air bearing system is less, a disadvantage of such a system is the increased manufacturing time. A mechanical bearing system has the advantage of been an off-the-shelf system with minimal assembly, whereas an air bearing system has to be designed specifically to the application. Another disadvantage is the required control program to switch the solenoid valves according to the courier's position. The additional costs associated with the above mentioned disadvantages increases the overall cost of the air bearing system.

10.2 FUTURE RESEARCH OPPORTUNITIES

The next stage of the project involves two main streams of research. The first stream is to develop the concept of CLSM MHS into a dual axis system. The second stream is to upgrade and implement the CLSM MHS into the manufacturing environment. The development of a dual axis CLSM MHS will add to the system's flexibility and increase the possible applications of the system. Many research centers are involved in the development of planar motors usually based on the Sawyer motor topology. Development of a dual axis cordless planar motor will have obvious advantages over a tethered planar motor. Early design work has been undertaken in this area [Filho et al].

The development of a dual axis system will require a re-design of the PM courier and armature platen. A PM courier capable of bi-directional motion will require a PM matrix. Research into Halbach magnetic arrays will allow the PM courier to travel in both directions. Asakawa [Asakawa],Hinds [Hinds], Ebihara [Ebihara et al] and Trumper [Trumper et al] have all studied magnetic matrices. The development of a dual axis armature platen will require extensive 3-D finite element analysis to be performed. A method will have to be developed to compensate for the lateral force developed by the motor. The lateral force causes the courier to skew. The reverse air bearing system could easily be extended for a dual axis CLSM. The idea has been successfully implemented and tested in the single axis CLSM MHS. An alternative mechanical bearing system is proposed by [Filho et al].

The second stream of research would be to advance the implementation of the CLSM MHS into a fully integrated assembly system integrated into the MR2L CIM cell. Focus would be placed on the development of an overhead manipulator and part feeders, together with the development of a communication protocol to ensure optimal control and synchronization of the material handling system and the overhead manipulator. This would ensure that accurate assembly tasks could be performed. Further research into position feedback devices which are suited to the application in which the CLSM is being applied will be required.

11. CONCLUSION

The objectives outlined for the project have driven the development of a Cordless Linear Synchronous Motor Material Handling System. The advanced material handling system was derived from the investigation into current material handling systems and their impact on manufacturing environments. The research and development in LSM technology is driven by the desire for precision positioning systems for advanced agile manufacturing development. The conceptualization, design and development of the cordless motor has led to the development of a novel bearing system which complemented the motor's performance. The reverse air bearing system allowed the courier to move freely without friction. The tetherless design of the material handling system has ensured increased flexibility and travel of the system. The study of position feedback devices and control systems led to the implementation of non contact position sensor and scalar control system which best suited the early development and testing of the motor. The operating system developed allows for the systems parameters to be changed easily. This allows for easy integration into other systems. The integration and interaction of the material handling system with robots, glue dispensers, part feeders and overhead manipulators allows for the creation of advanced assembly systems. The increased intelligence of the system, compared to conveyor systems, allows the new material handling system to integrate into the modern information based manufacturing environment. Applying mechatronic principles in the development of the component parts ensured that each received equal weighting. The integration of contributing technologies such as electrical and electronic engineering, mechanical engineering and computer based technologies has assisted in the synergetic operation of the individual components in the material handling system.

REFERENCES

[Accutech] Accutech Automation Pty (Ltd),Pretoria, SA,E-mail: charlg@accu. co. za, 1999.

[Allergri] T. H. Allergri, "Materials Handling : Principles and Practice", Van Nostrand Reinhold Company Limited., London, UK ,1984.

[Anoradl] Anorad Linear Motors, Anorad, Hauppauge, NY, USA, www.anorad.com

[Anorad_2] Anorad Linear Motors: Catalog, Anaorad Hauppauge, NY, US A. 1998.

[Anorad_3] Moving Magnet Lightning Series Catalog, Anorad Linear Motor Division, Anorad, Hauppauge, NY, USA, 1999

[Ansoft_l] Maxwell 2D Field Simulator, User's Reference, Ansoft Corporation, NY, USA, 1994.

[Ansoft_2] Maxwell 2D Field Simulator, Parametric Analysis Module User's Reference, Ansoft Corporation, NY, USA, 1994.

| Ansoft_3] Maxwell 2D Field Simulator: Software Documentation Help File, Ansoft Corporation, NY, USA, 1994.

[Asakawa] T. Asakawa, "Two Dimensional Precise Positioning Device for use in a Semiconductor Apparatus", US Patent Office, Patent No. 4 535 278, USA, 1985.

[Atherton et al] D.L Atherton, "Maglev using Permanent Magnets", IEEE Transactions on Magnetics, Vol 16, nol, pp 146-148.

[Balchin et al] M. J. Balchin, J. F. Eastham, P. C. Coles, "Full Scale Testing of a High Speed Linear Synchronous Motor and Calculation of End - Effects", IEEE Transactions on Magnetics, Vol. 24, No 6, pp 2892-2894, November 1988.

[Banner] Banner Engineering Corporation, Minneapolis, U.S.A,1999, www.baneng.com

[Basak et al1] A. Basak, A. F. Filho, "Three Dimensional Computation of Force in a Novel Brushless DC linear Motor", IEEE Transactions on Magnetics, Vol. 33, No. 2, pp 2030 - 2032, March 1997.

[Bodika et al_1] N. D. Bodika, C. G. Jeans, R. J. Cruise, C. F. Landy, "Methods of Detent Force Reduction in Linear Synchronous Motors", www.ee.wits.ac.za/ -machines/members/

[Brennemann et al] A. E. Bennemann, R. L. Hollis, "Magnetic and Optical-Fluorescence Position Sensing for Planar Linear Motors", Proceedings of International Conference on Intelligent Robots and Systems, pp 101-107, 1995.

[Bright] Bright, G, "Computer Aided Control, Data Transfer Processing, Path Planning and Guidance Techniques for Automated Guided Vehicles", PHD in Engineering, University of Natal, Durban, 1993.

[Bush-Vishniac et al] I. A. Wang, I. Busch-Vishniac, "A New Repulsive Magnetic Levitation Approach Using Permanent Magnetics and Air Core Electromagnets", IEEE Transactions on Magnetics, Vol. 30. No. 4, pp 1422-1432, Julyl994.

[**Constantinescu]** V. N Constantinescu, " Gas Lubrication." ,The American Society of Mechanical Engineers, New York, USA, 1969.

[Cruise et al_3] R. J. Cruise, J. F. Pritchard, C. F. Landy, "Linear Machines and the South African Mining Industry", www.ee.wits/~machines/members/rupert.html

[Deta Tau_1] Delta Tau Data Systems, California, U.S.A, www.deltatau.com.

[Delta Tau_2] PMAC2 Product Catalog, Delta Tau Data Systems, California, U.S. A,

[Dover] Dover Instruments, http://www.doverinstr.com/TA.html.

[Eagle_l] User Manual-PC30F and PC30G Series Boards, Eagle Technology, Cape Town, S.A.

[Eagle_2] Eagle Technology, Cape Town, S.A. ,2000, www.eagle.co.za

[Ebrihara et al] D. Ebrihara, M.Watada, "Study of a basic Structure of a Surface actuator.",IEEE Transactions on Magnetics, Vol. 25, No. 5,pp 3961-3981, 1989.

[Electro-Craft] "DC Motors, Speed Control, Servo Systems and Optical Encoders", The Electro-craft Engineering Handbook, Reliance Motion Control, Inc.,Washington, USA, 1998

[Ezenekwew et al] D. E. Ezenekwe, K. Lee, "Design of Air Bearing System for Fine Motion Application of Multi-DOF Spherical Actuators", Proceedings of te IEEE/ASME International Conference on Advanced Intelligent Mechatronics, pp 812 - 818, Atlanta, USA, September 1999.

[Filho et al] A.F. Filho, A. A. Susin, M.da Silveria, "Application of Neodymium Iron Boron Permanent Magnets on the Assembly of a Novel Planar Actuator", IEEE Trans. On Magnetics, Vol.35, No. 5, pp 4034 - 4036, September 1999.

[Firth] L. Firth, "The Giant Book of Questions and Answers.", Rainbow Books, New York, 1984.

[Fuller] J. L. Fuller, "Robotics: Introduction, Programming and Projects",Prentice-Hall Inc.,U.S.A, 1999

[Geary] P. J. Geary, "Fluid Film Bearings", British Scientific Instrument Research Association, London, United Kingdom 1961.

[Gieras] J.F Gieras, "Linear Induction Drives", Clarendon Press, Oxford, London, 1994.

[Gieras et all] J.F Gieras, Z. J Piech, "Linear Synchronous Motors: Transportation and Automation Systems." CRC Press, NY, United States, 1999.

[Giza_l] M. Giza, "300mm Travel Air Bearing X-Y Stage", Technical Article, www. doverinstr. com/T A. html.

[Grassam et al] N.S. Grassam, J.W. Powell, "Gas Lubricated Bearings", London Butterworths, London, 1964.

[Groover] M P Groover, "Automation, Production Systems, and Computer Integrated Manufacturing", Prentice Hall Inc., NY, USA, 1987

[Groover et al] M P. Groover, M Wiess, RNNagel, N G Ordrey, "Industrial Robotics: Technology, Programming and Applications", McGraw-Hill Inc, USA, 1986.

[Hanselman] Duane C. Hanselman," Brushless Permanent Magnet Motor Design", McGraw-Hill, USA, 1994.

[Hayashira et al] H. Hayashiya, H Ohsalci, "The control of Normal Force of a Linear Induction Motor for Non-contacting Steel Plate Conveyance."-Source unknown.

[Heetal] J. L. He, D. M. Rote, "Double -Row Loop-Coil Configuration for EDS Maglev Suspension, Guidance, And Electromagnetic Guidway Directional Switching." , IEEE Transactions on Magnetics, Vol. 30, No 6, pp 2956 - 2958, November 1993.

[Hinds] W. E Hinds, "Single Plane Orthogonal Movable Drive System."US Patent Office, Patent No. 4 654 571, USA, 1987.

[Hinds et al] W. E. Hinds, B. Nocito, "The Sawyer Linear Motor." , Theory and Application of Step Motors.", USA, 1974.

[Hippner] Post Graduate Course: DNEL5SE-Special Electrical Machines, Course Notes, Electrical Engineering, Natal University, South Africa, 1999.

[Hippner et al] M. Hippner, Z. Piech, "Ripple Free Linear Synchronous Motor.",International Conference on Electrical Machines, Istanbul, Turkey, 1998.

[Hocken et al] R. Hocken, M. E. Williams, D. L. Trumper, "Magnetic Bearing Stage for Photolithography", Annals of the CIRP, Vol 42, No 1 ,pp 607 - 609 1993.

[Hollisetal_l] R. L. Hollis, A. Quaid, "An Architecture for Agile Assembly", Proc. Am. Society of Precision Engineering, 10th Annual Meeting, USA, October 1995. Pages Unknown

|Hollis et al_2] R. L. Hollis, A. A. Rizzi, "Opportunities for Increased Intelligence and Autonomy in Robotic Systems for Manufacturing", 8th International Symposium of Robotics Research, Japan, 1997. Pages Unknown

[Hoole et al] H. Hoole, S. Ratnajeevan, "Computer-Aided Analysis and Design of Electromagnetic Devices", Elservier Science Publishers, New York, USA, 1989.

[Hwang et al] L. wang, J. Poarch, "Placement Repeatability Study of Two Flip Chip Die Attach Machines: Leadscrew vs Linear Motor", Proceedings of the IEEE/ASME International Conference on Advanced Intelligent Mechatronics, pp 478 - 483, Atlanta USA, September 1999.

[Die'] 0. R Ilic', "Analysis of the number of Automated Guided Vehicles Required in Flexible Manufacturing Systems." ,International Journal of Advanced Manufacturing Technology, Vol 9, Pg 382 - 389, 1984.

[INA] INA Lineartechnik, Linear Guidance Systems Catalog, 1998

[Jeans et al_l] C. G.Jeans, A. Hansa, R. J. Cruise, C. F. Landy, "Comparison between Surface Mounted And Buried Permanent Magnets in Linear Synchronous Motors", www.ee.wits.ac.za/~machines/members/george.html

[Jeans et al_2] C. G. Jeans, R. J. Cruise, C. F. Landy, "Improved Performance of a Linear Synchronous Motor by the Inclusion of an Aluminium Sheet", www.ee.wits.ac.za/~machines/members/george.html

[Khan] M. S. Khan, G Bright, "AGV Docking System for Computer Aided Production Engineering", Proceedings of the 5th Int. Conference on Computer-Aided Production Engineering, Durham, England,April 1999.

[Kim et al] Analysis and Implementation of a Tubular Motor with Halbach Magnet Array", IEEE 31st Industrial Applications Society Annual Meeting, Vol 1, 1996.pg 471-478, Sweden.

[Kollmorgen] Platinum Direct Drive Linear Motor On-line Catalog. Kollmorgen Motion Technologies Group, New York USA, 1998.www.kollmorgen.com

[LabView_l] User Manual, Lab View Graphical Programming for Instruments, National Instruments Corporation, Austin Texasl996.

[LabView_2] Function and VI Reference Manual, Lab View Graphical Programming for Instruments, National Instruments Corporation, Austin Texas 1996.

[Laithwaite et al_l] Prof. E. R. Laithwaite, H. R. Bolton, " Linear Motors with Transverse Flux", Proceedings of the IEE, Vol. 118, No. 12, pp 1761 - 1767 December 1971.

[Laithwaite et al_2] Prof. E. R. Laithwaite, FT Barwell," Applications of Linear Induction Motors to High Speed Transportation Systems", Proceedings of the

IEE, Vol. 116, No.5, pp 337 - 343, 1969.

[Landy et al] C. F. Landy, R. J. Cruise, "Linear Synchronous Motor Propelled Hoists.", www.ee.wits/~machines/members/rupert.html.

[Lequesne] B. Lequesne, "Permanent Magnet Linear Motors for Short Strokes",IEEE Transactions on Industry Applications, Vol.32, No. 1, pp 161 - 168, January/February 1996.

[Lindkvist] R.G.T. Lindkvist, "Handbook of Materials Handling", Ellis Horwood Limited Publishes, Chirchester, England, 1985.

[Lowther] D. A Lowther, P. P Silvester, "Computer Aided Design in Magnetics."Berlin-Springer, 1986.

[Luggen] William W. Luggen, " Flexible Manufacturing Cells and Systems", Prentice Hall, USA, 1991.

[Lynch] T. Lynch, "Air Bearing Enable Micro-inch Accuracy Stage.', Design News, Pages 96-97, April 1995.

[MagneMotion] Linear Synchronous Motors, MagneMotion Inc., 1999, www.magnemotion.com.linear.html

[Manda] B. S Manda, U. S. Palekar, "Recent Advances in the Design and Analysis of Material Handling Systems", Journal of Manufacturing Science and Engineering, Vol. 119, pp 841 - 848, November 1997.

[Materials] "Materials Handling Today", South African Institute of Materials Handling, November, 1999, SA.

[Meijer] Carl Meijer, "Electromagnetic Theory." Internal Course (DNEC3CE2) Notes, Department of Electronic Engineering, University of Natal, July 1995

[Miller] T.J. E Miller, "Brushless Permanent Magnet And Reluctance Motor Drives",Oxford University Press, New York, USA, 1989.

[Millerl] D. Miller, "The Illustrated History of Trucks and Buses", New Burlington Books, London, 1982.

[Moon] Francis C. Moon," Magneto-Solid Mechanics", John-Wiley and Sons, New York, 1984.

[Normag]	Northern Magnetics Linear Motor Technology, Normag - Baldor Electric Company, Santa Clarita, CA, USA. 1998. www.normag.com
[Nova]	Innova Laboratories Inc., San Diego, CA, USA, 1999, www2. connectnet. com/~innova/index. html
[Nysschen **et al]**	R. C. Nysschen, P. B. Me Shane, R. J. Cruise, C. F. Landy, "Design and Construction of A Levitated Vehicle Using a Single Excitation Source.", www.ee.wits/~machines/members/rupert.html
[Parker]	Rollin J. Parker, "Advances in Permanent Magnetism", John Wiley and Sons Inc., USA, 1990.
[Pemberton]	A.W. Pemberton, "Plant Layout and Materials Handling", McMillian Press, London, 1974.
[Pence]	I. W. Pence Jr, "A perspective on Material Handling Engineering: History and New Challenges", Journal of Manufacturing Science and Engineering, Vol. 119, pp 835 - 840,November 1997.
[Polgreen]	G. R. Polgreen, "New Applications of Modern Magnetics", McDonald and Company PTY., London , 1966.
[Potgieter]	J. Potgieter, "PC-Based Robotic Control System for Computer Integrated Manufacturing", Master of Science Thesis, School of Mechanical Engineering, University of Natal, Durban, 1998.
[Quaid et al_l]	A. Quaid, R L. Hollis, "Cooperative 2-DOF Robots for Precision Assembly", International Conference on Robotics and Automation, USA, 1966.
[Quaid et al_2]	A. Quaid, R. L. Hollis, Y. Xu, "Force Characterization and Commutation of Planar Linear Motors", IEEE ICRA Proceedings, USA, 1997.
[Renishaw]	*Laser Systems,* Renishaw pic, New Mills Gloucestershire, UK., 2000, www. renishaw. com/laserscale/laserwork html
[Rehg]	J. A. Rehg, "Introduction to Robotics in CIM Systems", Prentice-Hall, Fourth Edition, U.S A , 1997.
[Rhomberg]	Product Brochure, Sensick Industrial Sensors. South African Agents:

Rhomberg Africa.

[Robotworld] Robotworld, Motoman Inc. www.motoman.com/prodnav.htm

[Salant] M. A. Salant, "Introduction to Robotics.",McGraw - Hill Book Company, USA, 1988.

[Sanada et al] M. Sanada, S. Morimoto, Y Takeda, "Interior Permanent Magnet Linear Synchronous Motor for High Performance Drives", IEEE Transactions on Magnetics, Vol. 32, No. 5,pp 15 - 20, September 1996.

[Sandia] Sandia National Laboratory: Agile Manufacturing Prototyping System,", www.sandia.gov/AMPSfact.html

[Seki et al] K. Seki, K. Oka, M. Watada, S. Torii, D. Ebihara, "Pull in Control of the Linear Synchronous Motor with Discontinuously Arranged Primary." IEEE International Symposium on the Industrial Electronics, 1996, pg 260-265.

[Semipower] Semipower Systems Inc.,California, U.S.A., www.semipower.com

[Sul et al] S. Sul, H. Kim, J. Kim, "Thrust Ripple Free Control of a Cylindrical Linear Synchronous Motor Using Finite Element Method."IEEE 31 st Industrial Applications Society Annual Meeting, Vol 1, 1996.pg 42 - 46.

[Tio-lec] Product Information Brochure/ Quotation, Tio-lec (Pty)Ltd, Johannesburgh, South Africa, 1999

[Thornton et al] R. Thornton, E. Lohner, "The MagneTrack Linear Synchronous Motor Material Transport System", 1999, www.magnemotion.com,

[Tlale] N.S. Tlale, "An Intelligent Generic Gripper for Conventional Electronics Assembly", Master of Science Thesis, School of Mechanical Engineering, University of Natal, Durban, 1998.

[Townsend] M. Townsend, "Air Bearings Provide Unmatched Straitness of Travel." Technical Article, www.doverinstr.com/TA.html.

[Trilogy_l] PM Linear Motors, Trilogy Systems Corporation, USA, 1999 www.trilogysystems.com

[Trilogy_2] Trilogy: Linear Motor Technical Specifications, Catalog, 1998.

[Trumper et al] D. L. Trumper, W. Kim, M. E. Williams, " Design and Analysis Framework for Linear Permanent Magnet Machines",IEEE 29th Industrial Applications Society Annual Meeting, Vol 1, 1994pg 216 - 223

[Tzeng et al] Y. Tzeng, T. Wang, "Optimal Design of the Electromagnetic Levitation with Permanent and Electromagnets", IEEE Transactions on Magnetics, Vol. 30, No. 6, pp 4731 - 4733, November 1994.

[Wang et al] T.C. Wang, Y. Tzeng, "A New Electromagnetic Levitation System for Rapid Transit and High Speed Transportation", IEEE Trans, on Magnetics, Vol 30, No 6, pg 4734 - 4736, November, 1994

[White] J. A. White, "Design and Analysis of Integrated Manufacturing Systems: Material Handling In Integrated Manufacturing Systems.",National Academy Press, USA, 1987.

[Williams et al] R. Williams, J. R. Mately, Y. Arie, J. Rathee, "The effect of mass and pole strength on the levitation height on a magnet over a superconductor", Journal of Applied Physics, Vol 65, No. 9, pp 3583 - 3585, 1989.

[Yaskawa] Yaskawa Electronic Corporation, Japan, www.yaskawa.com.

[Yaskawa_2] VS mini V7 Series Instruction Manual, Yaskawa Electronic Corporation.

[Yamamura] S. Yamamura, " Theory of linear induction motors", University of Tokyo Press, Japan, 1972.

LIST OF SUPPLIERS

1. **Festo (PTY) LTD.**
   -Industrial pneumatic cylinders and systems.
   Tel: (031) 208-9116

2. **Varispeed:** Yaskawa Agents
   - Inverters and Drives
   Tel: (011)315-4592

3. **Dargells Engineering and machinery Sales (DEMS)**
   - Tufhol and Polycarbonates
   Tel: (031) 303-1347/8/9

4. **Durban Plastics (PTY) LTD.**
   - Perspec and Polycarbonates
   Tel: (031) 301-7511

5. **Eagle Technology**
   Multifunctional Data Acquisition Boards
   Tel: (021) 423-4943

6. **Natal Stainless Steel**
   - Stainless Steel
   Tel: (031)461-3611

7. **NDE Stainless Steel**
   - Stainless Steel
   Tel: (031) 700-5444

8. **Technical and General Distributions**
   - Permanent Magnet Material
   Tel: (011)886-7280

APPENDIX A

PERMANENT MA GNETDA TA

APPENDIX A

TABLE A1: Characteristic Properties of VACODYM and VACOMAX Magnets

Chwaeumao Propanlti « WCODYM ind V»COM«< il >m nnvenlun

Maunai			VACOtJYU »HR	VACQOVM XMWI	VATODVU xim	VACW7YU MIWI	VAcocm 175 HH	VACOOTM 170 WZ	VHCOCVM 450 HK	VACODYM 400 WZ	VACOMAX 225 HR	VACOMAX 225 WZ	WCOMAX 200	VACOMAX 170	WCOMAX 145	WCOMAX •IT	VtCOUAX »T	WCOMAX g«K
UannlJcanwnMon			NdFeB						j		Sm_2Co_{17}		6EC0,					
Ood.1			2*»10	2io/ao	2«W105	J10.T0)	140/IM	1PQ/IU	• 1WIT0	170/170	iso/eo	150'tO	VXV100	190/110	MO/129	M'I9O	9XV190	ao/no
!*-»*«.	**B,	(IMa|	IJO-I.M	i.u-i.ir	120-tJO	ijn-i.ir	1 19-113	1JM-I.11	. 1.0S-119	0I5-1M	•.9Q-l.1t	0M-I.09	o.n-iA	o.ao-i.00	OJS-O.M	• M-0.744	o.ao-o.w^	O.ga-0.64
Do**) chatty	^V (fH«	^A/n>)	Too-iom	(90400	•ao-iooo	•00- HO	aao-iooo	no-«M	no-«o»	•ao-aio	•00-400	5os-«a	)io-aoo	•n-reo	•00-720	•B-U9	496-120	'20-S00
	• trploU	*A/h,|	1000	lots.	1200	1200	1490	IU0	iaoo	IMO	1200	120C	BOO	1700	17M	MOO	2000	1KB
	"mm.	fiA/m)	900	•00	WOO	I0M	IMO	I3U	1700	1700	900	•00	1000	1300	1200	WOO	woo	ioo»
&»,r<»~"Y	'•"•—	Mmi	itatM	210-270	J0O-J35	210-270	J40-K0	iaa-4" -	• / >"1	170-220	190-240	150-200	I9O-H0	no-w	140-UO	n-iio	)0-U	ao-ao
Magnetization field strength |t*J	KM,	tlA/fTI]	tax	2500	29O0	2M0	2K0	2«0	7XC	MOO	MOO	um	1000	looo	?oorj	1000	2003	2000
Rev. temp. coefficient at temp. interval	TK(B) M-C-IOO*S	[%/K]	-0.11	-0.11	-O.10	-on	-0.10	-OIlO	•fl.10	-0.10	-O.O50	-0.030	-0.040	-0040	-4.040	b*» -0.011	MIV-O.010	-6.040
	WC-IWC		-	-	.	-	-0.12	•*. 12	-<i.ia	-4J.11	-0.035	-0.M1	-0049	-0.048	-0.045	-oxns.	-0.010	-
mu Doilhtous kn^.	T*«*	PC]	100	100	120	120	150	ISO	190	110	300	300	190	250	no	250	290	u
CuhaHxio.	t,	PC]	KXXB.3I0	appro. 110	anmx.110	•ixxn.110	•pprm.310	«{n».I10	. »pit«.3ra	•ppnn.310	•pprnn.900	•ppu.100	appot.llo	•ppnM.720	•ppmi.720	•tvrm.no	appra.no	WKPJ..720
Om«vtyplMI		*["1	7.4	7/4	T.4	1*	7.4	7/4	; 74	7.4	94	1.4	14	«S	•J	8.3	9.1	6.0
Specific electrical resistivity		[Ω mm²/m]	1J-1J	IA-14	1.4-1J	\A-\i	1,4-19	1.4-IJ	; i4-u	la-ii	OTJ-OM	o.rt-o.is	0 9-o.g	oj-o.a	o»-os	O.i-0%	0.9-O.9	11
Sp«*Ct>a<«		M/IHK3I	mvm.ua	appm.440	•nnx-MO	nnsui	Kpm.440	•Bpn>.440	1 tPCRH.440	•pprix.440	4O0TO.3W	approx. 390	•ppor-570	•pprm. 970	appn^JTO	nam.%n>	apm.370	-
TtaTnalwMucl*,		|w/|n.n|	•Broil	•pprgut	appmit	•ppmt	•ppn.1	«ni.I	1 appro.!	•ppRK.a	B00T9M1	•PP—.12	asm»i.n	appnx.10	•PP"«.1O	•pproLiO	•PPW.W	•J
Coefficient of thermal expansion	ll c	[10-6/K]	1	5	a	8	5	a	1 1	8	10	10	t	T	7	r	l	10
	1c		-1	-1	-1	-l	.1	-1	i-1 •	-T	a	12	a	11	11	11	11	-
YflUICJ Stm&MM		(IO'H'rwT^	1.9	IJ	u	u	1J	1.5	1S	IJ	1.9	IJ	u	11	VI	IJ	I.I	-
MWrnd		N<mm]	appro*. 270	•RXX.IT0	imKtn	appxx.ro	•RinnL270	•PPRM.270	.mm.in	ap[»ot270	90-190	n-iso	•<*«».<»	appnx.120	aporm.120	•pprea. 120	appro. 120	appro, wo
Compressive strength		[N/mm²]	.op™. 1080	appnvioso	•peraLiou	•ppw.1050	M^xIOM	•»*»-1050	• wcra. 1050	»P«.I090	approx. 850	appro*. I»	•Ptxs.1000	apprm. 1000	•ppra^WOO	•ppn». IOT»	apem. 1000	aenro.250
Vkanrortnm	HV		Kpprcn.STD	•ran».ro	tppnH.170	•rvo.no	Kcnv.1711	•pprQK.570	1 Mpna.570	appro.. 570	u>pn>H 940	appr^gM	annenBM	approx. 850	tpprox.9«0	•ppn».96O	appro.5H	appn». no
2£J£££**1"1C*	** •	N	70-flO	70H»	To-ao	7(H0	70-W	70-»0	70-00	70-«	40-50	•O-SO	S0-70	50-70	SO-70	10-70	SO-70	-

[1] Coating based on DIN 17 410 or IEC 404-8-1, respectively; the magnet values are normally superior to the IEC values.

[2] Details of the reversible coefficient of temperature as a function of temperature are shown in Fig. 11, Page 13.

* Dun «i anilialwif nn»0iM«pi»«TTi1nrrrT f»*r t"ah^rr–
Users are recommended ... solve temperatures above 150 °C or in general with regard to VACODYM
WC0OTM1xi VACOMAX are anisotropic materials, use reversible permeability at the working point is ... < 1.1
The exact value depends on the type of material and the geometry of the magnet.

* Oa !• to»•»«• tv pam air-pressed in an axial field.

WCCCTU<»«« WCOWMDOnot•>**«eM! ... the pamkitnnoiCOTWCM:oMrf»other

APPENDIX A cont.

TABLE A2: Magnetic characteristics of sintered NdFeB PMs manufactured in China. [Gieras et al]

Grade	Remanent magnetic flux density B_r, T	Coercivity H_c, kA/m	Intrinsic coercive force $_iH_c$ A/m	Maximum energy product $(BH)_{max}$, kJ/m^3
N27	1.02... 1.10	764...836	≥ 955	199...223
N30	1.08...1.15	796...860	≥ 955	223-247
N33	1.13... 1.17	844.-884	≥ 955	247-263
N35	1.17...1.21	876...915	≥ 955	263-286
N38	1.20 ...1.28	899. ..971	≥ 955	286...302
N27M	1.02-110	754-836	≥ 1194	199-223
N30M	1.08..1.15	796...860	≥ 1194	223-247
N33M	1.13-1.17	844-884	≥ 1194	247-263
N35M	1.17...1.21	876...915	≥ 1194	263-286
N27H	1.02...1.10	764-836	≥ 1353	199-223
N30H	1.08...1.15	796...860	≥ 1353	223-247
N33H	1.13...1.17	844...884	≥ 1353	247-263
N25H	1.17...1.21	876...915	≥ 1353	263-286
N27SH	1.02...1.10	7S4...836	≥ 1592	199...223
N30SH	1.08.. .1.15	796-860	≥ 1592	223-247
K33SH	1.13...1.17	844-884	≥ 1592	247-263
N35SH	1.16...1.22	876...915	≥ 1592	263.-279
N25UH	0.97...1.05	748-812	≥ 1910	183-207
N27UH	1.02...1.10	7B4...836	≥ 1910	199-223

TABLE A3: Physical properties of sintered NdFeB PMs manufactured in China. [Gieras et al]

Grade	Operating temperature °C	Temperature coefficient for B_r %/°C	Curie temp. °C	Specific mass density g/cm^3	Recoil permea-bility
N27	≤ 80	-0.11	310	7.4...7.5	1.1
N30	≤80	-0.11	310	7.4...7.5	1.1
N33	≤80	-o.u	310	7.4...7.5	1.1
N35	≤80	-0.11	310	7.4...7.S	l.l
N3B	≤ 80	-0.11	310	7.4...7.5	1.1
N27M	≤100	-0.11	320	7.4...7.5	1.1
N30M	≤ 100	-0.11	320	7.4...7.5	1.1
NS3M	≤ 100	-0.11	320	7.4...7.5	1.1
N3oM	≤ 100	-0.11	320	7.4.-7.5	1.1
N27H	≤ 120	-0.10	340	7.4..J.5	1.1
N30H	≤ 120	-0.10	340	7.4...7.5	1.1
N33H	≤ 120	-0.10	340	7.4...7.5	1.1
N35H	≤ 120	-0.10	340	7.4...7.5	1.1
N27SH	≤ 150	-0.10	340	7.4...7.5	1.1
N30SH	≤ 150	-0.10	340	7.4..J.5	1.1
N33SH	≤ 150	-0.10	340	7.4..J.5	1.1
N35SH	≤ 150	-0.10	340	7.4...7.5	1.1
N25UH	≤ 170	-0.10	340	7.4...7.5	1.1
N27UH	≤ 170	-0.10	340	7.4...7.0	1.1

APPENDIX A cont.

FIGURE A1: Demagnetization Curves for NdFeB - Grade35

NEO-35 DATA SHEET

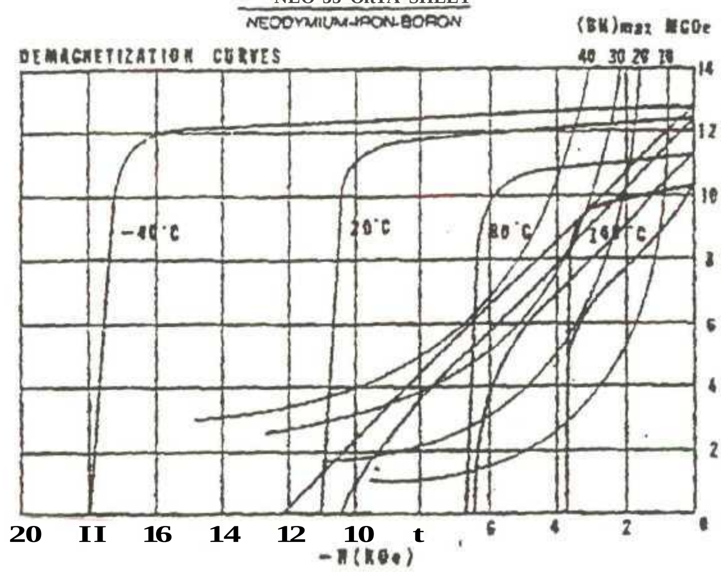

LISTING OF MATERIAL CHARACTERISTICS

NEO-35

Residual induction Br	KG	11.5-12.5
	T	1.15-1.25
Coercive force bHc	KOe	8.0-10.3
	KA/m	636-535
Intrinsic coercive force iHc	KOe	10.0-12.0
	KA/m	796-955
Max. energy product (BH) max	MGOe	33-35
	KJ/m³	263-287
Temperature coefficient of Br (0-100 C),	%/C	-0.12

Curie temperature Tc	°C	300-333
Density D	g/cm³	7.3-7.5
Vickers hardness Hv		500-600
Resistivity r	Ω-cm	1.6 × 10⁻⁴
Compressive strength σ	kg/cm²	7.4 × 10³
Working temperature	°C	< 80

APPENDIX A cont.

TABLE A4: Magnetic characteristics of bonded NdFeB PMs manufactured in China. (Gieras et al]

Grade	Remanent magnetic flux density B_{ri} T	Coercivity $H_{C!}$ kA/ra	Intrinsic coercive force iH_c A/m	Maximum energy product (BtfW, kJ/m^3
N36G	≥0.70	≥170	≥210	32...40
N44Z	≥0.47	≥360	≥540	40...48
N52Z	≥0.55	≥360	≥500	48...56
N60Z	≥0.68	≥380	≥680	56...64
N68G	≥0.60	≥410	≥1120	64.-72
N76Z	≥0.55	≥400	≥720	70...80
N84Z	≥0.70	≥450	≥850	80...88

TABLE A5: Physical properties of bonded NdFeB PMs manufactured in China. [Gieras et al]

Grade	Maximum. operating temperature °C	Temperature coefficient for B_r %/°C	Curie temp. °C °C	Specific mass density g/cm^3
N36G	70	≤-0.13	300	6.0
N44Z	110	≤-0.13	350	6.0
N52Z	120	≤-0.13	350	6.0
N60Z	120	≤-0.13	350	6.0
N68G	150	≤-0.13	305	6.0
N76G	150	≤-0.13	360	6.0
N48Z	150	≤-0.13	360	6.0

APPENDIX A cont.

TABLE A6: Magnetic Properties of Sintered Permanent Magnets.

tTEMIsSINTERED NdFeB PERMANENT MAGNET

MAGNETIC PROPERTIES OF SINTERED NdFeS PERMANENT MAGNET

LAUDE

烧结钕铁硼永磁体磁性能

GRADC	BT Residual Induction KBS	Coercive Force KOe	Mc Intrinsic Coercive force KOe	BHmax Maximum Energy Product MGOe	Working Temperature (max) ℃	TEMP COEFF OFBr 20℃−140℃ %℃	TEMPOS Oft* 20℃−140℃ %℃	CURE Temperature ℃
N-27	10.3-11.0	>9.0	>9.5	25-28	80	-0.12	-0.6	312
N-30	10.7-11.5	>9.0	>9.5	28-32	80	−0.12	-0.6	312
N-33	11.3—11.7	>9.0	>9.5	31—33	80	-0.12	-0.6	312
N-35	11.7—12.4	>9.5	>9.0	33-35	80	-0.12	-0.6	312
N-38	12.2-12.1	>9.5	>8.0	35—38	80	-0.12	-0.6	312
N-27H	10.3-11.0	>9.0	>17	25-28	100-120	-0.11	-0.6	320
N-30H	10.7-11.5	>9.5	>17	28-32	100-120	−0.11	-0.6	320
N-27SH	10.3-11.0	>9.0	>20	25-28	120-150	-0.1	-0.6	340
N-30SH	10.7-11.5	>9.5	>20	28-32	110-130	—0.1	-0.6	340

1.DENSITY.7.3-7.5G/CM2

2.MAGNET SHAPE,

DISKS-RINGS.CYLINDER,BLOCKS.ARCS

AND CUSTOMER REQUIRED SHAPES

3.COATING

Zn.Ni.AND RESIN COATING

MAGNA & LAUDE

MAANSHAN FOREIGN TRADE CORPORATION

ADDRESS:5/F .FOREIGN TRADE BUILDING .MAANSHAN CITY.ANHUI P. R.CHINA

FAX:+86 555 2484638 TEL:+86 555 2184538

APPENDIX B

Anorads LEB-S Brushless Linear Motor Series

APPENDIX B

Anorads LEB-S Brushless Motor Series

LEB-S

BRUSHLESS LINEAR MOTOR

- High force, epoxy core
- Enhanced cooling for high duty cycle
- No cogging, no magnetic attraction
- Mounting from all three sides
- Ideal for high precision/ smooth motion

For lequred force se*ct motor troe on p. ». For lesurwi wkxily wuc matching amplifier or p 85

LERS Specifications

Mm«r U«»e}		Symbol	Uulu	i£•*!.!			Ins-4-5			B U S			LERW-sr		
Cooling				NT	AT	V-	NC	AC	W	DC	AC	WV	NT	AC	W
CcttttMMS Faroe	4←! e JTO	Fc25	H	K	IOt	IIS	192	211	n	B>	Hi	MS	«J	422	4K
			hi	B-.	23	25	42	46	51	. 4 4	T	76	84	93	101
C««XJAM«S C»TTCfU	4t*l*23T)		Aim	34	3.7	4X	3.4	3.7	41	3.4	3.7	4.8	6.7	7.4	II
COtlUIMra* FflTW	4i»tt#lliT(	Fc125	N	11	30	91		179	in	244	260	293	IJt	3sa	291
			b	'8	K_JL..		36	I!	43	u	59	44	72	79	86
CAfettBMW CsTTCftt	(rmM 0 IBtl	uis	ARM	u	3.1	34	2.3	3!	3.4	u	11	14	1.7	u	kl
fMiFoTH	Mini	I.US	N	326	114	SK	B)	Ql	61	9n	977	B77	1WI	1313	HID
			lbs	72	72	72	143	143	143	215	21S	215	217	zn	2R
tai-Comm	>us»i	lp 0.25	An.	11.4	11.4	11.4	11.4	IK	IU	n4	IU	11.4	11.4	IU	11.4
Peak Force	(1 sec)	f»l	N	Oi	122	232	4E	4S	Mi	m	697	H7	929	•Z9	a
			ft)	51	S1	51	nn	IC	IC	153	IS3	13J	204	XX	2D4
Pa} Curaal	(1 ac)	lpl	AIM	L2	u	12 "	u		L3	12	u	8.2	lt.4	IU	IK
CnOiMtvf tower Low	t*u * tc*C)	ME	w	' 3Si	35.5	42.4	319	7LJ	MJ	m	ltu	mi	117JI	1414	m j
f am (MitUI 111 Tfcnc Paal		Kf	W/A mm	23.47	2X47	2117	MS	StS)	SU3	82.40	U40	KM	M.93	iUl	JtSJ
			la/Am	at	6.36	Ui	C33	us	IIS	18.79	un	U.7)	113	12.53	OSS
Back EMF	(pk)	ke	Vrms/m/sec	9.41	SO	TM	IUi	1W	MM	I14T	ttr	2X47	U9t	18.98	18.98
			Vrms/in/sec	UK	CJt	0.24	0.47	0.47	0.47	6.71	0.71	1.71	0.47	M7	147
laibiii	{m'nxt	£25	si	1.!	It	li	-J	SI	ij	?1	7JI	7i	3J	2t	2J
Idinitt </m «	ITTCI	uz	u	U	3.8	IC	72	73	TJ	IU	IU	iaj	3.6	5.8	U
tMDCtnn	(—1	I	•IE	1.4	1.4	u	2J	z1	U	4J	u	4.2	14	U	3.4
EtamalTVneCoiatnt		>	wms.	154	U4	IM	UI	0-W	154	dS4	1.S4	134	IS4	Ci4	>M
Mator CoutMit	n**HK mi	In	*!<•%	166	8.66	ME	O2S	uz	U2S	ISXC	ISM	15 »	17 J:	173!	17J!
			kl-<\	1.91	1.91	1.11	IB	2.09	24)	3.30	uo	3.30		311	Ul
Ibenul BeMUm		tit	°C/W	1.13	194	• 79	UT	l.<7	on	UI	UI	OJt	ut	in	oai
Mumm Ui! Tcwp4nt«re		m	°C	IK	US	US	I2S	12!	Ui	us	I3i	IS	IS	115	12!
QtflAutnUyWctfkl		*'	kg	8.4	14	0.4	17	«7	1.7	u	LI	11	u	1.6	Li
			lit	C!	S9	19	li	It	u	34	14	14	3.5	35	3.5
MirMttCMtrKlwn		F»	n	D	6	I	1	•	0	8	1	0	g	1	0
			lbs	D	J	•	•	t	1	0	•	0	•	t	0
Cooling Flow Rate		V	in	H/I	107.'	31	•A	93.1	u	M	TZJ	It	n/a	65.9	
			scrwoY	Kit	3.7	1	n/a	12	1	n/a	tr.	1	n/a	13	i
Cooling Supply Pressure		P	kPa	•d	207	241.5	n/a	207	27*	Ml	m	310.5	Ml	107	MS
			rsit	n/a	W	£	n/a	30	41	•0	31	45	1*1	30	SO

Note: Additional models available. all specifications are ± 10%

APPENDIX B cont.

Ordering Information

Coil Assembly

Example **LEB-S -8 -SP -WC2 -TE -HES**

O Numoerof Coil Set	a, **4,6,8**	
❷ Coil Winding Connection	S—Series	SP-Series/Parafiel
©Coding Type	*NC* -No Cooing **AC**-Air Cooing ***ACB*** -Double Sided Air CooBng	**WC** -Water Cooling *WCS* -Double Sided Water Cooing
© **Thermistor**	**TE**—Tnefnislw	*NT* -No Thermistor .
❺ Had Effect	*Mi-Ham* Efiect HB —Sinusoidal Hall Effect	**MET**—Trapezoidal Hail Effect *[US]* -Non Standard Mounting

Note: Hall eflect mounted on cabte side, otherwise indicate **JASJ**.

Magnet Assembly

Example ***LEBS'SSSmm***

O Magnet Assembly Length ***SSS, 3OO, 375,4SO, SBS. BOO,* 675, *7SO*** *mm*

Note: Magnet assembles can be butted together to provide longer length.

Cable Pinout

	Pin i Cflior	FunctM		lenyth
MOTOR 1EADS	• **RED**	**•A**		
(Siandard)	**WHT**	**oB**		**Olm**
	BLK	**«C**		**1ft**
	GRX	**GND**		
THERMISTORS	**Bll**	12St		**ELXm**
(Optional)	**BU**	12S^		in
HAH		**Tno**	**Sine**	
EFFECT	**RED**	**V+**	**1+**	
CONNECTOR	**BUi**	**S2**	**A+**	**0.3m**
(Optional)	**wm**	**SI**	**A-**	**lft**
	ORM	**S3**	**&+**	
	CRN		B-	
	BLK	**VKTN**	**1-**	

Nate; 1+ S mA Nominal; V* 5 • 24 rtc

Force Rating

a) Contnuous forces and currents are based on coil moving with an phases sharing the same load in smusctaal corraniraBon.

b)Ccat attached to aluminum heat sink 254 x 254x 25.4 mm (Iff x 10" x 17

c) Care must be taken to remove heat from the coil mounting pats and from the magnet plate.

d) For double-sided cooling, AC and WC, multtpiy continuous torces and currents oi AC2 by 1.1 and otWC2by 1.2, respectively.

e) For stand still conditions multiply continuous torce and continuous current by 0.9.

r) Coil moummgs on either of the two narrow sides reduces continuous force by 20%.

Magnet Assembly Specifications

a} Magnet assembly weight; 11.4 kgrn (0.64 Win).

b) Magnet pitch (180°) = 15 mm (0.59 ri).

c) Magnet assy, length = travel + coil length + hat tength (see example on p. 9].

d) AS evan lengths (e.g. 300.450,600,750) can be butted on either side.

e) All odd lengths (e.g. 225,375.525,675) can be butted only trom one side.

APPENDIX B cont.

LEB-S roinnrtflfirmrB-

Coil Assembly Outline

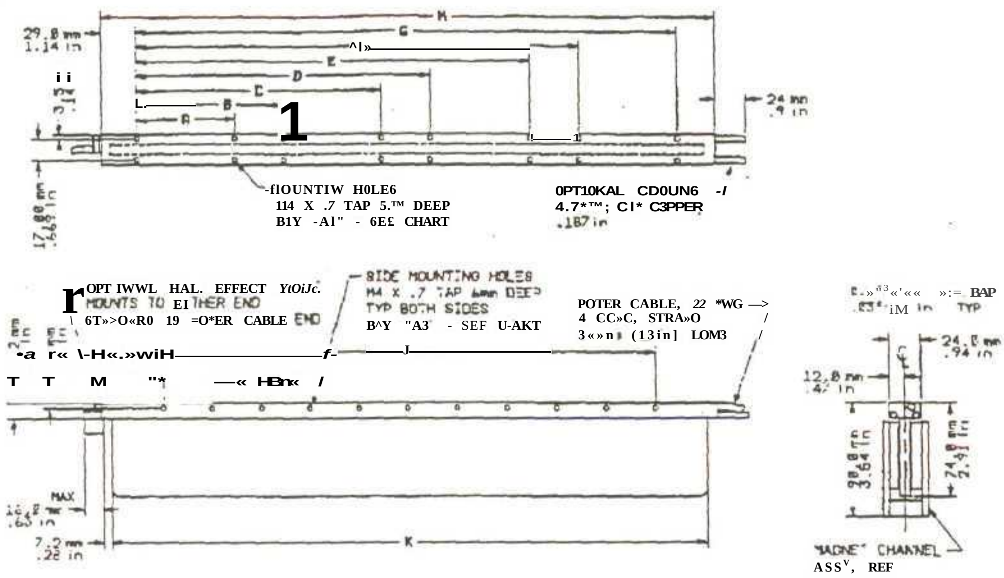

MOTOR		A	B	C	D	E	F	"ft?	H	J	K	A1	A2
LE&S-2	•n	80.00	-				-		140.00.	40.00	123.5		4
	ID	3.150							• isi-')	1.575	4.B6		
LE&&4	mm	(0.00	12D.0G	20O00	*	-	*	.	2NUD	16OX0	3.5	i>	10
	Is	X150	4.T34	7*71					10J4	U99	•••?.»		
LEB-S-6	nm	«uun	L2OO0	200.0(1	240.00	K0.0S	-		3SO.O3	230.V0		u	16
	U	2.150	4.724	7.874	94«	123MI			I4J6	usu	1O1		
LBBA*	DSD	80.00	120.00	200 00	240.00	320.110	360.00	*40J«l	snioo	400.UI	483.5	16	22
	in	3 130	4.724	7.874	9.449	12.59S	14.173	17J2i	M « .	15.748	19.U4		

CAD DISKS AVAILABLE

APPENDIX B cont.

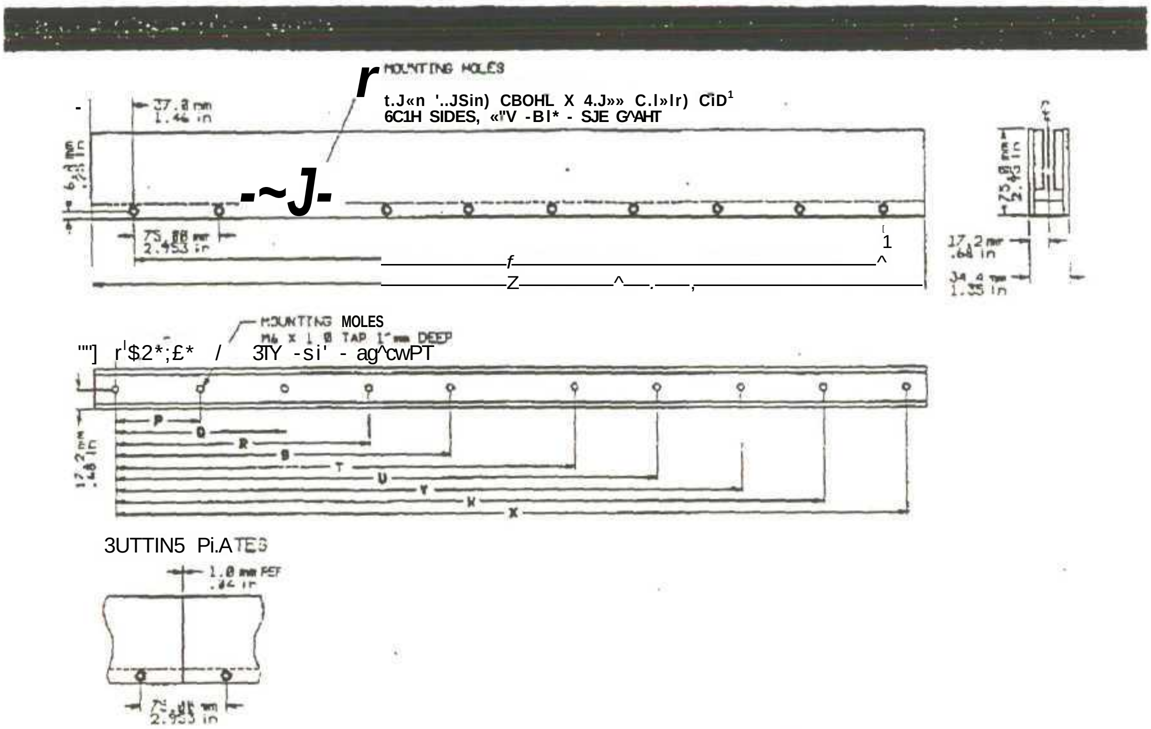

		P	Q	R	S	T	U	V	W	X	Y	Z	•njnr	B2(7TT
sac : • as	mm	75.90		187 X	-	-	-	-	-	-	1SOJ»	224.00		4
	In	2553	4.C29	•T.M2							S906	S.B19		
HO	mm	75-00	1ST JO		*	"	*	.	•	*	225.00	235.00	4	4
	In	ISO	73K2	10X15							8.B58	11.772		
• 375	rnm	7&00	150.00	18730	2CL51)	337 JO	-	.	•	.	300.00	374.00	5	t>
	In	Z953	S306	T.3S2		11287					113U	14.724		
450	nun	3.00	150.00	2S2.S0	•aim	412.SC	-	-	-	-	37S.O0	449.00	6	6
	III	1953	530G	1QJ3S		ItHO					U.7M	1T.S77		
• SB	Run	7SJ)11	1W.O0	22S.00		337 J5C		487.50	-	.	450.00	524.00	7	i
	in	1SS3	5^06	&en	102S	ixan	I&MO	19.in			17.717	20X30		
Ml)	omi	75.00	130.00	Z2S.00	33750	412iO	487^0	seuo	.	•	525.00	595.00	8	a
	In	29S3	SM6	8.85J	13.287		W.18J	2Z1«6			2O.fi69	•asm		
	mm	75.00	isaoo	22J.00	30&00	337 JO	41250	«7^0	SSL 50	etr.sv	buaoo	«74.O)	9	10
	M	i.«n	5S0f		11J11I	u»7	1G.240	19.133	22.146	25.098	23.S22	K£K		
"50	nu&	T5J»	150.00	225.00	300^0	412^0	487.50		(37.50	7L2.M	47S00	7WOC	111	in
	m		I Sid*	MM	Hill	UJ40	19.19S	22.M6	2SD96	2R0S1	2&S7!>	! W48R		

* THESE MAGNET CHANNELS HAVE SIMILAR MAGNETIC 1X.CS OM UCM INBi
THEREFORE, THEY CAN BE BUTTED TO OTHER MAGNtT C N A H N U I QNW» ™w ONE •tOK,

APPENDIX B cont.

Rated Parameters of LEB-S-2-S

Item	Value (unit)	
Continuous Force (@25°C)	96	N
Continuous Current (@25°C)	3.4	Arms
Continuous Force (@125°C)	81	N
Continuous Current (@125°C)	2.9	Anns
Peak Force (0.25s)	326	N
Peak Current (0.25s)	11.4	ATT15
Peak Force (1s)	232	N
Peak Current (1s)	8.2	Ams
Continuous Power (@125°C)	88.5	W
Force Constant	28.47	N/A
Back EMF (ptn)	9.49	V_{rms}/m/s
Resistance (@25°Cptn)	2.6	ohms
Resistance (@125°Cptn)	3.6	ohms
Inductance (ptn)	1.4	mH
Electrical Time Constant	0.54	ms
Motor Constant	8.66	N/W
Thermal Resistance	1.13	°C/W
Maximum Coil Temperature	125	°C
Coil Assembly Weight	0.4	kg
Dimensions:		
Magnetic Assembly	75 x 34	mm
Magnetic Pitch	15	mm
Coil Assembly Dimensions	140x66x8	mm
Coil Pitch	20	mm

APPENDIX C

COIL DESIGN AND MANUFACTURE DATA

APPENDIX C: Wire Calculations

Setup	lm	theta	magi	x	CoilW	coild	Fx(N/m)	Fy(N/m)	Thrust (N)	Normal (N)	Length	At	Kp	Acu	Icond	N	Acond	dcond	Cdeosity
Setup 1	100	324	10	23	7	78	105397	13445	12436846	1 58651	0.118	54 6	0785	42861	2.5	40	1 0715	1 168	2 3331234
Setup 2	150	324	10	23	7	78	153 024	12 803	18 056832	1 510754		54 6		42 861		60	07144	09537	3499685
Setup 3	200	324	10	23	7	78	200 65	12 139	23 6787	1 432402		54 6		42 861		80	05358	0 8259	46662467
Setup 4	250	*324*	*10*	*23*	7	7 8	248 276	11454	29 29658	135(572		54 6		*42.861*		*100*	0 4286	0 7387	*5 832233*
Setup 5	300	324	10	23	7	TT	295 901	10.747	34 916318	1.268146		54 6 "		42B61		120	0 3572	06744	6 9993701
Setup 6	350	324	10	23	7	78	343528	10.019	40.536068	1 182242		54 8		42 861		140	0 3062	0 6243	8 1659317
Setup 7	400	324	10	23	7	78	391 152	92695	46.155936	1093801		54 6		42 861		160	02679	0584	9.3324934
Setup B	450	324	10	23	7	78	438 777	8499	51 775686	1 002882		54.6		42 861		180	0 2381	0.5506	10499055
Setup 9	500	324	10	23	7	78	4B6 402	7.707	57.395436	0909428		54 8		42861		200	02143	05224	11 665617
Setup 10	550	324	10	23	7	78	534 028	6 8937	63 015068	08134568		54 6		42 861		220	0 1948	04981	12 832178
Setup 11	800	324	10	23	7	78	581.851	8 059	6B 634818	0 714962		54 8		42 881		240	01786	0 4768	1399874
Setup 12	650	»24	10	23	7	78	829 275	52029	74 25445	0 8139422		54 8		•12 861		260	0 1649	045B1	15 165302
Setup 13	700	324	10	23	7	78	678899	43255	79874082	0510409		54 8		42861		280	0.1531	0 4415	16 331863
Setup 14	750	324	10	23	7	7 B	724522	34269	85493598	0 4043742		54 6		42 861		300	0 1429	0 4265	17 498425
Setup 15	BOO	324	10	23	7	78	772 146	2 5068	91 113228	0 2957788		348		•12 B61		320	0 1339	0413	18664987
Setup 18	850	324	10	23	7	78	819 769	1 5066	96732742	01777788		54,6		42861		340	0 1261	0 4006	19031548
Setup 17	900	324	10	23	7	78	887 392	0.6021	102 35226	0071047B		54 9		42 861		360	0 1191	0 3893	20 99811
Setup 18	950	324	10	23	7	7.8	915014	•0 382	107 97165	-0045076		54.6		42861		380	0 1128	0 379	22 164672
Setup 19	1000	324	10	23	7	78	962637	-1.388	11359117	-0 163784		54 6		12861		400	0.1072	03694	23331234

dcond	071	mm
Cdensity	6.314	A/mm²
Turns	100	
Icond	2.5	A

Appendix C : Standard Copper Winding Wires

B.S.I. Standard Metric sizes of Copper Winding-Wires

Nom mm	Conductor diameter Max mm	Min mm	Equivalent inch	Sectional area sq.mm	Weight Per km kg	Nominal resistance at 20°C Per metre ohms	per kg ohms	Current rating at 4·65 amps per sq.mm † amps
SCQO	5-050	4'950	GT3S9	19-G3	T74-8	0-0006781	0-005029	31-30
+ 7S3	i-798	4-7C2	0«1870	17·72	157-5	0-000973O	0-006178	62'40
4·£00	4-54S	4-4S5	0-1772	15-90	141-4	0-001084-	<H)07666	73-95
4.-ZS0	A-293	-S-207	0-1673	14-19	125-1	U-00-.215	0-009839	
4-000	4-040	•$•360	0-157S	12E7	T1-.-7	0-0C1272	0-01228	5B-43
3·738	S-73S	3-712	0-U78	1T0i	5S-19	0-0015S1	O-C-1590	3136
3-SSO	3-588	3-5". 4	0-1398	S-SSS	87-M	0-001742	0-01 ?BO	46 03
3SS0	3-334.	3'3IS	O–3319		ra-33	0OO155&	0-02496	40-c9
	3-182	3--S18	0-12AQ	7-7S3	59·28	0OC2212	0-03--33	36-24
3-aaa	3-030	2·970	Q-11B1	7·069	22-34	0-002*39	0-033S1	32-87
2S00	z-raa	2-772	0-1:02	B-15S	54-74	0-002SOO	0-05115	28·63
2950	2--S77	2-S23	0-1043	S-5tS	43-43	Q-DC312S	306370	25-55
2-SilO	2'52S	2--175	0-C394.	4-909	43-64	0·0C3512	0-08C43	22-33
2·360	2-3S4	Z'336	O'CSCS	i-374	38-39	0-0029*1	0-1C13	20-34
2·240	2-262	2-21 a	0-08S2	3·941	35-03	0·004375	0·1249	ia-22
2-12O	I-U1	2-CS9	O-0S3S	3·530	3'. 33	0·004384	0-1656	16-41
	2-020	T-3S0	0-0787	3-T42	27-?3	0-00S-tas	0-1S65	-.4-61
7M0	T-919	VB81	0·0748	2-S35	25-21	0-KJ6C31	0-2."2	•3-:i
1·800	i-8t a	t-7S2	C-C709	2-545	22-52	0-00677S	0-299S	11-53
1-760	1-717	1-633	0·0669	2-270	20-18	0-007596	0·3784	10-53
7-eoo	V51S	1-5B4	0-C530	2-CI1	17-S7	0-0C8S7S	0-4799	5·349
t-SOtt	T-5:3	Vi3S	0-0591	1-767	15-71	0-0Q97S7	0-Q2H	a-r.7
1-400	1-4T4	'.-338	C-3SS1	t-338	13-69	0-0•125	0-6131	7 i 5a
	1-353	1-307	3·0520	1-363	72-17	0-C12B0	v<535	
1·250	1-263	1-237	0·0492	1-S7	10·91	O'CI^SS	1-228	5-70B
1·180	1-193	1-16S	0-C46S	1-094	9-722	0-01577	t-522	5-085
	1-131	1-109	00W1	C-9S52	B-75B	0-07730	1599	i-581
1-120	1-CM	--•049	0-04T7	g-5623	7-3£5	0-0*5=4	2-<!3V	i-IC3
J-Q60	I·010	0-990	3-03»<l	0-7fl54	5-9 B2	0-02193	3-'44	3-552
J 000	0·960	0·940	0-0374.	0-7088	6-301	O<32«32	3-B«0	3·236
0-S9Q						002710	4-751	2·953
0·900	0·903	0·891	0-C354	0-6362	5-658	0-0303S	S-022	2-539
0-8SO	0-a59	0-941	&-C335	DSS75	S-04S	0-0343D	7-^73	2-337
0-800	0-808	3-752	00315	0-5O27	4-469	0-C3SG3	S-933	2-0=4
Q-7SH	0-7 5S	a-742	C-02SS	3-4AT2	3·525	0C43S5	12-37	1·841
-Q-71Q	0-717	0-703	0·0230	0-3959	2-520			
0-570	0·577	0·563	0-C264	0-3526	3-T34	UOagso	15-60	1 ^
0-530	0·536	0·624	0C243	C-31'7	2·77".	0-05531	13-?6	T-315
oeco	0·605	0·584	0-C235	C2S27	2-5U	0-0eose	24-26	1--.45
	0·566	0·554	C-0220	0·2463	2190	0-070&O	31-56	1-025
0-330	0·526	0·524	3-0203	0·2206	1-9B1	o-C7at4	sa-as	

†4·65 amps per sq.mm is equivalent to 3000 amps per square inch. Local conditions may necessitate variation in this figure.
The conductor sizes in heavy italic print are preferred sizes and should be used wherever possible.

CONTINUED

Appendix C : Standard Copper Winding Wires

Concuctar diameter Nam mm	Max .Tim	Win irra	imiivnl.m ^icr	Sectional Area sc-nrn	Weight Ptr km to	Ncurinai nuonca «s 2D*C P-r nocn» cnms	per kg anms	Current *"P5 ifpoi p«r sq..-nmt €<-:»•
Q-SOO	C-SC-S	0-295	0-C197	0-*3c3	V>*6	0-06751	50-29	Q-S*3C
0-a7S	o-4ao	0-i70	0-0ifi7	0-772	1-575	0-037 3D	61-73	0-«2—2
-0-450	0-4S5	0-4-5	•0"D*77	C-1S9-3	*-414	0--.084.	78-6S	0-7395
0-425	0-43C	o-4":o	0-C1S7	0-1419	1-2S1	0-1215	96-35	06r95
0-400	C-405	C-395	0-C1 =7	312S7	1-1*7	C-1372	:22-3	0-58-12
C--375	o-3ao	0-370	0-0148	0-104	0-98*3	0-1531	155-3	0-513€
0·355	0-iS?	0-351	C-0- 40	0-09393	0-57 as	0' * 7-*-2	195·0	C -4603
C 235	0-333	0-331	0·0* 32	C-08B14	0-73 33	0-*.5=S	24S-6	0·4029
0' 375	0-2•?	0-311	0-0'2i	C-07 7=3	0-5S28	0-22*2	31S-3	0·3624
0-300	0-304	0-23 5	0·0·18	C07C5S	3-5234	0-2439	3S8-*.	3 32ST
0-lSa	0-234	C'2'c	o-ci-o	3061 £9	0^4?i	3-2800	SIT-3	0-2563
0-265	0-2SS	C-2S1	0C-1U	3-0S515	0-4903	3-3+23	637-3	0·2565
0-250	C–254-	C·242	0C09S	0-C49C3	ri-i3g4	3-35". 2	SC4.-3	C--22£2
0-2.2$	0-J4C	3-232	00C*-3	0-34374	0-3S83	0'354i	1.0:3-0	C-2C3-
0-22*	CZ27	3-22*.	c-ocaa	C03941	C-3303	0-<i375	1.2iS-C-	C-i8S2
C-2'2	0-215	0-209	O-O0S3	C-03530	o-sisa	C-4£8i	1,i5o-C	3-1S-"
0-200	3-2C3	0-*a7	•3 0379	3-C31£2	•3-2733	C·5483	-.,9=5-0	0-Uci
o-iao	0-193	0---37	0<O075	0-02335	O-2S21	C'Soai	2.412-3	O-iS-iS
0 1SO	0-183	0*.77	0-0071	3-025^5	0-22S2	0-S775	2.595-0	0-1133
0-170	0-173	Q-ia?	Q-C0B7	0-02270	0-2319	0-7*^36	3.764 0	OTOSi
O'ISD	C--S3	0-167	0-5052	O02CH	0--737	0-SS7S	4,793-0	0-0336
0-15O	C 153	0-147	0-0CE9	C01767	0T571	09757	6.211-0	0-0822
Otao	3-li3	0"*37	o-ooes	0-0'539	0-1363	V.20	S. 181-0	0C7T6
0-132	0-135	0-T29	0-W52	3-Ci 363	0-1217	•260	•0.3S3--0	0-063S
0-TZ5	0-*23	G-122	D-C04S	0-01227	0-1091	t -405	I2,a7S0	0-0571
0-112	0-1T 5	C-1C9	0-C044T	O-CO98S2	0-C37S3	1-750	19.9820	Q-W5B
O'TOO	G-"03	0-097	{JC0394	0-Q07B54	0-0€3B2	2-135	31.438·0	0-0365
0-030	G-Q£3	0-0S7	0-0C354	C-0C5362	0-03055	2.-7*0	47J14-0	0-0296
0080	3·033	0-C77	0-0035	C0CS027	C-04'tGlr	3-430	76.75T·0	00234
0-077	0-074	0-C6B	O-O02SO	0·003S53	0-0352C	4-355	123.722-0	Q-Q1S4
Q-OSJ	—	—	I>C02ia	0-C03'17	0-0277T	5-531	19S.W3-O	0-0145
o-oso	—	—	C-COZ36	0-C02327	0-02514	8-099	2*2.562-0	0-0132
0058	—	—	C·0022C	0C02453	0-02190	7·000	313.635·0	0-OT15
0-050	_	—	0001^97	0-30*. 9£3	0-C17A5	3-781	502.92"·0	o-ooa:
004S	—	—	0·00177	000*550	0-014T4	0-84	75Q.a2C0	0-0074
0-Q4-Q	—	–	0-0C157	CO01257	0-01117	13-72	t.223.290-0	0-WJ5&
0-C36	—	—	000142	0·0010'3	0-009043	16-94	1.372.330-0	0-0C47
Q-03S	—	—	0-C-3126	3 W0804-;	0-OC71SO	2"·44	2.998.5C1·0	0-0037
0-030	—	—	o-oona	3C-0O7OCS	0-0062B4	24-3S	:[SSI'.286-0	0-0033
002S	—	—	ocono	O-:005153	C--W3>i7".	2300	5. It 5.090-0	0-0029
0-<325	—	—	0C0D93	C-C0C4SC9	0C04364	35-12	B, 047,653 0	00023

*4·65 BPDI aar sq.rrm « ecuivalenr rq 3000 amos per square incJi. *Lacsi* *:c-nCmonj may necessaUni cansft vjfi*baii -Jl :fui llo-Jrm,

The conductor sizes in heavy italic are preferred sizes an ver possible.

APPENDIX
D

CLSM MHS

DESIGN AND ASSEMBL Y DRA WINGS

A.PPENIX U ^ o3. er Backiir Diensions

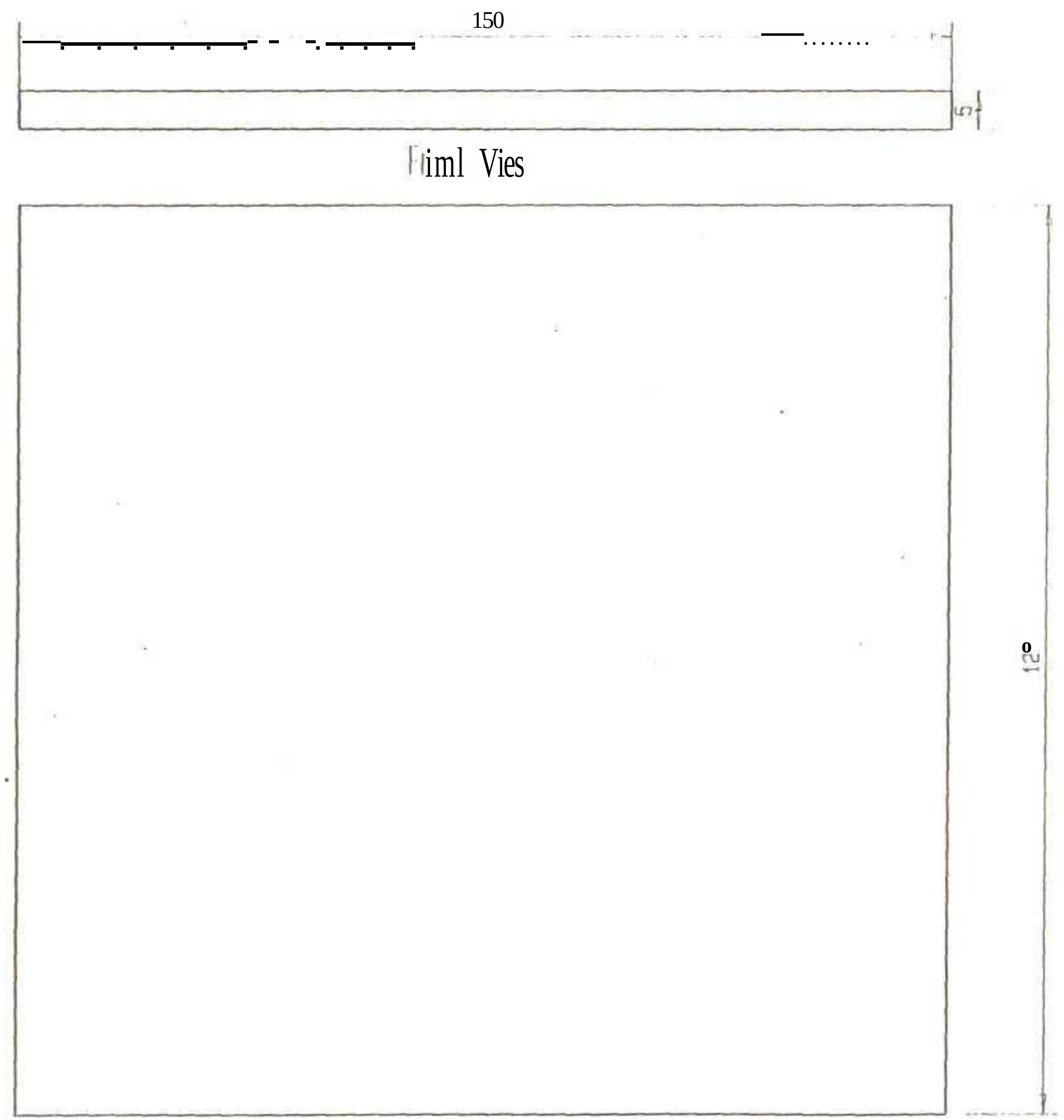

Fiml Vies

fop View

Par I : Hack iron

Helena!: IOI3Sleel

Halcnal finish: Cloned

Ho. llcq. :i (one)

		REV.	DATE	CHECKED	SCALE 1 : 1	UNIT'S : mm	PROJECT	No.
JNIVERSITY OF NATAL	Draflsperson	revQl	16/08/99	16/00/99	ESTIMATED MANUFACT. TIME: 2 Oays	STUDENT L. v. Lindsay	Cordless Linear Motor	MSC-11
School of Mechanical Engineering	Technician					SUPERVISOR Dr. G. Bright	TITLE Courier Backiron Design	
	WShop Manager							

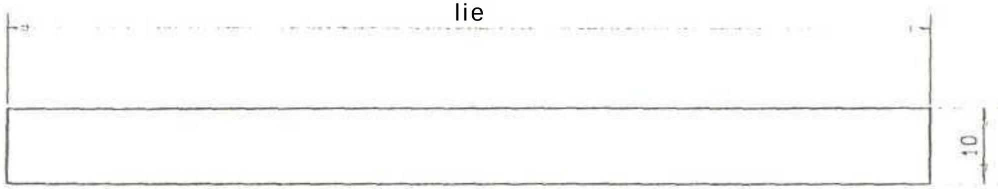

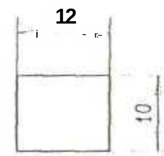

I rail to

Side View

IK) ICS

Hotlir ial: Ikfe Hiigmet

(luaitity: 10 (leu)

Sur laic 11nish: ime Coated

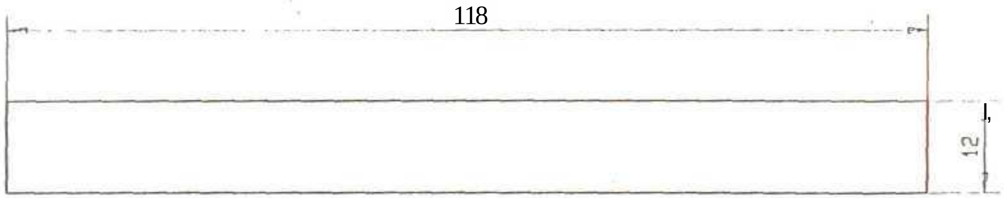

lop View

APPENDIX D_2 :nocrier M8 GTCJ 3 rt> © 3ensi©9s

NIVERSITY OF NATAL		REV.	DATE	CHECKED	SCALE 1:1	UNITS : mm	PROJECT Cordless Linear Motor	No. MSc-10
	Draftsperson	rev.104	08/08/99		ESTIMATED MANUFACT. TIME: 4-6 wks	STUDENT C.V. Lindsay		
hool of Meclianical Engineering	Technician					SUPERVISOR Dr. G. Bright	TITLE Courier Magnet Design	
	W'Shop Manager							

Material : lufnol tleclrical (Jraile

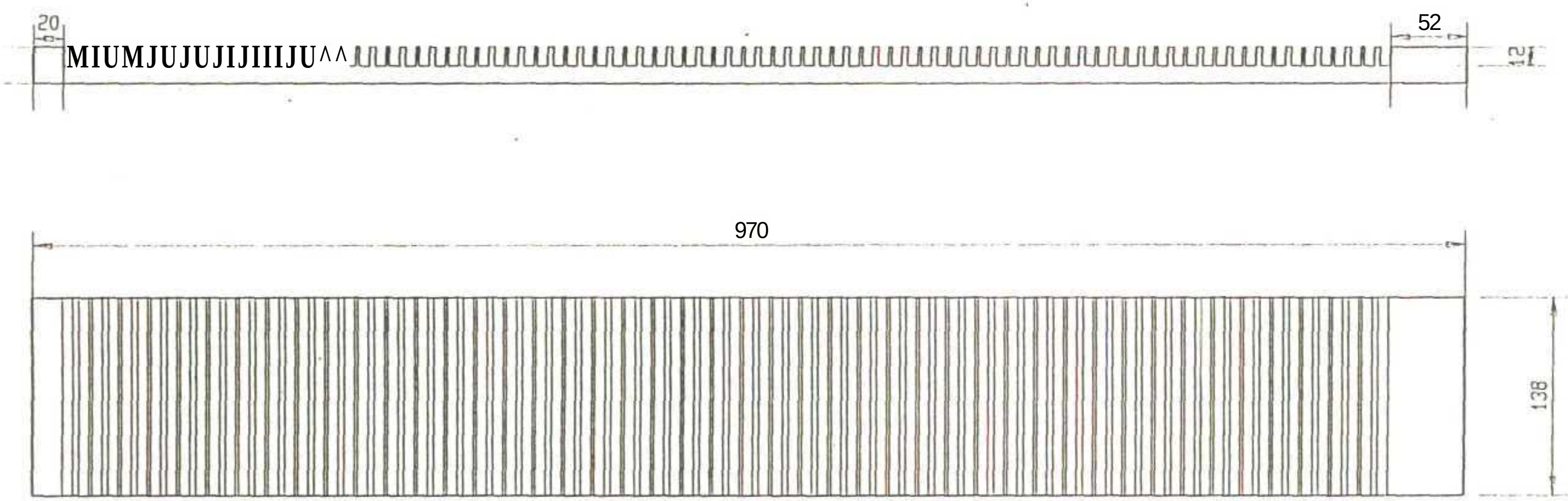

APPENDIX D_3 : Plate F esi

		REV.	DATE	CHECKED	SCALE 1:5	UNITS : mm	PROJECT	No.
JNIVERSITY OF NATAL	Draftsperson	revO3	11/08/99	16/08/99	ESTIMATED MANUFACT. TIME: 3 Days	STUDENT C.V Lindsay	Cordless Linear Motor	HSc.OI
iclιool of Mechanical Eiigiiteeriiig	Technician					SUPERVISOR Dr. G. Bright	TITLE Platen Construction	
	W'Shop Manager							

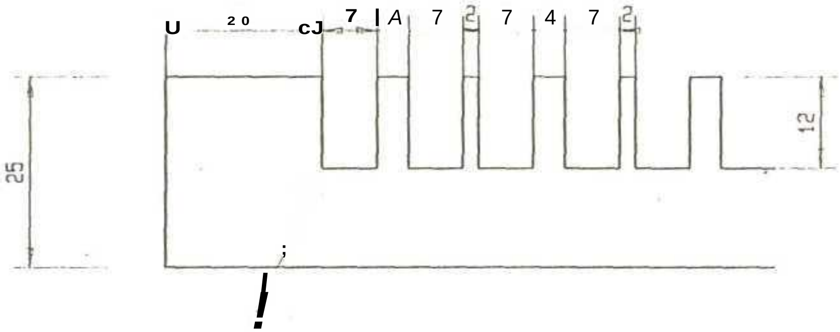

Zero Cutting Pionl

Hi 11 my Points from Zero Culling Point

O	II	,'0	31	.10	51	GO	'I	80	31
100	III	WO	-131	HO	151	Ilifl	1/1	180	191
,W\	,'Il	?A)	?3I	MO	N	260	2/1	280	291
300	311	320	331	340	351	360	3/1	300	391
400	411	420	431	440	451	460	4/1	400	4!)1
500	511	520	531	540	551	51)0	5/1	500	5'Jl
600	611	620	631	640	651	660	6/1	600	691
m	/I I	/20	/3I	/40	/5I	/60	ll\	/B0	/91
000	Oil	020	031	040	051	000	8/1	000	891

JNIVERSITY OF NATAL		REV.	DATE	CHECKED	SCALE 1 : 1	UNITS : mm	PROJECT Cordless Linear Motor	No. MSc_02
	Draftsperson	revO2	12/08/99	16/08/99	ESTIMATED MANUFACT. TIME: 3 Qays	STUDENT C. V. Lindsay		
Ichool of Mechanical Engineering	Technician						TITLE Platen Base Const.	
	W'Shop Manager					SUPERVISOR Dr. G. Bright		

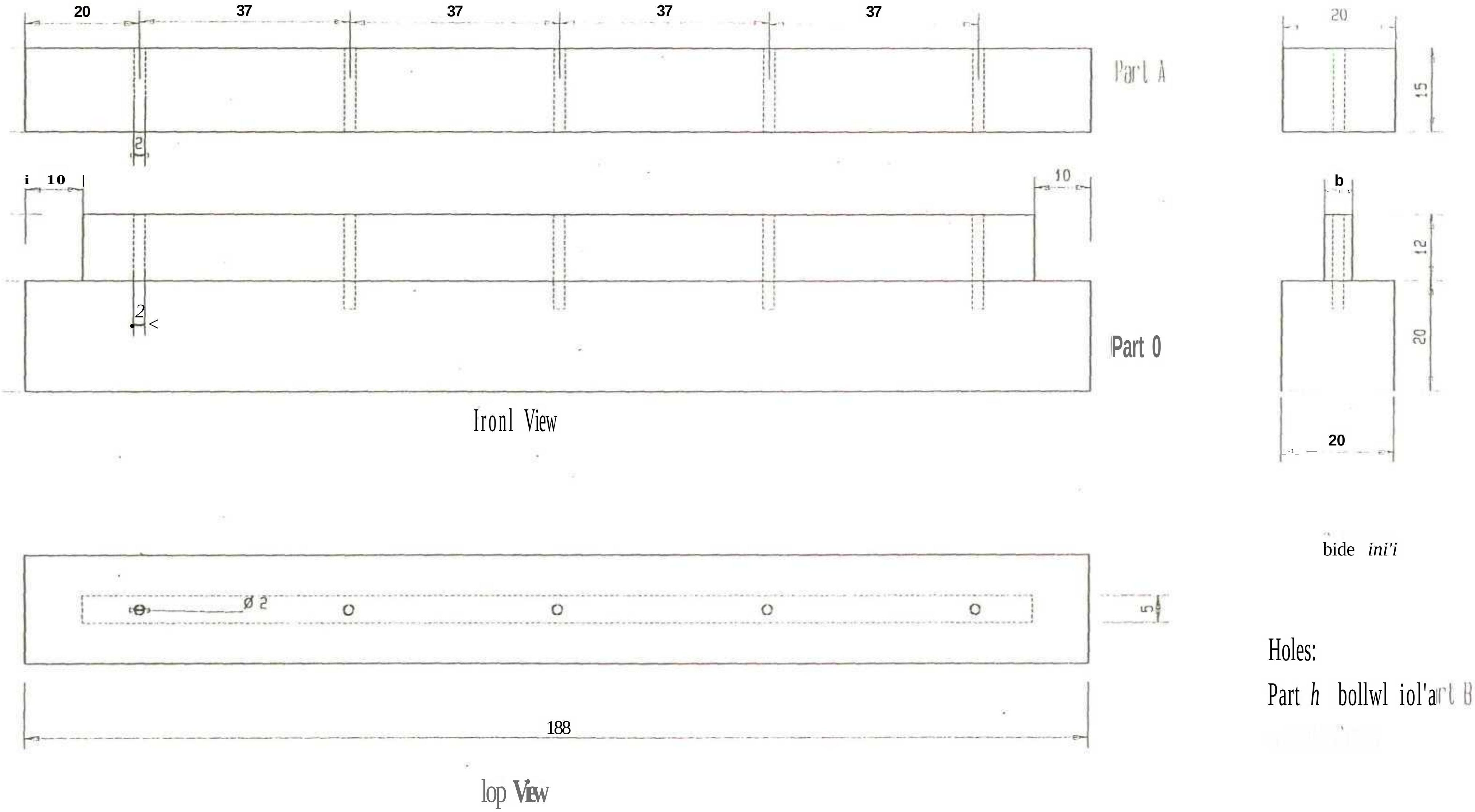

JNIVERSITY OF NATAL		REV.	DATE	CHECKED	SCALE 1:1	UNITS : mm	PROJECT Cordless Linear Motor	No. MSc-12
	Draftsperson				ESTIMATED MANUFACT. TIME: 2.days	STUDENT C.V. Lindsay	TITLE Former Design	
tchool of Mechanical Engineering	Technician					SUPERVISOR Dr. G. Bright		
	W'Shop Manager							

APPENDIX D_5:

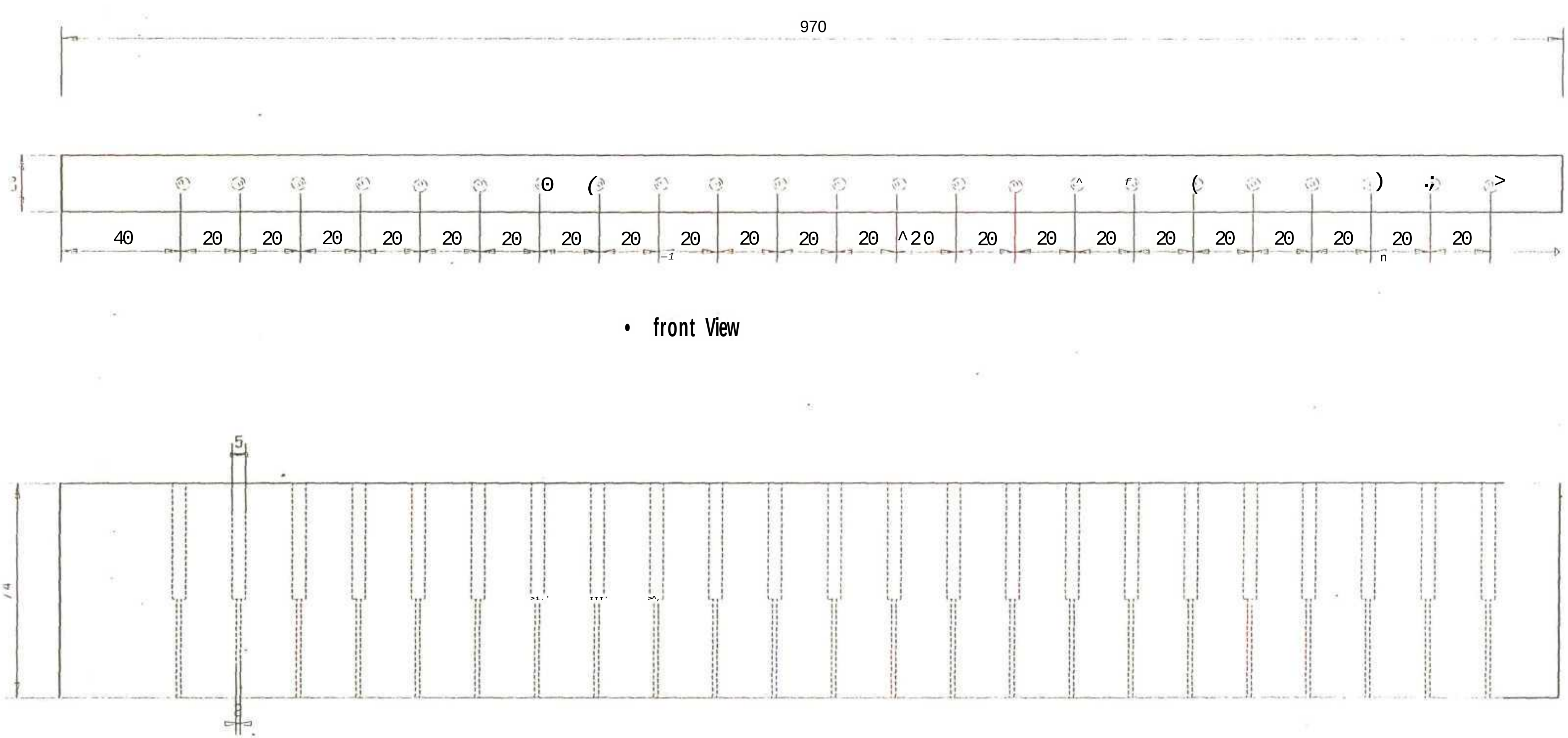

Hole: Side Bearings

Quantity: 1

UNIVERSITY OF NATAL		REV.	DATE	CHECKED	SCALE 1:2	UNITS : mm	PROJECT	No.
	Draftsperson	rev.1	18/08/99		ESTIMATED MANUFACT. TIME: 2 days	STUDENT C. V. Lindsay	Cordless Linear Motor	MSC-07
School of Mechanical Engineering	Technician					SUPERVISOR Dr. G. Bright	TITLE Side Bearing Design	
	W'Shop Manager							

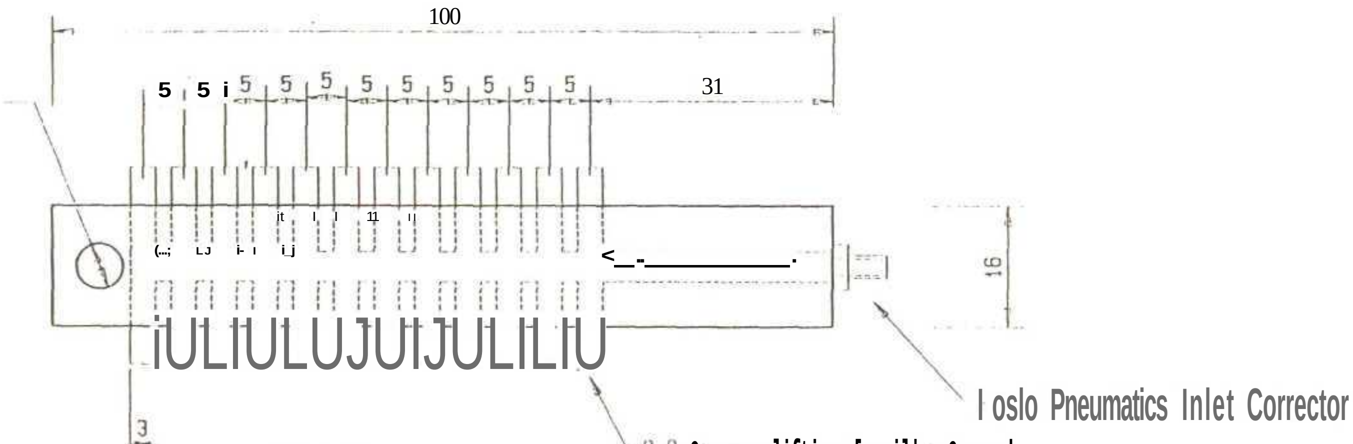

I rout View

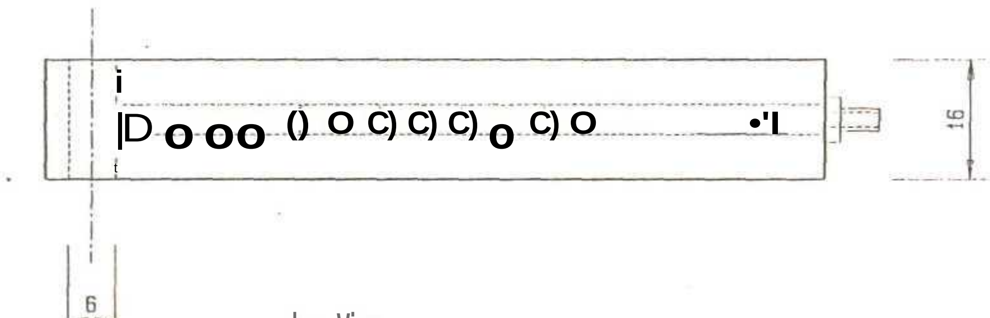

lop View

Holes

Material: 10 X10 mm Square Uar

Quantity: 0 (ciglitl

AP

ON :Air Manit a. esign

		REV.	DATE	CHECKED				
UNIVERSITY OF NATAL	Draftsperson				SCALE 1:1	UNITS : mm	PROJECT Cordless Linear Motor	No. MSc-13
School of Mechanical Engineering	Technician				ESTIMATED MANUFACT. TIME: 4 Qays	STUDENT C.V Lindsay	TITLE Air Mani folds	
	W'Shop Manager					SUPERVISOR Dr. G. Bright		

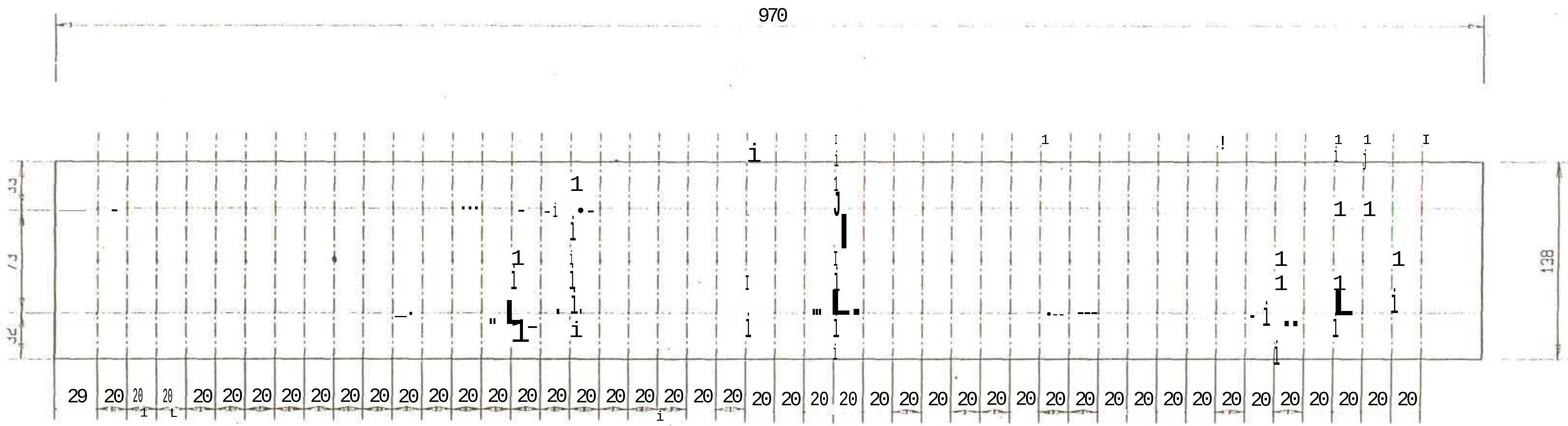

Note: Bearing Platen Surface

Orifice Design

Material : Polycarbonate (clear), 1.5 thick

Orifice Diameter : 1.5 mm

UNIVERSITY OF NATAL		REV.	DATE	CHECKED	SCALE 1:4	UNITS : mm	PROJECT Cordless Linear Motor	No. MSc-03
School of Mechanical Engineering	Draftsperson	VMM	19/08/99		ESTIMATED MANUFACT. TIME: 1Day	STUDENT C.V. Lindsay	TITLE Platen Bearing Design	
	Technician					SUPERVISOR Dr. G. Bright		
	W'Shop Manager							

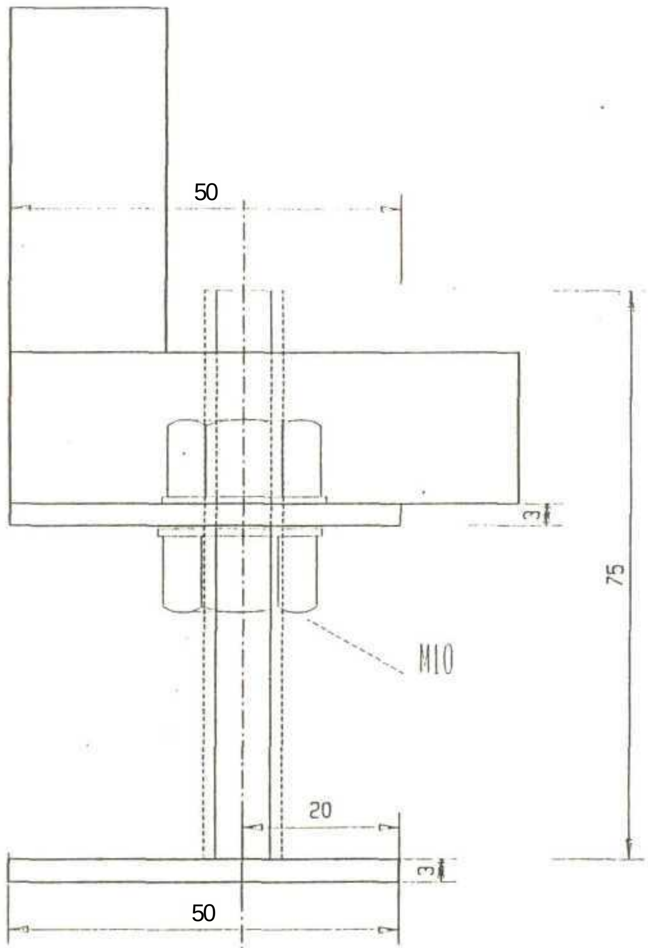

Hole U: Delai ol Slant)
Adjus toils

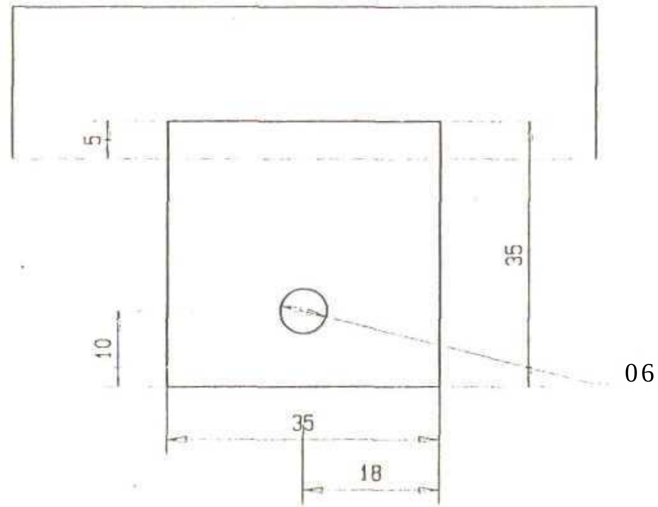

Hole A: Details of Air Man(old
Holder.
Position: lo Each Cross Hcnhor on Maid

See Uramng Frame.01
frame Design

		REV.	DATE	CHECKED	SCALE 1 : 1	UNITS : mm	PROJECT Cordless Linear Motor	No. MSc_05
UNIVERSITY OF NATAL	Draftsperson		IZ/08/99	19/08/99	ESTIMATED MANUFACT. TIME: 2 wks	STUDENT C.V. Lindsay	TITLE Detail Frame Design	
School of Mechanical Engineering	Technician					SUPERVISOR Dr. G. Bright		
	W'Shop Manager							

APPENDIX D

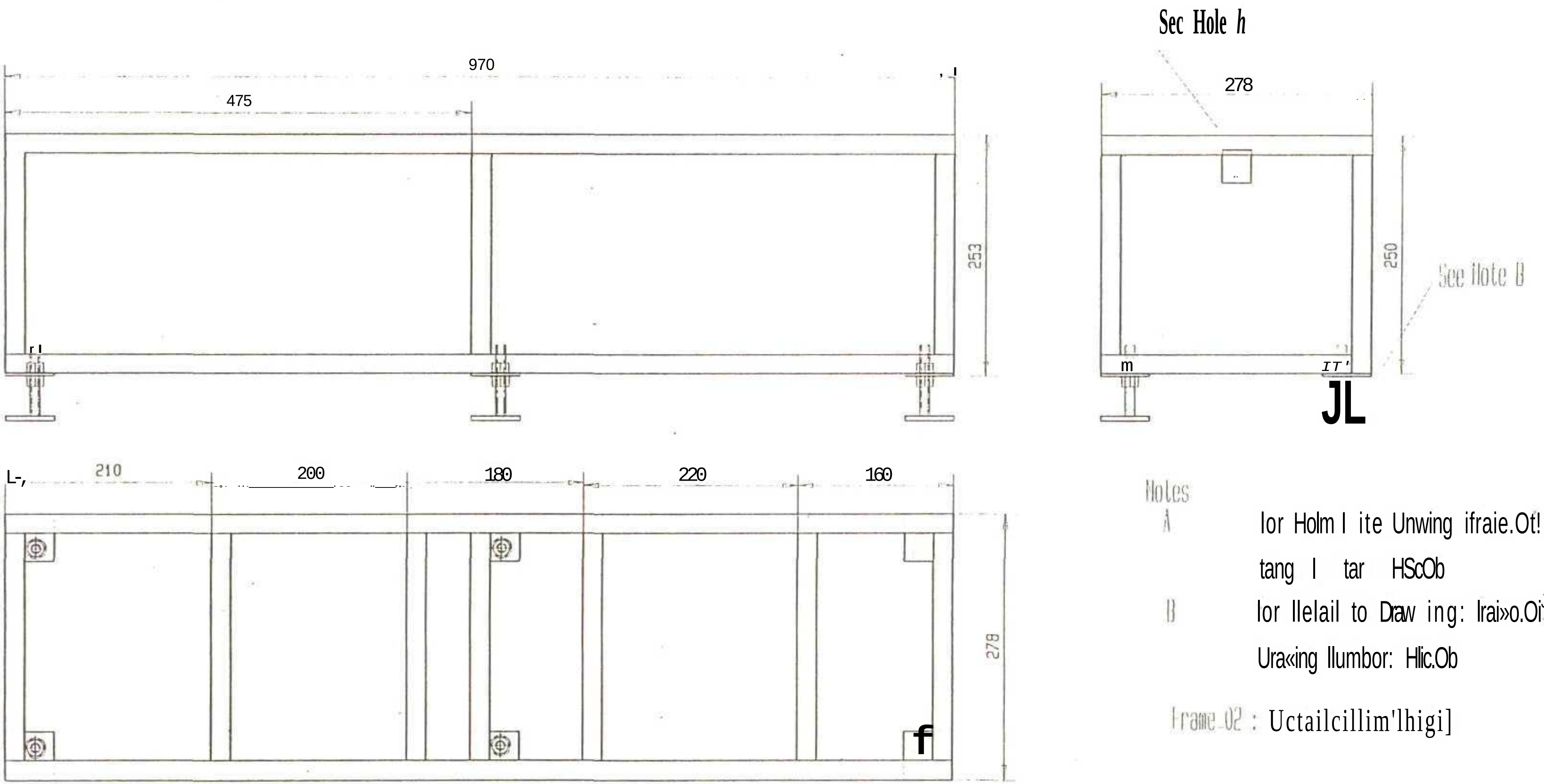

		REV.	DATE	CHECKED	1 SCALE 1:6	U7SUTS : mm	PROJECT Cordless Linear Motor	No. MSc-04
JNIVERSITY OF NATAL	Draftsperson	rev.02	17/00/99	19/08/99	ESTIMATED MANUFACT. TIME: p wks	STUDENT C.V. Lindsay		
cliool of Mechanical Engineering	Tecluiician					SUPERVISOR Dr. G. Bright	TITLE Iron Dos ion	
	W'Shop Manager							

APPENDIX D_9: Base Plate Design

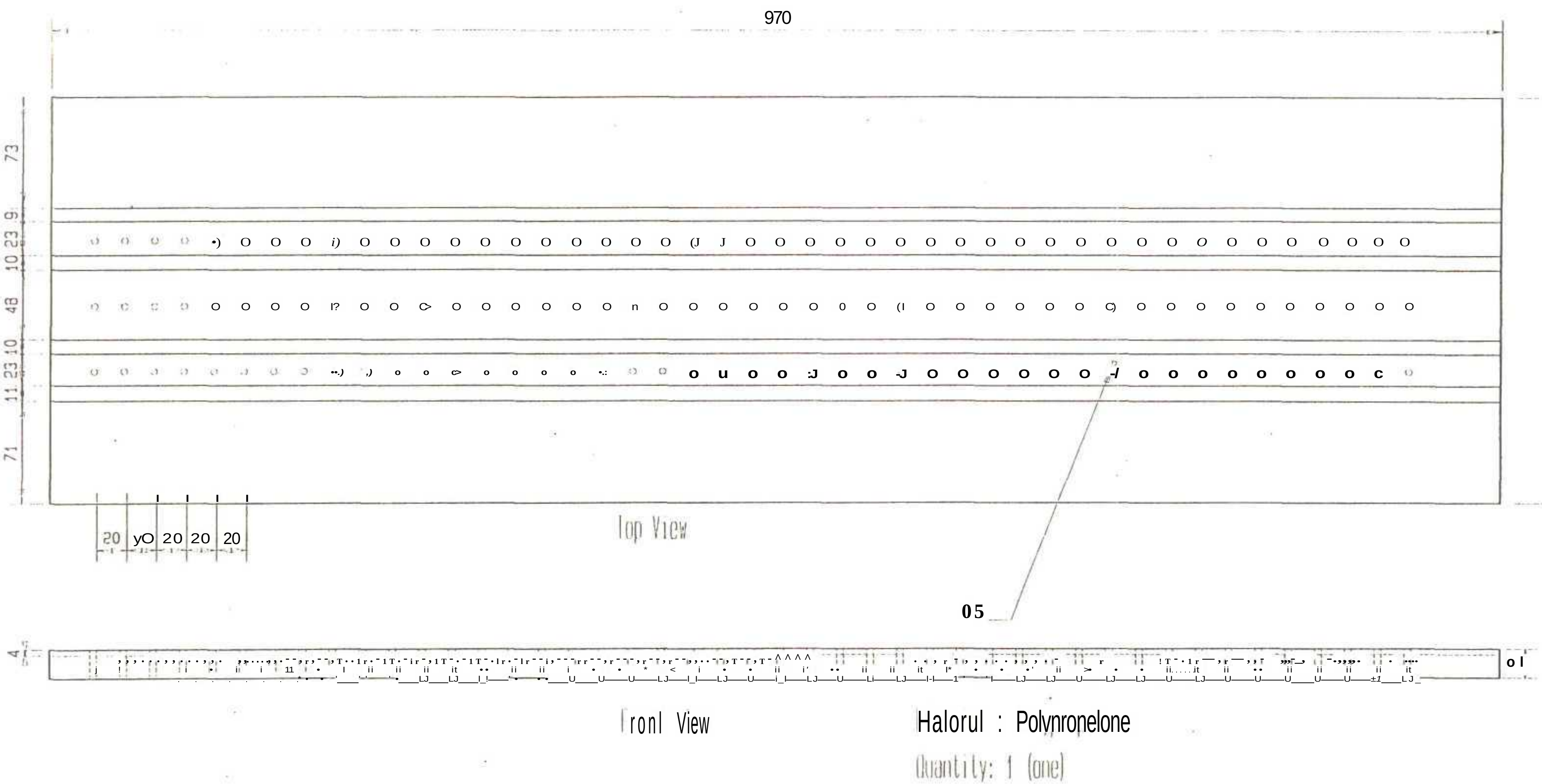

UNIVERSITY OF NATAL School of Mechanical Engineering		REV.	DATE	CHECKED	SCALE 1:4	UNITS : mm	PROJECT Cordless Linear Motor	No. MSc-0
	Draftsperson				ESTIMATED MANUFACT. TIME: 2 days	STUDENT C. V. Lindsay	TITLE Base Plate Design	
	Technician					SUPERVISOR Dr. G. Bright		
	W'Shop Manager							

APPENDIX D.9 : Side Wall Drawing

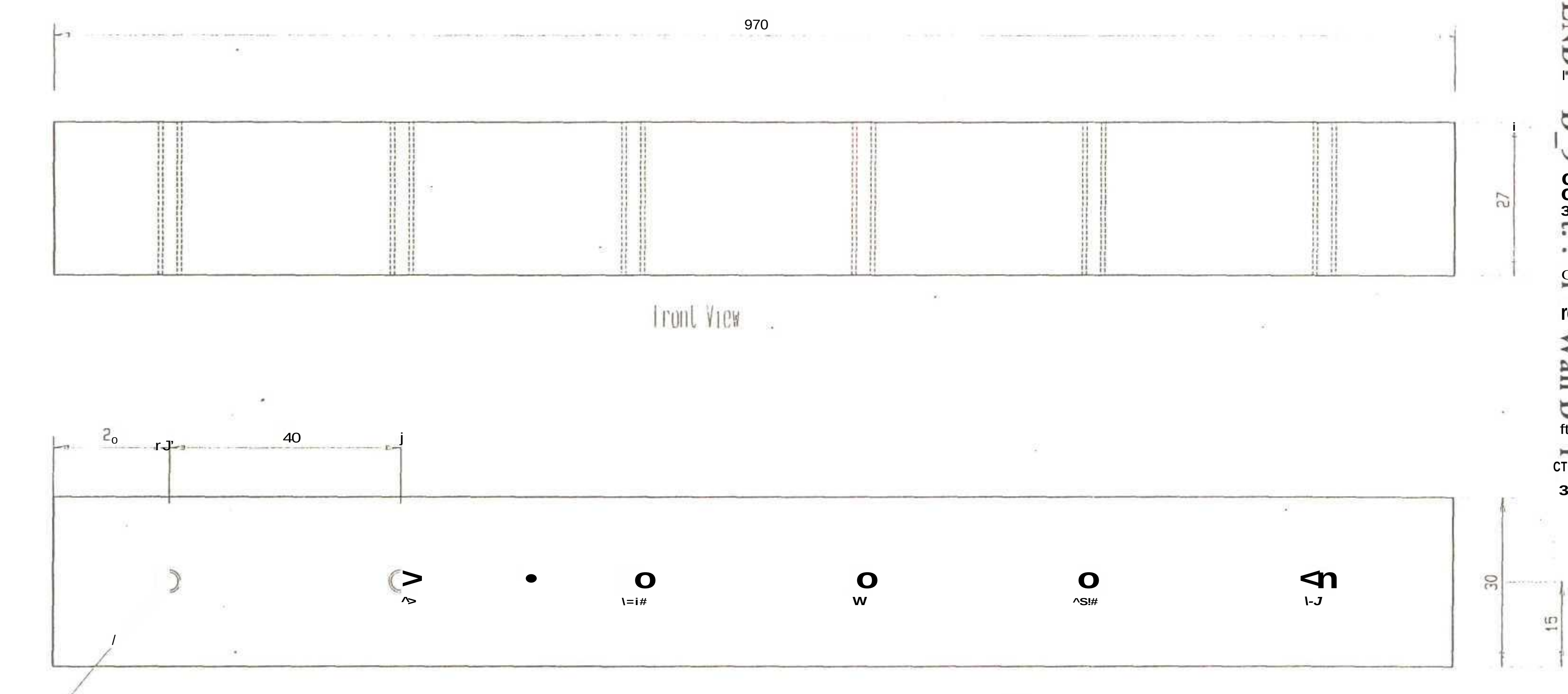

Note: Material : Polycarbonate

Quantity : 2 (two)

UNIVERSITY OF NATAL		REV.	DATE	CHECKED	SCALE 1:4	UNITS : mm	PROJECT Cordless Linear Motor	No. MSC-06
School of Mechanical Engineering	Draftsperson				ESTIMATED MANUFACT. TIME: 1 day	STUDENT N. S. Tlale	TITLE Side Wall Design	
	Technician					SUPERVISOR Dr. G. Bright		
	W'Shop Manager							

Con)Ioss Linear Motor Assunbly

Part A: Side Bearings
Part II: Hearim) linrfncc
Part C: Platen ta
Port II: Side Balls
Part L: Oase Plate
Parti: Irame

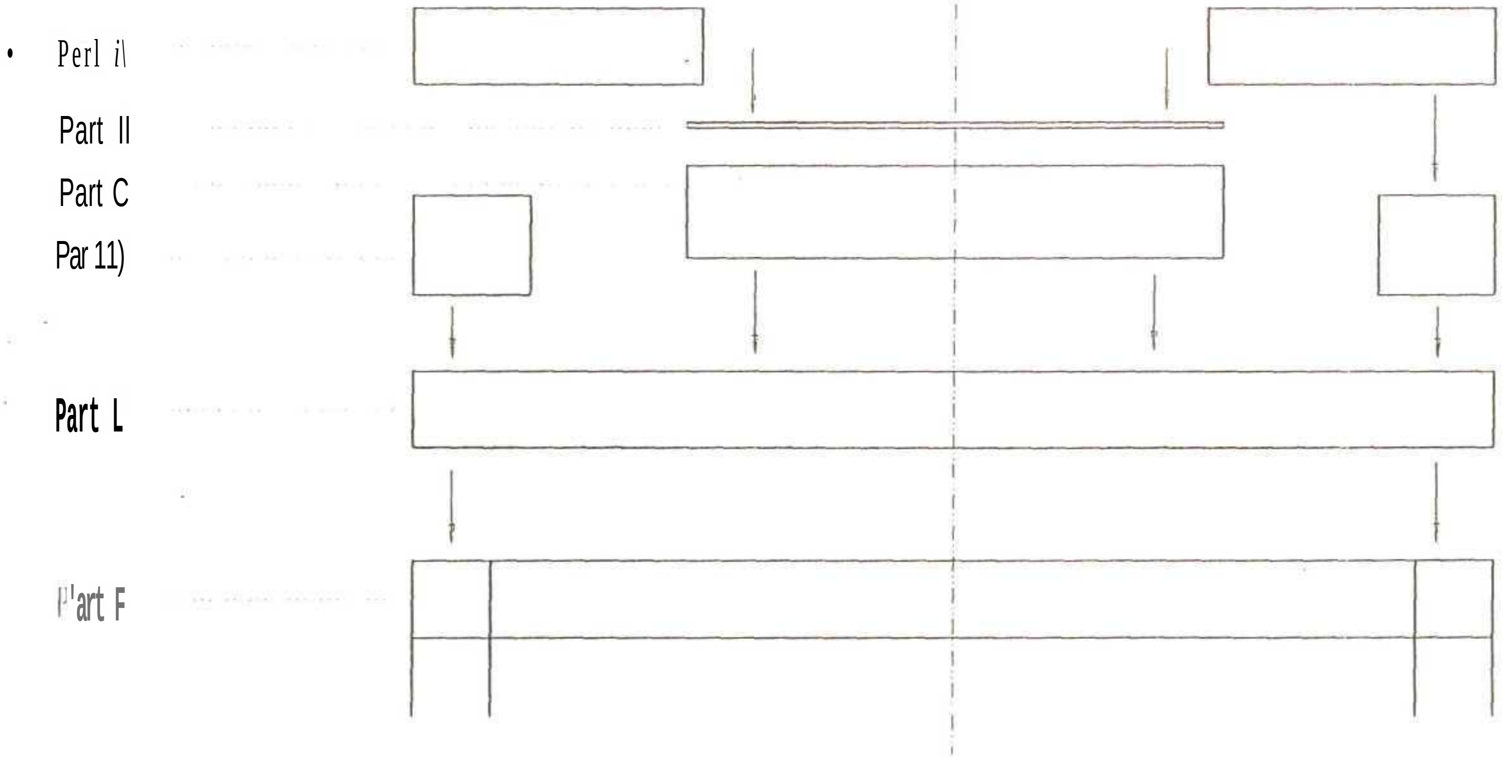

APPENDIX D

UNIVERSITY OF NATAL		REV.	DATE	CHECKED	SCALE 1:2	UNITS : mm	PROJECT Cordless Linear Motor	No. MSc-09
School of Mechanical Engineering	Draftsperson	rev.OJ	c*j/uu/yy		ESTIMATED MANUFACT. TFME" A riauc	STUDENT C.V Lindsay	TITLE Assembly Design	
	Technician					SUPERVISOR Dr. G. Bright		
	W'Sliop Manager							

APPENDIX E

ANALOG ULTRASONIC SENSOR

10-JA -2000 15:05 FROM D&I CONTROLS (PTY)LTD. TO 2603217 P.01

D & I Controls (Ply.) Ltd.

Reg.No.92/005515/07

P.O.Box 53367
YELLOWWOOD PARK 4011

i.i> VKLLC,W:OOL/ =APK SHOPPING CENTSE
YELLOWWOOD PARK 4011

TELEFÄX - MESSAGE

TSL.NO: (2731) 463-1833/4 rAX.NG; (2731) 4S5-1S9C

DATE:	1 J)[T%fl] JANUARY 2000
TO:	NATAL UNIVERSITY
FAX:	260321?
ATTENTION:	CRAIG LINDSAY
FROM:	DAVE LARSEN
PAGES:	SIX

Q&CTAIIQN: BA.NKER I^TRASQVTC SENSOK5

1 X Q45ULIU64 ACR
PRICE: JU 839^0 EACH EXa,?jI>ING VAT

1 X Q45ULIU64BCR
PRKIj R2 912.ru EACH EXCLUDING ^:AT

VALIDTTY; • QUOTATION IS VALID UNTIL 24TH JANX-AR1" 2000

STOCK: EX STOCK PPJOR TO SALE.

SPECIFICATION SHEETS HEREWITH.

WE THANK VOtJ FOR THIS ENQUIRY, IF WE CAN BE OF ANY FURTHER ASSISTANCE KINDLY CONTACT US.

REGARDS

DAVii LAP[1]AN.

the photoelectric specialist

Analog Q45U Ultrasonic Sensors

Piezoelectric Analog Proximity Mode Sensors with Push button or Remote Programming of Sensing Window Limits

Features

- Ultrasonic proximity detection from 100 to 1400 millimeters (4 to 55 inches)
- Push button TEACH mode programming of sensing window limits
- Digital filtering for exceptional immunity to electrical and acoustic "noise"
- Selectable 0 to 10V dc voltage sourcing or 4 to 20mA current sourcing analog outputs
- Selectable output slope: positive or negative with increasing target distance
- Wide operating temperature range of -25° to +70°C; all models include temperature compensation
- Rugged design for use in demanding sensing environments; rated IEC IP67, NEMA6P
- Choose models with integral 2 meter (6.5 foot) or 9 meter (30 foot) cable, or with mini-style or euro-style quick disconnect fitting
- Input for remote TEACH mode programming of window limits

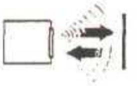

Ultrasonic

Analog Q45U Series Proximity Mode

Models	Temperature Compensation	Range	Cable	Supply Voltage	Output Type	Response Time
Q45ULIU64ACR Q45ULIU64ACRQ Q45ULIU64ACRQ6	Yes	100 mm-1.4 m (4 - 55 in)	2 m (6.5 ft) 5-Pin Mini QD 5-Pin Euro QD	15-24V dc	Selectable 0 - 10V dc or 4 - 20mA sourcing	Adjustable from 40 milliseconds to 1.28 seconds

Models with Temperature Compensation:
An increase in air temperature shifts both sensing window limits closer to the sensor. Conversely, a decrease in air temperature shifts both limits further away from the sensor. The shift is approximately 3.5% of the limit distance for a 20°C change in temperature.

Temperature compensated models maintain the position of both sensing window limits to within 1% of each limit distance over the range of from 0° to +50°C, and to within 2.5% over the full operating range of from -25° to +70°C.

For Q45U Ultrasonic Sensors:

i) 9 m (30 ft) cables are available by adding suffix **"W/30"** to the model number of the cabled sensor (e.g. - **Q45ULIU64ACR W/30)**

ii) A model with a QD connector requires an optional mating cable, see page 8.

Analog Q45U Ultrasonic Sensor

Near and Far Sensing Limit Settings:

The Q45U features a single push button for programming of sensing window near and far limits (Figure 1). See the programming procedure on page 4.

Status Indicators:

Status indicator LEDs are visible through the transparent, o-ring sealed Lexarf top cover. Indicator function in the **RUN** mode is, as follows:

- The green LED is on steadily whenever power is applied **to** the sensor, and flashes to indicate a current output fault.
- The red LED lights when an echo is received, and flashes at a rate that is proportional to echo strength.
- The yellow LED lights whenever the target is within the operating window limits.

The 5-segment moving dot LED indicator displays the relative position of the target within the programmed sensing window. The #1 LED flashes when the target is closer than the near limit. The #5 LED flashes when the target is beyond the far limit.

Output Response Settings:

IMPORTANT: Remove power before making any internal adjustments.

Using the two slots shown in Figure 1, a small flat-blade screwdriver may be used to lift up and remove the black inner cover to expose the 4-position DIP switch (Figure 2).

Those switches are used to program the following functions:

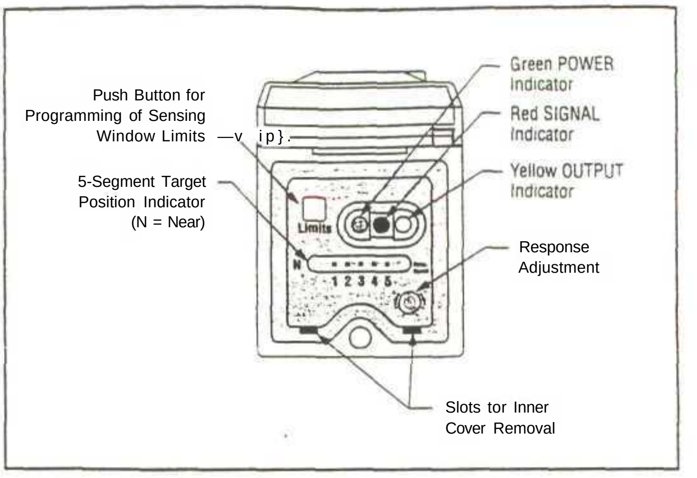

Figure 1. Analog Q45U Features

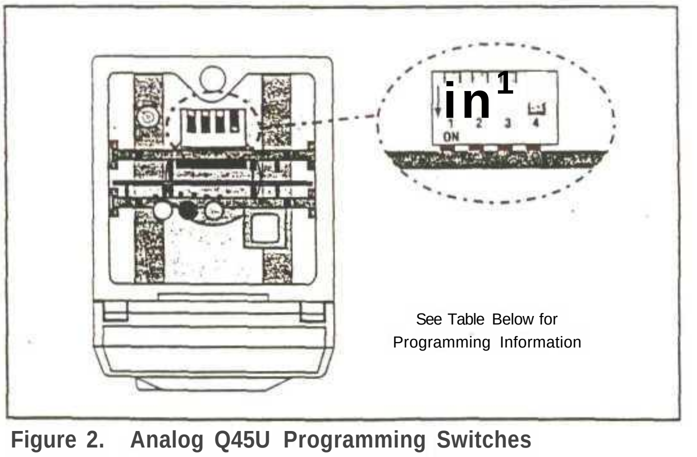

Figure 2. Analog Q45U Programming Switches

Switch	Function	Settings
1	**Output Slope**	On = Output value *increases* with distance Off* = Output value *decreases* with distance
2	**Output Mode**	On = Current output enabled Oft* = Voltage output enabled
3	**Loss of Echo**	On = Min - Max Mode Off* = Hold Mode
4	**Min - Max**	On* = Default to maximum output value Off = Default to minimum output value

"Indicates factory settings

Explanation of Programmable Output Functions:

Switch 1: Output Slope Select

On = Direct = Output value (voltage or current) increases with increasing distance of the target from the sensor
Off* = Inverse = Output value decreases with increasing distance of the target from the sensor

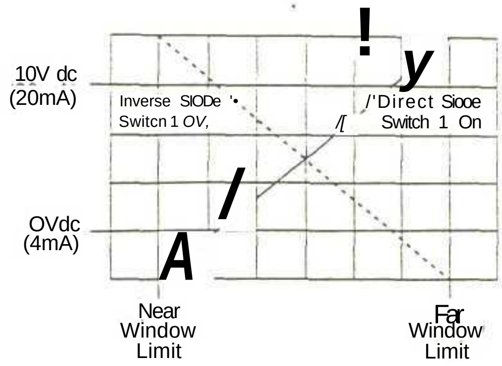

Figure 3. Output Slope

Switch 2: Output Mode Select

On = The 4 to 20mA current output (white wire) is enabled
Off* = The 0 to 10V dc voltage output (black wire) is enabled

This switch configures the D/A driver to use either the current output or the voltage output driver. **This output function can only be set with the power to the sensor turned off.**

Switch 3: Loss of Echo Mode Select

On = Min - Max Mode
Off* = Hold Mode

This switch determines the output response to the loss of echo. The "Hold Mode" (Switch 3 Off*) maintains the output at the value which was present at the time of echo loss. The "Min - Max Mode" (Switch 3 On) drives the output to either the minimum value (0V or 4mA or the maximum value (10V or 20mA) when the echo is lost. Minimum or maximum value is selected by Switch 4.

Switch 4: Min - Max Default

On* = Default to maximum output value at loss of echo
Off = Default to minimum output value at loss of echo

Switch 4 selects the output response to loss of echo when "Min - Max Mode" is selected by Switch 3 (see above).

Response Speed Adjustment

The speed of the output response is set using the single-turn potentiometer (see Figures 1 and 4). There are six values for response speed, which relate directly to the number of sensing cycles over which the output value is averaged (see the Response Speed Settings table, below). The response value is set by aligning the slot of the potentiometer with one of the marked positions. The positions are identified in Figure 4.

Response Speed Settings

Position	Response Speed
1	40 milliseconds (2 cycles)
2	80 milliseconds (4 cycles)
3	160 milliseconds (8 cycles)
4	320 milliseconds (16 cycles)
5	640 milliseconds (32 cycles)
6	1280 milliseconds (64 cycles)

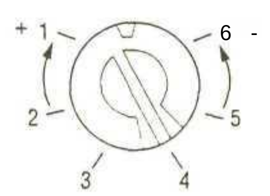

NOTE: This example shows the potentiometer set at position number 4. There are no numbers on the actual product label.

Figure 4. Response Adjustment Positions

Window **Limit Programming**

The "Limits" push button, located under the transparent top cover, is used to program the near and the far limits. The near limit may be set as close as 100 millimeters (4 inches) and the far limit may be set as far as 1400 millimeters (55 inches) from the transducer face. Minimum window width is 10 millimeters (0.4 inches). Whenever possible, use the actual target to be sensed when setting the window limits. The following procedure begins with the sensor in RUN mode.

Push Button		Indicator Status
Step 1 **ACCESS LIMIT PROGRAMMING MODE** Push and hold until green indicator turns off (approximately 2 seconds)	**Push Mil** Hold lor *i* 2 Seconds -A	Green: Goes off Yellow: Is on steadily to indicate ready for teaching first limit Red: Flashes to indicate strength of echo or is off if no target is present
Step 2 **SET FIRST LIMIT** (Near or Far) Place the target at the first limit and press the push button for less than 2 seconds	Push tor <2 Seconds y \ teftUt •i ^ U	Green: Remains off Yellow: Flashes at 2 Hz to indicate ready for teaching second limit Red: Comes on steadily for a moment, then resumes flashing to indicate strength of echo
Step 3 **SET SECOND LIMIT** (Far or Near) Place the target at the second limit and press the push button for less than 2 seconds	Push tor < 2 Seconds i; IKNI lmt \P 0 TZET	Green: Remains off, then comes on steadily (returns to **RUN** mode) Yellow: On steadily for a moment, then is either on or off to indicate output state (returns to **RUN** mode) Red: Comes on steadily for a moment, then resumes flashing to indicate strength of echo (returns to **RUN** mode)

Notes **regarding** window limit programming:

1) Either the near or far limit may be programmed, first.
2) There is a 2 minute time-out for programming of the first limit. The sensor will return to RUN mode with the previously programmed limits. There is no time-out between programming of the first and second limit.
3) The programming sequence may be cancelled at any time by pressing and holding the push button for ≥ 2 seconds. The sensor returns to RUN mode with the previously programmed limits.
4) During limit programming, the 5-segment moving dot indicator displays the relative target position between 0 and 1500 millimeters (the maximum recommended far limit position is 1400 millimeters).
5) If the target is positioned between 1400 and 1500 millimeters, the 5th segment of the moving dot indicator flashes to indicate that a valid echo is received, but the target is beyond the recommended 1400 millimeter maximum far limit.
6) If a limit is rejected during either programming step, the sensor will revert to the first limit programming step (Step 2 in .programming chart). This will be indicated by Green - off, Red - flashing to indicate signal strength, and Yellow - on steadily.
7) If both limits are accepted, the sensor **will** return to RUN mode, which is indicated by the Green LED coming on steadily.
8) If the target is held at the same position for programming of both limits, the sensor will establish a 10-millimeter wide sensing window, centered on the target position.

Analog Q45U Series Product Specifications	
Proximity Mode Range	Near limit: 100 mm (4.0 in) min Far limit: 1.4 m (55 in) max
Supply Voltage and Current	15 to 24V dc (10% maximum ripple) at 100mA, exclusive of load
Supply Protection Circuitry	Protected against reverse polarity and transient voltages
Output Configuration	One voltage sourcing and one current sourcing; one or the other output is enabled by internal programming switch #2. Output function may be programmed by a 4-position DIP switch located on top of the sensor, beneath the transparent o-ring sealed LEXAN[S] cover (see page 3 for complete information)
Output Rating	Voltage sourcing: 0 to 10V dc, 10mA maximum Current sourcing: 4 to 20mA, 1 to 500 ohm impedance
Output Protection Circuitry	Both outputs are protected against continuous overload and short circuit
Performance Specifications	Sensing Repeatability: ±0.1% of the measured distance (±0.25 mm minimum) Sensing Resolution: 0.25 mm (0.01 in) Analog Output Resolutions: 2mV, 3uA
Indicators	Three status LEDs: GREEN **glowing steadily** = power to sensor is "on" GREEN **flashing** = current output fault detected (indicates that the 4-20mA current path to ground has been opened) YELLOW **glowing steadily** = target **is'sensed** within the window limits (Yellow LED also indicates programming status during setup mode) RED **flashing** = indicates relative strength of received echo 5-segment moving dot LED indicates the position of the target within the sensing window
Construction	Molded VALOX- thermoplastic polyester housing, o-rıng sealed transparent LEXAN" top cover, and stainless steel hardware. Q45U sensors are designed to withstand 1200 psi washdown. The base of cabled models has a 7:"-14NPS internal conduit thread
Environmental Rating	Leakproof design is rated IEC IP67; NEMA 6P
Connections	2 m (6.5 ft) or 9 m (30 ft) attached cable, or 5-pin mini-style or 5-pin euro-style quick disconnect fitting
Operating Temperature	**Temperature:** -25 to +70°C (-13 to +158°F) **Maximum relative humidity:** 100%
Vibration and Mechanical Shock	All models meet Mil. Std. 202F requirements. Method 201A (Vibration: 10 to 60Hz max., double amplitude 0.06-inch, maximum acceleration 10G). Method 213B conditions H & I (Shock: 75G with unit operating; 100G for non-operation) Also meets IEC 947-5-2 requirements: 30G, 11 ms duration, half sine wave
Application Notes	**Minimum target size:** 10 mm x 10 mm aluminum plate at 500 mm (20 in) 35 mm x 35 mm aluminum plate at 1.4 m (55 in)

VALOX[5]and LEXAN[1]^ are registered trademarks of General Electric Company

Remote Window Limit Programming

The yellow wire of the Analog Q45U may be connected to a switch or process controller for remote programming of the sensing window limits. The programming procedure is the same as for the push button (see page 4).

A remote programming input is generated when +5 to 24V dc is applied to the yellow wire. The timing diagrams, below, define the required input pulses.

Step 1

Access Limit Programming Mode

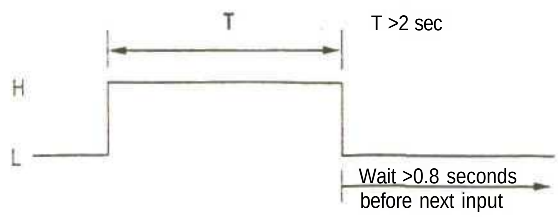

Step 2

Set First Limit
(Near or Far)

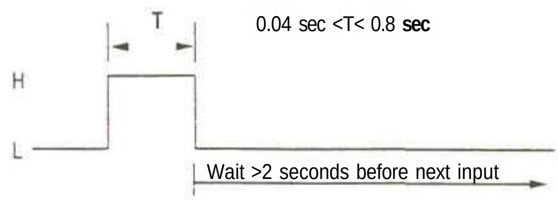

Step 3

Set Second Limit
(Far or Near)

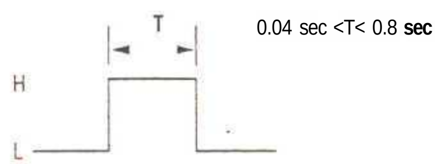

H = +5 to **24V dc**
L = <2V dc **(or open circuit)**

Notes regarding remote window limit programming:

1) The push button is disabled **during remote limit programming. (The remote** programming input is disabled during push button programming.)
2) Also see the **notes** regarding window limit programming on page **4.**

Analog Q45U Response Curves

Analog Q45U Effective Beam with Plate Target (Typical)

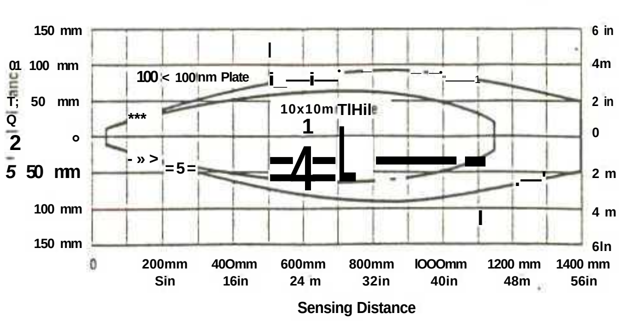

Analog Q45U Effective Beam with Rod Target (Typical)

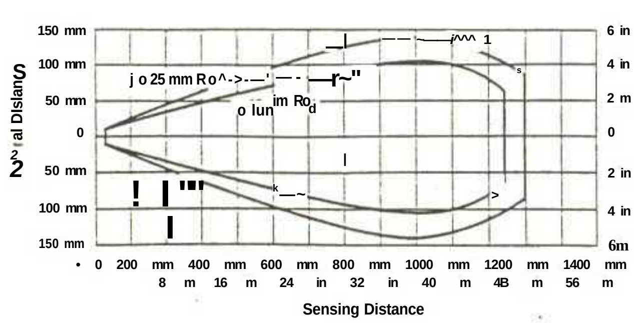

Analog **Q45U** Series Hookup Diagrams

Analog Q45U Sensor with Attached Cable

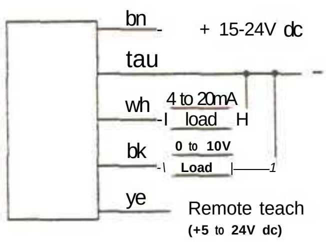

Analog Q45U Sensor with Quick Disconnect (5-Pin Mini-Style) ("Q" model Suffix)

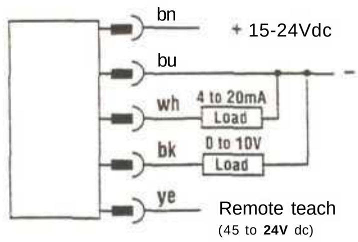

Analog Q45U Sensor with Quick Disconnect (5-Pin Euro-Style) ("Q6" model Suffix)

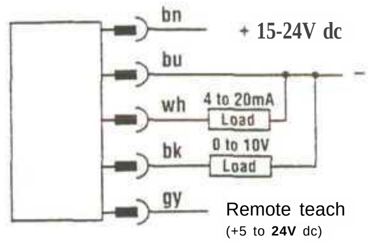

Quick Disconnect (QD) Option

Q45U Ultrasonic sensors are sold with either a 2 m (6.5 ft) or a 9 m (30 ft) attached cable, or with a 5-pin mini-style or 5-pin euro-style QD cable fitting.

For information on QD cables, see next page..

5-Pin Mini-Style Pin-out
(Cable Connector Shown)

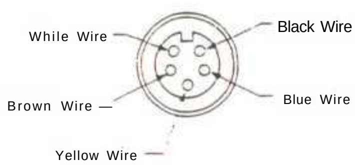

5-Pin Euro-Style Pin-out
(Cable Connector Shown)

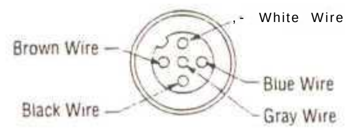

Q45U Series Dimension Information

Q45U Sensor with Cable Attached

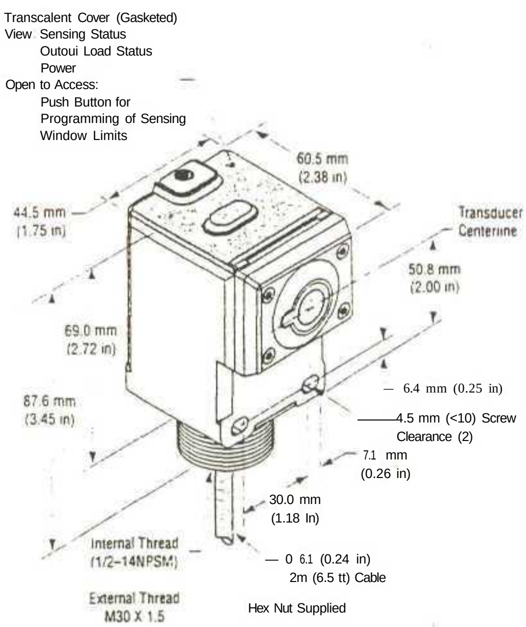

Q45U Sensor with 5-Pin Mini-Style QD ("Q" model Suffix)

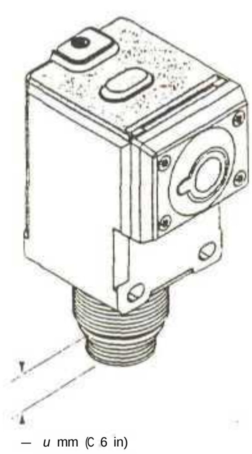

Q45U Sensor with 5-Pin Euro-Style QD ("Q6" model Suffix)

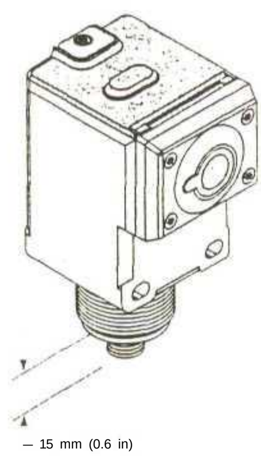

Analog Q45U Ultrasonic Sensor

QUICK DISCONNECT (QD) CABLES

Style	Model	Length	Connector
5-Pin Mini	MBCC-506 MBCC-512 MBCC-530	2 meters (6.5 ft) 4 meters (12 ft) 9 meters (30 ft)	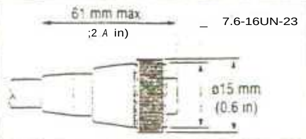
5-Pin Euro Straight	MQDC1-506 MQDC1-515 MQDC1-530	2 meters (6.5 ft) 5 meters (15 ft) 10 meters (30 ft)	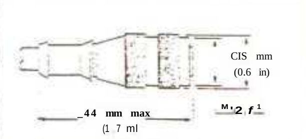
5-Pin Euro Right -angle	MQDC1-506RA MQDC1-515RA IYIQDC1-530RA	2 meters (6.5 ft) 4 meters (12 ft) 9 meters (30 ft)	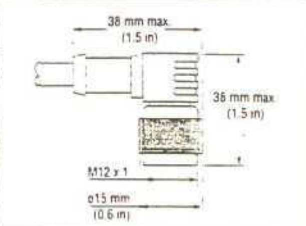

Mounting Brackets

Model	Description	Dimensions
SMB30S	• 30 mm swivel, black VAL0X* bracket • Stainless steel mounting hardware included	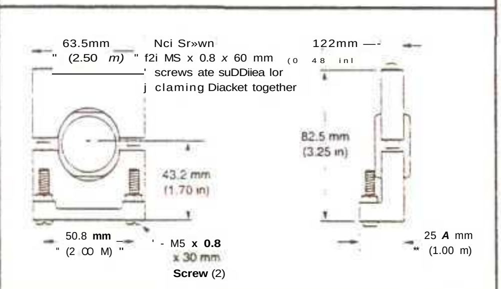
SMB30C	• 30 mm split clamp, black VALOX" bracket • Stainless steel mounting hardware included	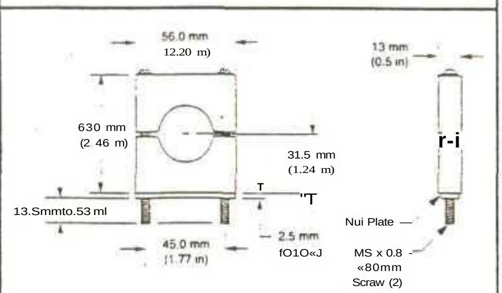
SMB30MM	• 30 mm, 11-gauge, stainless steel bracket with curved mounting slots for versatility and orientation • Clearance for M6 (V< in) hardware	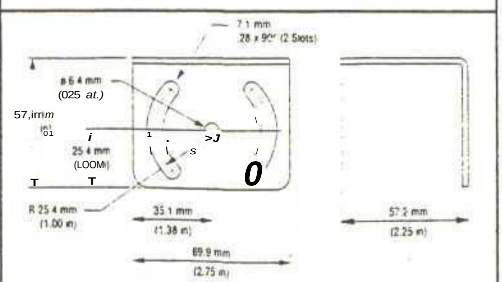

WARRANTY: Banner Engineering Corporation warrants it products to be free from defects for one year. Banner Engineering Corporation will repair or replace, free of charge, any product of its manufacture found to be defective at the time it is returned to the factory during the warranty period. This warranty does not cover damage or liability for the improper application of Banner products. This warranty is in lieu of any other warranty either expressed or implied.

WARNING These ultrasonic presence sensors do NOT include the self-checking redundant circuitry necessary to allow their use in personnel safety applications. A sensor failure or malfunction can result in either an energized or a de-energized sensor output condition.

Never use these products as sensing devices for personnel protection. Their use as a safety device may create an unsafe condition which could lead to serious injury or death.

Only MICRO-SCREEN" MINI-SCREEN', MULTI-SCREEN', MACHINE-GUARD" and PERIMETER-GUARD"' Systems, and other systems so designated, are designed to meet OSHA and ANSI machine safety standards for point-of-operation guarding devices. No other Banner sensors or controls are designed to meet these standards, and they must NOT be used as sensing devices for personnel protection.

the photoelectric specialist

APPENDIX F

SLOTTED OPTICAL SWITCH TECHNICAL DATA

/Question 6 overleaf

QT
0 PT2 ELECTfiDSI C S

SLOTTED OPTICAL SWITCH

H22A1/2/3

PACKAGE DIMENSIONS

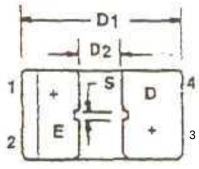

ST1340-01

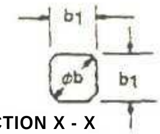

SECTION X - X
LEAD PROFILE

h E i

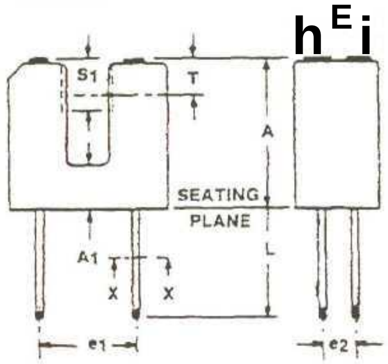

ET1340-02

SYMBOL	MILLIMETERS		INCHES		NOT^S
	MiN.	MAX.	MIN.	MAX.	
A	10.7	11.0	.422	,433	
A,	3.0	3.2	.119	.125	
ib	.600	.750	.024	.030	2
b,	.50 MOM.		.020 NOM.		2
C.	11.6	12.0	457	^472	
D,	3.0	32	.119	.129	
e,	6.9	7.S	zrz	.255	
1 e,	2.3	2.8	.091	.110	
1 E	£.15	6.35	.243	.249	
L	8.00		.315		
S	.65	1.0	.034	.039	
S,	3.45	3.75	.136	.147	
T	2.6 NOM.		.103 NOM.		3

NOTES:
1. INCH DIMENSIONS ARE DERIVED FROM MILLIMETERS.
2. FOUR LEADS. LEAD CROSS SECTION IS CONTROLLED BETWEEN 1.27mm (.030") FHOM SEATING PLANE AND THE END OF THE LEADS.
3. THE SENSING AREA IS DERNED BY THE "S" DIMENSION AND BY DIMENSION '7" ±Q.75mm (±.030 INCH).

PACKAGE OUTLINE

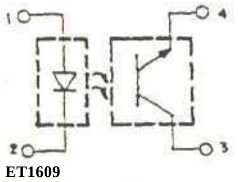

ET1609

DESCRIPTION

The H22A Slotted Optical Switch is a gallium arsenide light emitting diode coupled to a silicon photodarlington In a plastic housing. The packaging system is designed to optimize the mechanical resolution, coupling efficiency, ambient light rejection, cost and reliability. The gap in the housing provides a means of interrupting the signal with an opaque material, switching the output from an "ON" to an "OFF" state.

FEATURES

- Opaque housing
- Low cost
- .035" apertures
- High \ami

ABSOLUTE MAXIMUM RATINGS (T_A = 25°C Unless Otherwise Specified)

Storage Temperature . . . . -55°C to +100°C
Operating Temperature . . . . -55°C to +100°C
Soldering:
Lead Temperature (Iron) . . . . 240°C for 5 sec.[4,5]
Lead Temperature (Flow) . . . . 260°C for 10 sec.[3,4]

INPUT DIODE
Continuous Forward Current . . . . 60 mA
Reverse Voltage . . . . 6.0 Volts
Power Dissipation . . . . 100 mW[1]

OUTPUT TRANSISTOR
Collector-Emitter Voltage . . . . 30 Volts
Emitter-Collector Voltage . . . . 6 Volts
Power Dissipation . . . . 150 mW[2]

ELECTRICAL CHARACTERISTICS (T_A = 25°C Unless Otherwise Specified)

PARAMETER	SYMBOL	MIN.	TYP.	MAX.	UNITS	TEST CONDITIONS
INPUT DIODE						
Forward Voltage	V_F	—		1.7	V	I_F = 60 mA
Reverse Breakdown Voltage	V_R	6.0		—	V	I_R = 10 μA
Reverse Leakage Current	I_R	-		1.0	μA	V_R = 3 V
OUTPUT TRANSISTOR						
Emitter-Collector Breakdown	BV_{ECO}	6.0		—	V	I_E = 100 μA, Ee = 0
Collector-Emitter Breakdown	BV_{CEO}	30		—	V	I_C = 1 mA, Ee = 0
Collector-Emitter Leakage	I_{CEO}	—		100	nA	V_{CE} = 25 V, Ee = 0
COUPLED						
On-State Collector Current	$I_{C(ON)}$		See page 3.		mA	
Saturation Voltage	$V_{CE(SAT)}$		See page 3.		V	
Turn-On Time	t_{on}		See page 3.		μS	
Turn-Off Time	t_{off}		See page 3.		μS	

NOTES

1. Derate power dissipation linearly 1.33 mW/°C above 25°C.
2. Derate power dissipation linearly 2.00 mW/°C above 25°C.
3. RMA flux is recommended.
4. Methanol or Isopropyl alcohols are recommended as cleaning agents.
5. Soldering iron tip 1/16" (1.6 mm) from housing.

QT
PTDELECTB0K1CS

SLOTTED OPTICAL SWITCH

3

"CIONIJ V" CEI8AT1J "OB> AND t_{oft}

PARAMETER	SYMBOL	MIN.	TYP.	MAX.	UNrTS	TEST CONDITIONS
ON-STATE COLLECTOR CURRENT						
H22A1	I_{eaK}	0.15	—	- - — -•	mA	I_r = 5mA, V_{CE} = 5V
H22A2	'ctow	0.30	—	• •• —*	mA	I, = 5mA, V^ = 5V
H22A3	$I_{C(ON)}$	0.60	—	• : • — •	mA	I, = 5mA, Vn; = 5V
H22A1	$I_{C(ON)}$	1.0	—	— — -	mA	I_f = 20mA, V_{CE} «5V
H22A2	u	2.0	—	••.-—	mA	I_F = 20mA,V_{CE} = 5V
H22A3	'cra»	4.0	—	— — - -	mA	I, = 20mA, $V_=$ = 5V
H22A1	Iqwi	1.9	—	•. — •	mA	I, = 30mA, V_{CE} = 5V
H22A2	-'craw	3.0	—	—	mA	If = 30mA, V_{oE} = 5V
H22A3	$I_{C(ON)}$	5.5	—	. —	mA	I_f = 30mA, V_{CE} = 5V
SATURATION VOLTAGE						
H22A2	$V_{CE(SAT)}$	—	—	• 0.40	V	I_F = 20mA, I_c = 1.8mA
H22A3	VCtlSAT,	—	—	---0.40	V	1, = 20mA, L = 1.8mA
H22A1	VciWT,	—	• —	0.40	V	1, = 30mA, I_c = 1.8mA
Fum-On Time	t_{on}	—	8	—	μS	V_{cc} = 5V,I_F = 30 mA, R_L = 2.5KT1
turn-Off Time	t_{off}	-	50	— - •	jiS	V_{cc} = 5V, I_r = 30 mA, R_v = 2.5KTI

H22A1-3

TYPICAL CHARACTERISTICS

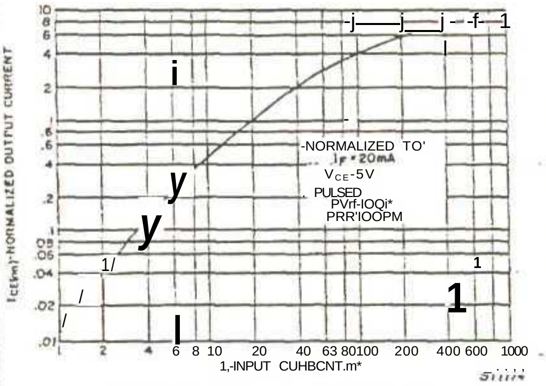

Fig. 1. *Output Current vs. Input Current*

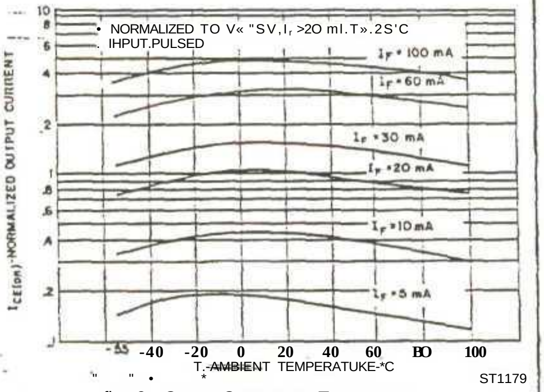

Fig. 2. *Output Current vs. Temperature*

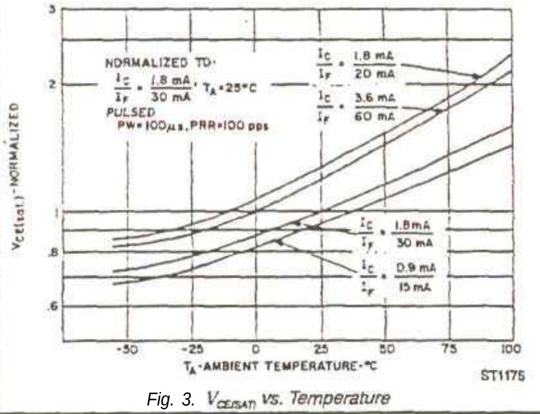

Fig. 3. $V_{CE(SAT)}$ *vs. Temperature*

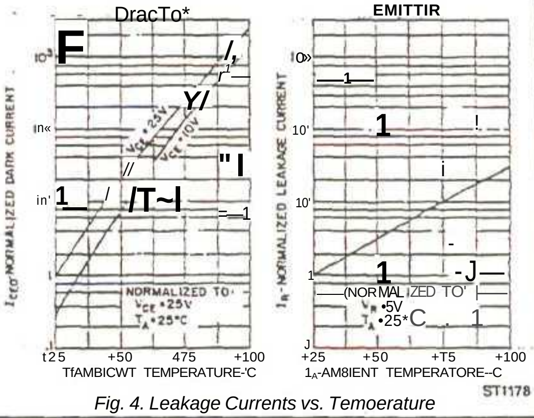

Fig. 4. *Leakage Currents vs. Temperature*

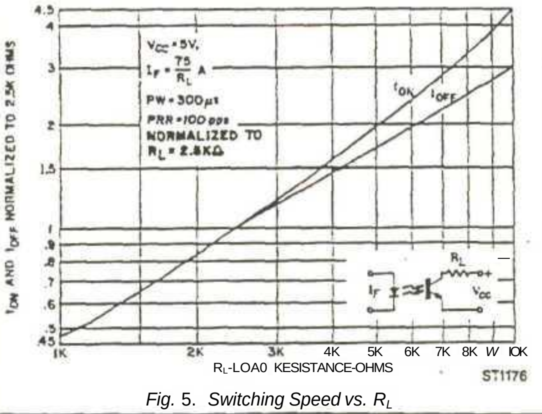

Fig. 5. *Switching Speed vs.* R_L

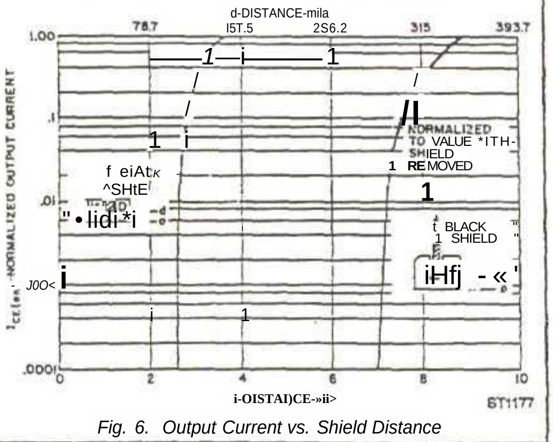

Fig. 6. *Output Current vs. Shield Distance*

APPENDIX G

YASKAWA VSMINIJ7 COMPA CT INVER TER:

WIRING AND CONSTANT DEFINITIONS/SETTINGS

Voltage Class		200V single-/ three-phase							400V three-phase*2						
Model CIMR-J7A□□□□	Three-phase	20P1	20P2	20P4	20P7	21P5	22P2	23P7	40P2	40P4	40P7	41P5	42P2	43P0	43P7
	Single-phase	B0P1	B0P2	B0P4	B0P7	B1P5	—	—	—	—	—	—	—	—	—
Max. Applicable Motor Output*2 kW (HP)		0.1 (0.13)	0.2 (0.25)	0.4 (0.5)	0.75 (1)	1.5 (2)	2.2 (3)	3.7 (5)	0.37 (0.5)	0.55 (0.75)	1.1 (1.5)	1.5 (2)	2.2 (3)	3.0 (4)	3.7 (5)
Output Characteristics	Inverter Capacity kVA	0.3	0.6	1.1	1.9	3.0	4.2	6.7	0.9	1.4	2.6	3.7	4.2	5.5	6.6
	Rated Output Current A	0.8	1.6	3	5	8	11	17.5	1.2	1.8	3.4	4.8	5.5	7.2	8.6

Category	Item	200V single-/ three-phase	400V three-phase
Output Characteristics	Max. Output Voltage V	3-phase, 200 to 230V (proportional to input voltage) Single-phase, 200 to 240V (proportional to input voltage)	3-phase, 380 to 460V (proportional to input voltage)
	Max. Output Frequency	400Hz (Programmable)	
Power Supply	Rated Input Voltage and Frequency	3-phase, 200 to 230V, 50/60HZ Single-phase, 200 to 240V, 50/60HZ	3-phase, 380 to 460V, 50/60Hz
	Allowable Voltage Function	-15% to +10%	
	Allowable Frequency Function	±5%	
Control Characteristics	Control Method	Sine wave PWM (V/f control)	
	Frequency Control Range	0.1 to 400Hz	
	Frequency Accuracy (Temperature Change)	Digital reference: ±0.01% (-10 to +50°C). Analog reference: ±0.5% (25±10°C)	
	Frequency Setting Resolution	Digital reference: 0.01Hz (less than 100Hz), 0.1Hz (100Hz or more) Analog reference: 1/1000 of max. output frequency	
	Output Frequency Resolution	0.01Hz	
	Overload Capacity	150% rated output current for one minute	
	Frequency Reference Signal	0 to 10VDC (20kΩ), 4 to 20mA (250Ω), 0 to 20mA (250Ω), frequency setting volume (selectable)	
	Accel/Decel Time	0.1 to 999 sec. (accel/decel time are independently programmed)	
	Braking Torque	Short-term average deceleration torque*3: 0.1, 0.2kW (0.13HP, 0.25HP): 150% or more; 0.4/0.75kW (0.5HP, 1HP): 100% or more; 1.5kW (2HP): 50% or more; 2.2kW (3HP) or more: 20% or more Continuous regenerative torque: Approx. 20%	
	V/f Characteristics	Possible to program any V/f pattern	
Protective Functions	Motor Overload Protection	Electronic thermal overload relay	
	Instantaneous Overcurrent	Motor coasts to a stop at approx. 250% of inverter rated current	
	Overload	Motor coasts to a stop after 1 minute at 150% of inverter rated output current	
	Overvoltage	Motor coasts to a stop if DC bus voltage exceed 410V	Motor coasts to a stop if DC bus voltage exceed 820V
	Undervoltage	Stops when DC bus voltage is approx. 200V or less (approx. 160V or less for single-phase series)	Stops when DC bus voltage is approx. 400V or less
	Momentary Power Loss	Following items are selectable: Not provided (stop if power loss is 15ms or longer), continuous operation if power loss is approx. 0.5s or shorter, continuous operation	
	Cooling Fin Overheat	Protected by electronic circuit	
	Stall Prevention Level	Can be set individual level during accel/decel, provided/not provided available during coast to a stop	
	Cooling Fan Fault	Protected by electronic circuit (fan lock detection)	
	Ground Fault	Protected by electronic circuit (operation level is approx. 250% of rated output current)	
	Power Charge Indication	ON until the DC bus voltage becomes 50V or less. RUN lamp stays ON or digital operator LED stays ON. (Charge LED is provided for 400V)	
Other Functions	Input Signals: Multi-function Input	Four of the following input signals are selectable: Forward/reverse run (3-wire sequence), fault reset, external fault (NO/NC contact input), multi-step speed operation, Jog command, accel/decel time select, external baseblock (NO/NC contact input), speed search command, UP/DOWN command, accel/decel hold command, LOCAL/REMOTE selection, communication/control circuit terminal selection, emergency stop fault, emergency stop alarm, self test	
	Output Signals: Multi-function Output	Following output signals are selectable (NO/NC contact output): Fault, running, zero speed, speed agreed, frequency detection (output frequency ≤ or ≥ set value), during overtorque detection, minor error, during baseblock, operation mode, inverter run ready, during fault retry, during undervoltage detection, reverse running, during speed seach, data output through communication	
	Standard Functions	Full-range automatic torque boost, slip compensation, 9-step speed operation (max.), restart after momentary power loss, DC injection braking current at stop/start (50% of inverter rated current, 0.5 sec, or less), frequency reference bias/gain, fault retry, speed search, frequency upper/lower limit setting, overtorque detection, frequency jump, accel/decel time switch, accel/decel prohibited, S-curve accel/decel, frequency reference with built-in volume, constants copy [Option :MEMOBUS communications (RS-485/422, max. 19.2kbps)]	
	Display: Status Indicator LED	RUN and ALARM provided as standard LED's	
	Display: Digital Operator	Available to monitor frequency reference, output frequency, output current	
	Terminals	Main circuit: screw terminals Control circuit: plug-in screw terminal	
	Wiring Distance between Inverter and Motor	100m (328ft) or less	
Enclosure		Open chassis (IP20) and NEMA 1	
Cooling Method		Cooling fan is provided for 200V, 0.75kW (1HP)(3-/single-phase), 400V, 1.5kW (2HP)(3-phase), others are self-cooling	
Environmental Conditions	Humidity	90% RH or less (non-condensing)	
	Storage Temperature*4	-20 to +60°C (-4 to 140°F)	
	Ambient Temperature	-10 to +50°C (14 to 122°F) (non-freezing)	
	Elevation	1000m (3280ft) or less	
	Vibration	Up to 9.8m/s² (1G) at 10 to 20Hz Up to 2m/s² (0.2G) at 20 to 50Hz	

*1: Under development
*2: Based on a standard 4-pole motor for max. applicable motor output. Select the inverter model within the allowable motor rated current.
*3: Shows deceleration torque for uncoupled motor decelerating from 60Hz with the shortest possible deceleration time.
*4: **Temperature during** shipping (for short period)

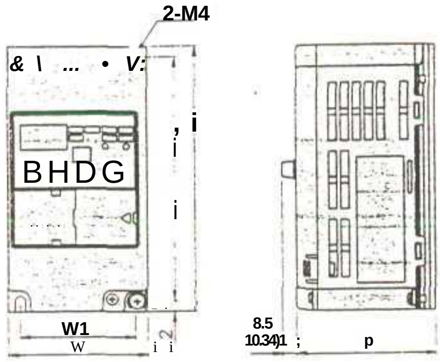

Figure 1

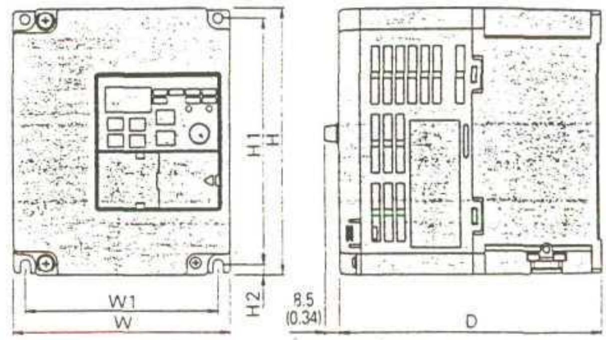

Figure 2

Voltage Class	Capacity kW (HP)	Fig- No.	Dimensions in mm (inches) W	H	D	W1	H1	H2	Mass kg (lb)	Heat Loss W Fin	Inside Unit	Total Heat Loss
200V Three-phase	0.1 (0.13)	1	68 (2.68)	128 (5.04)	70 (2.76)	56 (2.20)	118 (4.65)	5 (0.20)	0.5 (1.1)	3.7	9.3	13.0
	0.2 (0.25)									7.7	10.3	18.0
	0.4 (0.5)		68 (2.68)	128 (5.04)	102(4.16)	56 (2.20)	118 (4.65)	5 (0.20)	0.8(1.76)	15.8	12.3	28.1
	0.75(1)				122(4.80)				0.9(1.98)	28.4	16.7	45.1
	1.5(2)	2	108 (4.25)	128 (5.04)	129(5.08)	96 (3.78)	118 (4.65)	5 (0.20)	1.3(2.83)	53.7	19.1	72.8
	2.2 (3)				154 (6.06)				1.5(3.31)	60.4	34.4	94.8
	3.7 (5)		140(5.51)	128(5.04)	161(6.34)	128(5.04)	118(4.65)	5 (0.20)	2.1(4.63)	96.7	52.4	149.1
200V Single-phase	0.1 (0.13)	1	68 (2.68)	128 (5.04)	70 (2.76)	56 (2.20)	118 (4.65)	5 (0.20)	0.5(1.1)	3.7	10.4	14.1
	0.2 (0.25)									7.7	12.3	20.1
	0.4 (0.5)				112(4.41)				0.9(1.98)	15.8	16.1	31.9
	0.75(1)	2	108 (4.25)	128 (5.04)	129 (5.08)	96 (3.78)	118 (4.65)	5 (0.20)	1.5 (3.31)	28.4	23.0	51.4
	1.5 (2)				154(6.06)				1.5 (3.31)	53.7	29.1	82.8
400V Three-phase	0.37 (0.5)	Under Development										
	0.55 (0.75)											
	1.1 (1.5)											
	1.5(2)											
	2.2(3)											
	3.0 (4)											
	3.7 (5)											

■ Model Designation

C I MR — J 7 A A 2 0 P1

Inverter

VS mini J7 series

No.	Type
A	With digital operator (with analog volume)
B	Without digital operator
C	With digital operator (without analog volume)

No.	Specifications
A	Japan domestic standards

Conformed to C-UL US, CE marking. 200V Three-phase 3-7kW model accreditation pending

No.	Applicable maximum motor output
0P1	0.1kW (0.13HP)
0P2	0.2kW (0.25HP)
0P4	0.4kW (0.5HP)
0P7	0.75kW (1HP)
1P5	1.5kW(2HP)
2P2	2.2kW (3HP)
3P0	3.0kW (4HP)
3P7	3.7kW(5HP)

No.	Voltage Class
B	Single-phase 200V AC
2	Three-phase 200V AC
4	Three-phase 400VAC

■ Capacity Code Designation

2 0 P 1 0

No.	Phase / Volume
B	Single-phase 200VAC
2	Three-phase 200V AC
4	Three-phase 400V AC

No.	Applicable maximum motor output
0P1	0.1kW(0.13HP)
0P2	0.2kW (0.25HP)
0P4	0.4kW (0.5HP)
0P7	0.75kW(1HP)
1P5	1.5kW(2HP)
2P2	2.2kW(3HP)
3P0	3.0kW(4HP)
3P7	3.7kW(5HP)

No.	Protective structure
0	Open chassis (IP20)

■ Models

Voltage class	Description		Model	Capacity code to be filled in model □ (Max. applicable motor output kW) 0P1 (0.1)	0P2 (0.2)	0P4 (0.4)	0P7 (0.7)	1P5 (1.5)	2P2 (2.2)	3P0 (3.0)	3P7 (3.7)
Single-phase 200V	With Digital Operator	With Analog Volume	CIMR-J7AZB□	O	O	O	O	O	—	—	—
		Without Analog Volume	CIMR-J7CZB□								
	Without Digital Operator		CIMR-J7BZB□	O	O	O	O	O	—	—	—
Three-phase 200V	With Digital Operator	With Analog Volume	CIMR-J7AZ2□	O	O	O	O	O	O	—	O
		Without Analog Volume	CIMR-J7CZ2□								
	Without Digital Operator		CIMR-J7BZ2□	O	O	O	O	O	O	—	O
Three-phase 400V	With Digital Operator	With Analog Volume	CIMR-J7AZ4□	—	O	O	O	O	O	O	O
		Without Analog Volume	CIMR-J7CZ4□								
	Without Digital Operator		CIMR-J7BZ4□	—	O	O	O	O	O	O	O

Note: Models without cooling fin are available.
Contact your YASKAWA representative.

O: provided

STANDARD WIRING

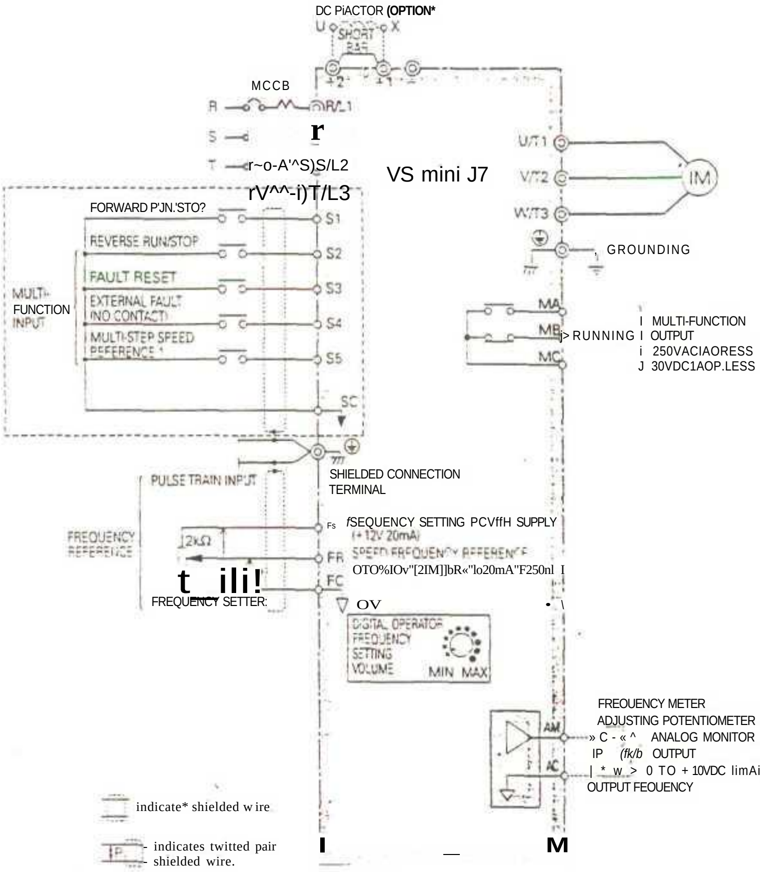

* shows the connection (or the following two kinds of sequence input (S1 to S5) signals: no-voltage contact and NPN transistor; (0V common). For a PNP transistor (+24V common), +24V external power supply is necessary

■ Model Description

Type			Terminal	Name	Function (Signal Level)	
Main Circuit			R/L1, S/L2, T/L3	AC Power Supply Input	Main circuit power supply input (Use R/L1 and S/L2 for single-phase power supply inverter. Do not use T/L3 of the models less than 0.75kW for other usage, such as a junction terminal)	
			U/T1, V/T2, W/T3	Inverter Output	For inverter output	
			+2, +1	DC Reactor Connection	Remove the short bar between +2 and +1 when connecting DC reactor (option)	
			+1, -	DC Power Supply Input	For power supply input (+1: positive electrode; - : negative electrode)*	
			⏚	Grounding	For grounding (Grounding should be conforming to the local grounding code.)	
Control Circuit	Input	Sequence	S1	Forward Run Input	Runs when CLOSED, stops when OPEN.	24VDC, 8mA photocoupler insulation
			S2	Multi-function Input Selection 2	Factory setting: Runs when CLOSED, stops when OPEN.	
			S3	Multi-function Input Selection 3	Factory setting: "Fault reset"	
			S4	Multi-function Input Selection 4	Factory setting: "External fault (NO contact)"	
			S5	Multi-function Input Selection 5	Factory setting: "Multi-step speed reference 1"	
			SC	Multi-function Input Selection Common	Common for control signal	
		Frequency reference	FS	Power Supply Terminal for Frequency Setting	+12V (allowable current: 20mA max.)	
			FR	Speed Frequency Reference	0 to +10V DC (20kΩ) or 4 to 20mA (250Ω), 0 to 20mA (250Ω) (resolution 1/1000)	
			FC	Frequency Reference Common	0V	
	Output	Multi-function Contact Output	MA	NO Contact Output	Factory setting: "Running"	Contact capacity 250VAC, 1A or less 30VDC, 1A or less
			MB	NO Contact Output		
			MC	Contact Output Common		
			AM	Analog Monitor Output	Factory setting: "Output frequency" 0 to +10V output	0 to 10V 2mA or less Resolution: 8bits
			AC	Analog Monitor Common	0V	

•DC power supply input terminal is not conformed to UL/cUL standard.

Function	Constant No. nzn	Function Name	Description	Setting Range	Min. Setting Unit	Initial	Ref. Page
Selecting Constant Group Initializing	01	Password	0 : nOI read and set, nO2 to n79 read only (FREF of digital operator can be set) 1 : nOI to n79 read and set 6 : Fault history clear 8 : Initialization-reset (multi-function terminal to initial setting) 9 :3-wire initialization-reset	0, 1.6. 8,9	-	l	17
Selecting Operation Mode	02	Run command selection	0 : Digital operator 1 : Control circuit terminal 2 : Communication	0to2	-	0	17
	03	Frequency reference selection	0 : Volume 1 : Frequency Reference 1 (n21) 2 : Control circuit terminal (0 to 10 V) 3 : Control circuit terminal (4 to 20 mA) 4 : Control circuit terminal (0 to 20 mA) 6 : Communication	0 to 4.6	-	0	
Selecting Stopping Method	04	Selecting Stopping Method	0 : Deceleration to stop 1 : Coast to a slop	0, 1	-	0	23
Reverse Run Prohibited	05	Selecting reverse run prohibited	0 : reverse run enabled 1 : reverse run disabled	0. 1	-	0	17
Selecting Digital Operator Key Function	06	Stop key function	0 : Stop key is always effective 1 : Stop key is effective when operated from digital operator	0, 1	-	0	23
	07	Selecune frequency reference in local mode	0: Volume 1 : Frequency reference 1 (n21)	0. 1	-	0	-
	08	Frequency reference setting method from digital operator	0 : Enter key used 1 : Enter key not used	0, 1		0	-
Setting V/f Pattern	09	Max. output frequency	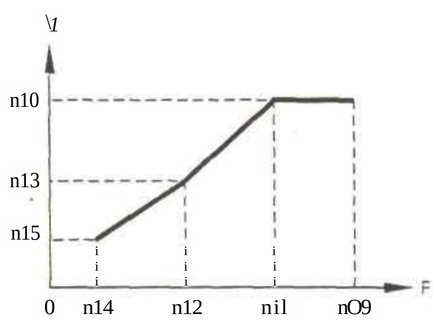	50.0 to 400Hz	O.I Hz (less than lOOHz) IHz (lOOHzor more)	60.0Hz	16 25
	10	Max. voltage		0.1 to 255V*	IV	200V	
	11	Max. voltage output frequency fbase frequency)		0.2 to 400Hz	0.1 Hz (less than lOOHz) IHz (lOOHzor more)	60.0Hz	
	12	Mid. output frequency		0.1 to 399Hz		1.5Hz	25
	13	Mid. output frequency voltage		0.1 to 255V	IV	12V*	
	14	Min. output frequency	When V/f pattern is a straight line, set n 14 and n16 to the same value. In this case. n15 is disregarded.	0.1 to lOHz	0.1 Hz	1.5H?.	
	15	Min. output frequency voltage		0.1 to 50V*	IV	12V*	

*: For 400V class inverter, the upper limit of voltage setting range and the setting value before shipment are twice that of (=400/200) 200V class.

Function	Constant No. n~zz:	Function Name	Description	Setting Range	Mm. Setting Unit	Initial	Ref. Page
Selecting Acceleration/ Deceleration Time	16	Acceleration time 1	Sets acceleration time in the unit when frequency reference changes from 0 to 100 %.	0.0 to 999	0.1s (less than 100s) Is (lOOsor more)	10.0s	16 19
	17	Deceleration lime 1	Sets deceleration time in the unit when frequency reference changes from 100 to 0 %.	0.0 to 999		10.0s	
	18	Acceleration time 2	Effective when acceleration lime 2 is selected at multi-function contact input selection. Setting is the same as n16.	0.0 to 999		10.0s	
	19	Deceleration time 2	Effective when deceleration time 2 is selected at multi-function contact input selection. Setting is the same as n17.	0.0 to 999		10.0s	
Selecting S-curve	20	S-curve selection	0 : S-curve not provided 1 :0.2 s 2 :0.5 s 3: 1.0s	0to3	-	0	20
Frequency Reference (fFREFl)	21	Frequency reference 1 (Master speed frequency reference)	Sets master speed frequency reference. Setting is the same as simple operation lamp IFREFI).	0.0 to 400Hz	0.1 Hz (less than lOOHz) 1 Hz (100 Hz or more)	6.0Hz	18
	22	Frequency reference 2	Sets second frequency reference. It is effective when multi-step speed reference 1 is selected in multi-function contact input.			O.OHz	
	23	Frequency reference 3	Sets third frequency reference. It is effective when multi-step speed reference 2 is selected in multi-function contact input.				
	24	Frequency reference 4	Sets fourth frequency reference. It is effective when multi-step speed references 1 and 2 are selected in multi-function contact input.				
	25	Frequency reference 5	Sets fifth frequency reference. It is effective when mulii-step speed reference 3 is selected in multi-function contact input.				
	26	Frequency reference 6	Sets sixth frequency reference. It is effective when multi-step speed references 1 and 3 are selected in multi-function contact input.				
	27	Frequency reference 7	Sets seventh frequency reference. It is effective when multi-step speed references 2 and 3 are selected in multi-function contact input.				
	28	Frequency reference 8	Sets eighth frequency reference. It is effective when multi-step speed references 1,2, and 3 are selected in multi-function contact input.				
	29	Jog frequency	Sets jog frequency. It is effective when jog frequency is selected in multi-function contact input.			6.0Hz	18 19
Frequency Reference Limit	30	Frequency reference upper limit	Sets upper limit of frequency reference in units of 1 %. Max. output frequency (nO9) is 100 %.	Oto 110%	1%	100%	19
	• 31	Frequency reference lower limit	Sets lower limit of frequency reference in units of 1 %. Max. output frequency (n09) is 100 %.	Oto 110%	1%	0%	
Motor Protection by Electronic Thermal	32	Motor rated current	Sets motor rated current of the molor nameplate. It is the standard current for motor electro-thermal protection.	0 to 120% of invener rated output current	0.1 A	Different according to invener cl|acily (kVA)	17 27
	33	Electronic thermal motor protection selection	0: Standard motor 1 : Inverter motor 2: No protection	Oto 2	-	0	27
	34	Electronic thermal motor protection time constant setting	Sets constant for motor protection. For standard and inverter motors (standard rating), 8min., for others (short period rating), 5min.	1 to 60min	Imin	8m in	
Selecting Cooling Fan Operation	35	Selecting cooling fan operation	0 : ON/OFF control (ON while running, OFF when stopped. ON for one minute after stopping.) 1 : Operates with power supply ON	0.1	-	0	-

Function	Constant No. rdj	Function Name	Description	Setting Range	Min. Setting Unit	Initial	Ret. Page
Selecting Sequence Input Functions	36	Multi-function input selection 2 (Terminal S2)	2 : REV run command (2-wire sequence) 3 : External fault (NO contact input) 4: External fault (NC contact input) 5: Fault reset 6: Multi-step speed reference 1 7: Multi-step speed reference 2 8 : Multi-step speed reference 3 10: Jog reference 11 : Accel/Decel time selection 12: External baseblock (NO contact input) 13 : External baseblock (NC contact input) 14 : Search command from maximum, output frequency 15 : Search command from set frequency 16: Accel/Decel prohibit 17: Local/Remote selection 18 : Comm./Contro! circuit terminal selection 19 : Emergency stop fault (NO contact input) 20: Emergency stop alarm (NO contact input) 21: Emergency stop fault (NC contact input) 22: Emergency stop alarm (NC contact input)	2 to 8 10 to 22	-	2	18 19 21 22 23
	37	Multi-function input selection 3 (Terminal S3)	0: FWD/REV run command (3-wire sequence) Other set items are same as n36	0.2 to 8, 10 to 22	-	5	
	38	Mulu-funcuon input selection 4 (Terminal S4)	Set items are same as n36	2 to 8 10 to 22	-	3	
	39	Multi-function input selection 5 (Terminal S5)	Set items are same as n36. 34; UP/DOWN command (Terminal S4 is UP command/DOWN command and the setiine of n3S is invalid) 35: Looplest (MEMOBUS)	2 to 8 10 to 22 34. 35	-	6	
Selecting Sequence Output Functions	40	Multi-function output selection 1 (Contact output terminal MA-MB-MC)	0: Fault 1 : Running 2 : Speed agreed 3: Zero speed 4 : Frequency detection 1 (Output frequency & Custom frequency detection) 5 : Frequency detection 2 (Output frequency i Custom frequency detection) 6 : Ovenorque detection (NO contact output) 7 : Ovenorque detection (NC contact output) 10: Minor fault (alarm displays) 11 : During baselock 12: Operation mode 13 : Invener operation ready 14: During fault retry 15 : Low voltage detecting 16: In REV running 17: Speed searching 18 : Output from communication	Oto7 10 to 18	-	1	25
Selecting Frequency Reference Functions	41*	Analog frequency reference gain	Sets internal reference level in units of 1 % when frequency reference voltage (current) is 10V (20mA). Max. output frequency (n09) is 100 %.	0 to 225%	1%	100%	19
	42*	Analog frequency reference bias	Sets internal reference level in units of 1 % when frequency reference voltage (current) is 0V (4mA or 0mA). Max. output frequency (n09) is 100 %.	-99 to 99%	1%	0%	19
	43	Filter time constant for analog frequency reference constant	Sets filter time constant for analog input primary lag. (to avoid noise)	0.00 to 2.00s	0.01s	0.10s	-
Selecting Analog Monitor Functions	44	Multi-function analog output (terminal AM-AC)	0: Output frequency (lOV/Max. frequency nO9) 1 : Output current (lOV/lnverter rated current)	0, 1	-	0	22
	45*	Analog monitor gain	Adjusts output voltage level of analog monitor, (ex.) when 3V is 100 % level, sets as n45 = 0.30	0.00 to 2.00	0.01	1.00	22

*: Can be changed during operation.

Function	Constant No. n~^	Function Name	Description	Setting Range	Min. Setting Unit	Initial	Ref. Page
Adjusting Carrier Frequency	46	Carrier frequency selection	Carrier frequency 1,2, 3.4: Set value X 2.5 Hz 7, 8, 9 : Proportional to output frequency of 2.5 kHz max. (lower limit 1 kHz)	1 to 4 7 to 9	-	4 Different according lo invcncr canacityftVA)	22
Momentary' Power Loss Ridethrough	47	Momentary power loss ridethrough method	0: Not provided 1 : Coniinuous operation after power recovery within the power loss ndethrough time. 2 : Coniinuous operation after power recovery (no fault output of UV1)	0to2	-	0	20
Fault Retry	48	Automatic retry attempts	Sets automatic retry limes after self-diagnosis when an inverter fault occurs.	Oto 10	1	0	20
Jump Frequency Control	49	Jump frequency 1	Sets frequency to jump. Disabled when setting value is 0.0.	0.0 to 400Hz	0.1 Hz (less than 100 Hz) 1Hz (100 Hz or more!	O.OHz	21
	50	Jump frequency 2					
	51	Jump frequency range	Sets the frequency ranse to jump. Disabled when setting value is 0.00.	0.0 to 25.5Hz	0.01 Hz		
DC Injection Braking	52	DC injection braking current	Sets current value at DC injection braking. Inverter rated current is 100 %.	Oio 100*	1%	50%	21 23
	53	DC injection braking time at stop	Sets DC injection braking time at ramp to stop tn units of 0.1 sec. Disabled at stop when the setting value is 0.0.	0.0 to 25.5s	0.1s	0.5s	23
	54	DC injection braking time at start	Sets DC injection braking time at start in units of 0.1 sec. Disabled at start when the setting value is 0.0.	0.0 lo 25.5s	0.1s	0.0s	21
Stall Prevention	55	Stall prevention during deceleration	0 : Enabled 1 : Disabled	0, 1	-	0	26
	56	Stall prevention level during acceleration	Scls stall prevention level in units of 1 * during acceleration, lnvcncr ralcd currcm is 100 9c (Notes: • Disabled with ituing of 200 4. • In consiam ouipm arci, prevention level is automatically lowered.)	30 to 2009c	1%	170%	
	57	Stall prevention level during running	Sets stall prevention level in units of 1 % during running. Inverter rated current is 100 9b. (Noie I Disabled with selling of 200 %)	30 to 200%	1%	160%	
Frequency Detection	58	Frequency detection (multi-function contact output)	Sets frequency to detect when selected frequency detection at multi-funclion contact output.	0.0 to 400Hz	O.iHz (less to 100 Hz) lHz (100 Hz or more)	O.OHz	21
Detecting Overtorque	59	Ovenorque detecting function selection	0: Detection disabled 1 : Detected during constant-speed running, and operation continues during and after detection. 2: Detected during constant-speed running, and invener output is shut OFF after detection. 3: Detected during running, and operation continues during and after detection. 4 : Detected duriing running, and invener output is shut OFF after detection.	Oto 4	-	0	20
Detecting Overtorque	60	Ovenorque detection level	Sets ovenorque detection level when detecting at multi-function contact output ahd multi-funclion photocoupler output. • Inverter rated current is)00% when detecting by current. • Motor rated torque is 100% when detecting by torque.	30 to 200%	1%	160%	20
	61	Ovenorque detection time	Sets overtorque detection time. Ovenorque is detected when the set time or the ovenorque detection level setting is exceeded.	0.1 10 10.0s	0.1s	0.1s	

Function	Constant No. nun	Function Name	Description	Setting Range	Min. Setting Unit	Initial	Ref. Page
Holding Output • Frequency	62	Hold output frequecy savins selection	Selects whether or not to save the frequency when holding at UP/DOWN command from multi-function input terminal. 0 : Output frequency is not saved while holding 1 : When holding more than 5 sec, saves output frequency at holding and operates at this frequency when restarted.	0.1	-	0	-
Torque Compensation	63*1	Torque compensation gain	Sets torque compensation gain in units of 0.1. Normally, no adjustment necessary.	0.0 to 2.5	0.1	1.0	25
Slip Compensation Function	64*1	Motor rated slip	Sets motor rated slip in units of 0.1 Hz.	0.0 to 20.0Hz	0.1 Hz	(Different according to inverter capacity (kVA))	-
	65*1	Motor no-load current	Sets motor no-load current proportional to the motor rated current.	0 to 99%	1%	(Different according to inverter capacity (kVA))	27
	66*1	Slip compensation gain	For motor slipping calculated from the output current, sets gain to correct output frequency in units of 0.1.	0.0 to 2.5	0.1	0.0	27
	67	Slip compensation time constant	Adjusts for unstable speed and slow speed response.	0.0 to 25.5s	0.1s	2.0s	-
MEMOBUS Communica-tion (when option unit is provided)	68	MEMOBUS time over detection	0 : Time over detection is enabled. (Coast to a slop) 1 : Time over detection is enabled. (Ramp to stop-Decel. 1) 2 : Time over detection is enabled. (Ramp to stop-Decel. 2) 3 : Time over detection is enabled. (Continue operation - alarm) 4 : Time over detection is disabled.	0to4	-	0	-
	69	MEMOBUS frequency reference and frequency monitor unil	0:0.1 Hz 1 : 0.01 Hz 2 : 30000/100% (30000=MAX. output frequency) 3:0.1 %	0to3	-	0	-
	70	MEMOBUS slave address	Allocates inverter MEMOBUS communication slave address between 0 to 32. Note: When set "0," ignores command from master and does not respond.	0to32	-	0	-
	71	MEMOBUS BPS selection	0: 2400 bps 1 : 4800 bps 2 : 9600 bps 3 : 19200 bps	0to3	-	2	-
	72	MEMOBUS parity selection	0: Even parity 1 : Odd parity 2 : No parity	0to2	-	0	-
	73	Transmission wailing time		0 to 65ms	lms	10ms	-
	74	RTS Control	0 : Enabled 1 : Disabled (RS-422: at 1 to 1 communication)	0. 1	-	0	-
Carrier Frequency Selection*2	75	Reducing carrier frequency selection at low speed	0 : Invalid 1 : Valid	0, 1	-	0	-
Control Copy Function*1	76	Constant copy function selection	rdy : READY vFy : VERIFY rEd : READ vA : Inverter capacity display Cpy : COPY Sno : software No. display	rdy, rEd cPy, uFu vA. Sno	-	rdy	-
	77	Constant Read selection prohibit	0 : READ prohibited I : READ allowed	0.1	-	0	-
Fault History	78	Fault history	Displays newest one fault (only lor monitoring)	-	-	-	-
Software Version	79	Software Version No.	Displays lowest 3 digits of software No. (only for monitoring)	-	-	-	-

*1. Can be changed during operation.
*2. Not built in for the software virsion VSP020OI0.

The set value displayed in [ ] is factory setting.

Programming features of VS mini J7 are explained according to the following items.

Item	Setting Function	Ref. Page
Items Should be Verified Before Operation	• Accel/decel lime setting • Adjusting motor torque • Motor rotation direction setting • LOCAL (operator) /REMOTE (control circuit terminal) selection • Motor rated current selling • Operation mode selection • Constant set-up	16 16 17 17 17 17 17
Setting Operating Condition	• Reverse run prohibit • Multi-step speed selection - Adjusting frequency setting signal • Operation at low speed • Adjusting frequency upper and lower limits • Using two accel/decel times • Automatic restart after momentary power loss • Soft-start characteristics • Torque detection • Continuing operation by automatic fault reset. • Frequency detection • Avoiding resonance • Operating coasting motor without trip • Holding accel/decel temporarily • Using frequency meter or ammeter • Reducing motor noise or leakage current	18 IS 19 19 19 19 20 20 20 20 21 21 21 22 22 22
Selecting Stopping Method	• Operator stop key selection • Selecting stopping method • Applying DC injection braking	23 23 23
Building Interface Circuits with Exlemal Devices	• Using input signals • Using output signals	23 25
Adjusting Motor Torque	• Adjusting torque according to application • Preventing motor from stalling (current limit)	25 26
Decreasing Motor Speed Fluctuation	• Slip compensation	27
Prolecting Motor	• Motor overload detection	27

Items Should be Verified Before Operation

Accel/decel time setting

Accel time 1, 2 [n16] [n18]

Decel time 1, 2 [n17] [n19]

Accel time : Sets the time needed for the motor to accelerate to the maximum output frequency from the stopped status.

Decel time : Sets the time needed for the motor to stop from the maximum output frequency.

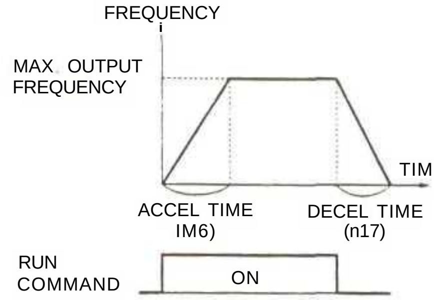

Adjusting motor torque

Max. output frequency [n09]

Max. voltage [n10]

Max. voltage output frequency [n11]

Sets the V/f pattern which matches the motor characteristics.

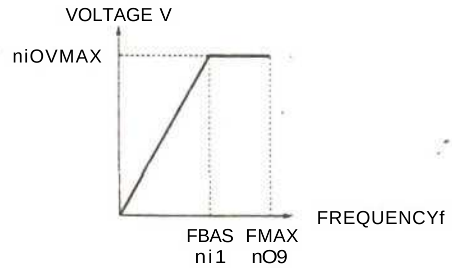

Motor rotation directiohsetting

FWD/REV direction seiection:fF/R]

Sets the motor rotation direction when run command is given by the digital operator.
FWD and REV run can be switched by pressing \K\ or 0key.

i-or- (FWD/RUN) r-fc<_ (REV/RUN)

LOCAL (operator)/REMOTE (control circuit terminal) selection

L0CAL/RJEMOTE switching |LO/RE|

Operation can be switched from digital operator or control circuit terminal. This function is valid only when stopped.

e.g. : Digital operator/control circuit terminal selection:

Operation mode selection nO2=l
Frequency reference selection nO3=2, 3 or 4
Local (LO) : Receives frequency reference (set at nO7) and run command from digital operator
Remote (RE) : Receives frequency reference (FR) and run command (terminals SI and S2) of circuit control terminal

* When local/remote selection function is allocated to multi-function input terminal, switching operation using \K\ and [v] keys is invalid.

Motor rated current setting

Motor rated current lor?*?]

Sets motor rated current. The following table shows the standard set value for each inverter capacity. When the applicable motor rated current value differs from the value listed below, change the set value.

VS mini J7 model CIMR-J7CDC2	20P1 B0P1	20P2 B0P2	20P4 B0P4	20P7 B0P7	21P5 B1P5	22P2	23P7
Max. Applicable Molor Output kw(HP)	0.1 (0.13)	0.2 (0.25)	0.4 (0.5)	0.75 (1)	1.5 (2)	2.2 (3)	3.7 (5)
Motor Current Factory Settina A	0.6	1.1	1.9	3.3	6.2	3.5	14.1

VS mini J7 model CIMR-J7□□□	40P2*	40P4*	40P7*	41P5*	42P2*	43P0*	43P7*
Max. Applicable Motor Output kw(HP)	0.37 (0.5)	0.55 (0.75)	1.1 (1.5)	1.5 (2)	2.2 (3)	3 (4)	3.7 (5)
Motor Current Factory Senina A	0.6	1.0	1.6	3.1	4.2	7.0	7.0

* : Under development

Operation mode selection

Run command selection In0^1

Frequency reference selection \r»OS\

Selects whether operation is performed by digital operator or control circuit terminal.

Setting	Run Command |r>C«?l
0	Operator
1	Control circuit terminal SI, S2
2	Communication

Setting	Frequency Reference | n S 3 |
0	Volume
1	Operator (Frequency reference 1) 1 o c » 1
2	Control circuit terminal FR (0 to 10V)
3	Control circuit terminal FR (4 to 20mA)
4	Control circuit terminal FR (0 to 20mA)
6	Communication (register No., 0002H)

Notes : When set to 2 or 3 (current input reference), dip switch setting must be changed. For details, refer to the instruction manual.

Constant set-up

Password InCJ !\

The following table describes the data which can be set or read when nOl is set.

Setting	Constant
0 (Constant write disable)	Only nOl can be set. nOl to n79 can be read
1	nOl to n79 read/set
6	Fault history clear
8*	Constant initialization (factory setting: 2-wire sequence)
9*	Constant initialization (3-wire sequence)

* Initialization resets the value to factory settinc

The set value displayed in |____| is factory setting.

Setting Operating Condition

Reverse run prohibit

Reverse run prohibit |«->O5l

"Reverse run disabled" setting does not accept a reverse run command from the control circuit terminal or digital operator. This setting is used for applications where a reverse run command can cause problems.

Setting	Description
0	Reverse run enabled.
1	Reverse run disabled.

Multi-step speed selection

Frequency reference FREF n21 to n29

Multi-function input terminal function selection n35 to n39

By combining frequency reference and input terminal function selections, up to 9-step speed can be set.

2-step speed change example
nO2 = 1 (Operation mode selection)
nO3 = 1 (Frequency reference selection)

n21 = 30.0Hz
n22 = 50.0Hz

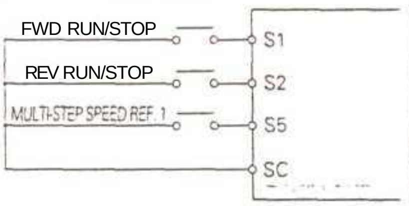

Note : When nO3 is set to 0. 2 .3, or 4, frequency reference 1 (n21) is disabled and frequency reference from volume (0) or control circuit terminal (FR) is enabled.

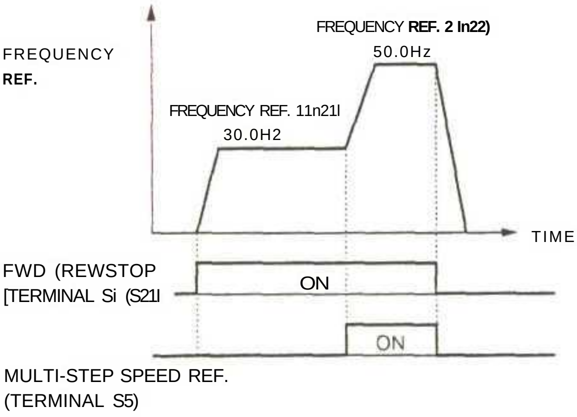

8-step speed change example
n02 = 1 (Operation mode selection)
n03 = 1 (Frequency reference selection)

n21 = 25.0Hz
n22 = 30.0 Hz
n23 = 35.0 Hz
n24 = 40.0 Hz
n25 = 45.0Hz
n26 = 50.0 Hz
n27 = 55.0 Hz
n28 = 60.0 Hz

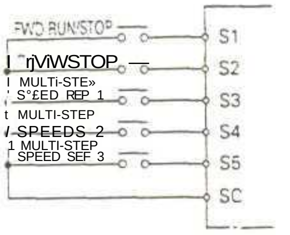

n37 = 6 (Multi-function input terminal S3)
n38 = 7 (Multi-function input terminal S4)
n39 = 8 (Multi-function input terminal S5)

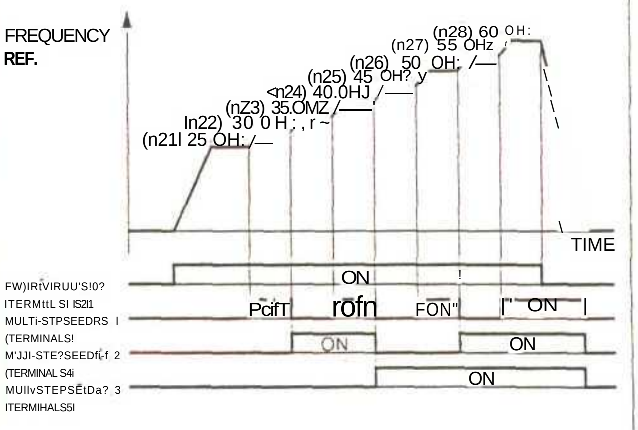

Adjusting frequency setting signal

Frequency reference gain JnW /|

Frequency reference bias |nS'd?| -

When the frequency reference is output by analog input of control circuit terminals FR and FC, the relation between analog voltage and frequency reference can be set.

Frequency reference gain (n41)

The analog input voltage value for the maximum output frequency (nO9) can be set in units of 1%.

Factory setting : 100%

Frequency reference bias (n42)

The frequency reference provided when analog input is 0V (4mA or 0mA) can be set in units of 1%.

[nO9 : Maximum output frequency = 100%]

Factory setting : 0%

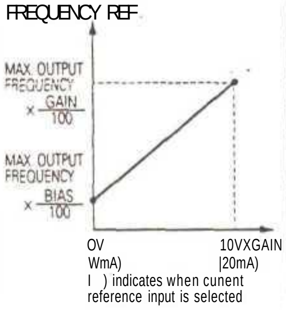

Gain : Outputs El % (ratio to max. output frequency nO9) at 10V.
^ n41 = SI %

Bias : Outputs [Hl% (ratio to max. output frequency nO9) at 0V.
^•n42=]B %

Typical Settings

- At 0 to 5V input

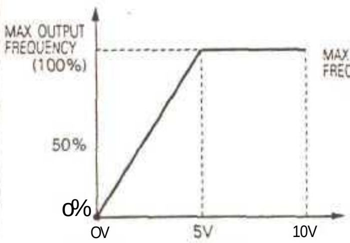

Gain Constant n41 =200
Bias- Constant n42=0

- To operate the inverter with frequency reference of 50% to 100% at 0 to 10V input

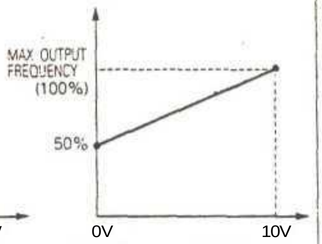

Gain: Constant n41 = 100
Bias. Constant n42=50

Operating at low speed

Jog frequency reference 1 FREF | |o<?9l

j Jog command selection k»36| to In 3!5

By inputting a jog command and then a forward (reverse) run command, operation is enabled at the jog frequency set in n29. When multi-step speed references 1. 2, or 3 are input simultaneously with the jog command, the jog command has priority.

Name	Constant no.	Setting
Jog frequency reference	n29	Factory setting : 6,0Hz
Jog command	n36 to n39	Set lo "10" for anv constant.

Adjusting frequency upper/and lower limits

Frequency'reference upper limit in351.^ _ i:;_ v!

Frequency reference lower limit |n3 «

Frequency reference upper limit (n30)

Sets the upper limit of the frequency reference in units of 1%.

[nO9 : Maximum output frequency = 100%]

Factory setting : 100%

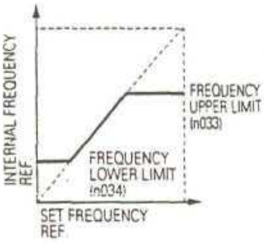

Frequency reference lower limit (n31)

Sets the lower limit of the frequency reference in units of 1%.

[n09 : Maximum output frequency = 100%)

When operating at frequency reference 0, operation continues at the frequency reference lower limit.

However, when frequency reference lower limit is set to less than the minimum output frequency (nl4), operation is disabled.

Factory setting : 0%

Using two accel/decel times: v-^; ;:.•;; .;;v-

Accel time 1,2' ";..' " -' - L. In «S| In 18\ •

Deceltime 1,2 ;• |r» »' 1\ \i-> SS\

Input terminal function selection In 361 to [n 351

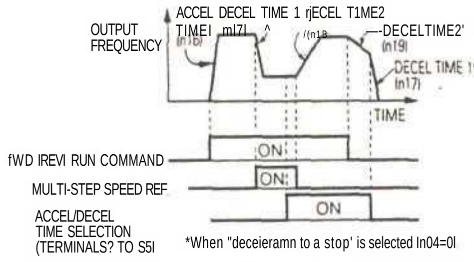

By setting input terminal function selection (one of n36 to n39) to "11" (accel/decel time select), accel/decel time is selected by turning ON/OFF the accel/decel time select (one terminal of S2 to S5).

AtOFF:nl6(acceltime 1)
nl7 (decel time 1)

At ON :nl8(acceltime2)
nl9 (decel time 2)

No.	Name	Unit*	Setting range	Initial setting
nl6	Accel time 1	0.1s	0.0 to 999s	10.0s
nl7	Decel time 1	0.1s	0.0 to 999s	10.0s
nlS	Accel time 2	0.1s	0.0 to 999s	10.0s
nl9	Decel time 2	0.1s	0.0 to 999s	10.0s

• Setting unit is Is when 100s or more.

- Accel time
  Set the time needed for output frequency to reach 100% from 0%.
- Decel time
  Set the time needed for output frequency to reach 0% from 100%.

The set value displayed in [ ] is factory setting.

Automatic restart after momentary power loss

Operation selection after momentary power loss lr> S' *?|

When momentary power loss occurs, operation restarts automatically.

Selling	Description
0	Continuous operation after momentary power loss not provided.
1*	Continuous operation after power recoverv within 0.5 second.
2*†	Continuous operation after cower recoverv (Fault output not provided).

* Hold the operation command to continue the operation after recovery from a momentary power loss,

t When 2 is selected, operation restarts if power supply voltage reaches its normal level. No fault signal is output.

Soft-start characteristics

S-curve accel/decel time selection \rnj?L

To prevent shock at machine start/stop, accel/decel can be performed in S-curve pattern.

Selling	S-curve charactenstic time
0	S-mrvc chanctenaic not provided
1	0.2 second
2	0.5 second
3	1.0 second

Note : S-curve characteristic lime is the time from accel/decel rate 0 lo a regular accel/decel determined by the set accel/decel lime.

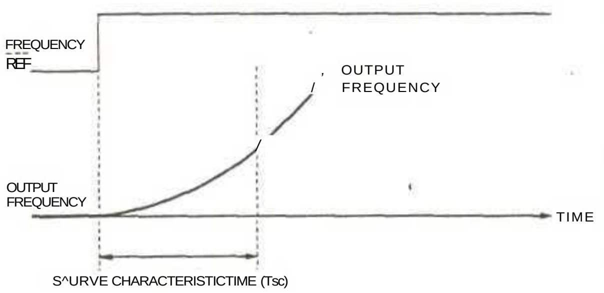

Time chart at FWD/REV run switching at deceleration to a stop

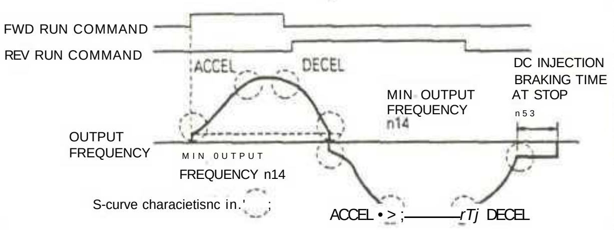

Torque detection

Overtorque detection function selection \r->SS\

Overtorque detection level 1<~>5C?|

Overtorque detection time . In 6 «|

If excessive load is applied to the machine, output current increase can be detected by output alarm signals at multi-function output terminals MA, MB and MC.
To output overtorque detection signal, set multi-function output terminal selection n40 to "overtorque detection (set 6 or 7)".

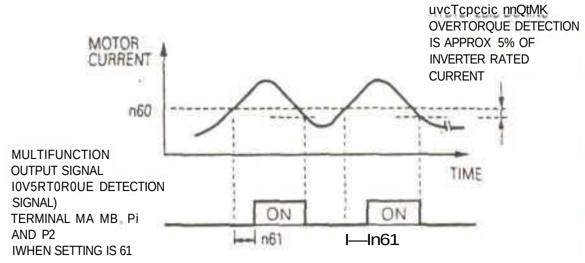

Overtorque detection function selection 1 (n59)

Seitins	Description
0	Ovenorque detection not provided.
1	Detected only during constant-speed running, and operation continues after detection.
2	Detected only during constant-speed running, and operation stops after detection.
3	Detected during running, and operation continues after detection.
4	Detected during running, and operation stops after detection.

Continuing operation by automatic fault reset

No. of fault retry times \r» S'Sl

Sets the inverter to restart and reset fault detection [overcurrent (OC) or overvoltage (OV)] after a fault occurs.
The number of self-diagnosis and retry attempts can be set at n48 up to 10 times.
The number of retry attempts are cleared to 0 in the following cases :

- If no other fault occurs within 10 minutes after retry
- When the fault reset signal is ON after the fault is detected
- Power supply is turned OFF

Frequency detection

Frequency detection level [Q58

Effective when output terminal function selections n40, are set to "frequency detection (setting : 4 or 5). "Frequency detection" turns ON when output frequency is higher or lower than the frequency detection level (n58).

Frequency detection 1 (Output frequency ≧ Frequency detection level)
(Set n40 to "4")

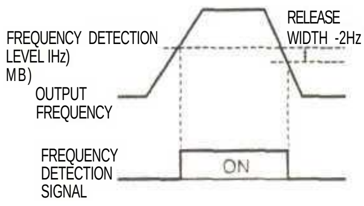

Frequency detection 2 (Output frequency S Frequency detection level)
(Set n40 to "5")

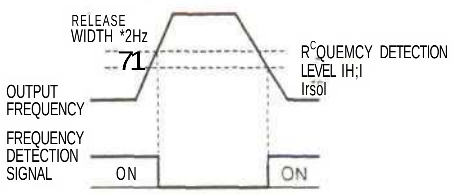

Avoiding resonance

Jump frequency 1, 2 n49 n50

Jump width \nS

This function allows the prohibition or "jumping" of critical frequencies so that the motor can operate without resonance caused by machine systems. This function is also used for dead band control. Setting the value to O.OHz disables this function.

Set jump frequency 1, 2 or 3 as follows:

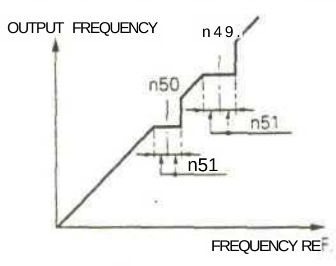

n49 ≧ n50

If this condition is not satisfied the inverter displays *Err-* for one second and restores the data to original settings.

Nole : Gradually changes without jumping during accel/decd.

Operating coasting motor without trip

Speed search command

Input terminal function selectfon lo 361 to In 351

DClnjectionbraking!at start

DC injection braking current lo Set

DC injection braking time at start |<->5S|

To operate coasting motor without trip, use the speed search command or DC injection braking at start.

Speed search command

Restarts a coasting motor without stopping it. This function enables smooth switching between motor commercial power supply operation and inverter operation.

Set input terminal function selection (n36 to n39) to "14" (search command from maximum output frequency) or "15" (search command from set frequency).

Build a sequence so that FWD (REV) run command is input at the same time as the search command or after the search command. If the run command is input before the search command, the search command becomes disabled.

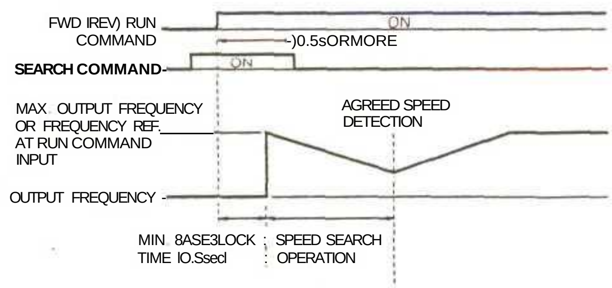

Time chart at search command input

DC injection braking at start

(n52. n54)

Restarts a coasting motor after stopping it. Set DC injection braking time at start in n54 in units of 0.1 second. Set DC injection braking current in n52 in units of 1%. When the setting of n54 is "0," DC injection braking is not performed and acceleration starts from the minimum output frequency.

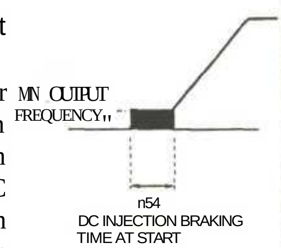

The set value displayed in [HZ!^is factor}' setting.

r

Holding accel/decel temporarily

Accel/decel hold command . • '

Input terminal function selection [<->35l to \n 3S\

To hold acceleration, input accel/decel hold command. The output frequency is maintained when the aceel/decel hold command is input during acceleration or deceleration.
The stop command releases the accel/decel hold and the operation ramps to stop while inputting accel/decel hold command.
Set input terminal function selection (n36 to n39) to 16 (accel/decel hold command).

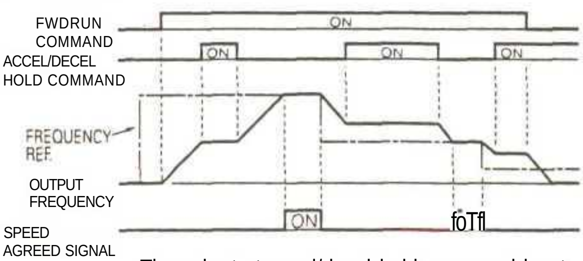

Time chart at accel/decel hold command input

Usihg.frequency;meterqr"ammetVfv..>v;;:-:

Analog monitor selection inHHl •--"•^v>': ^'-cv;--

Analog monitor gain . ••: |<->S'5|;"-^1** "..—:-^v'!//'•' -

Selects to output either output frequency or output current to analog output terminals AM-AC for monitoring.

Setting	Description
0	Output frequency
]	Output current

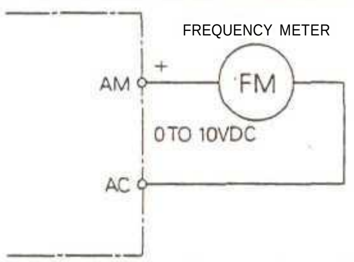

• Example of analog monitor gain adjustment
When using a frequency meter (full scale : 3V, 1mA) which indicates 0 to 60Hz at 0 to 3V.

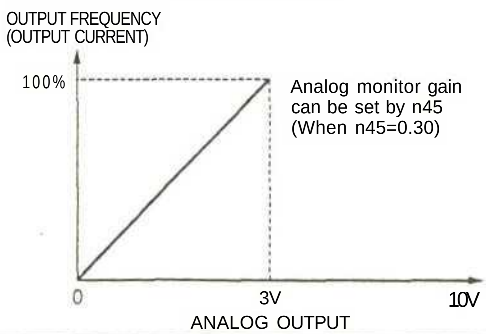

Reducing motor noise or leakage current

Carrier frequency lnS'61

Sets inverter output transistor swiching frequency (carrier frequency).

Seltins	Carrier frequency (Hz)	iMeullic noise from motor	Current leakace
1	2.5	Hieher	Smaller
2	5.0		1
3	7.5		
4	10.0		Larger
7 IO 9	Synchronized rypt with lower limit 1kHz and upper tail 15Hi	-	-

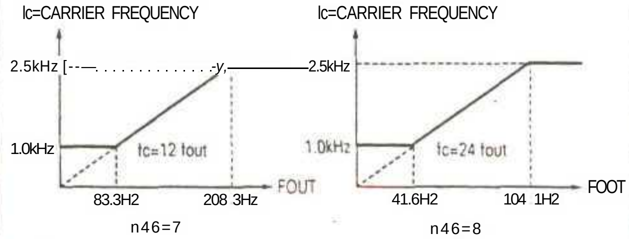

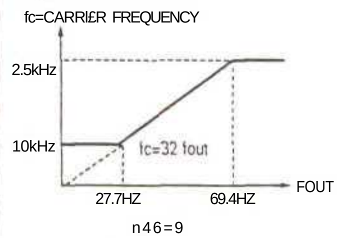

Carrier frequency initial value differs depending on inverter capacity as follows:

- 10kHz (setting n46 = 4): 200V three-phase 0.1 to 0.75kW
- 7.5kHz (setting n46 = 3): 200V three-phase 1.5 to 3.7kW
  200V single-phase, 1.5kW
  400V three-phase, all models

To change the initial value 7.5kHz to 10kHz, continuous output current must be lowered. For details, refer to the instruction manual.

Operator stop key selection

Operator stop key selection [illegible]

Selects processing when STOP key is depressed during operation from control circuit terminal or communication.

Setting	Description
0	STOP key effective when running from terminals or communication. When STOP key is depressed, the inverter stops according to the setting of constant n04. At this time, the digital operator displays " s r p " alarm (blinking). This stop command is held in the inverter until both forward and reverse run commands are open or operation command from communication is "0".
1	STOP key ineffective when running from terminals or communication.

Selecting stopping method

Stopping method selection [illegible]

Selects the stopping method suitable for application.

Setting	Description
0	Deceleration to stop
1	Coast to stop

• Deceleration to stop

Example when accel/decel time 1 is selected

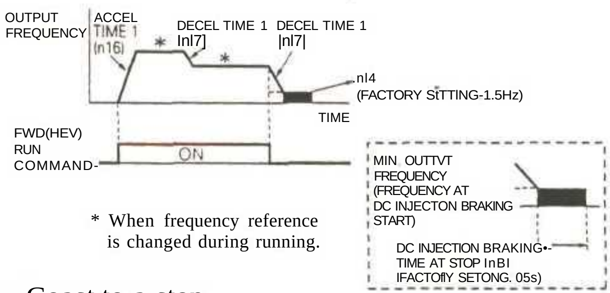

* When frequency reference is changed during running.

• Coast to a stop

Example when accel/decel time 1 is selected

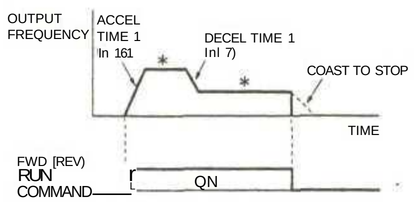

* When frequency reference is changed during running.

Applying DC injection braking

DC injection braking current [illegible]

DC injection braking time at stop [illegible]

When coasting to a stop is specified in stopping method selection (n04), DC injection braking at stop does not operate.

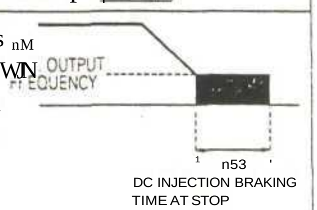

Using input signals

Input terminal function selection [illegible]

Multi-function input terminals S2 to S5 functions can be changed when necessary by setting constants n36 to n39, respectively. The same value can not be set to different constant setting.

- Terminal S2 function : Set to n36 : Factory setting 2
- Terminal S3 function : Set to n37 : Factory setting 5
- Terminal S4 function : Set to n38 : Factory setting 3
- Terminal S5 function : Set to n39 : Factory setting 6

Setting	Function Name	Description	Ref. Page
0	FWD/REV run command (3-wire sequence selection)	Setting enabled only for n052	24
2	REV run command (2-wire sequence)	-	-
3	External fault (NO contact input)	Inverter stops by external fault signal input. Digital operator display is "EFD*"	-
4	External fault (NC contact input)		
5	Fault reset	Resets fault. It is disabled with run signal entered.	-
6	Multi-step speed reference 1	-	18
7	Multi-step speed reference 2	-	
8	Multi-step speed reference 3	-	
10	Jog command	-	19
11	Accel/decel time select	-	19
12	External baseblock (NO contact input)	Motor coasts to stop by this signal input. Digital operator display "fab" (blinking).	-
13	External baseblock (NC contact input)		
14	Search command from max. output frequency	Speed search command signal	21
15	Search command from set frequency		
16	Accel/decel hold command	-	22
17	LOCAL/REMOTE selection	-	24
18	Communication/Control circuit terminal selection	-	24
19	Emergency stop fault (NO contact input)	Inverter stops by emergency stop signal input according to stopping method selection (n04). When frequency deceleration to a stop (n04=0) is selected, inverter decelerates to a stop according to decel time setting 2 (n19). Digital operator displays "%rP" (lights at fault, blinks at alarm).	-
20	Emergency stop alarm (NO contact input)		-
21	Emergency stop fault (NC contact input)		-
22	Emergency stop alarm (NC contact input)		-
34	UP/DOWN command	Setting is enabled only for n39.	24
35	Self-test	Setting is enabled only for n39.	-

* : A number 2 to 5 is displayed in -3 corresponding to the number of terminal S2 to S5 respectively.

The set value displayed in I___I is factor)' setting.

Terminal function at 3-wire sequence selection

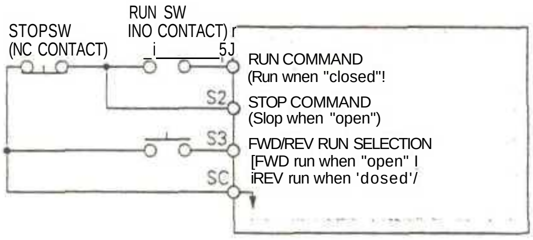

LOCAL/REMOTE select (setting : 17)

Select operation reference by the digital operator or by the control circuit terminal.

LOCAL/REMOTE select is valid only during stop.

Open : Run by setting at run command selection (nO2) and frequency reference selection (nO3).

Closed : Run by frequency reference and run command from digital operator.

e.g. : When the digital operator/control circuit terminal selection setting is nO2 = 1 and nO3 = 2,3 or 4

Open : Receives frequency reference (terminal FR, RP) and run command (terminals SI to S5) from control circuit terminal

Closed : Receives frequency reference (setting at nO7) and run command from digital operator.

Communication/control circuit terminal selection (setting : 18)

Selects operation reference by communication or by control circuit terminal. Communication/control circuit terminal selection is valid only during stop.

Open : Run according to the setting at nO2 and nO3 (operation method selection).

Closed : Run by frequency reference and run command from communication.

e.g. : When used for communication/control circuit terminal selection, set nO2 = 1 and nO3 = 2, 3 or 4

Open : Receives frequency reference (terminal FR) and run command (terminals SI to S5) from control circuit terminal

Closed: Receives frequency reference and run command from communication

UP/DOWN command (setting : n39 = 34)

With the FWD (REV) run command entered, accel/decel is enabled by inputting the UP or DOWN signals to control circuit terminals S4 and S5 without changing the frequency reference, so that operation can be perfomed at the desired speed. When UP/DOWN commands are specified by n39. any function set to n38 becomes disabled; terminal S4 becomes an input terminal for UP command and terminal S5 for DOWN command.

Control circuit terminal S4 (UP command)	Closed	Open	Open	Closed
Control circuit terminal S5 (DOWN command)	Open	Closed	Open	Closed
Operation status	Accel	Decel	Hold	Hold

*: Effective only when with option unit.

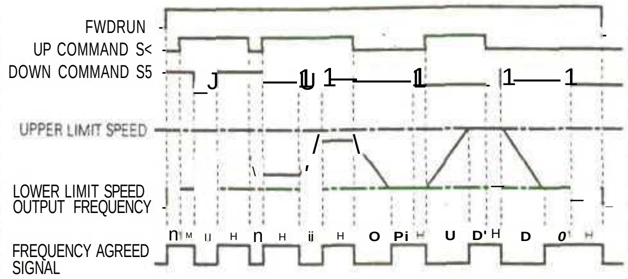

Time chart at UP/DOWN command input

U = UP (accelerating) status
D = DOWN (decelerating) status
H = HOLD (constant speed) status
Ul = UP siatus. clamping at upper limit speed
Dl = DOWN status, clamping at lower limit speed

Notes :
- When UP/DOWN command is selected, the upper limit speed is set regardless of frequency reference.
  Upper limit speed = Max. output frequency (nO9) x Frequency reference upper limit (n30)/100
- The lower limit speed is the largest value among min. output frequency (n!4) and frequency reference lower limit (n31).
- When the FWD (REV) run command is input, operation starts at the lower limit speed without UP/DOWN command.
- When the jog command is input while running by the UP/DOWN command, the jog command has priority. The UP/DOWN command can not be input together with multi-step speed reference.
- By setting hold output frequency memory selection (n62) to 1, the output frequency during hold can be saved.

Sean; it n6?	Description
0	Output frequency during hold is not saved.
1	After 5 sec. of hold state, the output frequency during hold is saved and the operation will restart with the saved output frequency

Using output signals

Multi-function output terminal function selection n40

Multi-function output terminal MA and MB, functions can be changed when necessary by setting constants n40.

• Terminal MA and MB functions: Set to n40

Setting	Function Name	Description	Ref. Page
0	Fault	"Closed" (ON) when inverter fault occurs.	-
1	Running	"Closed" (ON) when FWD or REV run command is input, or when the inverter outputs voltage.	-
2	Speed agreed	-	Figure below
3	Zero speed	"Closed" (ON) when the inverter output frequency is less than min. output frequency	-
4	Frequency detection 1 (output frequency ≥ frequency detection level)	-	21
5	Frequency detection 2 (output frequency ≤ frequency detection level)	-	21
6	Overtorque detection (NO contact output)	-	20
7	Overtorque detection (NC contact output)	-	20
10	Minor fault (alarm display)	-	28
11	During baseblock	"Closed" (ON) when the inverter output is shut off.	-
12	Operation mode	"Closed" (ON) when "LOCAL" is selected by LOCAL/REMOTE selection	-
13	Inverter run ready	**"Closed" (ON) when the inverter is ready to operate without any fault.**	-
14	In fault retry	**"Closed" (ON) during** fault retry.	-
15	Low voltage (UV) detected	"Closed" (ON) when the inverter is detecting low voltage.	-
16	In REV run	-	-
17	In speed search	"Closed" (ON) during speed search of inverter.	21
18	Data output from communication	**• By command from MEMOBUS communication, multi-function output terminal is operated independently from the inverter operation.**	-

Factory settings n40 : 1

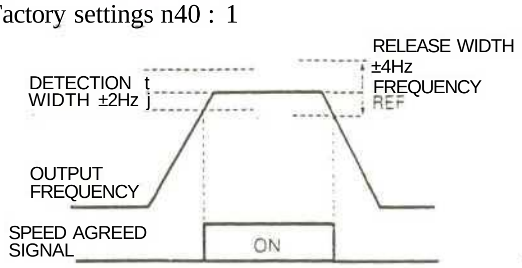

Setting example of "Speed agreed signal" (setting = 2)

Adjusting Motor Torque

Adjusting torque according to application

Max. output frequency: n09

Max. voltage: n10

Max. voltage output frequency: n11

Mid. output frequency: n12

Mid. output frequency voltage: n13

Min. output frequency: n14

Min. output frequency voltage: n15

Torque compensation gain: n63

Adjust motor torque by using "V/f pattern" and "full-range automatic torque boost".

V/f pattern setting

Set V/f pattern by n09 to n15 as described below. Set each pattern when using a special motor (high-speed motor, etc.) or when requiring special torque adjustment of machine.

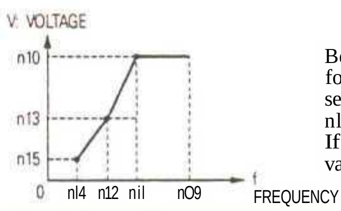

Be sure to satisfy the following conditions for the setting of n09 to n15.

n14 ≤ n12 < n11 ≤ n09

If n14 = n12 is set, the set value of n13 is disabled.

Constants No.	Name	Unit	Setting Range	Initial Setting
n09	Max. output frequency	0.1 Hz	50.0 to 400Hz	60.0Hz
n10	Max. voltage	1V	1 to 255V	200V*
n11	Max. voltage output frequency (base frequency)	0.1 Hz	0.2 to 400Hz	60.0Hz
n12	Mid. output frequency	0.1 Hz	0.1 to 399Hz	1.5Hz
n13	Mid. output frequency voltage	1V	1 to 255V	12V*
n14	Min. output frequency	0.1 Hz	0.1 to 10.0Hz	1.5Hz
n15	Min. output frequency voltage	1V	1 to 50V	12V*

Note : Refer to the instruction manual for details of setting.
* : Twice for 400V class.

Full-range automatic torque boost

Motor torque requirement changes according to load conditions. Full-range automatic torque boost adjusts voltage of V/f pattern according to the requirement. The VS mini J7 automatically adjusts the voltage during constant-speed operation as well as during acceleration. The required torque is calculated by the inverter.

Normally, no adjustment is necessary for torque compensation gain (n63 factory setting = 1.0). When the wiring distance between the inverter and the motor is long, or when the motor generates vibration, change the torque compensation gain. In these cases, reset the V/f pattern (n09 to n15).

The set value displayed in [ ] is factory setting.

Preventing motor from stalling (Current limit)

Stall prevention (current limit) level during accel	n56
Stall prevention (current limit) level during running	n57
Stall prevention during decel	n55

Stall prevention (current limit) level during accel (n56)

Automatically adjusts the output frequency and the output current according to the load to continue operation without stalling the motor.

During acceleration if the output current exceeds 170% of the inverter rated current [the value set for n56], acceleration stops and then frequency is maintained.

When the output current goes down to 170% [the value set for n56], acceleration starts. Inverter rated current becomes 100%.

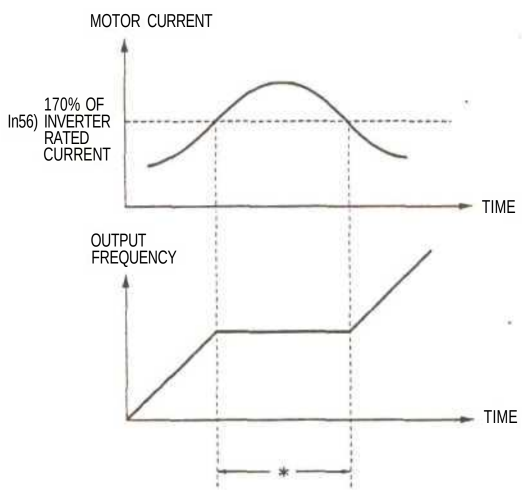

*Holds the acceleration to prevent the motor from stalling.

Factory setting of n56 = 170%
When set to 200%, this function becomes disabled.

In the constant output area [output frequency ≥ max. voltage output frequency (n11)], the stall prevention level during acceleration is automatically decreased by the following equation.

Stall prevention (current limit) level during accel in constant output area

$$= 170\% \text{ [n56 setting]} \times \frac{\text{Max. voltage output frequency (n11)}}{\text{Output frequency}}$$

Stall prevention (current limit) level during running

During agreed speed if the output current exceeds 160% of the inverter rated current [the value set for n57], deceleration starts.

When the output current exceeds 160% [the value set for n57], deceleration continues.

When the output current goes down to the value, acceleration starts, up to the set frequency.

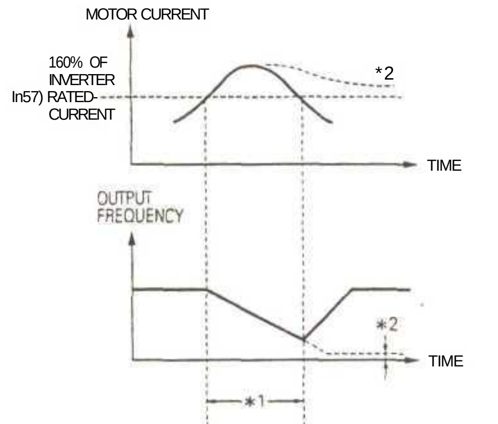

*1 Decreases frequency to prevent the motor from stalling.
*2. If the output current does not become set level or less, the operation will be held at the min. output frequency

Factory setting of n57 = 160%
When set to 200%, this function becomes disabled.

Stall prevention (current limit) during deceleration (n55)

To prevent overvoltage during deceleration, the inverter automatically extends the deceleration time according to the value of main circuit DC voltage.

Setting	Stall prevention during deceleration
0	Provided
1	Not Provided

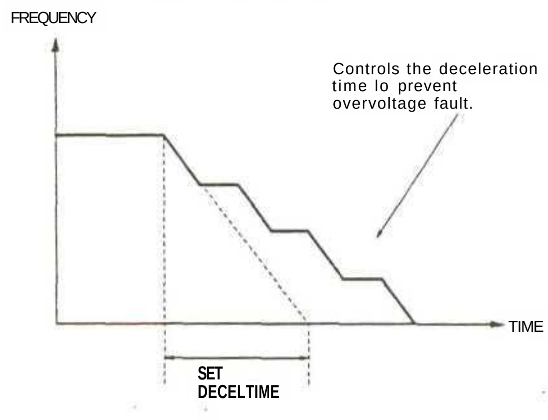

Decreasing Motor Speed Fluctuation

Slip compensation vv:;;/:

Slip compensation gain |nSS|

Motor no-load current IrtSSl

As the load becomes larger, the motor speed is reduced and motor slip value is increased when V/f control mode is selected.
The slip compensating function controls the motor speed at a constant value even if the laod varies. When inverter output current is equal to the motor rated current, compensation frequency is added to the output frequency.

$$\text{Compensation frequency} = \text{Motor rated slip value (n64)} \times \frac{\text{Output current} - \text{Motor no-load current (n65)}}{\text{Motor rated current (n32)} - \text{Motor no-load current (n65)}} \times \text{Slip compensation gain (n66)}$$

Constants

Constant No.	Function Name	Setting Unit	Setting Range	Factory Setting
n32	Motor rated current	O.IA	Oto 120% of inverter rated current	*
n64	Motor rated slip	O.lHz	0.0to20.0Hz	*
n66	Slip compensation gain	0.1	0.0 to 2.5	0.0
n65	Motor no-load current	1%	Oto 99% (100% = motor rated current n32)	*
n67	Slip compensation primary delay time	0.1s	0.0 to 25.5s When 0.0s is set. delay time becomes 2.0s	2.0s

* : Differs depending on invener capacity.

Notes : • When output frequency < min. output frequency (nl4), slip compensation is not performed.
• During regenerative operation, slip compensation is not performed.

Motor Protection

Motor overload detection

Motor rated curTent7i-v^y'^^ •.;-•!.-'. I<i5<?|

Electronic'thermal motor protection selection |r>33|

Electronic thermal motor protection time constants setting |n3*-f|

The VS mini J7 protects against motor overload with a built-in electronic thermal overload relay.

Motor rated current (electric thermal base current) (n32)
Set to the rated current value shown on the motor nameplate.

Motor overload protection selection (n33)

Setting	Electronic Thermal Characteristics
0	For standard motor
1	For invener motor
2	Electronic thermal motor protection not provided

Motor overload protection selection (n34)
The initial value is 8 min. of standard rating. Set 5-min. rating for short-term rating.
When operating with one invener connected to one motor, an external thermal relay is not required.
When operating severad motors with one inverter, install a thermal relay on each motor.

Standard motors and inverter motors
Motors are classified standard motors and inverter motors according to its cooling capabilities. Therefore, the motor overload function operates differently between motor types.

	Cooling Effect	Torque Characteristic	Electronic Thermal
Standard Motors	Since designed for operation with commercial power supply, cooling effect is lowered as speed lowered.	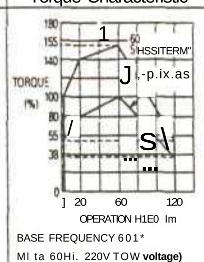 As the motor temperature rise is controlled at low-speed operation, the load should be limited.	"OL1" error (motor overload protection) occurs when continuously operated at 50/60Hz or less at 100% load.
Inverter Motors	Designed for heat-resistant in case of lowered cooling capability in low-speed range (approx. 6Hz).	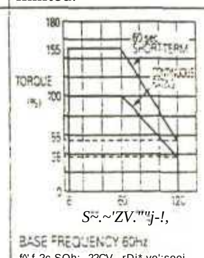 For continuous operation in low-speed range, use invclet motors.	Electric thermal overload protection not activated even when continuously operated at 50/60Hz or less at 100% load.

-&• : ON 6 : BLINKING • : OFF

Alarms and Corrective Actions

Alarm Display Digital Operator	Alarm Display RUN (Green) ALARM (Red)	Inverter Status	Explanation	Causes and Corrective Actions
i t LJLJ BLINKING	O 6	Warning Does not output fault. Automatically recover after the fault eliminated	UV (Main circuit low voltage) Main circuit DC voltage drops below the low-voltage detection level while the inverter output is OFF. Detection level 200V class: Approx. 200V or less (for single-phase, approx. 160V or less) 400V class: Approx. 400V or less Control power fault: Control power fault delected while inverter stopped.	Check the following : • Power supply voltage • Main circuit power supply wiring is connected. • Terminal screws arc securely lightened.
OLJ BLINKING			**OV (Main circuit overvoltage)** Main circuit DC voltage exceeds the overvoltage detection level while the inverter output is OFF. Detection level 200V class : Approx. 410V or more 400V class : Approx. 820V or more	Check the power supply voltage.
oH BUNKING			OH (Cooling fin overheat) Intake air temperature rises while the inverter is stopped.	Check the intake air temperature.
CAL BL1NKING			CAL (MEMOBUS in waiting) After power ON with nO2 (operation mode selection) set to 2 and n03 (frequency reference selection) to 6. normal transmission data is not received from PLC.	Check communication devices and transmission signals.
oPD			OP (Setting error) OPE D (Constant setting error when setting constants from MEMOBUS) OP1 : Same set values are input to constants n36 lo n39 for multi-function input selection. OP2 : Improper size comparison of setting for V/f constants nO9,nll,nl2andnl4 OP3 : Set value of motor rated current (n32) exceeds 150 °lc of inverter rating. OP4 : Frequency reference upper limit (n30) < Frequency reference lower limit (n31) OPS : Improper size comparison among jump frequency 1 (n49), 2 (n50) OP9 : Carrier frequency (n46) setting error	Check set value.
oL 3 BLINKING	6		OL3 (Overtorque detection) Inverter output current exceeds overtorque detection level (n60)	Decrease load, increase accel/decel time.
SE< BLINKING			SER (sequence error) Inverter received LOCAL/REMOTE selection command signal, or communication/control circuit selection command signal during operation.	Check external circuit (sequence).
fob BUNKING	6 or g 6		BB (external base blocked) Inverter stops output upon receiving an external base block signal. (Note : Resetting external base block signal restarts operation.	Check external circuit (sequence).
EF BLINKING			EF (FWD and REV command simultaneous input) FWD command and REV command from control circuit terminal are simultaneously "Closed". When command is "Closed" for 500ms and more, inverter stops operation by setting stopping method selection (nO4).	Check external circuit (sequence).
srp BLINKING			STP (Operator function stop) STOP/RESET key is pressed during running by FWD or REV command from control circuit terminal or communication. In this case, inverter stops operation by setting of stopping method selection (nO4). STP (emergency stop) At receiving emergency stop alarm signal, inverter stops operation by setting of stopping method selection (nO4).	> Open FWD or REV command from control circuit terminal. • Check external circuit (sequence)
FRr> BLINKING			FAN (Cooling **fan fault)** Cooling fan is locked.	Check the followings : • Cooling fan • Power supply connection of cooling fan
CE BLINKING			CE (MEMOBUS **communication fault)** Communication data are not received normally	Check communication devices and communication singals.

Faults and Corrective /Actions

Fault Display: Digital Operator	Fault Display: RUN (Green) ALARM (Red)	Inverter Status	Explanation	Causes and Corrective Actions
oC	• ☼	Protective Operation Output is shutt OFF and motor coasts to a stop.	**OC (overcurrent)** Invener output current **momentarily exceeds** approx. 250 % of rated current	Check the following and restart: • Short-circuit or grounding at inverter output side • Excessive load GD[2] • Extremely rapid accel/decel time (n16 to n19) • Special motor **used** • Starting motor during coasting • Motor of a capacity greater than the inverter rating has been started. • Magnetic contactor open/closed at the inverter output side
Uu2			**UV2 (control power supply fault)** Voltage fault of control power supply is detected.	Tum OFF, and ON power. If the fault remains. replace the invener.
ou			**OV (main circuit overvoltage)** Main circuit DC voltage exceeds the overvoltage detection level due to excessive regenerative energy from the motor. Detection level 200V class : approx. 410V and more 400V class : approx. 820V and more	• Insufficient decel time (constants n17 and n19) • Large minus load at lowenng (elevator, etc.) ⬇ • Increase decel time. • Connect optional braking resistor.
Uu1			**UV1 (main circuit low-voltage)** Main circuit DC voltage drops below the low-voltage detection level while inverter output is ON. Detection level 200V class : approx. 200V and less (approx. 160V and less lor single-phase) 400V class : approx. 400V and less	• Reduction of input power supply voltage • Open phase of input supply • Occurrence of momentary power loss ⬇ Check the following: • Power supply voltage • Main circuit power supply wiring is connected • Terminal screws are securely tightened.
oH			**OH (cooling fin overheat)** Temperature rise due to inverter overload operation or intake air temperature rise.	• Excessive load • Improper V/f pattern setting • Insufficient accel time if the fault occurs during acceleration • Intake air temperature exceeding 50 ℃ • Cooling fan is stopped. ⬇ Check the following: • Load size • V/f pattern setting (n09 to n15) • Intake air temperature
oL1			**OL1 (motor overload)** Motor overload protection activated by built-in electronic thermal overload relay.	• Check the load size and V/f pattern setting (n09 to n15) • Set n36 to the rated current on motor nameplate.
oL2			OL2 **(inverter overload)** Invener overload protection activated by built-in electronic thermal overload relay.	• Check the load size and V/f pattern setting (n09 to n15) * Check the invener capacity
oL3			OL3 **(overtorque detection)** When V/f mode is selected, invener output current exceeds the ovenoraue detection level (n60). If ovenorque is detected, invener operates according to the setting at n59)	Check the driven machine and correct the cause of the fault, or increase the value of n60 up to the highest allowable value for the machine.
GF			GF **(ground fault)** Invener output ground fault is dectected.	Check the connection at output side wiring and the motor.

Faults and Corrective Actions (Cont'd)

Fault Display		Inverter Status	Explanation	Causes and Corrective Actions
Digital Operator	RUN (Green) ALARM (Red)			
EFD			EFD (external fault) Received an external fault signal. EFO : External fault command from MEMOBUS EF2 : External fault input from control circuit terminal S2 EF3 : External fault input from control circuit terminal S3 EF4 : External fault input from control circuit terminal S4 EF5 : External fauli input from control circuit terminal S5	Check external circuit (sequence).
F r-tn LJLJ			**CPF-00 (CPF : control circuit fault)** Communication with digital operator is disabled even 5 sec. after power is ON.	Turn OFF power, then turn ON power again. If fault remains, replace the inverter.
LJ I		Protection Operation	**CPF-01** Communication fauli occurrs for 5 sec. or more after communication started with digital operator	Turn OFF power, then turn ON power again. If fault remains, replace the inverter.
FO'-i	● -33-	Output is shutt OFF and motor coasts to a stop.	CPF-04 EEPROM fault of inverter control circuit	• Save all the constant data, then initialize the constants (refer to page 17 for initialization of constants) • Turn OFF power, then ON again. If the fault remains, replace the inverter.
FOS			CPF-OS A/D convener fault of inverter control circuit	Turn OFF power, and ON again. If fault remains, replace the inverter.
FOS			CPF-06 • Optional card connection fault • Non-applicable option card is connected.	> Turn OFF power and properly connect the card, then tum ON power. • Check the inverter software NO (n79).
LJ I			CPF-07 Digital operator control circuit (EEPROM. A/D converter fauli	Tum OFF power once, then tum ON power again. If fault remains, replace the inverter.
CE			**CE (MEMOBUS fault)** Communication data cannot be received properly.	Check communication device and signals.
srp	O ☼ or ● -ft	Stops according to constant setting	**STP (emergency stop)** At receiving an emergency stop fault signal, **inverter stops** output by setting stopping method selection (nO4)	**Check external circuit (sequence).**
OFF	● ●	Protective Operation Output is shutt OFF and motor coasts to a stop.	• Insufficient power supply voltage • Control power supply fault • Hardware fault	Check the following: • Power supply voltage • Main circuit power supply wiring • Terminal screws are securely tightened. • External control circuit (sequence) • Replace the inverter

Noise Countermeasures

The low-noise type uses high-carrier frequency PWM control, and compared to the low-carrier type tends to suffer from increased electromagnetic interference (EMI). Following are suggestions that may be effective in reducing EMI effects in your installation:

- Lower the carrier frequency (constant n46) and the interference will be reduced.
- A line noise filter is effective in eliminating sensor malfunction or AM radio static (see page 35).
- To eliminate inductive noise from the inverter power line, separate the signal lines [recommended 30cm (11.8in), minimum 10cm (3.94in)] and use twisted-pair shielded cable.

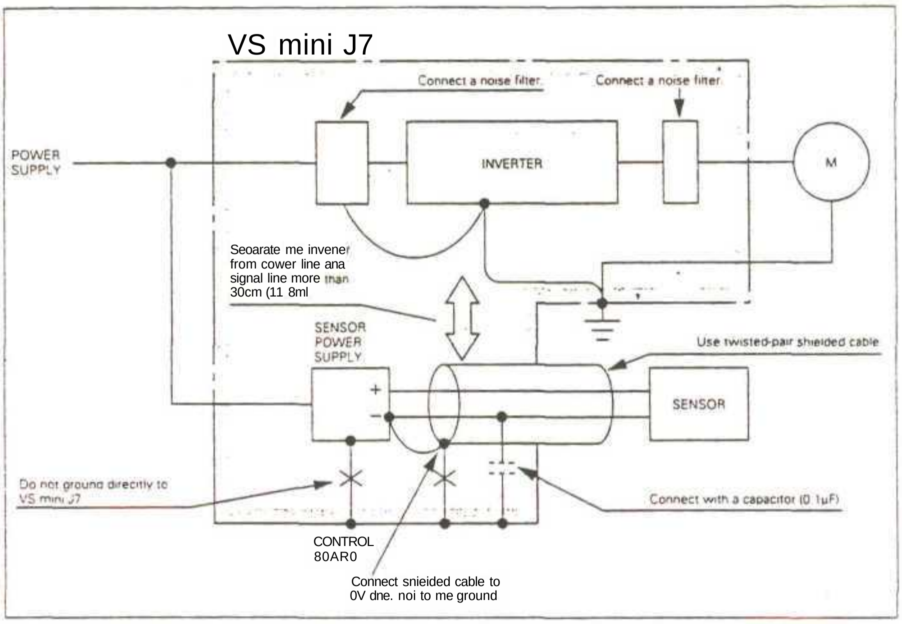

From the JEMA report

Current Leakage Countermeasures

A floating capacitance exists between the invener power line and other drive lines, and between ground (earth) and the motor. This may carry high-frequency leakage current and affect other equipment. This phenomenon varies with the carrier frequency and the wiring distance between invener and motor. The following measures may help to minimize the effects.

	Phenomenon	Countermeasures
Current Leakage to Ground (eanh)	Malfunction of ground fault interrupters and leakage relays	• Lower the carrier frequency (constant n46) • Use a ground fault interrupter resistant to high frequencies (e. g. Mitsubishi Electric NV Series)
Inter-line Leakage Current	Malfunction of external thermal overload relays due to high-frequency component of leakage current	• Lower the carrier frequency (constant n46) • Use an inverter with a built-in electronic thermal overload relay.

Wiring distance between inverter and motor, and setting of carrier frequency

Wiring Distance	Up to 50m (164.0ft)	Up to 100m (328.1ft)	More than 100m (328.1ft)
Allowable carrier frequency (Constant n46 set value)	lOkHzorless (1 to 4. 7, 8,9)	5kHz or less (1,2,7.8,9)	2.5kHz or less (1.7.8.9)

Output Noise Filter

(Tohoku Metal Industries Co., Ltd.)

Example

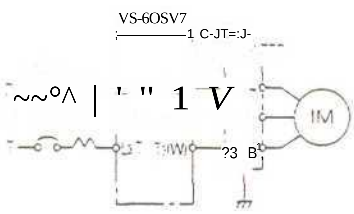

Specifications

Spec. / Voltage	Max. Applicable Motor Output kW (HP)	Inverter Capacity kVA	Model	Rated Current A	Part Code No.
200V Three-phase	ai 10.13)	C.3	LF >luK«	K'	FILdUK*'
	0.2 (0i5)	0 6	LF-.'IOk*	Id	FIL(««KXJS
	O< 10.5)	1.1	LF-'IOkA	Id	FtIKKKW*
	0.75(1)	1.9	LF-5IOK4	Id	FILI««i(>s
	1.5(2)	3.0	LF-.'IOKA	III	F1L(KXX*A
	2-2(3)	«	LF-.'Sik*	:u	F1LI«»»"
	3.7(5)	6.7	Lr.^ok^.	2ii	FILIH»I*^U
	5.5(7.51.7.5110)	9.5.13	LF-J50k».	Mi	FILIKXX170
400V class Three-phase	0.2 (0.251.0<(C.5)	0.9. Vi	LF-JIIIKE	II'	riL(««m:i
	0.75(1)	2.6	LF-.illIKB	Hi	FIL n u n 1
	1.5(2)	3.7	LF-JHIKB	II'	FILIUIDTI
	2.2(3)	Ai	LF-HOKB	Id	FILUIKI'I
	3.0(Z2).3.7(5)	5.5.7.0	LF-'IOKB	W	FIL«««)"]
	5.5(7.51.7.5(10)	11.K	LF-.-:ilkB	:0	FIL IXKIO";

Note: Contact your YASKAWA representative for single-phase, 200V class models.

Dimensions

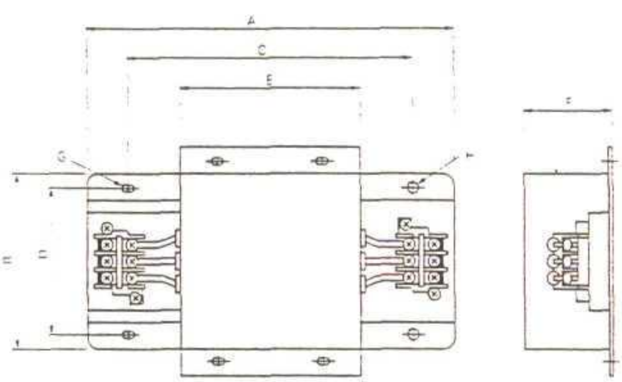

Model	Terminal Plate	A	B	C	D	E	F	G	H	Approx. Mass kg (lb)
LF-310KA	TE-K5.5M4	[illegible]	[illegible]	[illegible]	[illegible]	[illegible]	[illegible]	[illegible]	[illegible]	[illegible]
LF-320KA	TE-K5.5M4	[illegible]	[illegible]	[illegible]	[illegible]	[illegible]	[illegible]	[illegible]	[illegible]	[illegible]
LF-350KA	TE-KZ2M5	[illegible]	[illegible]	[illegible]	[illegible]	[illegible]	[illegible]	[illegible]	[illegible]	[illegible]
LF-310KB	TE-K5.5M4	[illegible]	[illegible]	[illegible]	[illegible]	[illegible]	[illegible]	[illegible]	[illegible]	[illegible]
LF-320KB	TE-K5.5M4	[illegible]	[illegible]	[illegible]	[illegible]	[illegible]	[illegible]	[illegible]	[illegible]	[illegible]

Digital Operator for Remote Operation (MODEL JVOP-146)

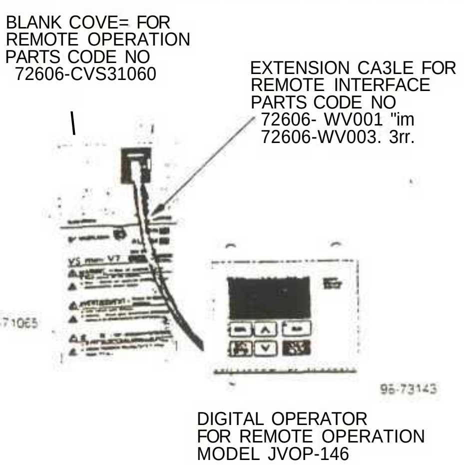

Dimensions in mm (inches)

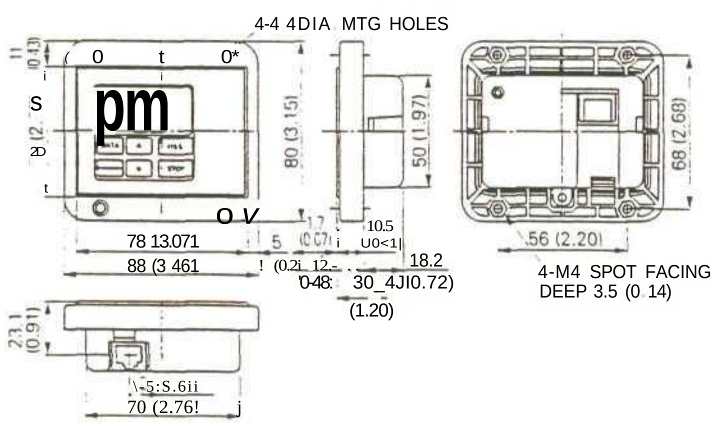

Note: Order digital operator, cable, and blank cover separately.

SI-N Communication Interface Unit

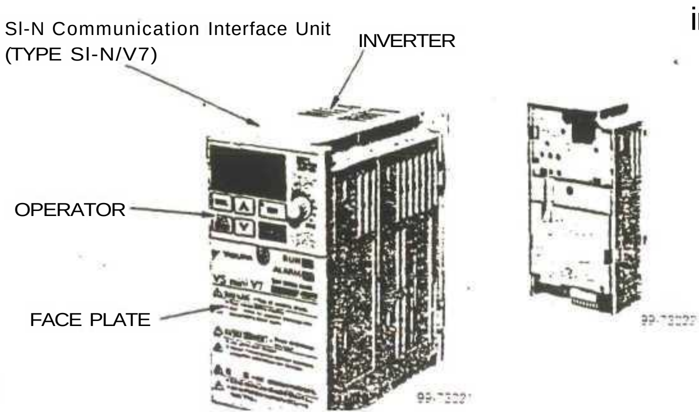

Dimensions in mm (inches)

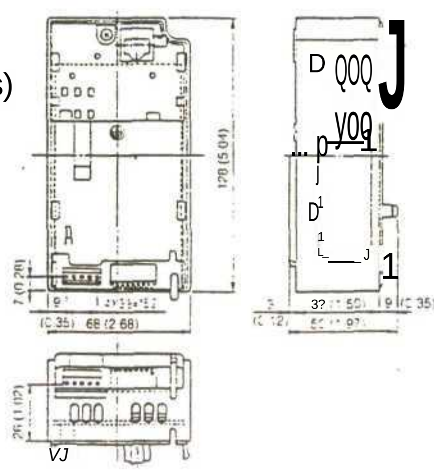

■ Wiring the Main Circuit

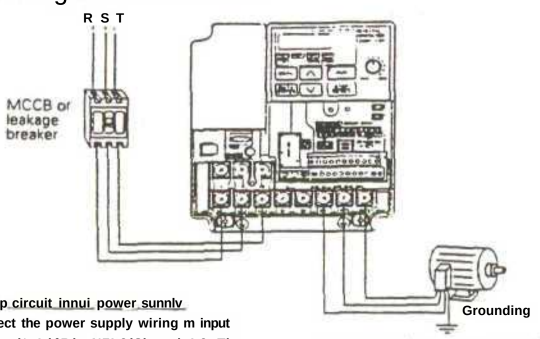

• **Mgip circuit innui power sunnlv**
Connect the power supply wiring m input terminal* LlfRl. N7L2(S) and L3<T) |L1(R). N7L2(S) for single-phase specifications}. Never connect them 10 VfT\,V/T2.W/T3. B I. B2. -. +1. or +2. Otherwise Ihe invener may be damaged. Stngle-pha« f2OOV class. OJ.Hw or less) tnvencr can connect lermiruil TVUV Never use the terminal v. iih other purposes.
(mp Single-phase (200V class. 0.75kW or less) in verier can connect terminal T/L.V Never use Ihe terminal with other purposes.

*** Grounding (Use groundtcrroinal © .)**
Make sun: to ground the ground terminal © according to the local grounding code- Never ground ihe VS mini in common with welding machine*, motors, or other electrical equipment.
When several VS mini units are used side by side, ground each unit as shown in examples Do not loop the ground wires.

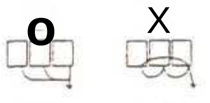

• **Braking re si si or connection (optional)**
To connect the braking resistor, cui the protector on terminals B1 and B2.
To protect the braking resistor from overheating, install a thermal overload relay between the braking resistor and the tnvener This provides a sequence which shuts off the power supply, by a thermal relay trip contact.
Ilse this same procedure when connecting a braking resistor unit.

• **Invener nuip**[ul]
Connect the motor terminals to U. V, W.

Wirmp the main circuit terminals
Pass the cables through wiring hole and connect. Be sure to mount the cover in unoriginal position.

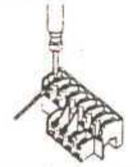

Connect with a Phitltps (plus) screwdriver.

• Wiring the Control Circuit

Only basic insulation is provided Tor the control circuit terminals. Additional insulation may be necessary in the end product.

• Control Circuit terminals

Pass the cable through wiring hole and connect. Be sure to mount the cover in its original position.

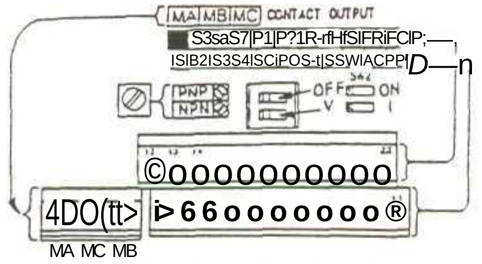

• SWI can be changed according to input signal polarity.
OV common: NPN side
24 common: PNP side
Refer to page 65 for SW2.

Wiring the control circuit terminals

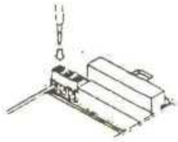

Screwdriver blade width

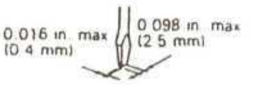

Insert the wire into the lower pun of ihe terminal block and connect it lighily wilh ;i screwdriver.

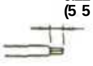

Wire sheath strip length inusi be ().22in. (5.5mm).

Open the front cover and verify thai the strip length is 0.22in. (5.5mm).

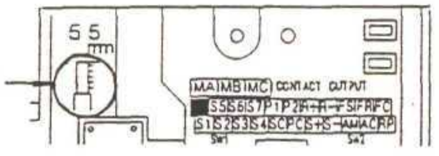

• Wiring Inspection

After completing wiring, check Ihe following :

D Wiring is proper.

• Wire clippings or screws are not left in Ihe unit.

D Screws are securely lightened.

D Bare wire in ihe terminal does not contact other terminals.

NOTE

If the FWD (REV) run command is given during the operation reference selection (n003=l) from ihe control circuit terminal, the motor will stan automatically after the main circuit input power supply is turned ON.

• Simple Data Setting

Volume setting (Refer to 5. OPERATING THE INVERTER) and digital setting are both available for simple accel/decel operation of the VS mini. Frequency setting volume is set with initial setting (n0O4=O)

Following is an example in which the function LED's are used to set frequency reference, acceleration time, deceleration time, and motor direction.

Operaoon Steps	Operator Display	LED Display	Status Indicator LED
1. Turn ON trie power suppry.	0.00	FREF	RUN ALARM
2. Set consort n004 ID 1.	1	PRGM	RUN ALARM
3. Set the Mowing constants. nO19:15.0 (acceleration wne) nO20 :5.0 (deceteraoon time)	15.0 5.0	PRGM	RUN ALARM
4. Select forward or reverse run by pressing [M X Q Key. NOTE Examne tie application. (Never Htad REW when reverse lun is prchbned.)	For- (Forward) or rEu (Reverse)	F/R	RUN ALARM
5. Sei the referent* by pressing [Tjtx [» Key	6000	FREF	RUN ALARM
6. Press fHUNI	0.00-60.00	FOUT	RUN ALARM
7. Press STOP to stop.	60.00-*0.00	FOUT	RUN ALARM

■ Using V/f Mode

| Adjusting torque according to application |

Adjust moior torque by using "V/f pattern" and "full-range automatic torque boost".

• V/f pattern setting

Set V/f pattern by nOl I to nO17 as described below. Set each pattern when using a special motor (high-speed motor, etc.) or when requiring special torque adjustment of machine.

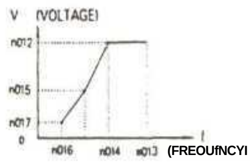

Be sure lo satisfy the following conditions for the setting of nOl I to n017.

nOl6£nOl4<nO13£nOll

If nOl6 = nOl4 is set. the set value of n015 is disabled.

Constants No.	Name	Unit	Setting range	Initial Setting
nOU	Mai. outom keqmncy	0.1 H2	50.0 to 400.0HZ	60.0Hz
n012	Max. vonapi	IV	1 tO i!bi CV (O 1 lo 510 OV)	zoo uv HOO OV)
not 3	Max vollaoB output trcouOTcv »»•*• tieguartcy)	0.1 Hz	0.2 to 400.0HZ	60 0H2
nO14	Md. outoul fcvQuency	0.1Hz	0 1 to 399 9Hz	1 5Hz
n015	M«. 0UCU1 lreouancy weape	IV	0.1 to 255.0V (0 1 to 510.0V)	12.0V (24.0V)
nO16	Mm. output beouency	0.1H2	0.1 to 10.0HZ	1.5Hz
nO17	Mm. output trsouancrvMaoe	1V	1 to 50.0V (0.1 to 100.0V)	12.0V (24.0V)

• Typical setting of V/f pattern

Set the V/f pattern according to the application as described below. For 400V class, the voltage values (nOl2, nOl5. and n0l7) should be doubled. When running at a frequency exceeding 50Hz/6OHz, change the maximum output frequency (nOl I).

Note :Be sure lo set the maximum output frequency according lo the motor characteristics.

(I) For general-purpose applications

Motor Specification : 60Hz (Factory setting)

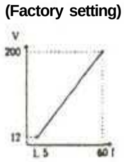

Constant	Setiina
non	60.0
nO12	200.0
nO13	60.0
nO14	1.5
nO15	12.0
nO16	1.5
nO17	12,0

Motor Specification : 50Hz

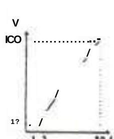

Ccneaan	Semno
nOU	50.0
nO12	2000
nO13	50 0
n0i4	1.3
n0i5	120
nO16	1.3
nO17	12 0

02) For fans/pumps

Motor Specification : 60Hz

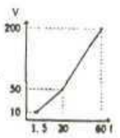

COTKWI	Setima
n011	60.0
n012	200.0
n013	60.0
nOK	30.0
n015	50.0
nO16	1.5
n017	10.0

Motor Specification :50H2

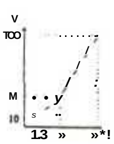

C^nsart	Senina
nO11	50,0
nO12	200.0
nO13	50.0
nOH	25.0
nO15	50 0
nO16	1.3
P017	10.0

(3) For applications requiring high starting torque

Motor Specification : 60Hz

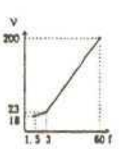

Constant	Setltna
non	60.0
P012	200.0
n013	60 0
nOK	3.0
n015	23.0
n016	1.5
"PI?	16.0

Motor Specification : 50Hz

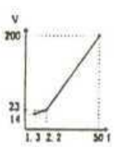

Constart	S>t1tno
nOjl	50.0
nO12	200.0
nO13	50.0
nOK	2.2
nO15	23.0
nOl£	1.3
nO17	14.0

Increasing voltage of V/f pattern increases motor torque, but an excessive increase may cause motor overexcilation. motor overheat or vibration.

Note : n012 is to he set to motor rated voltage.

• Full-range auiom.ilic torque boost (only when V/f mode is selected. n002=0)

Motor torque requirement changes according to load conditions. Full-range automatic lorquc boost adjusts voltage of V/f pattern according to the requirement. The VS mini automatically adjusts the voltage during constant-speed operation as well as during acceleration.

The required lorquc is calculated by the inverter.

This ensures lriplcss operation and energy-saving effects.

IQuiput voltagctct [Automatic torque boost gain (n!03)| x [Required iorquc|

• Operation

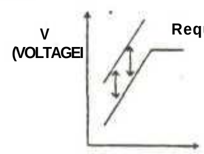

Normally, no adjustment is necessary for automatic torque boost gain (n!03 factory selling: 1.0). When the wiring distance between the inverter and the motor is long, or when the motor generates vibration, change the automatic torque boost gam. In Ihese cases, set the V/f pattern (nOl I to n()!7).

Adjusting frequency upper and lower limits

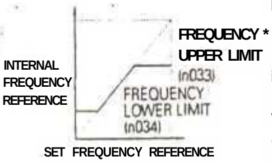

• **Frequency reference upper limit (nO33)**
Sets the upper limit of the frequency reference in units of 1%.
(nOI l: Maximum output frequency = 100%)
Factory setting: 100%

• **Frequency reference lower limit (nO34)**
Sets Ihe lower limit of ihe frequency reference in units of 1%.
(nOI 1: Maximum output frequency = 100%)
When operating at frequency reference 0, operation is continued at the frequency reference lower limit.
However, when frequency reference lower limit is set to less than the minimum output frequency (nO16), operation is not performed.
Factory setting: 0%

Using two accel/decel limes

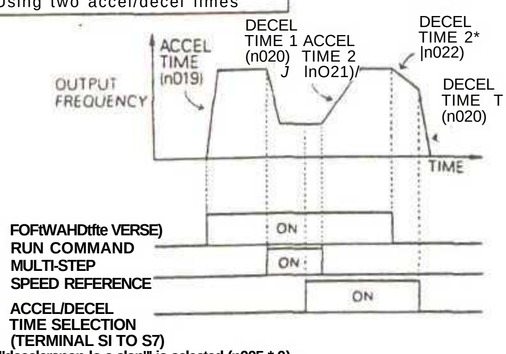

• When "dccclcranon lo a slop'" is selected (n005 * 0).

By setting input terminal function selection (either of n050 to nO56) to "I I (accel/decel lime select)", accel/decel lime is selected by turning ON/OFF the aceel/dcccl lime sclcci (terminal SI lo ST).

At OFF : nOI9(accel lime I)
n020(deccl lime I)
AION : nU2I (acccl lime 2)
nO22 (deed lime 2)

No.	Name	Unit	Setting range	Initial setting
nO19	Accel time 1	Refer to n0t8 setting	Reler to n018 setting	10 0s
n020	Decel time 1			100s
nO21	Accel lime 2			10 0s
nO22	Decel lime 2			10.0s

nOI8 selling

No.		Unit	Setting range
nO18	0	0.1 sec.	0.0-999.9sec. (lOOOsec. or less) 1000-6000sec (1000sec. or more)
	1	0.01 sec	0.00-99.99sec (lOOsec. o' less) 100.0-600.Osec (lOOsec. or more)

. Constant nOI8 can be set during stop.
. If the numeric value exceeded 600.0 sec. is set for ihc accel/decel time when n018 = 0(in units of 0.1 sec), "I"cannot be sel tonOIR.

• Accel time
Set the time needed for output frequency to reach 100% from *0%.*

• Decel time
Set the lime needed for output frequency lo reach 0% from 100%.

Automatic restart after momentary power loss (nO81)

When momentary power loss occurs, operation restarts automatically.

Setting	DescrtDtion
0	Continuous operation alter momentary power loss not provided.
!•	Continuous operation after power recovery within momentary power loss ndethru time
2*t	Continuous operation attei power recovery (Fault output not provided)

• Hold Ihe operation command lo continue the opcrnutHi after recovery from a momentary power loss,
t When *2* is selected, operation restarts il no»er supply voltape reaches us normal level. No fault sipnal is oulpul.

Terminal lunction at 3-wire sequence selection

When 0 is set at the terminal S3 (n()5l). icmiin.il SI becomes run command, terminal S2 becomes stop command, and terminal S3 becomes FWD/REV run command.

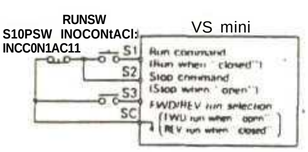

• LOCAL/REMOTE select (selling: 17)
. Selecis operation reference by the digital operator or by the multi-function input terminal.
. LOCAL/REMOTE select is available only during stop.
Open : Run according lo the selling of run command selection (n(J03) or frequency reference selection (n004).
Closed : Run by frequency reference and run command from Ihe digital operator.
^Frequency reference changes according to the selling of nOO8 (local mode).
(Example) Set nO03 = 1, n004 = 2, nO08 = 0.
Open : Run by frequency reference from multi-function input terminal FR and run command from multi-function input terminals SI to S7.
Closed : Run by volume frequency reference and run command from ihe digital operator.

.^UP/DOWN command (setting: nO56 = 034)
With the FWD (REV) run command entered, accel/decel is enabled by inputting the UP or DOWN signals to multi-function input terminals S6 and S7 without changing the frequency reference, so that operation can be performed at the desired speed. When UP/DOWN commands are perilled by nO56. any function set lo nO55 becomes disabled: terminal S6 becomes an input terminal for the UP command and terminal S7 for the DOWN command.

Multi-lunciion Input Terminal 86 (UP command)	Closed	Open	Open	Closed
Multifunction Input Terminal 87 (DOWN command)	Open	Closed	Open	Closed
Operation Status	Accel	Decel	Hold	Hold

Reducing motor noise or leakage current (n080)

Set inverter output transistor switching frequency (carrier frequency).

Setting	Catner Frequency (kHz)	Metallic Noise from Motor	Noise and Current Leakaae
7	12 tout	Higher	Smaller
8	21 foul		
9	36 lout		
1	25		
2	5.0	Not audible	
3	7.5		Larger
4	10.0		

Setting values 7. 8. or 9 multiplies ouipul frequency according to output frequency value.

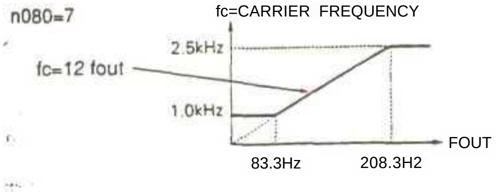

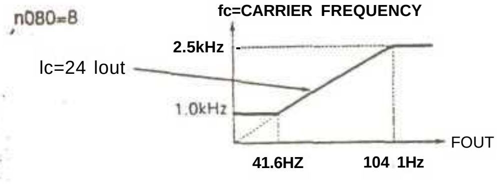

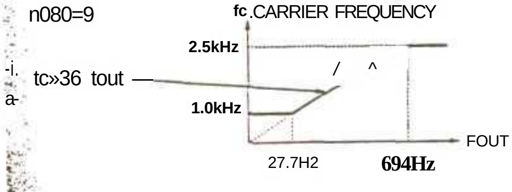

■ Selecting Stopping Method

Selecting slopping method (nOO5)

Selects the slopping method suitable for application.

Setling	Description
0	Deceleration to stop
1	Coast to stop

• Deceleration to slop
Example when accel/decel lime 1 is selected

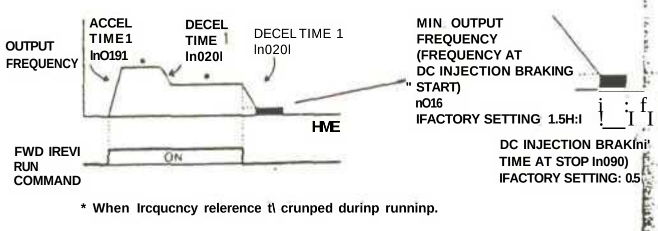

* When Ircqucncy relerence t\ crunped durinp runninp.

Upon removal of the FWD (REV) run command, the motor decelerates it the decel role determined by the time set 10 dcccl time I (nO2O) and DC injection braking is applied immediately before stop. If the decel time is shori or the load inertia is large, overvoltage (OV) fault may occur at deceleration. In this case, increase the decel time or install a optional braking resistor.

Braking torque : Without braking resistor: Approx. 20% torque of motor rating
With braking resisior: Approx. 150% torque of motor rating

• Coast to slop
Example when acccl/dccel lime I is selected

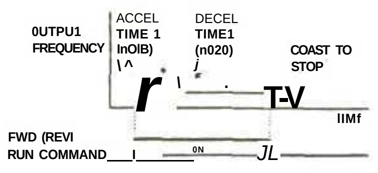

• When frequency relerence is chanped during running.

Upon removal of the FWD (REV) run command, the motor starts coasting.

Applying DC injection braking

• DC injection braking current (nO89)
Sets DC injection braking current in units of I %. (Invener rated currcnt=IOO%)

• DC injection braking time al stop (n090)
Sets the DC injection braking time at stopping in units of 0.1 second. When the setting of n()90 is 0, DC injection braking is nol performed btil invener output is shut OFF at the timing of DC injection braking slarl.

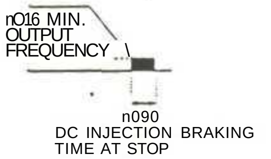

When coasting to a stop is specified in stopping method selection (n(X)5), DC injection braking at stop does not operate.

Inverter Constant Value Settings

[illegible]	4	[illegible]	0	[illegible]	2	[illegible]	0.1	[illegible]	-	[illegible]	0	[illegible]	0	[illegible]	rdy
[illegible]	0	[illegible]	0	[illegible]	3	[illegible]	0	[illegible]	-	[illegible]	0	[illegible]	0	[illegible]	0
[illegible]	1	[illegible]	0	[illegible]	5	[illegible]	0	[illegible]	1	[illegible]	0	[illegible]	0	[illegible]	1.oL1
[illegible]	2	[illegible]	0	[illegible]	6	[illegible]	10	[illegible]	0.3	[illegible]	1	[illegible]	2	[illegible]	0021
[illegible]	0	[illegible]	0	[illegible]	7	[illegible]	4	[illegible]	6.5	[illegible]	1	[illegible]	0		
[illegible]	0	[illegible]	0	[illegible]	10	[illegible]	0	[illegible]	2.5	[illegible]	1	[illegible]	10		
[illegible]	0	[illegible]	0	[illegible]	0	[illegible]	0	[illegible]	2.575	[illegible]	0	[illegible]	0		
[illegible]	1	[illegible]	100	[illegible]	1	[illegible]	0	[illegible]	19.07	[illegible]	0	[illegible]	3		
[illegible]	0	[illegible]	0	[illegible]	2	[illegible]	0	[illegible]	150	[illegible]	100	[illegible]	120		
[illegible]	D	[illegible]	0	[illegible]	10	[illegible]	0	[illegible]	55	[illegible]	0	[illegible]	16		
[illegible]	50	[illegible]	1	[illegible]	0	[illegible]	0	[illegible]	0	[illegible]	0	[illegible]	10		
[illegible]	220	[illegible]	0	[illegible]	0.1	[illegible]	-	[illegible]	0	[illegible]	0	[illegible]	5		
[illegible]	50	[illegible]	8	[illegible]	-	[illegible]	-	[illegible]	0	[illegible]	1	[illegible]	1		
[illegible]	1 3	[illegible]	0	[illegible]	-	[illegible]	50	[illegible]	0	[illegible]	0	[illegible]	0		
[illegible]	12	[illegible]	.	[illegible]	0	[illegible]	0.5	[illegible]	0	[illegible]	223.7	[illegible]	-		
[illegible]	1 5	[illegible]	-	[illegible]	0	[illegible]	0	[illegible]	0	[illegible]	50	[illegible]	-		
[illegible]	12	[illegible]	-	[illegible]	1	[illegible]	0	[illegible]	-	[illegible]	12	[illegible]	-		
[illegible]	0	[illegible]	-	[illegible]	100	[illegible]	170	[illegible]	-	[illegible]	1	[illegible]	-		
[illegible]	5	[illegible]	-	[illegible]	0	[illegible]	160	[illegible]	-	[illegible]	0	[illegible]	-		
[illegible]	0.5	[illegible]	-	[illegible]	0.1	[illegible]	0	[illegible]	0	[illegible]	0.5	[illegible]	-		
[illegible]	10	[illegible]	-	[illegible]	100	[illegible]	0	[illegible]		[illegible]	0.2	[illegible]	-		
[illegible]	10	[illegible]	-	[illegible]	0	[illegible]	0	[illegible]	0	[illegible]	-	[illegible]	-		
[illegible]	0	[illegible]	-	[illegible]	0.1	[illegible]	160	[illegible]	0	[illegible]	-	[illegible]	-		
[illegible]	9	[illegible]	-	[illegible]	100	[illegible]	0.1	[illegible]	0	[illegible]	2500	[illegible]	-		
[illegible]	0	[illegible]	1	[illegible]	0	[illegible]	0	[illegible]	0	[illegible]	0	[illegible]	0		

Table G1: Inverter Constant Settings.

APPENDIX H

PC30GADATA
A CQUISITION BOARD

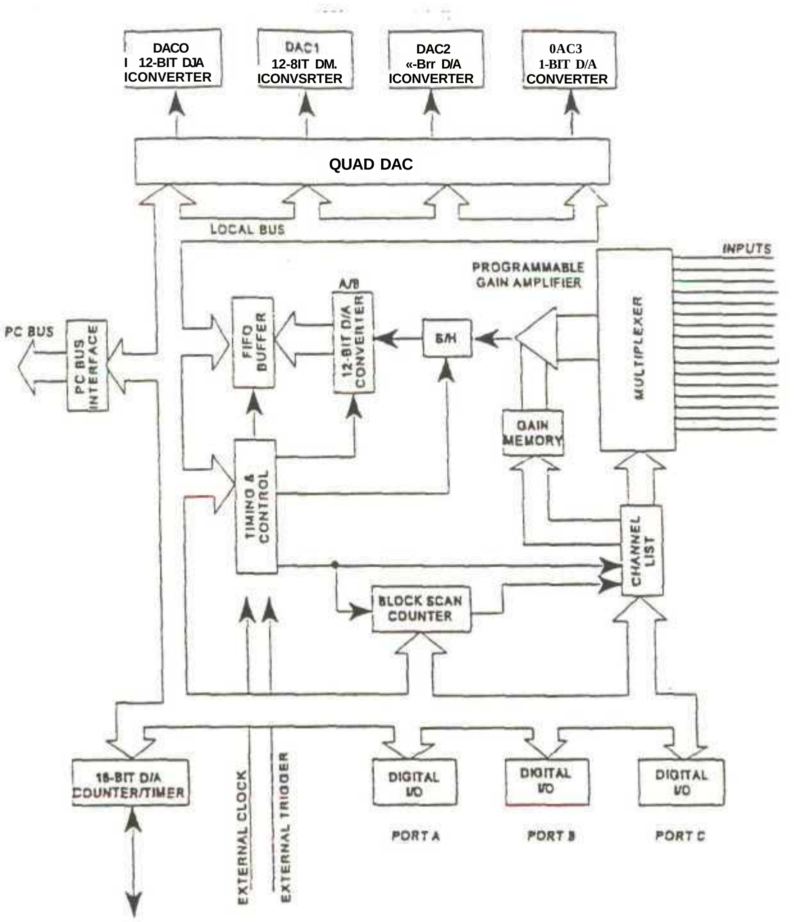

Figure 2-1. PC30 Board Block Diagram

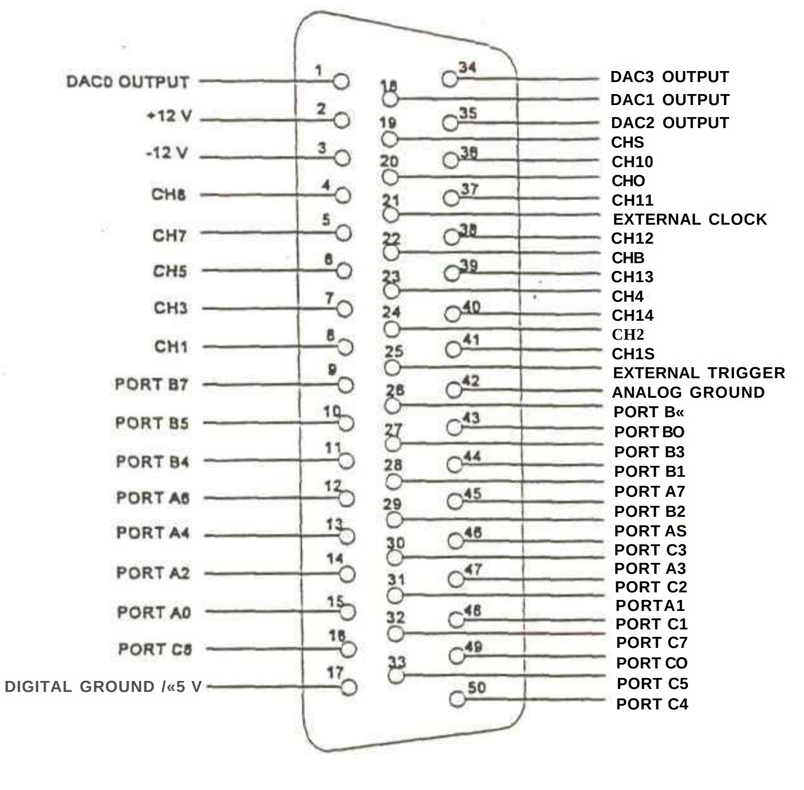

Figure 4-1. PC30 Connector (as seen from the rear of the PQ

Signal Definitions

a. CHO - **CH15.** These are the analog input lines. Note that no more than ±10V must be applied to these pins. In differential mode, channel 8 serves as the return line for input channel 0, channel 9 as that for input channel 1 etc.

b. **ANALOG GROUND.** One analog ground line is provided. The analog input lines are measured relative to AGND.

c. DACO OUTPUT. This is the analog output line for DACO.

d. D AC1 OUTPUT. This is the analog output line for DAC1.

e. **DAC2** OUTPUT. This is the analog output line for DAC2.

f. DAC3 OUTPUT. This is the analog output line for DAC3.

g. +12V. This line provides a +12V power supply to the user's interface. Maximum permissible current draw is 125 mA.

h. -12V. This line provides a -12V power supply to the user's interface. Maximum permissible current draw is 125 mA.

i. **Digital Ground/** +5V. This line is jumper selectable to provide either a digital ground connection, or a source of+5V (+125 mA) power. Digital ground is the ground return line for the digital inputs and outputs. Any digital circuitry tied to the digital lines should be referenced to these lines. It is internally connected to analog ground.

j. **Port** A0 - A7. This is the first digital I/O port, digital I/O port 0. It is configurable into a number of operating modes under software control.

k. **Port** BO - B7. Digital 170 port 1. It is configurable into a number of operating modes under software control.

1. **Port CO** - C7. Digital I/O port 2. It is configurable into a number of • operating modes under software control.

m. **External Trigger.** This line is jumper selectable **to** provide either a clock or trigger signal to the A/D, and may be read under software control. It is TTL compatible. This line can also be configured as an output to synchronize boards in master/slave modes.

n. **External Clock.** This line interfaces to the uncommitted counter/timer, and can be jumpered to perform a variety of functions, as described in the previous chapter. It may be configured either as an input or output and is also TTL compatible.

1 Tablet	Analos Inputs
]dumber of Channels	16 single-ended or 8 differential (software selectable)
]dumber of Channels with simultaneous sample/hold	16 single ended only
Resolution	12-bits(lin4096)
Total System Accuracy (absolute accuracy)	± 1 bit LSB (for Gain of 1)
Linearity: Integral Differential	±0.05% FS i3/. LSB max.
A/D Input Voltage - Ranges	±5V, ±10V, 0 to 10V (PC30G, PC30GA) ±5V, ±10V (PC30F, PC30FA) ±5V (PC30GAS4.PC30GAS16, PC30FAS4.PC30FAS16)
Data Acquisition Rate	PC30G: 100kHz, PC30F: 330kHz (G<1000) PC30G: 100kHz, PC30F: 100kHz (G=1000)
Input Impedance: 1 On Channel 1 Off Channel	 10M/20pF lOM/lOOpF
Offset Voltage Input Bias Current Input Bias Offset Drift	±5 LSB adjustable to 0 il00pA/°C ±30ppm/°C
Input Gains: Ranges Gain Error Gain Accuracy CMRR for various gains Monotonicity	 1,10,100, 1000 or 1, 2,4, 8 (SAV selectable) Adjustable to 0 0.25% max, 0.05% typical for gains < 1000 l%max,0.1%forg=1000 0to70°C
Temperature Drift: Full Scale Error Drift Bipolar Zero Drift Gain	 6 ppm/°C (PC30Fx) 1 ppm/°C (PC30Fx) ±30 ppm/°C
Input Over voltage Protection	±12V
A/D FIFO Buffer Size	16 samples
Channel Gain/Queue Length	31
A/D Clock: Internal Clock Clock frequency tolerance Clock Drift Internal Clock Divider External Clock External Trigger Channel List (queue) Length Block Scan Mode	 2 MHz or 8 MHz (software selectable) 0.01% 10 ppm/°C 2x 16 bit stages TIL compatible TTL compatible 31 Up to 256 channels per block; all channels converted at max. thruput on each clock pulse
Noise Levels (p-p)	G=l: ±1 bit; G=10: ±1 bit; G=100: ±2 bits Noise levels will vary according to environmental conditions
Data Acquisition Modes	Polled I/O, Interrupts, Single and Dual Channel DMA

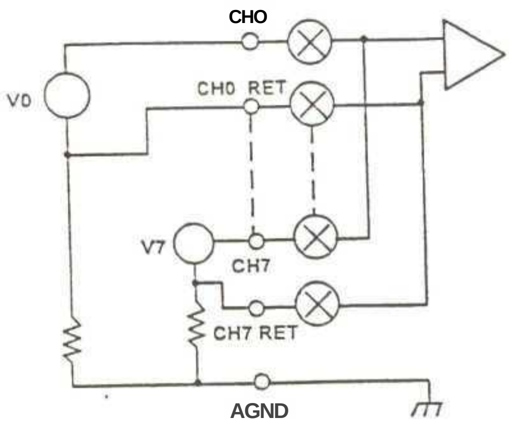

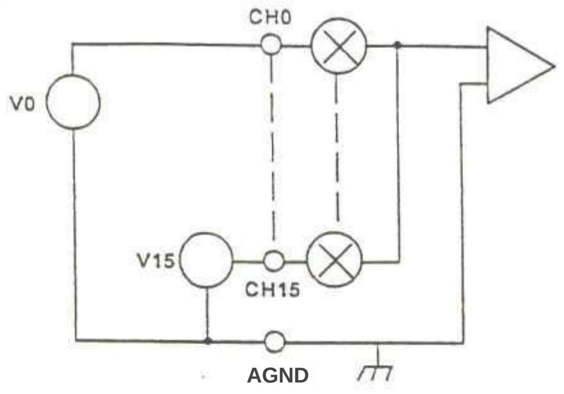

Figure 4-2. Single Ended Analog Inputs

Figure 4-3. Differential Analog Inputs

Table 2	Analog Outputs
Number of channels	4
Resolution	Two 12-bit, two 8-bit
Accuracy	±1 LSB (12-bit), 0 LSB (8-bit)
Differential Nonlinearity	±1 LSB max.
Output Ranges	±5V, ±10V, 0 to 13 V (software selecuble)
Offset Error	Unipolar: *VA* LSB typical, 1 LSB max. (12 bit) Bipolar: ^{X}A LSB typical, 2 LSB max. (12 bit)
Gain: Ranges Error	xl, x2 2 LSB typical, 5 LSB (12 bit)
Settling time to ^{l}A LSB	1 0 ^ max. in a Load of 500 p, 2 kQ
Throughput Rate	500 kHz (depending on computer)
Temperature Drift	100 ppm/°C of full scale
Max. Current Output Source	5 mA maximum
Monotonicity	0to70°C

Table 3	Digital I/O
Number of I/O Lines	24 in 3 ports (8255 PPI)
Voltage Compatibility	TTL
Interface Selection	Programmable for simple I/O, strobed I/O or handshake I/O.
Max. Input Voltage	5.5V
Max. Current Source/Sink	ilmA

Table 4	Timer/Counter Specifications
Resolution	16 bits
Voltage Compatibility	TTL
Number of Counters	3 (2 used for A/D timing)

Table 5	PC Interface
Base Address	0 - 1FFF DIP Switch selectable
Number of Registers	32 8 bit registers
Interrupts	Register selectable for end of conversion, DMA block or timer
DMA	Dual channel jumper selectable to levels 5, 6 or 7
I/O Connector	50-way female D-tvue (same as PC30 series')

Table 6	Environmental Specifications
Operating Temperature	0to70°C
Storage Temperature	-55tol50°C
Relative Humidity	5% to 95% noncondensinp

Table 7	Power Requirements
+5 V	500 mAtyp.
+12 V	100 mAtyp.
-12 V	100 mAtyp.

Table 8	Physical
Dimensions	193 mm long, 111 mm high (excluding gold edger connector, DB50 connector and bracket)

Table 9 Software Support
Register compatible with older PC30 series boards
Supported by EDR Software Development Kit
DOS language support
Windows 3.1 language support (DLL)
Win 95 language support
Labview, LabWindows/Labtech Notebook drivers available
Visual Basic Custom Controls available
DASYLab support
Test Point support

EAGLE TECHNOLOGY TITLE: PC 30F/G A/0 D/A BOARD	DOC NO: PC3OF/G REV1C FLENAME: 30F8A.PCB DATE 15/1/96	DESIGNER: SHAFIQUE ALLE

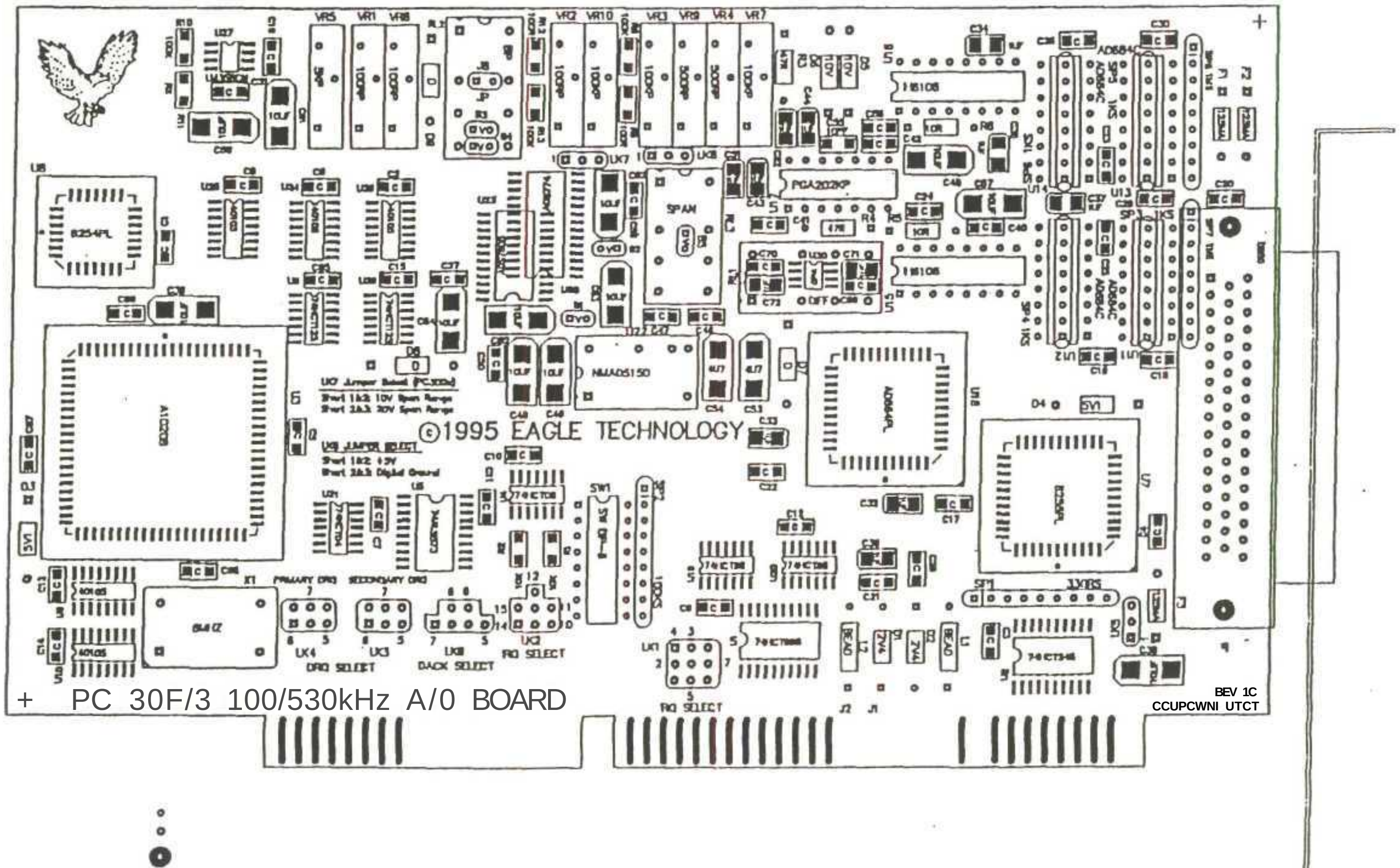

APPENDIX I

CLSMMHS WIRING DIA GRAMS

PC30GA Data Transfer Cable:

50 Pin D-Type Male Connector

PC30GA	Description	Pin No	Cable Colour
DACO	Analogue output	1	Red
+12V	DC Supply	2	Blue
-12 V	DC Supply	3	Green
CH8	Analogue input	4	Yellow
CH7	Analogue input	5	White
CH5	Analogue input	6	Black
CH3	Analogue input	7	Brown
CH1	Analogue input	8	Purple
B7	Digital I/O	9	Orange
B5	Digital I/O	10	Pink
B4	Digital I/O	11	Turquoise
A6	Digital I/O	12	Grey
A4	Digital I/O	13	Red/Blue
A2	Digital I/O	14	Red/Green
AO	Digital I/O	15	Yellow/Red
C6	Digital I/O	16	White/Red
D-Gnd	Digital GND	17	red/Black
Dad	Analogue output	18	Red/Brown
CH9	Analogue input	19	Yellow/Blue
CHO	Analogue input	20	White/Blue
CLK	External Clock	21	Blue/Black
CH6	Analogue input	22	Orange/Blue
CH4	Analogue input	23	Green/Blue
CH2	Analogue input	24	Grey/Blue
TRG	External trigger	25	Yellow/Green
B6	Digital I/O	26	Red
B3	Digital I/O	27	Blue
A7	Digital I/O	28	Green
A5	Digital I/O	29	Yellow
A3	Digital I/O	30	White
A1	Digital I/O	31	Black
C7	Digital I/O	32	Brown
C5	Digital I/O	33	Purple
DAC3	Analogue output	34	Orange
DAC2	Analogue output	35	Pink
CH10	Analogue input	36	Turquoise
CH11	Analogue input	37	Grey
CH12	Analogue input	38	Red/Blue
CH13	Analogue input	39	Red/Green
CH14	Analogue input	40	Yellow/Red
CH15	Analogue input	41	White/Red
A-Gnd	Analogue Ground	42	red/Black
BO	Digital I/O	43	Red/Brown
B1	Digital I/O	44	Yellow/Blue
B2	Digital I/O	45	White/Blue
C3	Digital I/O	46	Blue/Black
C2	Digital I/O	47	Orange/Blue
C1	Digital I/O	48	Green/Blue
CO	Digital I/O	49	Grey/Blue
C4	Digital I/O	50	Yellow/Green

PC30GA CARD -Plant Wiring Configuration

Pin No.	Name	Plant Interface	Colour
20	CHO	Ultrasonic Sensor Output (0-1 OV)	Black
8	CH1	Spare -	—
24	CH2	Spare -	-
7	CH3	Spare -	-
23	CH4	Spare -	-
6	CH5	Spare -	-
22	CH6	Spare -	-
5	CH7	Spare -	-
4	CH8	Spare -	-
19	CH9	Spare -	-
36	CH10	Spare -	-
37	CH11	Spare -	**
38	CH12	Spare -	-
39	CH13	Spare -	-
40	CH14	Spare -	-
41	CH15	Spare -	-
1	DACO	Frequency Reference (0-1 OV)	Purple
18	DAC1	Run/Forward Relay	White
35	DAC2	Spare -	-
34	DAC3	Run/Reverse Relay	Green
2	+12V	Spare -	-
3	-12 V	Spare -	-
42	Analogue GND		Black
21	External Clock	Spare -	-
25	External trigger	Spare -	-
15	AO	Spare -	-
31	A1	Spare -	-
14	A2	Spare -	-
30	A3	Spare -	-
13	A4	Spare -	-
29	A5	Spare -	-
12	A6	Spare -	-
28	A7	Spare -	-
43	BO	Spare -	-
44	B1	Spare -	-
45	B2	Spare -	-
27	B3	Spare -	-
11	B4	Spare -	-
10	B5	Spare -	-
26	B6	Spare -	-
9	B7	Spare -	-
49	CO	Air Bearing Relayi	White
48	C1	Air Bearing Relay2	Green
47	C2	Air Bearing Retay3	Yellow
46	C3	Air Bearing Relay4	Grey
50	C4	Air Bearing Retay5	Pink
33	C5	Air Bearing Relay6	Blue
16	C6	Air Bearing Relay7	Red
32	C7	Air Bearing Relay8	Turquoise
17	Digital GND		Black

Wiring Distribution Board

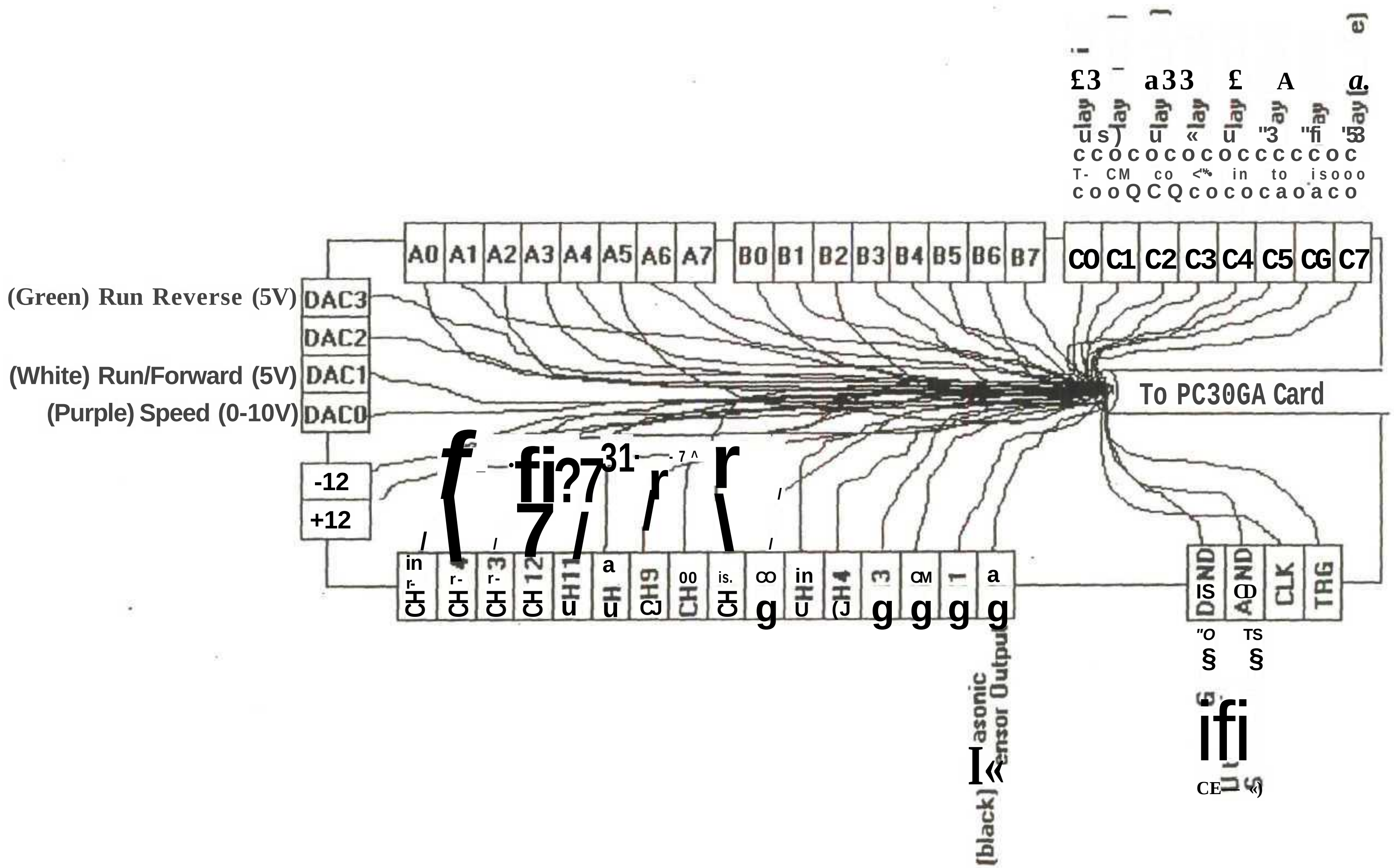

Air Bearing Solenoid Valve Switching Circuit :AB1- AB4

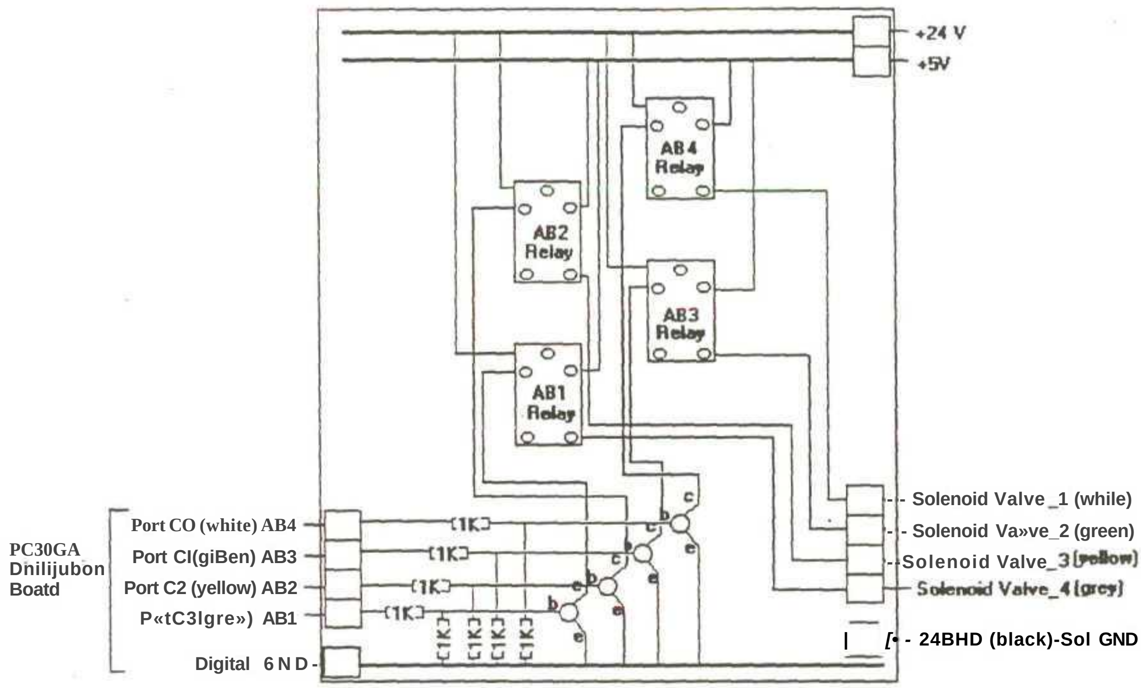

Air Bearing Solenoid Valve Switching Circuit :AB5- AB8

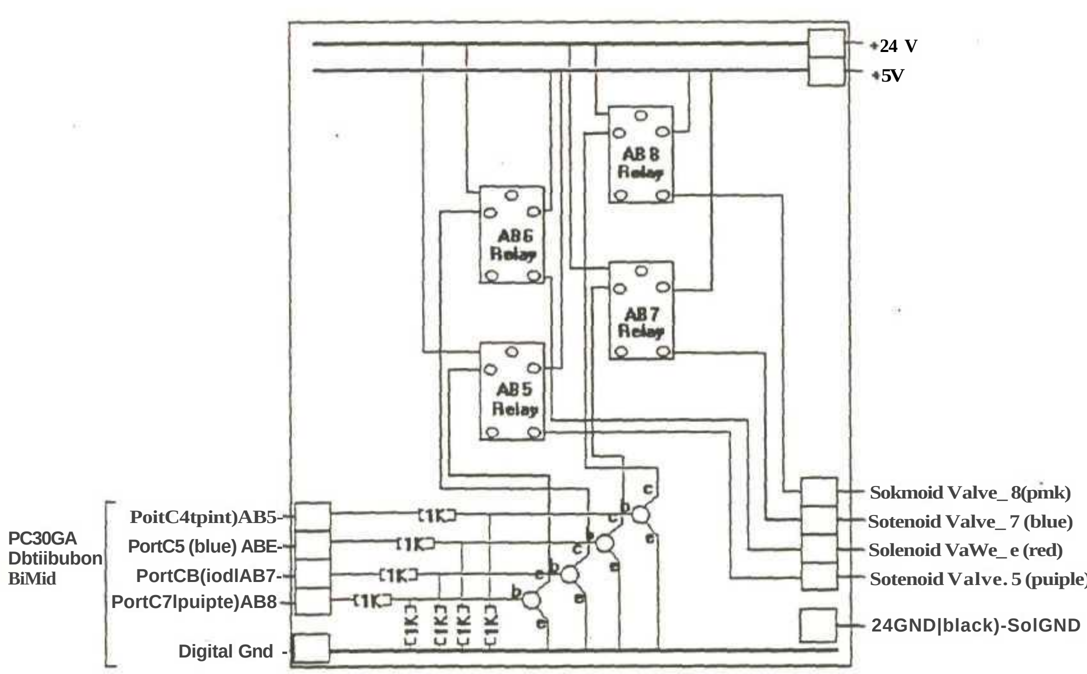

FESTO CPV Solenoid Valve Terminal: Pin Configuration

Wire Colour	*Pin No.*
white	1
green	2
yellow	3
grey	4
pink	5
blue	6
red	7
violet	8
black	9

Inveter Control Circuit Switching Circuit

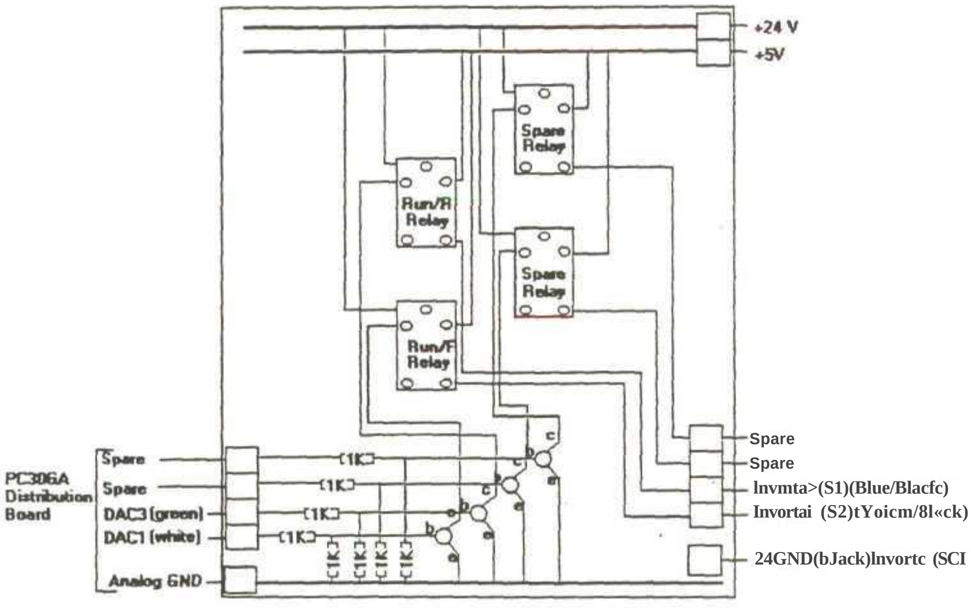

Inverter Wiring Configuration

Inverter Main Circuit Wiring

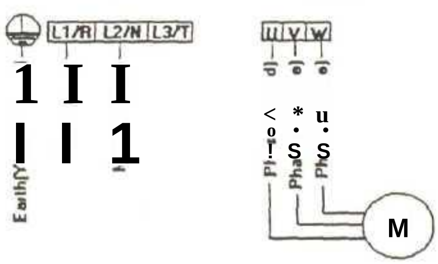

Inverter Control Circuit

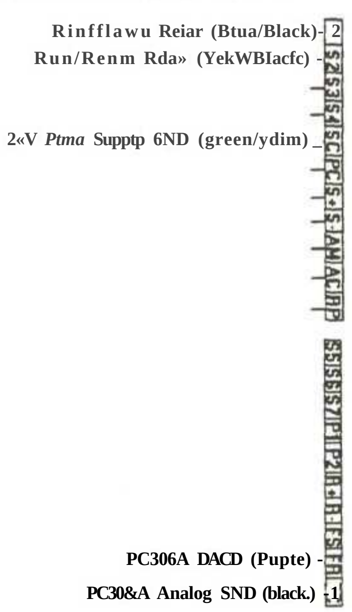

APPENDIX J

LABVIEW GRAPHICAL PROGRAMS

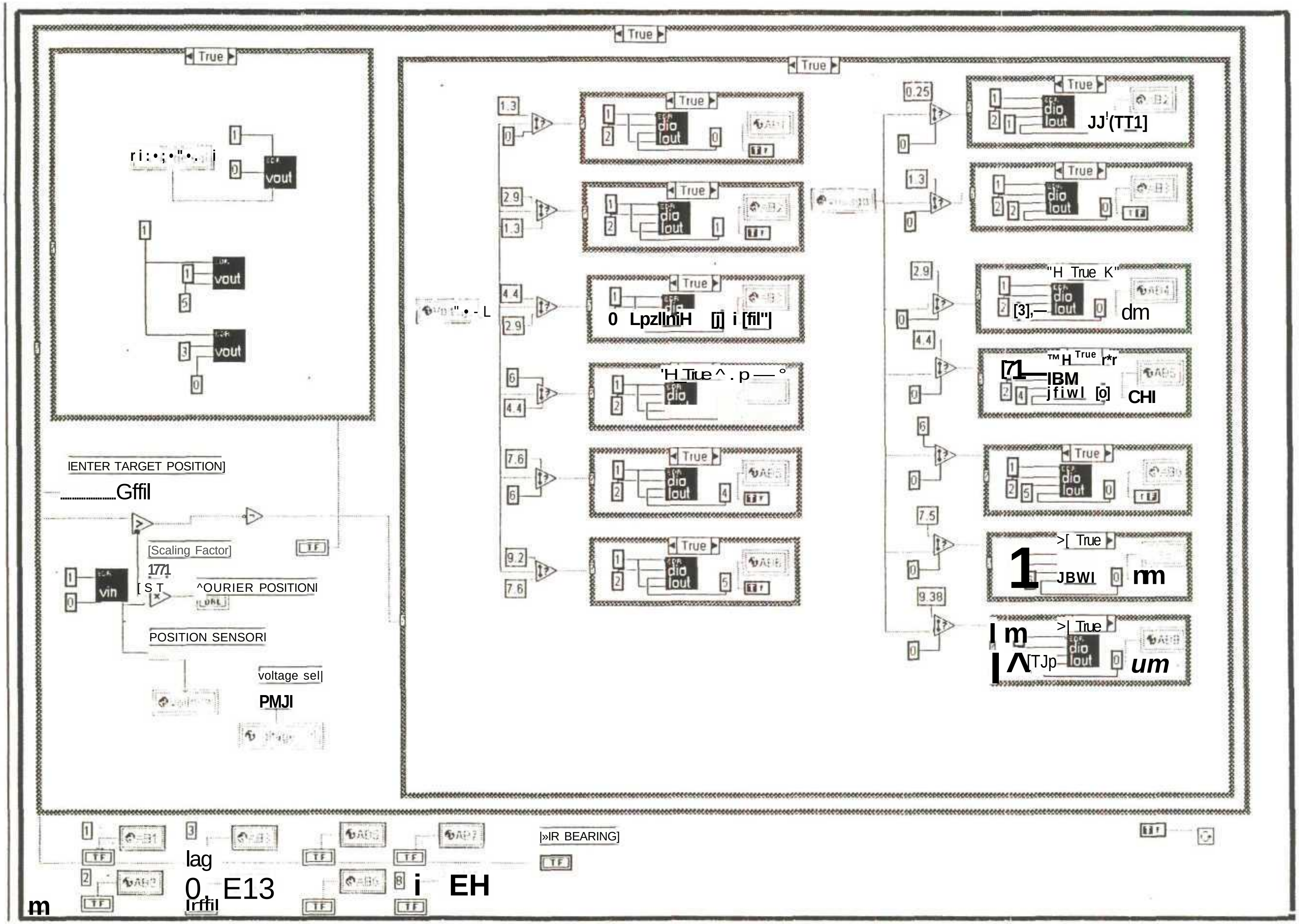
True
vout
vin
dio
lout
ENTER TARGET POSITION
Scaling Factor
POSITION SENSOR
voltage sel
IR BEARING
1.3
2.9
4.4
6
7.6
9.2
0.25
7.5
9.38

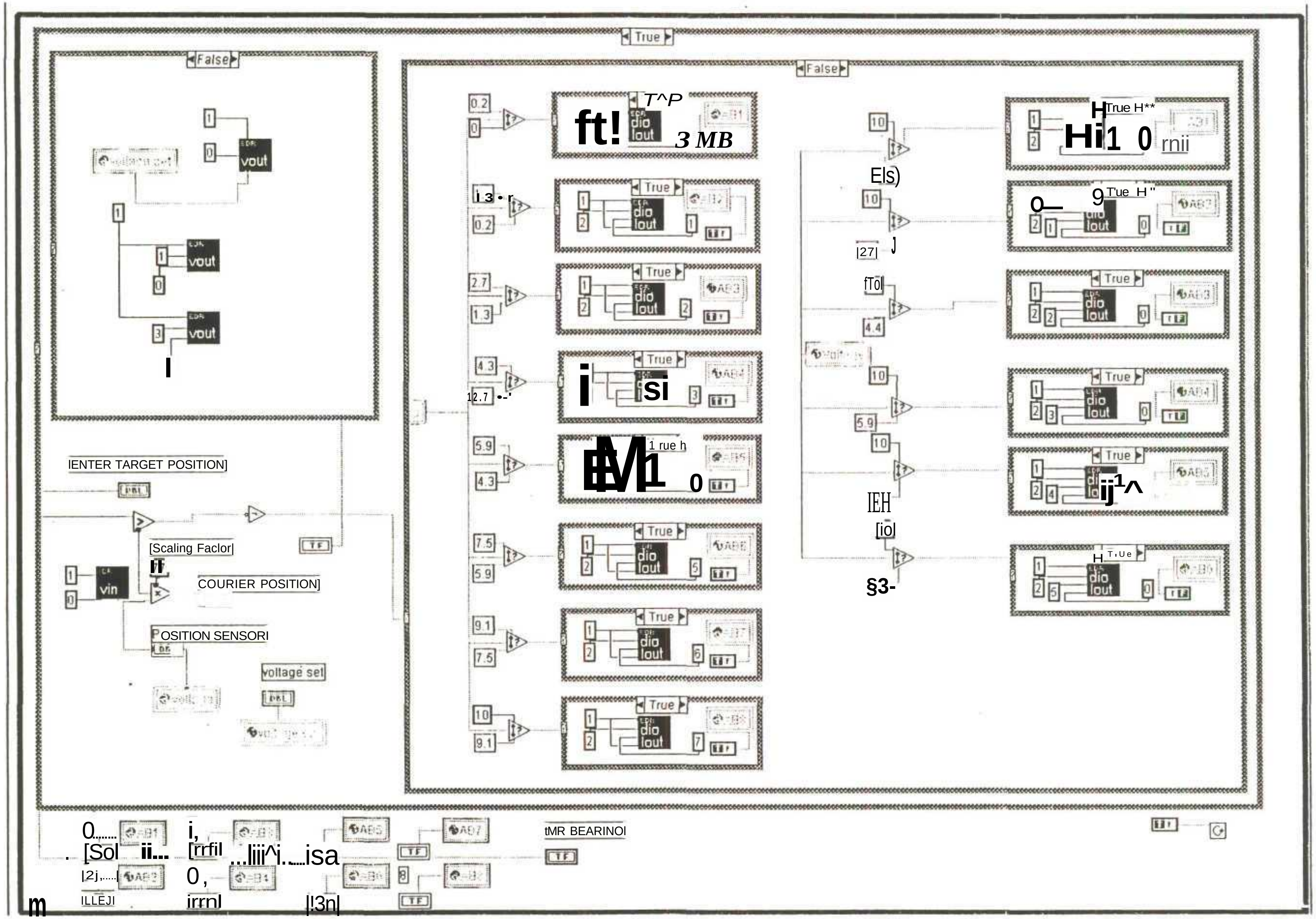

True
False
vout
vin
dio
Iout
ENTER TARGET POSITION
Scaling Factor
COURIER POSITION
POSITION SENSOR
voltage set
MR BEARING

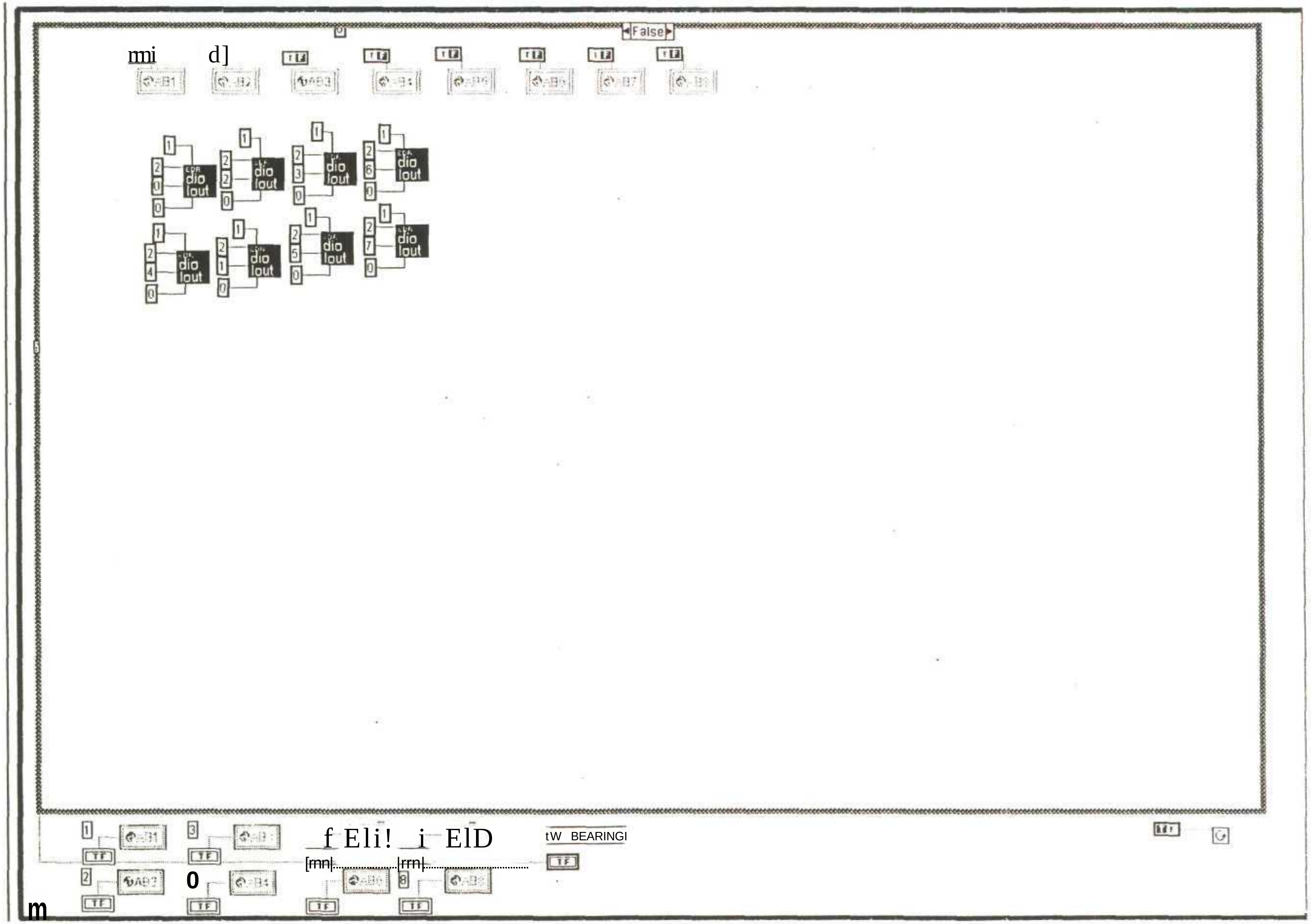
False
dio
Iout
BEARING

CLSM MHS FRONT PAGE

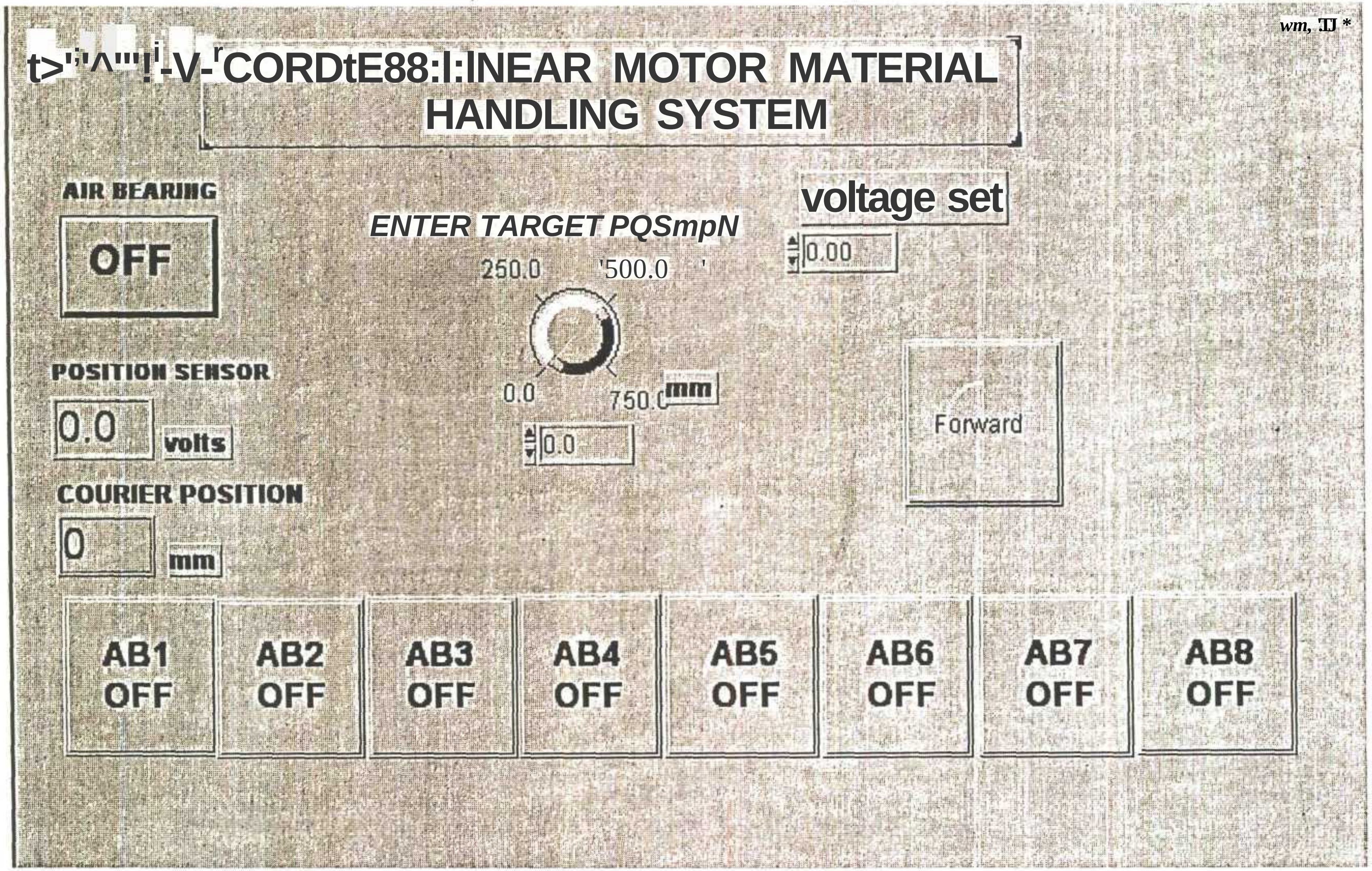

APPENDIX K

PUBLICATIONS

Proceedings of the 5th International Conference

COMPUTER INTEGRATED MANUFACTURING

Technologies For New Millennium Manufacturing

28 - 30 March 2000
Singapore

In conjunction with
ICCIM 2000 Pre-Conference Workshops,
ILA 2000 - The 2nd Asia Pacific Forum on Integrated Logistics Solutions,
TLA 2000 - The 2nd Asia Pacific Exhibition for Transportation & Logistics,
Technology Hub 200 - The 1st Asia Pacific IT Exhibition in
Manufacturing and Logistic Solutions.

Volume 1

Editors

J. Singh, S. C. Lew and R. Gay

Gintic
Institute of Manufacturing Technology

Nanyang Technological University

DAAAM INTERNATIONAL - VIENNA - AUSTRIA

RESULT OF THE REVIEW OF THE PAPER (L-04)

Title: **Intelligent Material Handling System for Advanced Electronic Component Inspections**

Author(s): **Lindsay, C; Tlale, S. & Bright, G.**

Dear Colleague, Vienna, 22-06-2000

I am happy to inform you that your paper is reviewed and accepted in the final program of the **11th DAAAM International Symposium: intelligent Manufacturing & Automation: Man-Machine-Nature"** which will be held from **19-21" October 2000, in Opatija, Croatia.** Please make slight modifications on your paper as specified below, and send us the hard and soft copy of it.
In order to have the paper appear in the proceedings, please pay the conference fee. The conference fee for authors and participants is 250.- Euro. You can pay reduced conference fee of 220.- Euro if you are paying it before 2000-08-01. The conference fee for the students is 100.- Euro paid before 2000-08-01 or 125.- Euro paid after 2000-08-01. The conference fee should be sent to the Bank Austria Count No. 22911856900 BLZ 12000, DAAAM-2000. The money transfer charge has to be paid by sender.

We are looking forward to see you in Opatija in October 2000
With best regards from Vienna
I am sincerelyjvours^

I'resident of DAAAM International
l^rdjessor Branko Katalinic

DANUBE ADRIA ASSOCIATION FOR AUTOMATION & MANUFACTURING
DAAAM INTERNATIONAL
VIENNA

Robotics and Computer-Integrated Manufacturing

EDITOR
Professor Agostino Villa
Dipanmcnto di Sistemi di Produzione cd
Economia dell' Azienda
Politecnico di Torina
Corso Duca degli Abruzzi 24
10129 Torino
ITALY
Tel: +39 11 564 7233
Fax: +39 11 564 7299
e-mail: villa@aitiena.poliic.il
EDITOR-IN-CHIEF: Professor **Andre Sharon**

Torino, Jume 7, 2000

Prof. Craig LINDSAY
School of Mechanical Engineering
University of Natal
BURBAN 4041

copy to: **Dr. Alison SEEDHOUSE**
RCIM Issue Manager
ELSEVIER Science LTD
Bampfylde Street
Exeter EX1 2AH. England

Dear Prof. Lindsay,

RE: Advanced material handling system for Computer Integrated mAnufacturing.
Reference No: RCIM/AV/10/99

I am pleased to inform you that the above paper has been accepted for publication in ***Robotics and Computer Integrated Manufacturing..***

Proofs will be sent out to you in due course and your paper will appear in the next available issue.

A copyright transfer form will also sent you, and I would be grateful if you could sign and return it to **The Production Controller, *Robotics and Computer Integrated Manufacturing*, ELSEVIER Sciences Ltd., The Boulevard, Landford Lane, Kidlington, Oxford, 0X5 1GB, England.** Please, be sure to include also biographical notes of up to 100 words for each author, describing career details and current research interests. Any further enquiries regarding your paper should now be directed to The Production Controller.

Yours sincerely,

Agostino Villa, Professor